AD NUMBER

ADB005327

NEW LIMITATION CHANGE

TO

Approved for public release, distribution unlimited

FROM

Distribution authorized to U.S. Gov't. agencies only; test and evaluation; June 1973. Other requests shall be referred to U. S. Army Engineer Waterways Experiment Station, Vicksburg, Mississippi

AUTHORITY

d/a ltr, 23 Jun 1976.

TECHNICAL REPORT M-73-3

EFFECTS OF TERRAIN ON THE PROPAGATION OF MICROSEISMIC WAVES AND IMPLANTATION CHARACTERISTICS OF AIR-DELIVERED SENSORS AT FORT HUACHUCA, ARIZONA

WET- AND DRY-SEASON CONDITIONS

by

H. W. West, B. Rohani

June 1973

Sponsored by U. S. Army Test and Evaluation Command, U. S. Army Electronics Proving Ground, Fort Huachuca, Arizona

Conducted by U. S. Army Engineer Waterways Experiment Station
Mobility and Environmental Systems Laboratory
Vicksburg, Mississippi

Destroy this report when no longer needed. Do not return it to the originator.

The findings in this report are not to be construed as an official Department of the Army position unless so designated by other authorized documents.

TECHNICAL REPORT M-73-3

EFFECTS OF TERRAIN ON THE PROPAGATION OF MICROSEISMIC WAVES AND IMPLANTATION CHARACTERISTICS OF AIR-DELIVERED SENSORS AT FORT HUACHUCA, ARIZONA

WET- AND DRY-SEASON CONDITIONS

by

H. W. West, B. Rohani

June 1973

Sponsored by U. S. Army Test and Evaluation Command, U. S. Army Electronics Proving Ground, Fort Huachuca, Arizona
Project: 9-C0-002-000-010

Conducted by U. S. Army Engineer Waterways Experiment Station
Mobility and Environmental Systems Laboratory
Vicksburg, Mississippi

ARMY-MRC VICKSBURG MISS

THE CONTENTS OF THIS REPORT ARE NOT TO BE USED FOR ADVERTISING, PUBLICATION, OR PROMOTIONAL PURPOSES. CITATION OF TRADE NAMES DOES NOT CONSTITUTE AN OFFICIAL ENDORSEMENT OR APPROVAL OF THE USE OF SUCH COMMERCIAL PRODUCTS.

FOREWORD

The study reported herein was sponsored by the U. S. Army Electronics Proving Ground (AEPG) of the U. S. Army Test and Evaluation Command under Project 9-CO-002-000-010, "Sensor Surveillance System." It was conducted by personnel of the U. S. Army Engineer Waterways Experiment Station (WES) during the period August 1971 through December 1972 under the direct supervision of Mr. Bob O. Benn, Acting Chief, Environmental Research Branch (ERB), Mobility and Environmental Systems Laboratory (MESL), and under the general supervision of Messrs. W. G. Shockley, Chief, MESL, and W. E. Grabau, Chief, Environmental Systems Division. Field tests were performed in August 1971 (wet season) and March 1972 (dry season). Personnel making significant contributions were Messrs. H. W. West (Project Engineer), of the Environmental Simulation Branch, M. A. Zappi, Environmental Characterization Branch, and C. Miller, B. T. Helmuth, and C. Lebron, SP4 T. Engdahl, and SP4 B. Shumard of ERB; Messrs. J. R. Curro, R. E. Leach, M. Carlson, D. H. Douglas, E. Perry, and L. O. Steen, and Dr. B. Rohani of the Soil Dynamics Division, Soils and Pavements Laboratory (SPL); Mr. J. D. Broughton, Geology Branch, SPL; and Messrs. M. Savage and S. W. Guy of the Operations Branch, Instrumentation Services Division.

The reduction of seismic and environmental data and mapping of the seismic intrusion detector test areas were accomplished by Mr. Curro. The theoretical depth-of-penetration predictions of the air-delivered sensors were produced by Dr. Rohani. The report was prepared by Mr. West and Dr. Rohani.

Acknowledgment is made to Messrs. L. Jay, Project Coordinator, Colin Giorgi, and Merle Wittmeyer, and LT Gary Wills of the AEPG, Fort Huachuca, Arizona, for their many contributions to the field

Huachuca, Arizona, for their many contributions to the field experimental program, including the establishment of meteorological stations within the Fort Huachuca East Range, acquiring test vehicles, obtaining high-speed photographs for the determination of impact velocities of the ADSID/S sensors, and providing personnel support for conducting special seismic tests; and to SP4 W. Richardson and SP4 K. Gilliland of the AEPG for their assistance and cooperation in obtaining environmental data and conducting seismic response tests. Acknowledgment is also made to CPT E. R. Bedard and SGT Serfass of the Combat Surveillance Electronic Warfare School, Unattended Ground Sensor Division, Fort Huachuca, for their assistance and cooperation in obtaining penetration data on the ADSID/S sensors.

Director of WES during this study and preparation of this report was COL Ernest D. Peixotto, CE. Technical Director was Mr. F. R. Brown.

CONTENTS

CONTENTS

NOTATION

C_D	Drag coefficient associated with projectile penetration, dimensionless
CPR	Cone penetration resistance, kPa
E	Young's modulus of elasticity, kg/cm^2
f	Frequency corresponding to SPV, Hz
G	Shear modulus, kPa
M	Bulk (constrained) modulus
P	Hydrostatic pressure, kg/cm^2
PPV	Peak particle velocity, cm/sec
PSPV	Peak summed particle velocity, cm/sec
rms	Root mean square
SPV	Summed particle velocity, cm/sec
t	Time, sec
T_1, T_2	Thickness of refraction layers 1 and 2, respectively, cm
V_P	Compression (primary) wave velocity, m/sec
V_R	Rayleigh wave velocity, m/sec
V_S	Shear wave velocity, m/sec
V_T	Total volume of soil sample, cm^3
W	Moisture (or water) content of soil sample, %
W_s	Weight of solids within soil sample, g
W_T	Total weight of wet soil, g
W_w	Weight of water within soil sample, g
γ_d	Soil dry density, g/cm^3
δ	Angle of friction between projectile and soil, deg
ε_a	Axial strain, %
$\varepsilon_a - \varepsilon_r$	Deviator strain, kg/cm^2

ζ	Viscous damping coefficient, dimensionless
λ	Lamés stress constant, kg/sec^2
μ	Coefficient of friction between projectile and soil, dimensionless
ν	Poisson's ratio
ρ	Initial wet density of soil, g/cm^3
ρ_p	Current wet density of soil, g/cm^3
ρ_p/ρ	Soil compressibility parameter, dimensionless
σ_a	Axial stress, kg/cm^2
σ_r	Radial stress; also confining pressure, kg/cm^2
$\sigma_a - \sigma_r$	Deviator stress, kg/cm^2
$\left(\sigma_a - \sigma_r\right)_{max}$	Stress difference at failure
$\left(\sigma_a + 2\sigma_r\right)/3$	Mean normal stress, kg/cm^2
σ_u	Ultimate soil shear strength, kg/cm^2
ϕ	Angle of internal friction, deg

CONVERSION FACTORS, METRIC TO BRITISH AND BRITISH TO METRIC UNITS OF MEASUREMENT

Units of measurement used in this report can be converted as follows:

Multiply	By	To Obtain
Metric to British		
millimeters	0.03947	inches
centimeters	0.0328	feet
centimeters per second	1.968	feet per minute
square centimeters	0.1550	square inches
cubic centimeters	0.06102	cubic inches
meters	3.281	feet
meters per second	2.237	miles per hour
kilometers	0.6214	miles
square kilometers	0.3861	square miles
kilograms	2.205	pounds
kilograms per square centimeter	14.223	pounds per square inch
grams	0.0022	pounds
grams per cubic centimeter	0.0361	pounds per cubic inch
kilopascals (kilonewtons per square meter)	0.1450	pounds per square inch
Celsius or Kelvin degrees	9/5	Fahrenheit degrees*
British to Metric		
inches	0.0254	meters
pounds per square inch	6.8948	kilopascals (= kilonewtons per square meter)
cubic feet	0.0283	cubic meters
miles (U. S. statute)	1609.344	meters
feet	0.3048	meters

* To obtain Fahrenheit (F) readings from Celsius (C) readings, use the following equation: $F = 9/5(C) + 32$. To obtain Fahrenheit from Kelvin (K), use: $F = 9/5(K - 273.15) + 32$.

SUMMARY

To obtain a quantitative basis for experiment design decisions regarding evaluation of seismic intrusion detector (SID) systems, test areas were selected (one for hand-emplaced SID's and six for air-implanted SID's) and special seismic and environmental field experiments were conducted at Fort Huachuca, Arizona, during August 1971 and March 1972. Data obtained were assumed to be representative of wet- and dry-terrain conditions at the test sites. This report discusses the selection of the SID test areas, their wet- and dry-terrain characteristics, and the procedures for collecting environmental data and conducting seismic response tests (i.e. man-walking, drop-hammer, M151 wheeled and M577 tracked vehicles, ambient and induced noises). Also presented are experimental detection distance data on the hand-emplaced miniaturized SID (MINISID), and experimental data on the depth of penetration and angle of impact of the air-delivered seismic intrusion detector/short (ADSID/S).

This report also presents a theoretical system for modeling the quantitative effects of the terrain on SID detection performance and methods by which SID test results can be extrapolated from one site condition to another. This system has been implemented on the U. S. Army Engineer Waterways Experiment Station computer and involves (a) acquisition of terrain and seismic data for input to the model, (b) exercising the model for each set of terrain factor data, and (c) portraying the performance predictions for each set of terrain and seismic factor data.

A system of equations is presented for determining soil penetration and deceleration of air-delivered SID's. The system employs a series of computer routines that treat the soil as an elastic-plastic, strain-hardening, and compressible medium. The inputs for the penetration equations are the dynamic stress-strain data obtained from laboratory triaxial compression and uniaxial strain tests.

The hand-emplacement area was found to provide near-ideal terrain conditions for performing engineering tests of hand-emplaced SID's. Surface and subsurface terrain data of the area show more variation from site to site than between wet- and dry-season conditions. The seismic responses measured at the 10 test sites within the hand-emplacement area show some site-to-site variation, and this variation should be considered in SID engineering testing; however, it is believed that this variation can be accounted for analytically and, therefore,

will not necessarily result in any erratic or inconsistent results in engineering tests performed on the hand-emplaced SID's. The variations in seismic response parameters portrayed by airdrop areas 1 and 4-6, measured in the dry season, generally indicate that the detection performance of air-implanted SID's can be evaluated for a large range of terrain conditions. The variation in these conditions allows the testing of air-implanted SID's under varying stress conditions (i.e. high to low rigid-body deceleration values) and under a variety of soil strength conditions.

The theoretical detection prediction scheme and/or concepts provide an analytical framework for predicting SID performance for man-walking targets in various world terrains. The scheme requires specific terrain and seismic input data for execution, and as a result, four types of maps were prepared. These include (a) terrain factor complex maps for subsurface layers 1 and 2 to provide inputs to the theoretical seismic wave propagation model, (b) surface condition maps to be used with the forcing function model under development, (c) seismic response factor complex maps to show the relative seismic response of the hand-emplacement area, and (d) SID one-man walking detection performance map. The predicted depths of penetration of the ADSID/S compared reasonably well with the very limited experimental penetration data; they show the depth of penetrations to be very dependent upon near-surface moisture conditions.

Appendix A describes the operating principles of hand-emplaced miniaturized SID's and air-delivered SID's used in special tests to yield data for aiding in the evaluation of the techniques for predicting SID performance. Appendix B describes the test sites and contains supplementary refraction seismic data. Appendix C presents the equations for predicting penetration depths and deceleration values for air-implanted SID's. Appendix D describes the computer models used to predict SID detection performance.

EFFECTS OF TERRAIN ON THE PROPAGATION OF MICROSEISMIC WAVES AND IMPLANTATION CHARACTERISTICS OF AIR-DELIVERED SENSORS AT FORT HUACHUCA, ARIZONA WET- AND DRY-SEASON CONDITIONS

PART I: INTRODUCTION

Background

1. The U. S. Army Electronics Proving Ground (AEPG), Fort Huachuca, Arizona, has the responsibility for developing methodology and conducting engineering tests for the U. S. Army Test and Evaluation Command (TECOM) for the purpose of evaluating seismic intrusion detection systems.

2. The development of a capability for testing the engineering adequacy and operational suitability of seismic intrusion detection devices must necessarily rest on an understanding of the physical phenomena involved in the detection process. Generally, a seismic intrusion detector (SID) is intended to provide, at a minimum, the information that something (hereafter referred to as a target) is moving across the terrain within some specified distance from the SID. It would, of course, be far better if more information could be obtained, and thus efforts have been made to design SID's that will provide information on target characteristics (i.e. will discriminate among types of targets), target rate of movement, target direction, and target range.

3. The detection process alone (i.e. determination that there is a target within a given area) is relatively complex, and with the addition of other types of information, the process becomes very complex indeed. In view of this, it seems appropriate to provide a brief discussion of the detection process and of the physical phenomena involved therein.

Transfer of energy from
seismic source to substrate

4. The detection process consists of a sequence of interrelated physical phenomena (fig. 1). The sequence starts with the target.

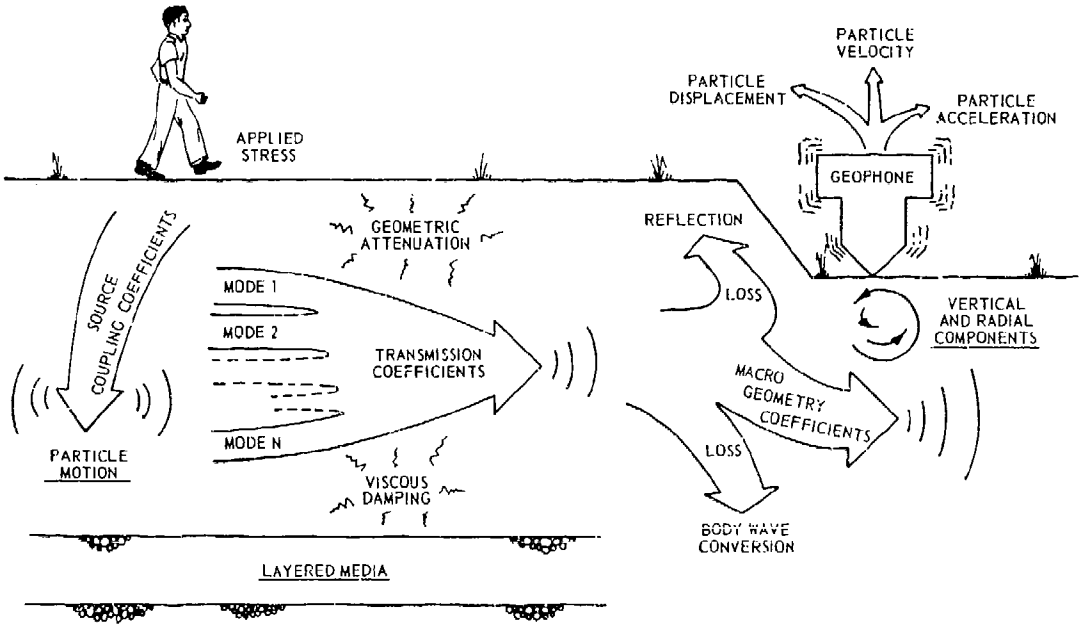

Fig. 1. Signal generation and propagation of microseismic waves

Anything that moves on the surface of the ground applies a force to the substrate. The thing may be a man, a vehicle, the pressure pulse of an acoustic wave, an animal, or even trees being moved slightly by the wind. If the force is raised to a level such that the substrate is stressed enough to deform, even if only minutely, the energy is carried away from the point of deformation by seismic waves. The implications of the statement that anything that applies a force to the substrate of sufficient magnitude to stress and deform it will produce a seismic wave train should be thoroughly understood. For example, wind blowing through trees and shrubs transmits forces down the stems and into the substrate, and the deformations result in the generation of seismic wave trains. Those waves are not qualitatively different from the ones

produced by a moving tank. A passing train produces seismic signals; so does traffic on highways. Factories produce seismic signals. In fact, the active crust of the earth produces seismic wave trains throughout the surface of the globe. No area on the planet is entirely free of such extraneous wave trains, and those waves will inevitably be sensed by military SID's, just as will the waves from a military target. The point is that if one is interested in detecting a specific type of target "false alarms" will always occur; the only point of issue is their frequency.

5. The amplitude and, to some degree, the type of seismic wave generated depends upon its stress history. For example, a walking man applies a localized force at the point of each footfall, and that force and the resultant substrate stress are characterized by a particular relationship between magnitude and time. That is, the force is not applied instantaneously; rather, it rises and falls according to a particular pattern, even though the entire time involved is only a fraction of a second. This "force-time history" can vary remarkably. The major variations can be classed as: (a) variations in the nature of the target itself, and (b) variations in the nature of the substrate (soil, rock, pavement, snow, or any other material composing the medium on which the target is moving).

6. Variations in the nature of the target are important because they result in differing rates and magnitudes of force application to the substrate. That is, they affect the force-time history by which the available energy is applied to the substrate. The major potential variations are size of the mass and rate of force application.

7. Other things being equal, a large mass will result in greater forces than a small mass, and these will, of course, be reflected in the force-time history. Thus, a large man tends to produce a force-time history different from that of a small man; this also is true for large and small vehicles.

8. Again other things being equal, a force applied rapidly will produce a force-time history different from that of the same force applied slowly. Thus, a man placing his feet slowly and carefully on

the ground will produce a force-time history significantly different from that produced by the same man walking normally. Similar differences occur in the force-time histories of vehicles. For example, a wheeled vehicle moving on a smooth, even surface applies force relatively smoothly, without sharp discontinuities in force level. On the other hand, the track pads of a tracked vehicle strike the ground sequentially, and thus produce a force-time history consisting of a series of high and low force levels. Obviously, the rate at which those cycles occur is a function of vehicle speed. This situation becomes even more complex if the surface over which the vehicle is moving is irregular, since in this instance the dynamic response of the vehicle, regardless of whether it is wheeled or tracked, will result in maxima and minima in the force applied to the substrate.

9. Variations in the nature of the substrate may also affect the force-time history, since that history is a record of the relation between force and time as measured at a specific point. If the surface is soft and spongy, the thing applying the force (i.e. an infantryman's foot, the track pad of a tank, etc.) requires a longer time between initial contact and achievement of maximum force level than would be the case on a firm, hard surface. Thus, the force-time histories of the two situations will not be identical, even though no intrinsic changes in the character of the target are present. One implication of this is that the force-time history of a man walking in a sod-covered area will be different from that of the same man walking at the same pace in an area of bare ground.

10. The force applied to the ground surface creates a set of stresses in the substrate material, and if the stress level is high enough, measurable deformation occurs. The energy of deformation is then carried away from the point of deformation by seismic waves. Thus it follows that the stress-time history and the characteristics of the substrate materials control the nature and magnitude of the seismic waves.

11. There are three major seismic wave modes, all of which move radially outward from a point of substrate deformation (i.e. the point

at which stress is applied): (a) compression waves (P-waves), in which the principal particle motion is along a radial; (b) shear waves (S-waves), in which the principal particle motion is at right angles to a radial; and (c) surface waves (Rayleigh waves), in which the principal particle motion is elliptical, with the plane of motion chiefly perpendicular to the surface of the propagating medium and the major axis of the ellipse usually subparallel to the surface. Compression waves move in all directions, so that the advancing wave front is approximately a hemisphere. Shear waves also move in all directions, so that the advancing wave front is also approximately a hemisphere. However, they do not necessarily move at the same velocity as the P-wave, even in the same material. Unlike P-waves and S-waves, Rayleigh waves move only at shallow depths and parallel to the surface, so that at a point a few meters from the target, the advancing wave front is cylindrical, with the vertical axis of the cylinder at the target. For all practical purposes, Rayleigh waves (assuming very low amplitudes such as are of interest in SID utilization and design) affect a substrate zone equal to about one-half wavelength. Amplitudes of Rayleigh waves are at a maximum at the surface and decrease progressively with depth. The propagation velocities are not the same as those of either P-waves or the S-waves.

12. Generally, both P-waves and S-waves are diffracted in the direction of greater substrate densities, and since nearly all natural substrates increase in density with depth, these waves tend to diffract downward. The result is that they appear to attenuate very rapidly at the surface. They may, however, reflect from a subsurface discontinuity and reappear at the surface at some distance from the target. Thus there may be zones in which the P-waves and S-waves cannot be detected at the surface. Conversely, the Rayleigh wave propagates only along the surface; thus there can be no discontinuities in the area over which the signal can be detected. This, and the fact that about two-thirds of the energy at the source is carried away in the Rayleigh wave, is the principal reason for choosing the Rayleigh wave as the mode upon which to base SID designs.

13. All seismic waves are affected by the nature of the materials through which they propagate. However, since the Rayleigh wave is the principal mode of interest, the following discussion will be restricted to matters of concern to Rayleigh wave propagation.

14. The "ideal" situation for the propagation of Rayleigh waves would consist of a completely homogeneous elastic half-space. Anything that departs from these ideal conditions serves to attenuate the wave form more rapidly than would be the case by purely geometric attenuation (i.e. the attenuation resulting from the same amount of energy being applied over a longer wave front as the wave moves outward away from the source). There are several basic types of nonhomogeneities commonly found in nature. The dramatic effects of nonhomogeneities on wave propagation stem primarily from the fact that each type of material tends to act as a specific medium for a specific suite of wave frequencies. That is, a specific type of material tends to propagate certain frequencies more efficiently than others. The result is that substrate materials act as selective filters. For example, most targets generate a seismic wave train (or signal) consisting of a complex of frequencies (or wavelengths) ranging from very low (i.e. very long waves) to very high (i.e. very short waves). Generally, the signal contains a broad spectrum of frequencies as it emerges from the source. However, as the wave train moves radially away from the source, two things happen to it. First, since each frequency tends to propagate at a slightly different speed, the wave train tends to separate into sections, each having a characteristic frequency. This effect is usually not obvious, since the process rarely has time to produce complete frequency separation before the wave train dies completely away.

15. Second, some frequencies are propagated efficiently over rather long distances and others die out quickly. The effect of this phenomenon is to filter out some of the original frequencies, leaving a signal characterized only by those frequencies that are efficiently propagated. In practical terms, the implication is that, in some terrains and at long detection distances, all targets tend to be characterized by wave trains exhibiting the same frequencies. It is obvious that

in such situations, virtually all targets will look the same insofar as the frequency composition of their signatures is concerned.

16. There are several basic types of variations in substrate characteristics, each of which interacts with the seismic wave trains in specific ways. One such basic type is stratification. Nearly all substrates are stratified to some degree, and many are divided very sharply into distinct layers. For example, most agricultural areas are characterized by soils having a minimum of three more-or-less distinct strata: (a) a disturbed layer, down to plow depth, consisting of relatively low-density materials; (b) a layer in which the parent material is only partially modified by soil-forming processes; and (c) a layer consisting of the original parent material, which is often rock. Each such layer tends to be characterized by somewhat different propagation characteristics, with the result that the seismic waves try to propagate independently through each. The interference that occurs at the interfaces absorbs energy, and the wave as a whole therefore tends to attenuate rapidly. Many other conditions of stratification also occur; the hand of man is not required to produce them.

17. It should be noted that stratification is not a constant with respect to time. The most common cause of a change in stratification is a change in moisture content. The presence of water in a soil affects the overall density, the intraparticle adhesion, and in some cases even particle orientation, all of which change the elasticity and/or viscosity of the soil, and therefore the wave propagation characteristics. The effects of moisture are often dramatic. For example, the deep, nearly homogeneous, silty sand soils that occur along the Gulf Coast of the United States seem superficially to approach the ideal as a propagation medium and, indeed, do approach the ideal during periods when moisture content is uniform throughout the soil mass. However, during and for a short period after rain, the near-surface soil stratum is near saturation, whereas the soil at depth has a much lower amount of contained water. The result is an effective, if temporary, stratification that may result in a more rapid attenuation of the seismic wave than would normally be the case. In practical terms, this means that the

effective detection range of a SID might be significantly reduced during the period of stratification. Somewhat similar situations can occur and persist for longer periods; for example, detection distances in some tropical situations are characteristically less during the wet season than during the dry.

18. A change in stratification of the kind described above may also result in a change in the frequency characteristics of the signal as a function of time. The reason for this is that a wet soil may not efficiently propagate the same frequencies as the same soil in a dry state. The practical effect of this phenomenon (see paragraphs 14 and 15) is that the signals arriving from the same target at the same distance may be different in wet and dry seasons.

19. A second basic type of variation in substrate characteristics is facies changes. Nearly all substrates change laterally to some extent, and in many geographic situations such changes occur abruptly and within short distances. This phenomenon may have important effects on seismic wave propagation if an interface occurs between the target and the SID. For example, consider a situation in which the first half of the propagation medium consists of a material that efficiently propagates low-frequency waves, but quickly attenuates high-frequency waves, and the second half consists of a material that efficiently transmits high-frequency waves, but not low-frequency waves. The signal leaves the target with a normal spectral composition of both high and low frequencies. During the first half of the path, all of the high frequencies are attenuated and lost, so that only low frequencies remain as the signal crosses the interface between material types. Since the second type will efficiently transmit only high frequencies, the low frequencies will be quickly attenuated and lost, leaving nothing. The practical implication of this is that a seismic wave train may be eliminated in a distance less than would be the effective detection distance if the entire propagation path were in either one of the substrate types.

20. Nonhomogeneities in the soil mass are a third basic type of variation in substrate characteristics. Many substrate materials consist of particles that are both small with respect to the size (i.e.

wavelength) of the seismic waves that propagate through the substrate and also materials with particles roughly equal to the size of the propagating wave. On the other hand, many soils consist of aggregates of different materials, some of which contain relatively large-size particles such as boulders in sand. The effect is somewhat like plums in a pudding. In addition to the size disparity, there are many situations in which the "plums" exhibit elastic and/or viscous properties markedly different from those of the matrix material.

21. Such internal nonhomogeneities may arise from a number of causes. For example, the widespread boulder-clays of the northeastern United States are materials in which the matrix is basically silty clay, and the plums are cobbles and boulders of solid rock. In forested areas, the nonhomogeneity may be caused by the roots of trees. In arid and subarid climates, discontinuous masses of caliche (a form of calcium carbonate) may form in the soil. In the Arctic the plums may be ice wedges buried in the soil.

22. Generally, substrate materials exhibiting this type of nonhomogeneity attenuate all seismic waves much more rapidly than a homogeneous material of comparable elastic and viscous properties. However, the effect is usually more dramatic on high frequencies than on low. The reasons are to be found in the frequency-dependence of propagation efficiencies (paragraph 14). For example, consider a material such as a fine sand with large rocks in which the matrix efficiently propagates low frequencies. A broad-spectrum signal propagating through such a material will be rapidly attenuated because of a complex of phenomena: The high-frequency components are quickly filtered out because of the properties of the matrix, the low frequencies are attenuated because the basic wave forms are distorted as they pass around the plums, and so on.

23. Yet another basic type of variation occurs as changes in surface geometry. Very few terrains exhibit perfectly planar surfaces, which is the ideal situation for the propagation of Rayleigh waves. Instead, nearly all are irregular to some degree. Generally, the more irregular the topographic surface, the less efficient is the propagation of the Rayleigh wave. There is, however, one important proviso; namely,

that the irregularities be large enough to significantly interfere with the wave form, but not so large that one or more wave forms can be accommodated on the feature. Since the wavelengths that are of primary interest from the point of view of SID design and utilization vary in length from about 2 to 50 m,* it is obvious that surface geometry feature size is also frequency-dependent. That is, a feature (such as a ditch) that is a meter across may well interfere significantly with the propagation of a high-frequency wave (i.e. a wave having a length of only a few meters); whereas it might not interfere significantly with a low-frequency wave (i.e. a wave having a length of tens of meters). The converse is also possible; that is, a high-frequency wave may not be significantly affected by a feature tens of meters across, because several complete wave forms of the high-frequency wave can be accommodated on it.

Transfer of seismic
energy from substrate to SID

24. The previous paragraphs have dealt with the transfer of energy from a seismic source to the substrate and the propagation of seismic waves within the substrate. The following paragraphs present a brief discussion of the phenomena dealing with the transfer of seismic energy from the vibrating medium (i.e. substrate) to the SID.

25. As the propagating seismic wave passes the geophone of the SID, the geophone is carried along by the motion of the substrate particles, if the geophone is properly placed in contact with the ground, and if certain other conditions are met. In the case of hand-emplaced SID's, the various conditions are relatively easy to meet, but this is not necessarily the case with air-delivered or artillery-delivered devices. There are three major conditions that can affect SID performance: (a) depth of penetration (or emplacement), (b) geophone attitude, and (c) coupling of the geophone with the substrate material.

26. In the context of penetration depth, it must be recalled that

* A table of factors for converting metric units of measurement to British units and British units of measurement to metric units is presented on page xi.

the particle motion produced by a Rayleigh wave is at a maximum at the surface, and that the amplitude decreases as a function of the ratio depth/wavelength of the substrate material and becomes effectively undetectable at a ratio of 1.2 in almost all substrate materials.[1] The practical effect of this characteristic of the wave mode is that maximum detection distance (or range) is achieved when the geophone is at or very close to the surface. Thus, if a geophone is emplaced at a depth of 1 m, it may not detect a target that is readily detected by a geophone placed at the surface, because the amplitude of the particle motion at that depth will be somewhat lower. This effect becomes more and more pronounced with depth, even in nonstratified substrates.

27. If the substrate is strongly stratified, the effect may be even more pronounced. This situation can occur if the second layer has propagation characteristics markedly different from those of the surface layer. In this situation, it is common to find that very little of the available energy is coupled into the second layer, and therefore the particle motion is very small. Thus, a geophone emplaced in the second layer may be scarcely affected by a wave passing above it and which is propagating almost entirely in the surface layer.

28. From these considerations, it is evident that depth of penetration of the geophone is critical. If it is placed too deep, the geophone may be below the zone in which active particle motion is taking place.

29. All existing SID's, and nearly all those presently in design stages, utilize geophones that operate at maximum efficiency when the axis of the geophone is parallel to the pull of gravity. The point is that the geophone should be vertical with respect to sea surface, not vertical with respect to the substrate surface (except when sea level surface and the substrate surfaces are parallel). The geophones become less efficient with increasing angles of inclination, and most become completely inoperative at angles from the vertical of between 45 and 60 deg, depending upon type. The practical effect of this phenomenon is that two SID's placed virtually side by side will not necessarily detect the same target. If one geophone is vertical and the

other is at some angle, the vertical geophone will characteristically achieve greater detection ranges than the one emplaced at an angle. It is also apparent that the probable detection range of an air- or artillery-delivered SID cannot be reliably estimated unless the attitude of the SID geophone is known.

30. In order for the particle motion produced by the wave to be sensed by the geophone, the case of the geophone must move as if it were a substrate particle. Generally, this can only be achieved if the geophone is in intimate and solid contact with the substrate. If it is not, only a fraction of the real particle motion may be transferred to the geophone, with the result that the geophone will record the passing of a wave having an apparent amplitude of much less than that of the real wave. The practical effect of this phenomenon is, again, a reduction in the detection range.

31. Failure to achieve adequate coupling can arise from several mechanisms. For example, the impact of an air-delivered SID may "crater" the substrate, leaving only the very tip of the projectile embedded in the ground. This limited surface contact may be inadequate to transfer all of the motion from the substrate to the SID. The impact of the SID may, in some soil types, cause the soil to surge away from the projectile body, resulting in a tubular cavity. The walls of the cavity may break and collapse into the space between the cavity wall and the projectile, which results in a very loose material actually in contact with the SID. The loose material may act as an energy-absorbing system, effectively preventing any significant amount of seismic motion from penetrating to the SID. The practical effect, of course, is to reduce the effective detection range of the device.

32. Finally, the passing seismic wave produces appropriate motion in the geophone, and the geophone then sends an electrical analog signal to the SID logic, which the logic then processes in some way. The precise operation of the logic is of major importance in any attempt to predict detection range. One example may suffice.

33. Let it be assumed that a particular SID has a logic system that will transmit a "detection" alarm only when a particular wave

amplitude is exceeded four times within a 5-sec period. Thus, in effect, the logic "listens" for a particular wave amplitude. When it "hears" it, it stores the memory away for future reference, and continues to store away similar memories for a period of 5 sec. It then adds the memories, and if the total is four or more, it transmits an alarm.

34. Now let it be assumed that the SID is in a place where there is a cyclic background "noise" (i.e. a wave train generated by some situation in the ambient environment), which occurs in such a way that the threshold amplitude of the SID is exceeded once every 2 sec. The SID, of course, hears the background noise signals, but since only two such events occur in each 5-sec period, the SID does not alarm. Now let it be assumed that an intruder approaches the position of the SID. At some point, while the intruder is still some distance away, the SID will begin to hear some of the intruder's footsteps. It will not hear them all, at first, because of natural variations in the intruder's pace, because of slight changes in the character of the surface, and so on. However, the SID adds the record of those footsteps that it does hear to the background noise events, and when the total exceeds four in a 5-sec period, the SID alarms. In this situation, the practical effect of the background was to increase the apparent sensitivity of the SID, since it achieved a detection at a distance that it would not have achieved had there been no background seismic events.

35. Now let it be assumed that the same SID is emplaced in a region in which the background noise exceeds the threshold amplitude on a random schedule, rather than on a regular cyclic schedule. Given this situation, a number of things may occur. First, a chance concentration of noise events may cause the SID to alarm in the complete absence of an intruder. A different concentration may produce the same effect as that described in paragraph 34 above, thus producing an abnormally long detection distance. A still different random concentration of noise events might also saturate the SID logic, in which case an intruder could pass through the area without detection, since the SID would be alarming constantly; the signals added by the intruder could not be

differentiated from those of the background noise. The point is that the effects of background seismic events are not necessarily either consistent or constant. At the extremes, they can produce what appears to be abnormal sensitivity in a sensor, and they can prevent detection entirely.

Scope of engineering tests

36. From the preceding discussion, it is apparent that any objective test of a SID should, if possible, account quantitatively for all of the potential variables that have been described. Only in this way is it possible to achieve confidence that the system is operating as intended, and only in this way can its true performance characteristics be established.

Objectives

37. The overall objective of the seismic and environmental study reported herein was to improve procedures for conducting engineering tests to evaluate various SID systems. The specific objectives were to:

a. Determine the significant terrain and/or seismic response factors required for interpreting the engineering test results and extrapolating the results to other test conditions.

b. Determine the variation (i.e. site to site and season to season) in the significant environmental and microseismic response factors measured at Fort Huachuca.

c. Develop and/or assemble field data collection procedures for the acquisition of the significant terrain and seismic response data.

d. Map the distribution of the terrain and microseismic response factors of the hand-emplacement test area considered significant to the engineering evaluation (i.e. those factors related to the prediction of SID detection range) of a typical Phase III SID system.

e. Examine WES analytical systems to determine their usefulness in extrapolating SID test results.

f. Determine theoretical estimates of the depth of penetration and deceleration for a typical air-delivered SID in selected airdrop test areas under varying terrain conditions (i.e. under two different moisture conditions that were assumed to be typical of wet- and dry-terrain conditions, respectively).

Approach

38. To provide a quantitative basis for making experiment design decisions in regard to evaluating SID systems, test areas were selected (one area for hand-emplaced SID's and six areas for air-implanted SID's) and special seismic and environmental field experiments were conducted by WES personnel at Fort Huachuca, Arizona, during August 1971 and March 1972, respectively. Data obtained during these periods were assumed to be representative of the respective wet- and dry-terrain conditions at Fort Huachuca. Also, special tests with air-implanted SID's were conducted at Fort Huachuca by Combat Surveillance Electronic Warfare School (CSEWS) personnel during August 1972 to provide experimental data on the depth of penetration of SID's in the Fort Huachuca terrain.

Sensor detection performance

39. To provide a framework for studying the quantitative effects of the terrain on SID detection performance, the detection problem was divided into efforts to develop procedures or models to describe the following phenomena:

a. The transfer of energy from the target to the substrate material.

b. The propagation of the microseismic waves within the substrate materials.

c. The transfer of energy from the vibrating medium (substrate) to a SID.

d. The response of the sensor logic to the vibrating medium.

These four facets of the seismic detection problem are related as shown in fig. 2. Each facet was studied within the framework of theoretical

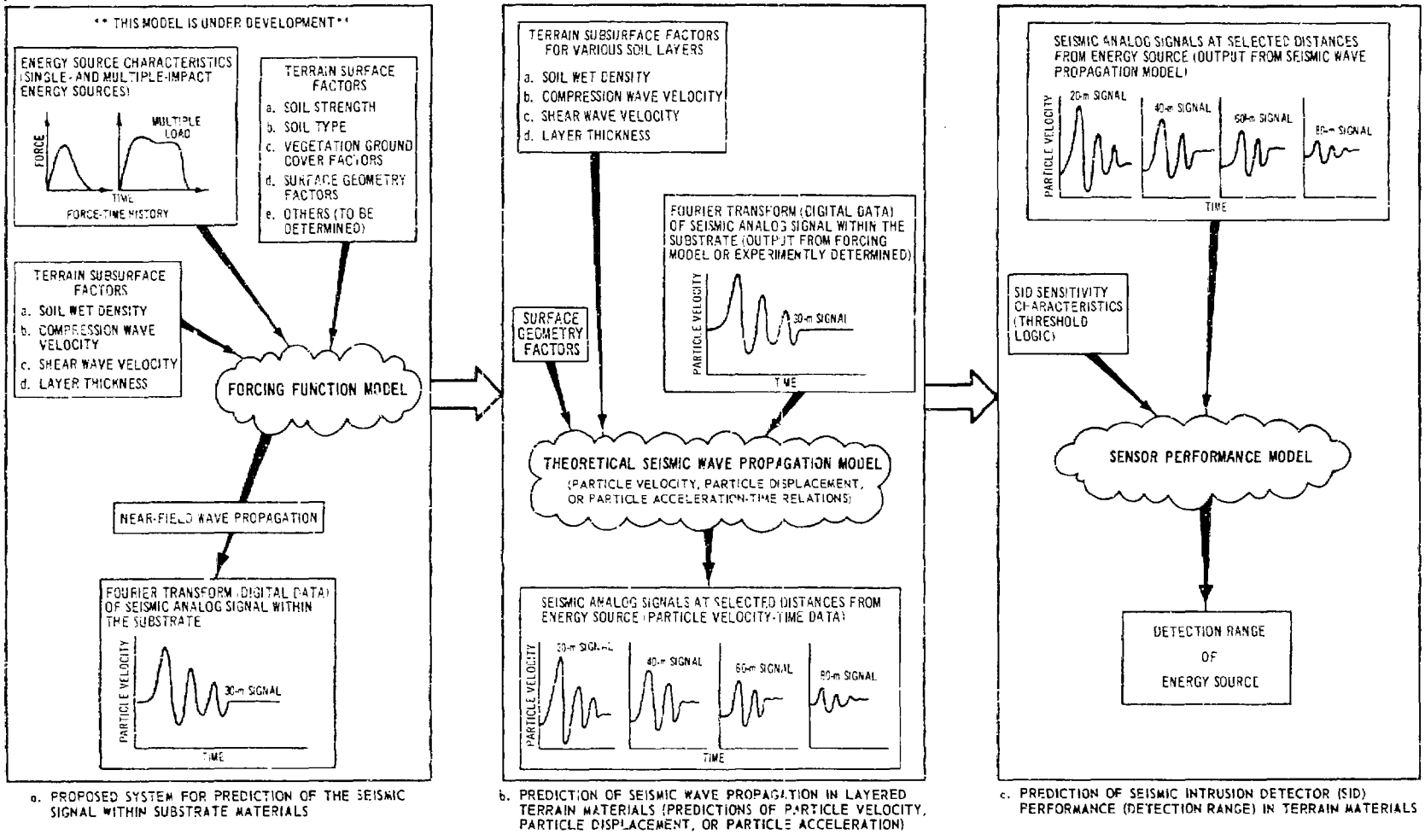

Fig. 2. WES analytical system for the prediction of SID performance in terrain materials

mechanics; and, where possible, mathematical models that closely simulate the phenomena involved in each facet were formulated. The input requirements of the models define the data that must be measured or inferred to make a prediction.

40. The performance prediction procedures form the keystone for extrapolating SID test results from one site condition to another. The concept for extrapolation or comparison of SID performance in different areas is shown graphically in fig. 3. The system involves (a) acquisition and mapping of the terrain data required by the various models, (b) exercising the forcing function and wave propagation submodels for each set of terrain factor data, and (c) portraying the performance prediction for each set of terrain factor data.

Sensor air-implantation performance

41. The development of quantitative tools for predicting the performance of air-implanted sensors has been restricted to studies of air-delivered SID (ADSID/S) soil penetration and deceleration. The approach to the soil penetration problem employs a series of computer routines that treat the soil as an elastic-plastic, strain-hardening, compressible medium. The dynamic stress-strain data required as input to the computer routines are obtained from laboratory triaxial compression and uniaxial strain tests.

Program structure

42. In practice, the entire research effort was divided into three subprograms, and those subprograms are used as the basis for the structure of this report. Thus, each subprogram is described in a part, as follows:

a. Part II: Sensor Test Areas, Test Procedures, and Environmental Characterization. This includes a description of the process of test area selection, the test program, the data collection and processing methods employed, and related matters.

b. Part III: Analysis of Data. This includes an analysis of both environmental and seismic response data, a discussion of seismic propagation models and their

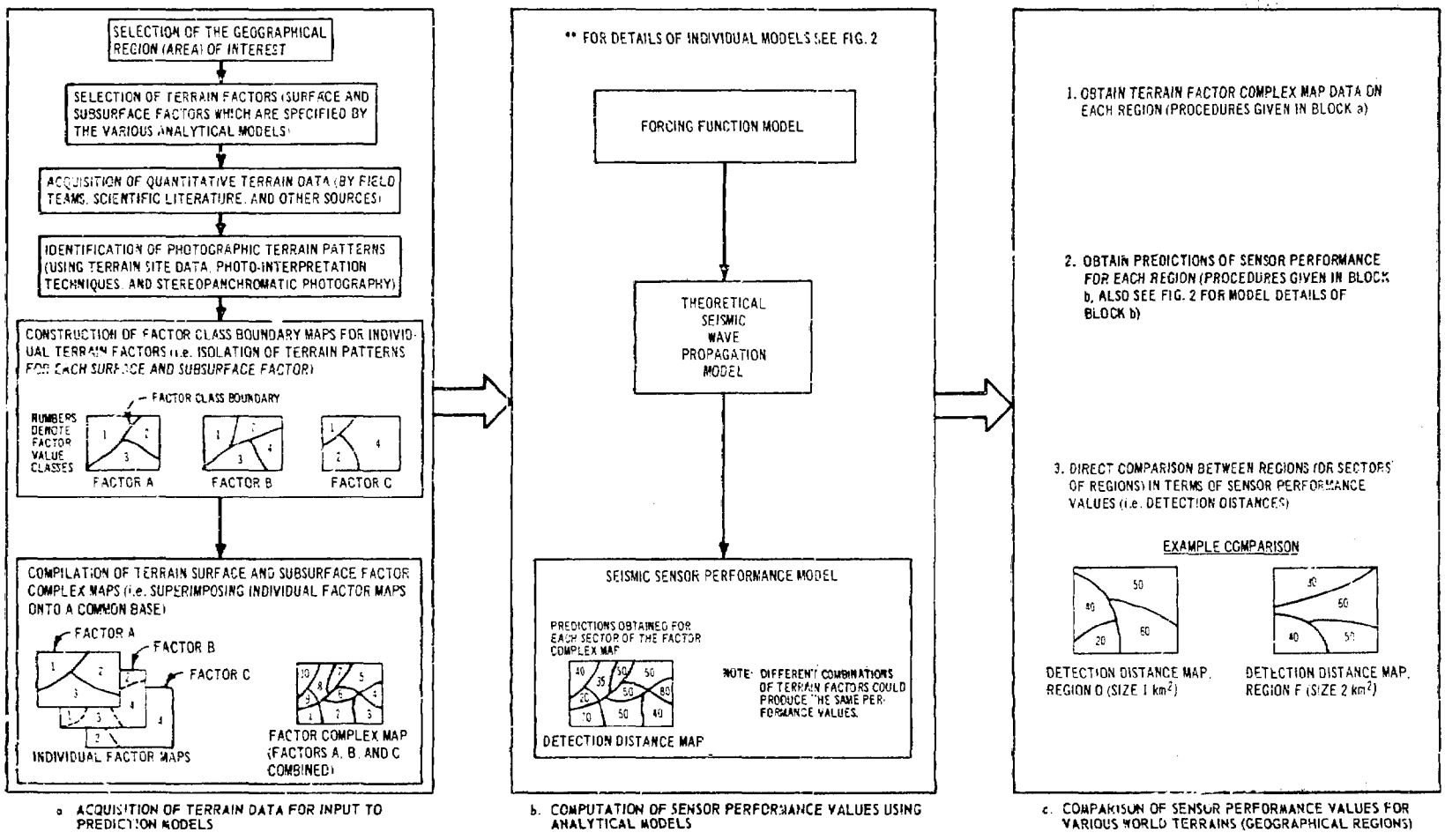

Fig. 3. WES system for obtaining SID performance predictions for various world terrains (i.e. geographical regions)

utilization, a discussion of sensor implantation data and models, and related matters.

c. Part IV: Mapping of Terrain and Seismic Response Factors and SID Performance Values. This includes a discussion of techniques developed for mapping terrain factors related to seismic sensor utilization, and related matters.

Definitions

43. Certain terms used in this report are defined as follows:

a. Coefficient of friction (μ): The coefficient of friction between the projectile (or sensor) and the soil, dimensionless.

b. Compressibility parameter (ρ_p/ρ): The ratio of the current wet density (ρ_p) of the substrate material to the initial wet density (ρ) of the substrate material. Symbolically the compressibility parameter, $\rho_p/\rho = \exp \varepsilon_v$, where ε_v is the vertical or axial strain.

c. Compression wave velocity (V_P): The speed of a compression (primary) wave through a medium. Compression waves have the greatest velocity of any elastic wave in the same medium. The motion of the particles is parallel to the direction of propagation. V_P is defined mathematically as

$$V_P = \left(\frac{\lambda + 2G}{\bar{\rho}}\right)^{1/2}$$

where

V_P = compression wave velocity, LT^{-1}

λ = Lamés constant, FL^{-2}

G = shear modulus, FL^{-2}

$\bar{\rho}$ = mass density or soil wet density divided by gravitational constant, g, $FL^{-4}T^2$

d. Cone penetration resistance (CPR): The force, in kilopascals, required to make a 30-deg right circular cone

of 3.23 cm^2 base (or projected area) penetrate a soil mass. The CPR is commonly accepted as a dimensionless index of the shear resistance of the soil. The CPR of the surface soil and the average CPR of the 0- to 45-cm layer are used in this report.

e. Drag coefficient (C_D): The coefficient representing the geometry of the frontal face of the projectile and the frictional forces acting on the projectile during a penetration event, dimensionless.

f. Moisture (or water) content (W): The ratio of the weight of water (W_w) in a sample of soil to the dry weight of solids (W_s) in the sample, expressed as a percentage. It can be written

$$W = \frac{W_w}{W_s}$$

g. Peak particle velocity (PPV): The maximum positive amplitude of the time rate of change of a particle of the medium with respect to a specified reference frame. The particle velocity was measured in the time domain by the geophones used in this study.

h. Peak summed particle velocity (PSPV): The peak or maximum value of SPV.

i. Rayleigh wave velocity (V_R): The speed of a Rayleigh wave (particle motion is elliptically retrograde and parallel to the direction of propagation) along the free surface of a medium; depends on Poisson's ratio (ν) of the medium. For values of Poisson's ratio $0 < \nu < 0.5$, the Rayleigh wave velocity has the range $0.875V_S < V_R < 0.955V_S$, where V_S = shear wave velocity, LT^{-1}.

j. Root mean square (rms) velocity: The velocity corresponding to the square root of the sum of the squares of the individual velocities (i.e. the particle velocity at each frequency component) within the seismic wave.

k. Shear wave velocity (V_S): The speed of a shear wave (particle motion of the medium is perpendicular to the direction of propagation) through a medium. Mathematically, $V_S = (G/\bar{\rho})^{1/2}$

l. Span: Absolute difference between the maximum positive and maximum negative amplitudes (or velocities) within the seismic wave.

m. Sum-frequency (f): The frequency at which the maximum value of PSPV occurs on the SPV-versus-frequency relations.

n. Summed particle velocity (SPV): The particle velocity summed in the frequency domain over a 7-Hz bandwidth. The summation is accomplished by performing a Fourier transform to the analog particle velocity recording (time domain) and converting it to the frequency domain.

o. Thickness of refraction soil layers (T_1 and T_2): The thickness of layer 1 (T_1) is the vertical depth to the interface between the surface and the next deeper layer as distinguished by their differing compression (primary) wave velocities. The thickness of layer 2 (T_2) is the vertical depth from the bottom of the first layer, as determined above, to the surface of the next layer. The compression wave velocities of these two layers are determined by techniques of refraction seismology. The above-defined layers often, but do not necessarily, correspond to soil layers as defined in soil mechanics studies. Mathematically, the thickness of layer 1 is

$$T_1 = \frac{X_1}{2}\sqrt{\frac{V_{P2} - V_{P1}}{V_{P2} + V_{P1}}}$$

where

T_1 = thickness of first refraction layer, m

X_1 = distance from the seismic source to point at which first change in compression wave velocity occurs, m

V_{P1} = compression wave velocity in first layer, m/sec

V_{P2} = compression wave velocity in second layer, m/sec

The thickness of layer 2 is determined by:

$$T_2 = \frac{X_2}{2}\sqrt{\frac{V_{P3} - V_{P2}}{V_{P3} + V_{P2}}} - \frac{T_1}{6}$$

where

T_2 = thickness of the second layer, m

X_2 = distance from the seismic source to the point at which second change in compression wave velocity occurs, m

V_{P3} = compression wave velocity in third layer, m/sec

It should be noted that a subsurface layer will not be detected if the substrate material is an infinite, homogeneous, isotropic, elastic medium.

p. Ultimate shear strength (σ_u): The maximum or ultimate shear stress of the substrate material. Mathematically,

$$\sigma_u = \frac{\left(\sigma_a - \sigma_r\right)_{max}}{\sqrt{3}}, \frac{kg}{cm^2}$$

where

σ_a = axial stress, kg/cm^2

σ_r = radial stress (also confining pressure), kg/cm^2

q. Wet density (ρ): Wet unit weight; the total weight (W_T) of the wet soil (solids plus moisture) from a soil sample per unit of total soil volume (V_T) of the sample (volume of solids plus voids). Symbolically this is

$$\rho = \frac{W_T}{V_T}, \frac{g}{cm^3}$$

r. Young's modulus of elasticity (E): Young's modulus is

the stress-strain ratio in simple tension or compression. Mathematically

$$E = \frac{d(\sigma_a - \sigma_r)}{d\varepsilon_a}$$

where

d = differential

σ_a = axial stress, kg/cm^2

σ_r = radial stress (also confining pressure), kg/cm^2

ε_a = axial strain, percent

PART II: SENSOR TEST AREAS, TEST PROCEDURES, AND ENVIRONMENTAL CHARACTERIZATION

44. This part of the report discusses the selection of the SID test areas, their terrain characteristics and the procedures used in collecting environmental data and in conducting seismic response tests (i.e. man-walking, drop-hammer, vehicle, and ambient or induced noise), hand-emplaced miniaturized SID (MINISID) performance tests, and ADSID/S air-implantation tests.

45. The field program consisted of (a) field reconnaissance and site selection, (b) environmental data collection to provide input to the sensor detection and implantation performance models, (c) seismic response tests to establish the seismic response characteristics of the various test sites at Fort Huachuca, and (d) data collection for verification of the sensor detection and implantation performance models.

46. The data collected for the environmental characterization are listed below.

a. Input requirements for detection performance model:
   (1) Transfer of energy from source to substrate:
      (a) Surface soil moisture content, percent
      (b) Surface soil wet density, g/cm^3
      (c) Surface soil type (Unified Soil Classification System, USCS)
      (d) Surface soil strength (CPR), kPa
      (e) Surface vegetation ground cover height, cm; and density of ground cover
   (2) Propagation of seismic waves:
      (a) Thickness of refraction layer, cm (each layer)
      (b) Compression wave velocity m/sec (each layer)
      (c) Shear wave velocity, m/sec (each layer)
      (d) Soil wet density, g/cm^3 (each layer)
      (e) Surface terrain profiles, xyz coordinates

b. Input requirements for sensor implantation performance model:

(1) Initial Young's modulus of elasticity (E), kg/cm^2

(2) Ultimate shear strength (σ_u), kg/cm^2

(3) Compressibility parameter (ρ_p/ρ), dimensionless

(4) Soil wet density (ρ), g/cm^3

(5) Coefficient of friction between the projectile and the soil (μ), dimensionless

(6) Drag coefficient (C_D), dimensionless

Note: These data are determined from laboratory tests on bulk samples obtained in the field.

c. Background meteorological data:

(1) Air temperature, deg Celsius

(2) Wind speed, m/sec

(3) Wind direction, deg

(4) Precipitation (rainfall, snowfall), cm

47. The tests conducted for seismic responses are listed below.

a. Basic tests for model development:

(1) Man walking

(2) Drop hammer, or controlled source

(3) Vehicle

(4) Ambient or induced noise

b. Tests to verify prediction models:

(1) Sensor detection performance (MINISID tests)

(2) Sensor implantation performance (ADSID/S tests)

Location and Climate of Fort Huachuca Reservation

48. The Fort Huachuca Reservation is in Cochise County, Arizona, about 76 km north of the Mexican border. The reservation is on the northeast flank of the Huachuca Mountains and on the southern part of the San Pedro River drainage basin. The climate is mild and sunny and the annual precipitation is about 36 cm (15-yr record, 1956-1970) of which approximately 1.6 cm is the water equivalent of 16 cm of snow. The precipitation distributed by months is as follows. (For a detailed summary of the meteorological data at Fort Huachuca, see reference 2.)

Month	Precipitation cm	Month	Precipitation cm
January	1.52 (0.17)*	July	11.30
February	1.45 (0.48)	August	9.22
March	1.45 (0.41)	September	4.14
April	0.48 (0.07)	October	1.70 (0.02)
May	0.18	November	1.24 (0.20)
June	1.02	December	2.62 (0.31)
		Total	36.32 (1.6)

* Numbers in parentheses indicate snow.

49. The mean daily maximum temperature varies between 15 and 19 C (Celsius) during the winter months (November-March) and between 23 and 32 C during the summer months (April-October); whereas the mean daily minimum temperature varies between 1 and 8 C during the winter months and between 11 and 19 C during the summer months. The prevailing winds during the months of September-May are in a southwesterly direction (225 deg) and during the months of June-August are in a westerly direction (270-285 deg). The mean wind speed during all months is approximately 3 to 4 m/sec, although peak wind gusts with speeds up to approximately 19 to 26 m/sec occur during all times of the year.

50. The field program was conducted at the following selected areas on the East Range of the Fort Huachuca Reservation and at the Willcox Playa near Willcox, Arizona:

a. A hand-emplacement area (trapezoidal-shaped with an area of approximately 3 sq km).

b. Six airdrop (i.e. air-implantation) areas (rectangular-shaped, each 100 m wide and 1200 m long). Five areas were located on the Fort Huachuca East Range and one at Willcox Playa.

c. Special airdrop area used by CSEWS for testing ADSID/S.

Test Areas

51. All test areas were in Fort Huachuca's East Range (fig. 4), except airdrop area 6, which was in a flat lake bed (Willcox Playa), near Willcox, Arizona (fig. 5). The East Range covers approximately 117 sq km and lies, in general, on an alluvial apron along the northeast flank of the Huachuca Mountains. Near the eastern boundary of the range, the alluvial apron merges into the floodplain of the San Pedro River. The East Range is drained by intermittent streams (arroyos), which flow either northerly to the Babocomari River or easterly to the San Pedro River. Most of the arroyos are well incised, contain steep, near-vertical banks, and vary in width from 1 to 2 m to as much as 200 m.

52. The general terrain is relatively flat, except for the northeast corner, which is flanked by hills some of which reach heights of 100 m above the surrounding terrain. The predominantly flat areas vary between el 1230 and 1360.* The soils are predominantly fine-to-coarse sands (classified SC by the USCS) with a small mixture of silt and/or clay. Gravels, cobbles, and boulders up to 30 cm in diameter are also quite prevalent within the substrate and usually occur within 25 cm of the surface. The upper banks of the arroyos normally contain gravels and large stones embedded in the fine-to-coarse sands. Most of the soils on the East Range are strongly calcareous, and hardpans of nodular caliche are present. Caliche deposits were also noted in a few scattered areas, but were normally found at depths greater than 1 m below the surface. The caliche, in most cases, seems to develop as a thin, layered, local deposit.

53. Vegetation at the East Range includes desert grass, mesquite, creosote bush, acacia, and an unidentified bush (probably burro bush). Stands of yucca and a few cacti were also present, mostly on the slopes of the arroyos, but were not very abundant (i.e. they were widely

---

* All elevations (el) cited herein are in meters referred to mean sea level.

Fig. 4. Aerial mosaic showing location of hand-emplacement and airdrop test areas on the East Range, Fort Huachuca, Arizona. (For a larger print of this figure, see map 1 in pocket inside back cover.)

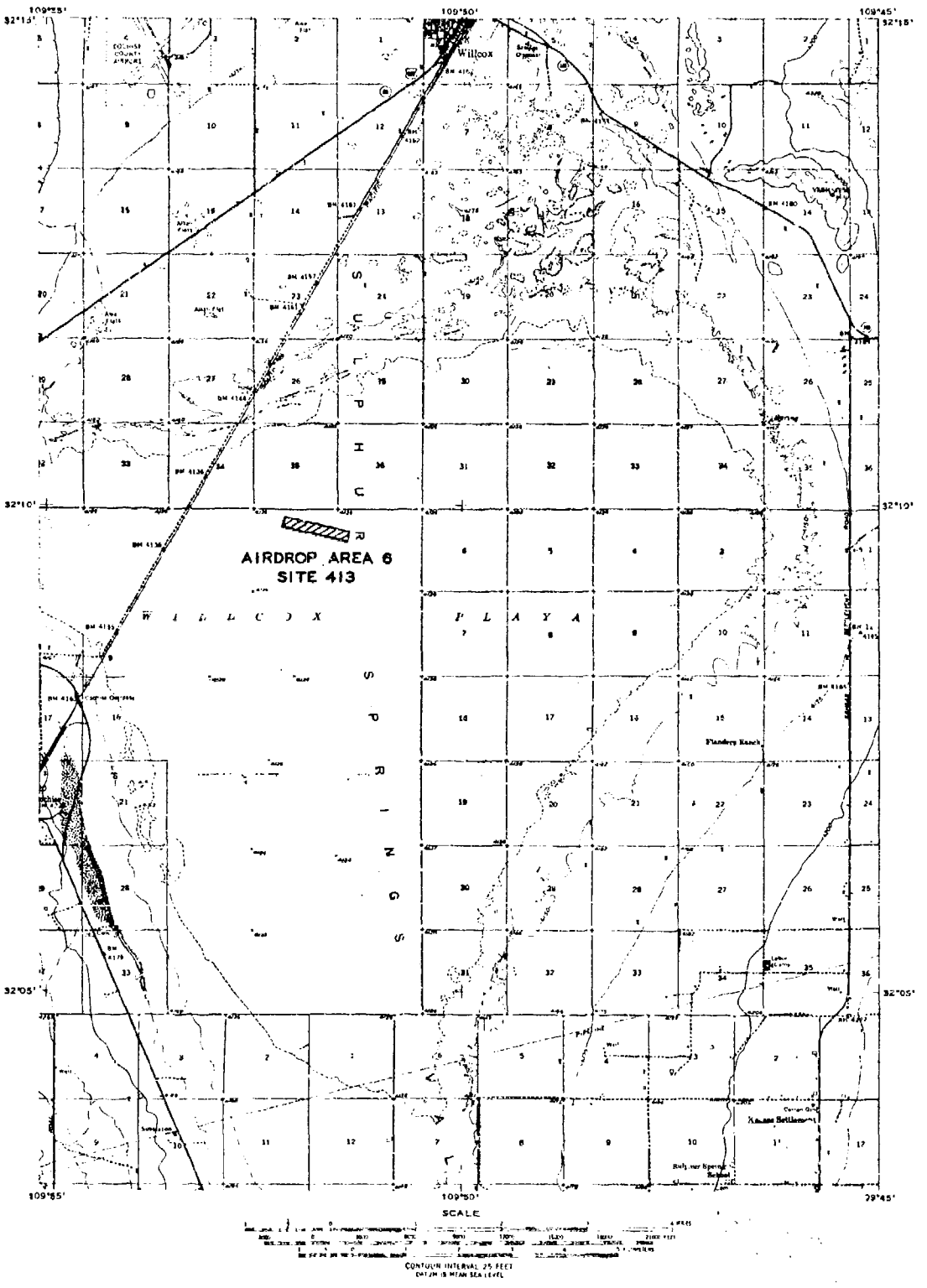

Fig. 5. Location of airdrop test area 6 in Willcox Playa

spaced). The vegetation in general was most dense in the bottoms and along the upper banks of the arroyos.

Hand-emplacement test area

54. The trapezoidal-shaped area selected for conducting tests with hand-emplaced SID's was in the south-southwest part of the East Range (see fig. 4). The north boundary was 2880 m long, the east boundary 2040 m, the south boundary 2970 m, and the west boundary 1680 m. The geographical coordinates of the four corners of the area are as follows:

NE corner:	lat. 31°36'52" N long. 110°15'50" W
SE corner:	lat. 31°35'53" N long. 110°14'59" W
NW corner:	lat. 31°35'43" N long. 110°17'17" W
SW corner:	lat. 31°34'55" N long. 110°16'38" W

55. This area was selected as being representative of most of the physiographic, geologic, vegetation, and soils conditions found on the East Range; it contained numerous homogeneous, relatively flat areas suitable for man-walking tests. Also, its network of unimproved roads and trails provided sites for vehicle tests, and it was sufficiently removed from the high-activity (i.e. noise) areas. The east-west orientation of its long axis (see fig. 4) afforded the use of the area for testing with minimum dissection by drainage channels (arroyos).

Airdrop test areas

56. The airdrop areas were selected to provide a variety of soils materials ranging in penetration difficulty from relatively easy to extremely difficult. The areas were tentatively selected on the basis of available published data, topographic and geologic maps, and by a stereoscopic examination of the air photos, whereby photo patterns were isolated on the basis of their tone, texture, and geometry. The final selection of the airdrop areas was made after a detailed ground reconnaissance of the East Range. The airdrop area at Willcox Playa (see fig. 5) was near the center of the large playa and was selected to

provide an easily penetrable, deep, near-homogeneous material for testing air-implanted SID's.

57. Airdrop areas 1-6 were rectangular in shape (each 100 m by 1200 m) and were positioned at the following geographical locations (coordinates are in reference to the SE corner of each area).

a. Airdrop area 1: lat. 31°38'13" N
long. 110°16'40" W

b. Airdrop area 2: lat. 31°39'57" N
long. 110°14'12" W

c. Airdrop area 3: lat. 31°36'36" N
long. 110°18'15" W

d. Airdrop area 4: lat. 31°37'57" N
long. 110°14'10" W

e. Airdrop area 5: lat. 31°38'19" N
long. 110°12'31" W

f. Airdrop area 6: lat. 32°09'47" N
long. 110°51'06" W

58. A special airdrop area selected by CSEWS for conducting drop tests with an ADSID/S had approximately the same dimensions as the other airdrop areas. It was located at lat. 31°35'27" N and long. 110°13'36" W. The terrain description of the special airdrop area and the results of the experimental tests with the ADSIS/S are included herein for comparison with the other airdrop areas and for evaluating the theoretical depth-of-penetration predictions presented herein.

59. Terrain conditions of the various areas are discussed below:

a. Airdrop area 1, positioned at el 4270 on the east side of and parallel to an unimproved airstrip, had a general slope of approximately 3 deg from south to north and very few irregularities along the ground surface. The substrate material varied from a loose sandy silt (classified SC by the USCS) to a reddish-brown clayey sand (SC), except for the northernmost end (last 20 m). Here the substrate materials consisted of a coarse sand with caliche nodules and considerable amounts of gravel, cobbles, and rocks up to 10 to 15 cm in diameter.

b. Airdrop area 2 was situated at el 4350 on the west slope

of an igneous hill near the northeast corner of the East Range (see fig. 4). This area was selected because it represented the upper range of soil strengths that might be encountered on the East Range. The ground surface along the area was very irregular and consisted of a coarse gravelly sand with some cobbles and boulders up to 50 cm in diameter. Patches of bedrock were exposed within the area.

c. Airdrop area 3 was a rather large arroyo whose top width was approximately 200 m and bottom width was approximately 150 m. The ground surface along the bed of the arroyo was relatively flat and was composed of a fine-to-coarse sand with some mixture of silt and clay (SC to SM by USCS). A small, but deeply entrenched, wash channel (2 m wide and 5-7 m deep) was also in the main bed of the arroyo. This wash channel contained an assortment of sand, gravel, pebbles, and a few small boulders. The bed of the arroyo also contained a very dense stand of reeds (a species of grass) 1 to 2 m in height.

d. Airdrop area 4 was on an alluvial plain of the San Pedro River at el 4150 (fig. 4). The ground surface along the center-line length was relatively flat (less than 2-deg slope), but along the southwest-northwest boundary it was very irregular as a result of numerous small, well-defined wash channels. The substrate material consisted of a loose, gray, sandy silt with pebbles in the surface layer (0-10 cm) and a firm, light-brown, sandy clay with various amounts of friable caliche down to a depth of 1 m. A layer of caliche approximately 30 cm thick was encountered at a depth of approximately 1 m near the southwest corner of the area. The dominant vegetation consisted of creosote bush approximately 1.5 m in height, with a few very widely spaced mesquite trees 2-3 m in height.

e. Airdrop area 5 was also in an alluvial plain of the

San Pedro River at el 4100-4150 (fig. 4). The topography was slightly undulating as a result of small well-defined wash channels that drain the area in the east-northeast direction. The substrate materials in general consisted of a sandy silt (SC) in the surface layer (0-10 cm) and a very hard, compact, sandy silt with inclusions of pebbles and caliche in the subsurface layer (10-120 cm). A layer of white caliche was also detected at a depth of approximately 100 cm in the southeast part of the area. Vegetation covering the area was composed of a relatively dense mixture of creosote bush (height 1-1.5 m) and acacia (height 1-1.5 m).

f. Airdrop area 6 was in a rather large lake bed (Willcox Playa) (see fig. 5). The topography was extremely flat and very smooth. The substrate material in the 0- to 20-cm layer was a compact, brown, silty clay (CL), and in the 20- to 150-m layer it was a homogeneous, blue-green to black clay (CH). The playa contained no vegetation and is inundated during certain periods of the year (July-September).

g. Special CSEWS airdrop area was on an unimproved airstrip located approximately 2 km west of the hand-emplacement area (see fig. 4) at el 4300. The substrate material varied from sandy silt to clayey sand (SC) with small amounts of gravel and small pebbles. The ground surface was relatively smooth and contained a small grass cover along the outer edges of the airstrip.

Seismic Response Tests

Test site selection

60. Within each sensor test area, one or more sites were selected for conducting seismic response tests and collecting environmental data. In the hand-emplacement area, 10 sites (sites 335-342, 348, and 349) were selected for conducting man-walking and drop-hammer seismic

response tests, and two sites (cross-country sites 344 and 345) were selected for conducting vehicle seismic response tests. The locations of all sites are shown on the aerial mosaic in fig. 6. Within each airdrop test area, except for the special CSEWS area, one site was selected for conducting man-walking and drop-hammer seismic response tests. All man-walking and drop-hammer test sites were, in most cases, in areas portraying the least ground surface irregularity within the general area.

Test site layout

61. Sites were prepared in a specified manner for the tests (drop-hammer, man-walking, and moving-vehicle tests). For the drop-hammer and man-walking tests, a reference line 110 m long was established by placing wood stakes at 5-m intervals. For the two vehicle cross-country test sites, a reference line 1100 m long was established by placing wood stakes at 50-m intervals. Typical site layouts are shown in fig. 7.

Test procedures

62. The seismic responses, or analog signatures, resulting from a walking man and a controlled source (drop-hammer) were measured at each test site. Also, the ambient background noise and any induced noises that occurred during testing were recorded. Special vehicle tests were also conducted in the hand-emplacement area with two military vehicles (M151 Jeep and M577 Armored Command Post). The following paragraphs discuss the instrumentation used and the procedures for each type of test.

63. Instrumentation. The analog signatures resulting from a walking man, a hammer drop, or a moving vehicle were measured with the following scientific geophones: a Mark Products Model L-4-3D (three-dimensional geophone) positioned at sta 0 (see fig. 7) and a Mark Products L-4-1D (one-dimensional, or vertical, geophone) positioned at sta -5 for the man-walking and drop-hammer tests, and an L-4-3D geophone positioned at sta 0 for the vehicle tests. The natural frequency of the geophones was 1 Hz. The L-4-3D geophone was emplaced by excavating a hole approximately 30 cm in diameter and 22 cm deep and orienting the three internal geophones as follows: The vertical geophone was normal to the ground surface, the radial geophone was parallel to the reference line, and the transverse geophone was perpendicular to the line. The

Fig. 6. Location of test sites, hand-emplacement test area

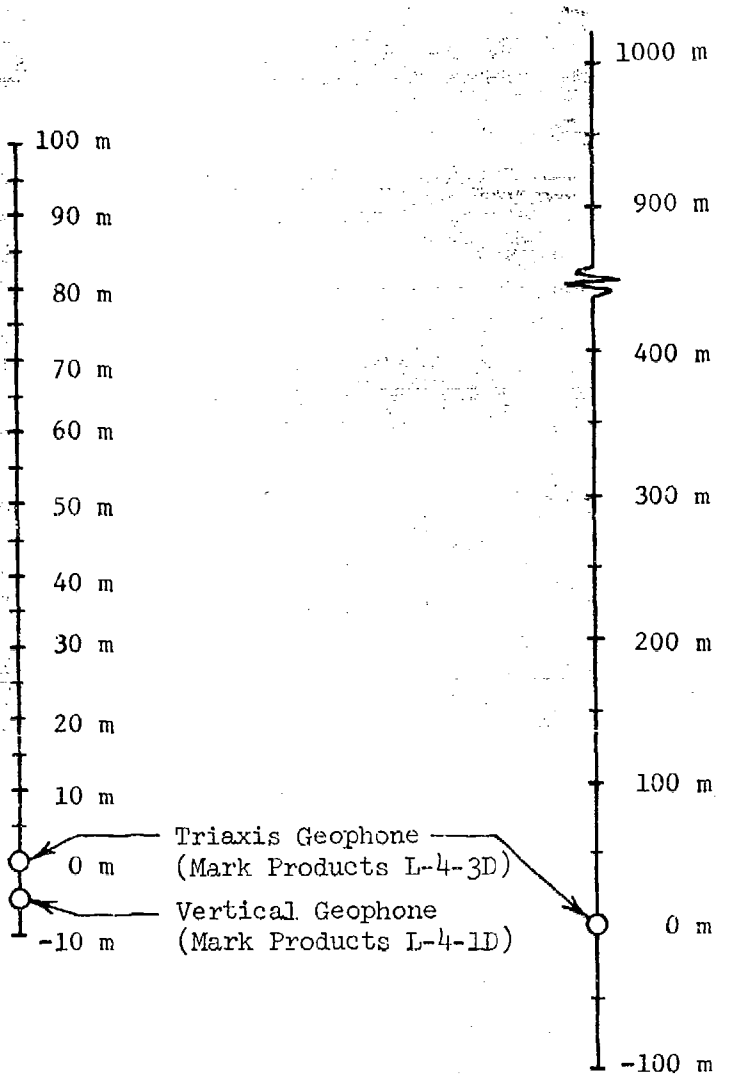

a. Drop-hammer and man-walking site layout (distance markers at 5-m intervals)

b. Vehicle site layout (distance markers at 50-m intervals)

Fig. 7. Site layouts for seismic response tests

material removed from the hole was then tightly packed around and also spread over the top of the geophone. The same emplacement procedure was used for the L-4-1D geophone at sta -5, except that a hole approximately 20 cm in diameter was excavated. Fig. 8 shows two geophones in place.

64. Seismic analog signatures were recorded on analog FM magnetic tape and on a direct-print oscillograph (fig. 9), which were housed in

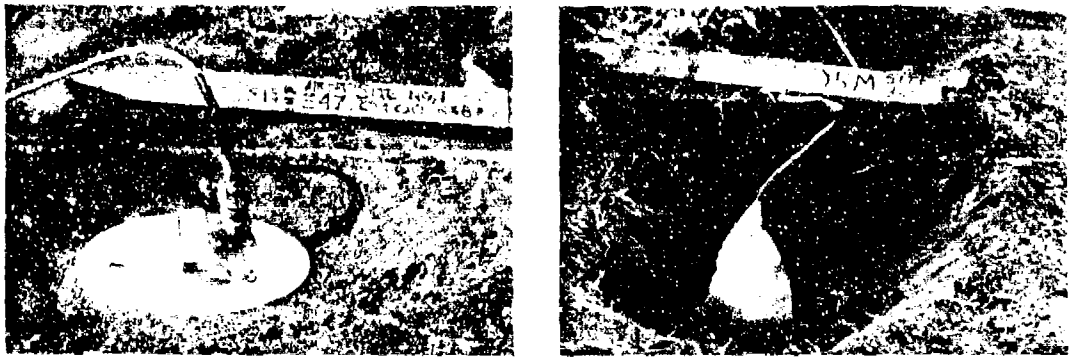

a. Three-dimensional (L-4-3D) geophone in place

b. Vertical (L-4-1D) geophone in place

Fig. 8. Emplacement of geophones

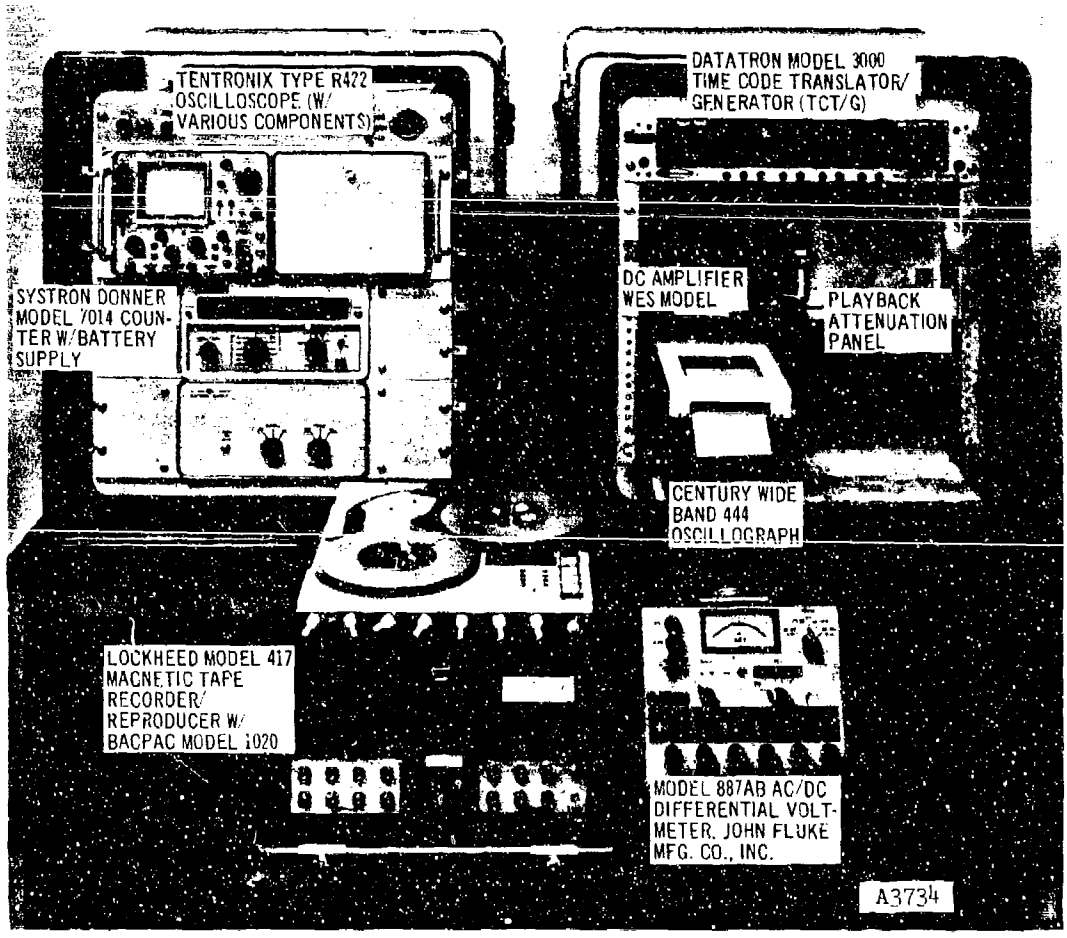

Fig. 9. Battery-powered instrumentation used to obtain seismic response data

a mobile, self-contained vehicle that was normally positioned approximately 50-75 m from the site (or walk line). A wide-band-frequency (2-300 Hz) battery-powered recording system was used to obtain continuous high-quality data and an adequate dynamic range. All instruments used in the seismic tests were calibrated in accordance with the National Bureau of Standards procedures, and no filtering of any type was used. Seven channels were used to record the following:

a. Four particle velocity measurements (one three-dimensional geophone array at sta 0 and one vertical geophone at sta -5).

b. One time code.

c. One voice comment or remote acoustic data (microphone).

d. One location of energy source (position indicator).

65. Man-walking tests. In a man-walking test, a man walked at a constant rate along the prescribed 110-m path, starting from sta +100. During the test, radio communication was maintained between the man and the recorder for positioning each footstep (i.e. each foot encounter with the ground) along the line. Prior to the actual test, a practice walk was made to establish a step of uniform length and rate.

66. Drop-hammer tests. A special drop-hammer apparatus (fig. 10), designed by U. S. Army Engineer Waterways Experiment Station (WES) was a controlled energy source whose seismic response could be compared in amplitude and frequency with that resulting from an average footstep. A sample analog signature from the drop hammer is compared with that from a footstep in fig. 11. The hammer, which consists of a 9.9-kg annular weight with a Teflon sleeve, is connected by a metal guidepost to the footing, which is a plywood base topped by two layers of 0.2-cm-thick hard rubber and two layers of 1.9-cm-thick soft foam rubber. In a drop-hammer test the hammer was dropped two times at each 5-m station along the reference line starting at sta 0 and continuing out to the distance at which the seismic signal could not be detected over the system and ambient noise level. Before the hammer was placed on the soil at each 5-m station, surface litter was removed, and the hammer was positioned so that it would drop vertically and have uniform contact with the ground.

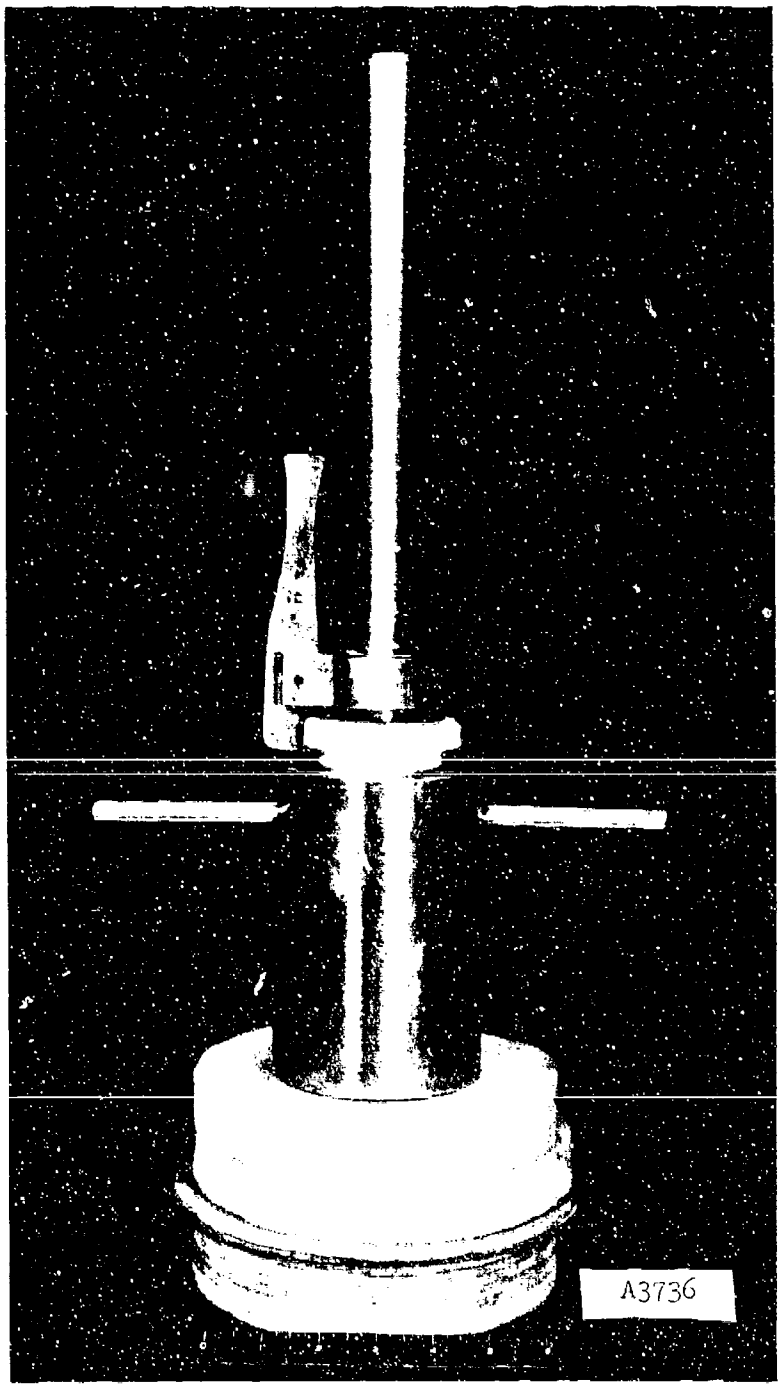

Fig. 10. Drop-hammer apparatus

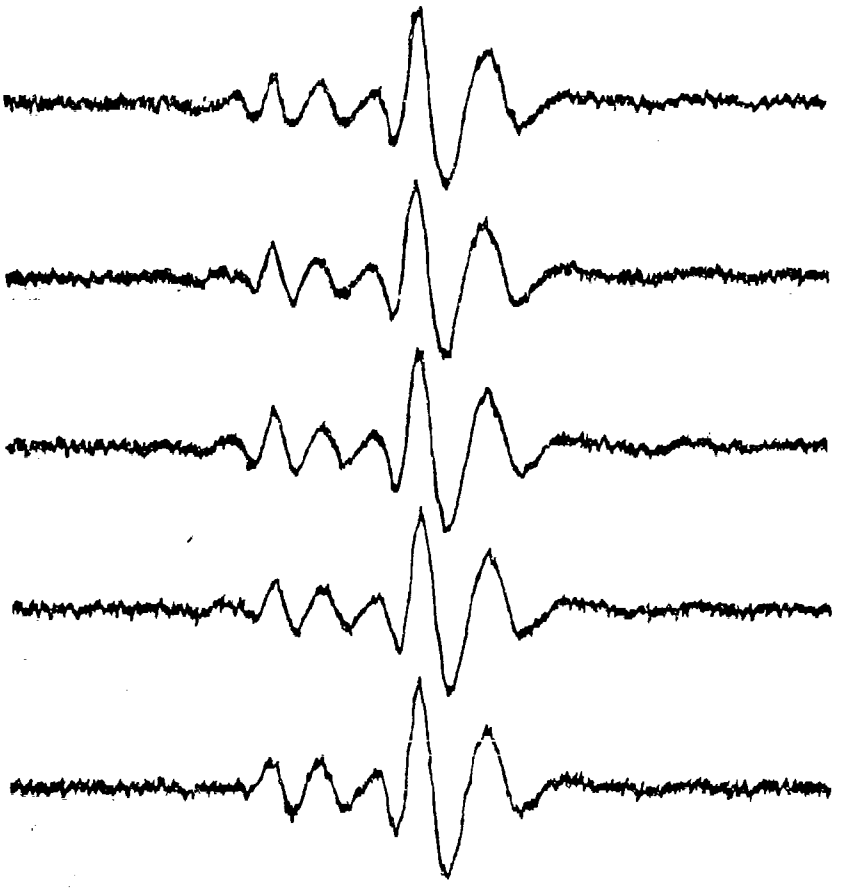

a. DROP-HAMMER SIGNATURES FOR FIVE DROPS

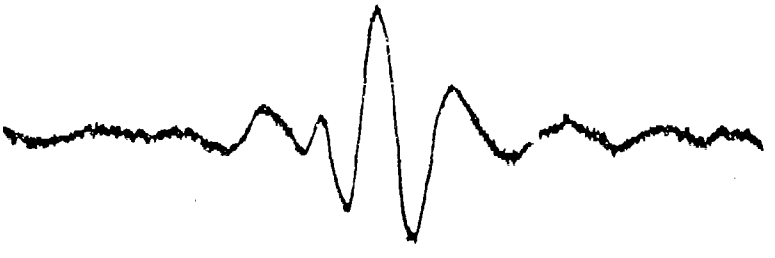

b. FOOTSTEP SIGNATURE

NOTE: THESE RECORDS WERE OBTAINED FROM THE VERTICAL GEOPHONE FOR THE 10-METER DISTANCE.

SCALE, TIME

0 10 20 MSEC

Fig. 11. Comparison of drop-hammer and footstep signatures

67. Vehicle tests. Vehicle tests were conducted in the hand-emplacement area with two vehicles (M151 and M577) in the same manner as the man-walking tests. A vehicle was positioned at some arbitrary distance beyond sta +1000 so that it could attain a preselected speed upon reaching sta +1000. Speeds of 8 and 32 km/hr were used, and two tests were conducted at each speed.

MINISID and ADSID/S Tests

MINISID tests

68. Man-walking tests were also conducted with four Phase III MINISID's at each of the seismic test sites to yield data for aiding in the evaluation of the techniques for predicting SID performance. (For a discussion of MINISID operating principles see Appendix A.) The MINISID test procedures are discussed below.

69. A small trench approximately 5 cm wide, 10 cm long, and 5 cm deep was excavated at sta 0 (fig. 7) for emplacement of the four MINISID geophones. Each geophone was placed in the trench by hand and forced down until its spike was completely below the bottom of the small trench. After the geophone was in place and as nearly vertical as possible (the MINISID geophone senses the vertical component of the seismic wave), slight pressure was applied to the side of the geophone to ensure that it did not move and was in firm contact with the soil. Emplacement of the four MINISID's is shown in fig. 12. Once the geophones were

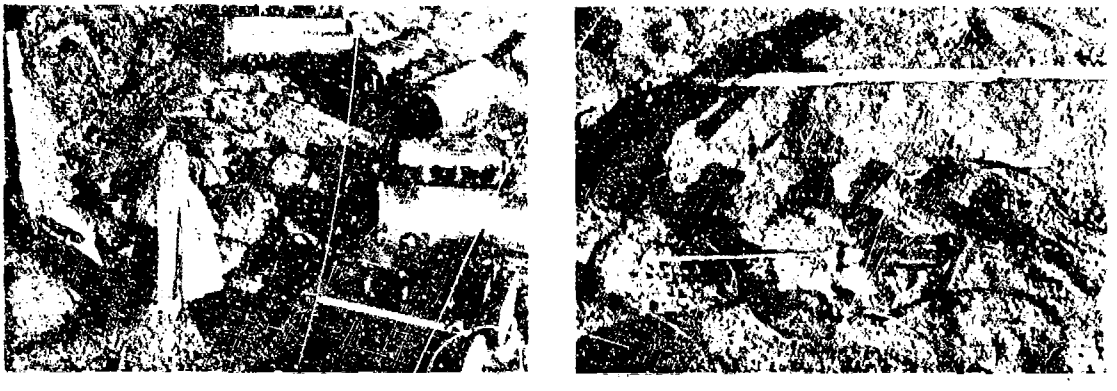

a. Geophones and detectors b. Geophone in trench

Fig. 12. Emplacement of MINISID geophones

emplaced, the material removed from the trench was tightly packed around and loosely spread over the top of each of the geophones.

70. The triggering of the MINISID's was monitored by using a portatale that was positioned in the instrumentation van located approximately 50-75 m from the walk line. The four MINISID's were set on the following gains.

a. MINISID A: Low gain.

b. MINISID's B and C: Medium gain.

c. MINISID D: High gain.

71. Individual walks were made for each of the four MINISID's. For the first test (i.e., MINISID A, which was set on low gain) a man walked from sta +100 down the 110-m line until an activation was indicated on the portatale. At the point of activation the man was signaled, by radio, to stop the walk and to determine his position (i.e. distance) with reference to the MINISID. This distance was recorded as the detection distance of the MINISID. The man then walked back to sta +100, or at least 15 m back from the detection distance, paused for approximately 30-45 sec, and then started walking down the line again. Walk tests were conducted until the MINISID's had triggered several times for each gain setting, respectively.

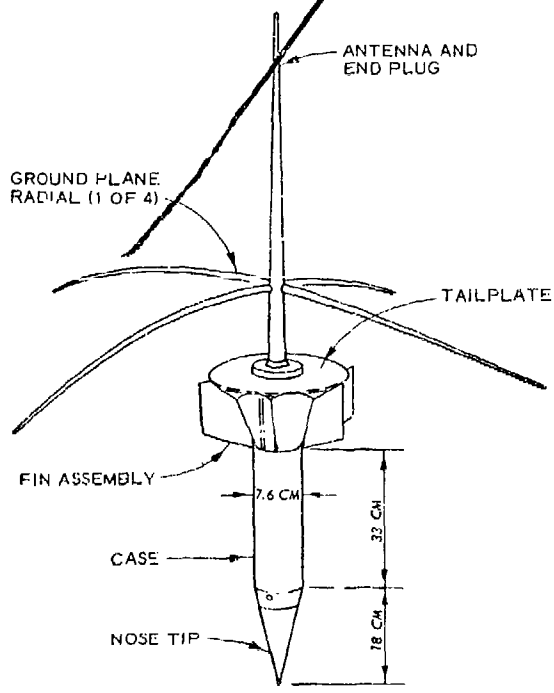

Fig. 13. ADSID/S sensor

ADSID/S tests

72. Airdrop tests were conducted by personnel of CSEWS at Fort Huachuca during August 1972 with a dummy (i.e. not instrumented) Phase III ADSID/S, MA-37, at the special airdrop area (unimproved airstrip) described above. Fig. 13 is a drawing of the ADSID/S. The results of these experimental tests have been

included herein to aid in the evaluation of the techniques for predicting the penetration performance (i.e. depths of penetration) of the ADSID/S's. These tests are discussed below.

73. There were 120 ADSID/S's delivered from a fixed-wing aircraft by dropping three sensors on each of several passes over a marked target area. The drop interval for the three sensors was regulated by an intervalometer mechanism and normally resulted in a ground impact spacing of 100-150 m. After each completed aircraft flyby, a CSEWS field team assisted by one man from WES visited the impact area to determine each sensor's depth of penetration (i.e. penetration depth measured along the longitudinal axis of the impact trajectory), angle of impact with respect to the vertical, and data on the terrain conditions (i.e. moisture content, density, cone penetration resistance). In addition, the AEPG provided a team to take high-speed photographs for the determination of the near-surface impact velocities for 11 of the sensor tests (tests 5, 9, 11, 12, 34, 36, 75, 76, and 78-80).

Ambient- and Induced-Noise Tests

74. The seismic motion resulting from both the ambient or natural noise and any induced noises created by aircraft (fixed- and rotary-wing), vehicles traveling along roads near the areas, wind gusts, rain, etc., were recorded at each test site. Approximately 60 sec of data were recorded at each site as follows: The ambient seismic motion was measured at a time when members of the test team were quiet and motionless and normally before the start of a drop-hammer test; in the case of induced noises, the seismic motions were measured as they occurred during testing.

Environmental Characterization

75. To obtain information that allows the SID test results to be evaluated within a rigorous theoretical framework, specific environmental data are required. For convenience, the environmental data

collected can be considered in support of: (a) the seismic response tests and/or the prediction of sensor detection performance, and (b) sensor implantation performance. The data requirements for each category are listed in paragraphs 46a and b.

76. In general, the terrain factors required (except soil type, Atterberg limits, and soil particle sizes) are sensitive in varying degrees to changes in moisture content and temperature. For this reason the field data collection program was conducted under conditions assumed to be representative of wet- and dry-season conditions. It was recognized that the probability of sampling the extreme ranges of moisture content during only one sample period each within the dry and wet seasons was very remote. Therefore, it was decided that meteorological data from which soil moisture content can be derived should be collected at specific locations for at least a complete yearly cycle. The meteorological data collected are compatible with the WES computer model[3] for predicting soil moisture in the 0- to 15- and 15- to 30-cm layers and include:

a. Air temperature, deg C.

b. Wind speed, m/sec.

c. Wind direction, deg.

d. Precipitation (rainfall, snowfall), cm.

77. The meteorological data were measured by AEPG personnel at three locations within the East Range (see fig. 4), and were recorded continuously during the period July 1971 to the time of this study. The data were recorded on paper strip charts and, therefore, must be manually extracted and put in a computer-compatible format before soil moisture data can be obtained. This work is not within the scope of this study; however, data were extracted from the records and tabulated for the times of the seismic response tests for each of the sites and are included in table 1.

78. As stated above, the meteorological data were obtained to provide a means for estimating the range of soil moisture contents at the East Range SID test sites. A secondary, but important, use of the meteorological data is the interpretation of causes for high ambient

seismic noise caused by meteorological phenomena. For example, as stated in paragraphs 4 and 74, wind blowing against vegetation can cause considerable seismic noise, and for this reason, a cursory description of vegetation was made in the field program. The vegetation factors for which data have been obtained include:

a. Tree type (species).

b. Stem base diameter(s), cm; and number of stem components per plant assemblage.

c. Tree height, cm.

d. Average tree spacing, cm.

e. Tree crown characteristics (diameter and depth), cm.

f. Depth, cm; and density of ground cover.

Data collection procedures (sensor detection performance requirements)

79. Soil moisture-density and USCS classification. In support of seismic response testing, soil samples for describing the substrate were obtained by digging a pit to a depth of 1 m near sta +5 at sites 335-342, 347-349, and 410-413. Also, for three sites (sites 336, 338, and 340) a hole approximately 10 cm in diameter was hand-augered to a depth of 3 m. Compact soil prevented sampling beyond the 1-m depth at the other sites. Soil samples from which moisture content and wet density were determined were obtained at the surface and at depths of 50 and 100 cm in the test pit, and in the hand-augered holes, at additional depths of 150, 200, and 300 cm, respectively. Bulk samples were taken at various depths (as specified by the field geologist) to obtain USCS classification for each identifiable soil layer. Soil moisture content, density, and classification data for the wet and dry seasons for the surface layer and layers 1 and 2 of the various sites (335-342, 347-349, and 410-413) are listed in table 2. A comparison of the moisture data for the wet and dry seasons is given in table 3. The surface soil plasticity and liquid limit data (Atterberg limits) for the sites within the hand-emplacement test area are compared in fig. 14.

80. CPR measurements. Cone penetrometer readings (a measure of soil strength) were obtained at each site, at six stations (0, +10, +20,

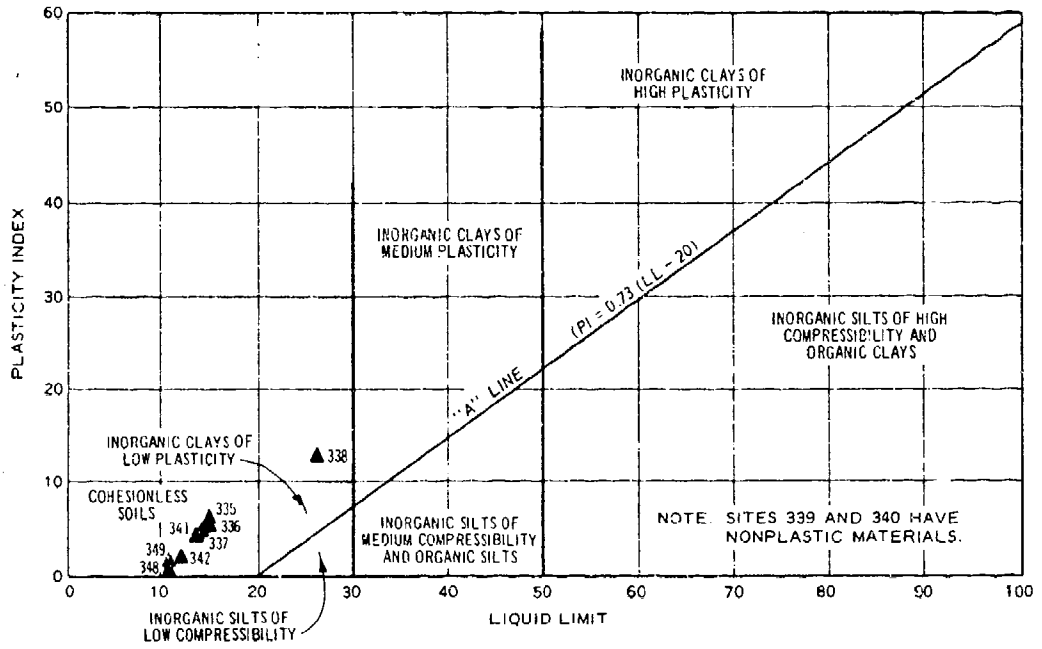

Fig. 14. Surface soil plasticity and liquid limit data for 10 sites within the hand-emplacement test area

+30, +40, and +50) along the line at the surface and at 2.5-cm increments to a depth of 15 cm, and then at 7.5-cm increments to a depth of 45 cm (when possible). The cone penetrometer data for the wet and dry seasons for all sites except the CSEWS airdrop area are given in tables 2 and 4. The CPR data for the CSEWS area for each sensor's location are given in table 5.

81. Compression wave velocity and thickness of layers. To obtain a measure of the compression wave velocity and thickness of the refraction layers, a refraction seismic survey was conducted at the various sites with the WES modified Geo-Space Corporation GT-2B, 12-channel portable seismograph (fig. 15). The refraction survey consisted of emplacing 11 geophones at specified intervals (3 m for the dry season and 5 m for the wet season) between two stations (0 and +30, and 0 and +50) and recording the arrival times of the initial seismic impulse at each respective geophone. The seismic signal was generated by a hammer blow at each end of the refraction line (i.e. sta 0 and +30, or sta 0 and +50). Refraction data (compression wave velocities and thicknesses of

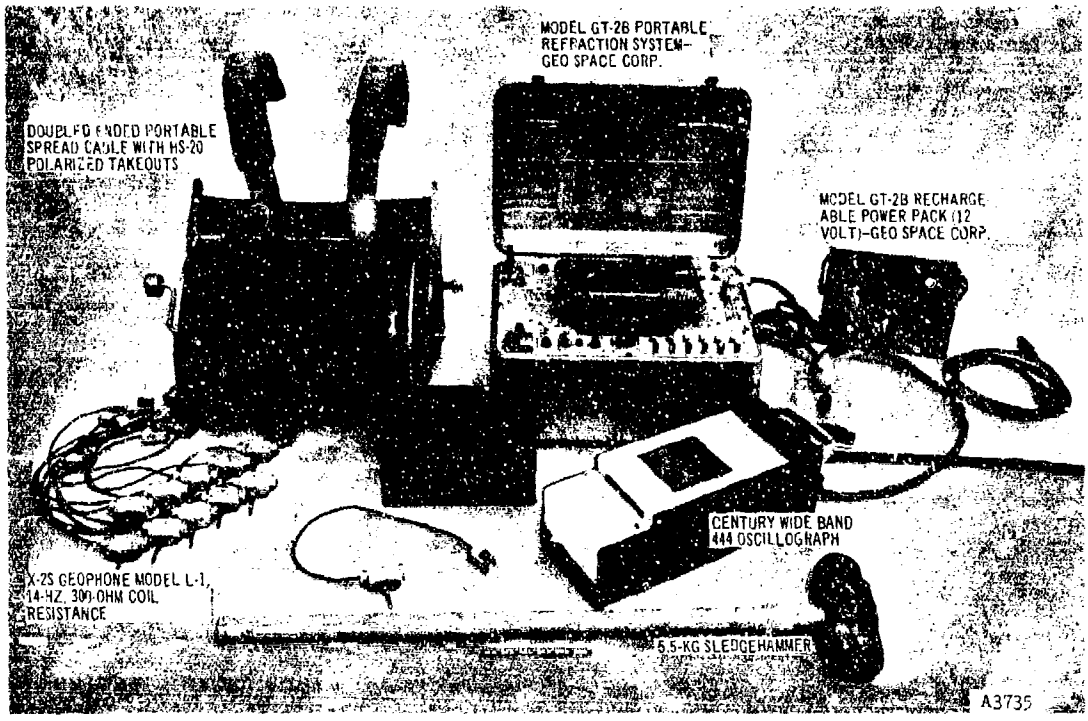

Fig. 15. Instrumentation used in seismic refraction tests

layers) for the wet- and dry-season conditions are summarized for the surface and first and second refraction layers in table 2. The refraction data portrayed in a time-versus-distance format for the sites are included in Appendix B, figs. B12-B39.

82. Shear wave velocity. For this study the surface shear wave velocity was considered equal to the measured surface (Rayleigh) wave velocity (see paragraph 43i). The shear wave velocity was determined by comparing similar distinct wave forms from the time-displacement refraction records of six successive geophones. The shear wave velocity was calculated by dividing the distance (3 m) between successive geophones by the time lag between similar wave shapes. The depth at which this calculated velocity applies was computed as one-half the wavelength of the wave used in determining the shear wave velocity. (The wavelength is the wave period multiplied by the wave velocity.) By using several successive geophones, various depths and their corresponding velocities were determined. From these data the shear wave velocity for various selected depths, such as the first-layer refraction depth (or

thickness), was computed. The shear wave velocity data for the various sites are contained in table 2.

83. Topography. Ground surface configuration data were obtained by surveying a detailed profile along each 110-m drop-hammer and man-walking test site and each 1100-m vehicle test site. Since the drop-hammer and man-walking sites selected were in relatively flat terrain, there were very few terrain surface changes along the 110-m line. In the cross-country vehicle test sites (sites 343 and 344), a few minor elevation changes occurred along the 1100-m lines, but these changes were not abrupt; therefore, the effect on the seismic response would probably be quite small. The surface configuration data for the drop-hammer and man-walking sites and the vehicle sites have not been included in this report.

84. Vegetation. The vegetation surrounding each man-walking and drop-hammer site was described by determining the plant type (species), stem base diameters, heights, spacing, number of stems per plant, and crown characteristics (diameter and depth) of the dominant and codominant plants in the population, and determining the amount of grass or other low-growing plants that occupied the site. Also, the height of ground cover along the 110-m line was measured and recorded. The vegetation data describing the various sites are listed in table 6. General terrain descriptions of the various sites are given in paragraphs 2-13, Appendix B.

Data collection procedures
(sensor-implantation requirements)

85. In support of providing input data for the theoretical equations that predict the depth of penetration of air-delivered SID's, special soil samples were obtained at depths of 30, 90, and 120 cm from two locations within each of airdrop areas 1, 4, and 5, respectively. The locations of the soil pits in each of the three areas are shown in fig. 16. The equations used to predict the depths of penetration are described in Appendix C. The input requirements for the sensor-implantation equations are listed in paragraph 46b.

86. Data on E, σ_u, ρ_p/ρ, μ, and C_D were obtained from

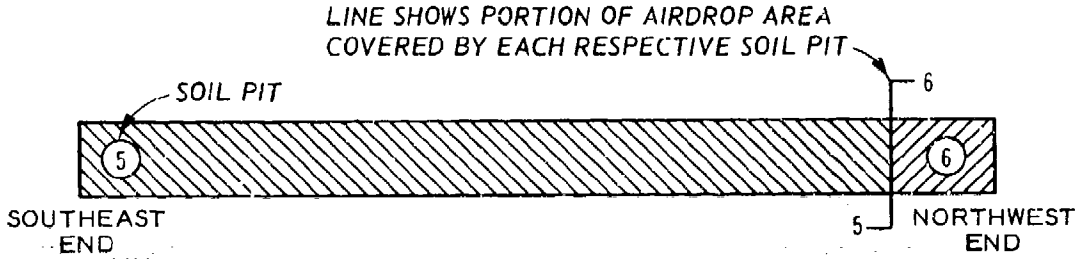

a. AIRDROP AREA 1

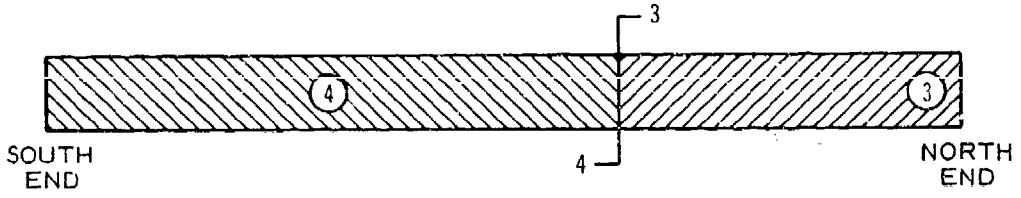

b. AIRDROP AREA 4

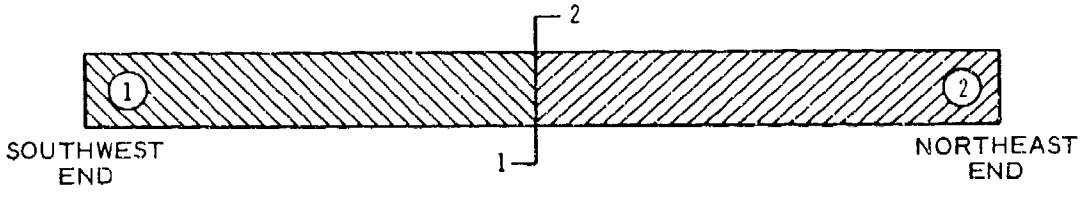

c. AIRDROP AREA 5

NOTE: AREA SIZE 100 BY 1200 m.

Fig. 16. Locations of soil pits, airdrop areas 1, 4, and 5

the results of special uniaxial strain and triaxial compression tests. These special laboratory tests were performed on a soil sample from the 30-m depth at each site, at two moisture contents believed to be representative of the wet and dry conditions at the site. The laboratory tests (uniaxial and triaxial) and data reduction procedures are documented in detail in references 4-8. The results of the laboratory tests are briefly discussed below.

87. The uniaxial strain tests were conducted by rapidly loading a laterally constrained soil sample and measuring its axial strain-time response. The results from a typical test are shown in fig. 17 and consist of stress-time, strain-time, and stress-strain relations.

88. The triaxial tests were conducted by rapidly loading a confined (confining pressures from 0 to approximately 68,950 kPa, or 10,000 psi) soil sample to failure (i.e. failure in 15-40 msec). The results from a typical test, shown in figs. 18-20, consist of (a) relations of deviator stress (i.e. vertical stress-radial stress) versus axial strain (fig. 18), (b) relations of mean normal stress to maximum stress difference (fig. 19), and (c) relations of shear to normal stress (fig. 20). The input parameters for the penetration equations were derived from the laboratory test results as described below.

89. Initial Young's modulus of elasticity, E . This parameter was obtained from the initial slope of the deviator stress-axial strain relation as shown in the example in fig. 18. Mathematically, E equals $d(\sigma_a - \sigma_r)/d\varepsilon_a$. In the example the average initial slope for two soil samples is given.

90. Compressibility parameter, ρ_p/ρ . The compressibility parameter was determined from the equation of continuity as follows:

$$\frac{\rho_p}{\rho} = \exp(\varepsilon_v) \tag{1}$$

where

ρ_p = current wet density of the substrate material

ρ = initial wet density of the substrate material

ε_v = vertical or axial strain

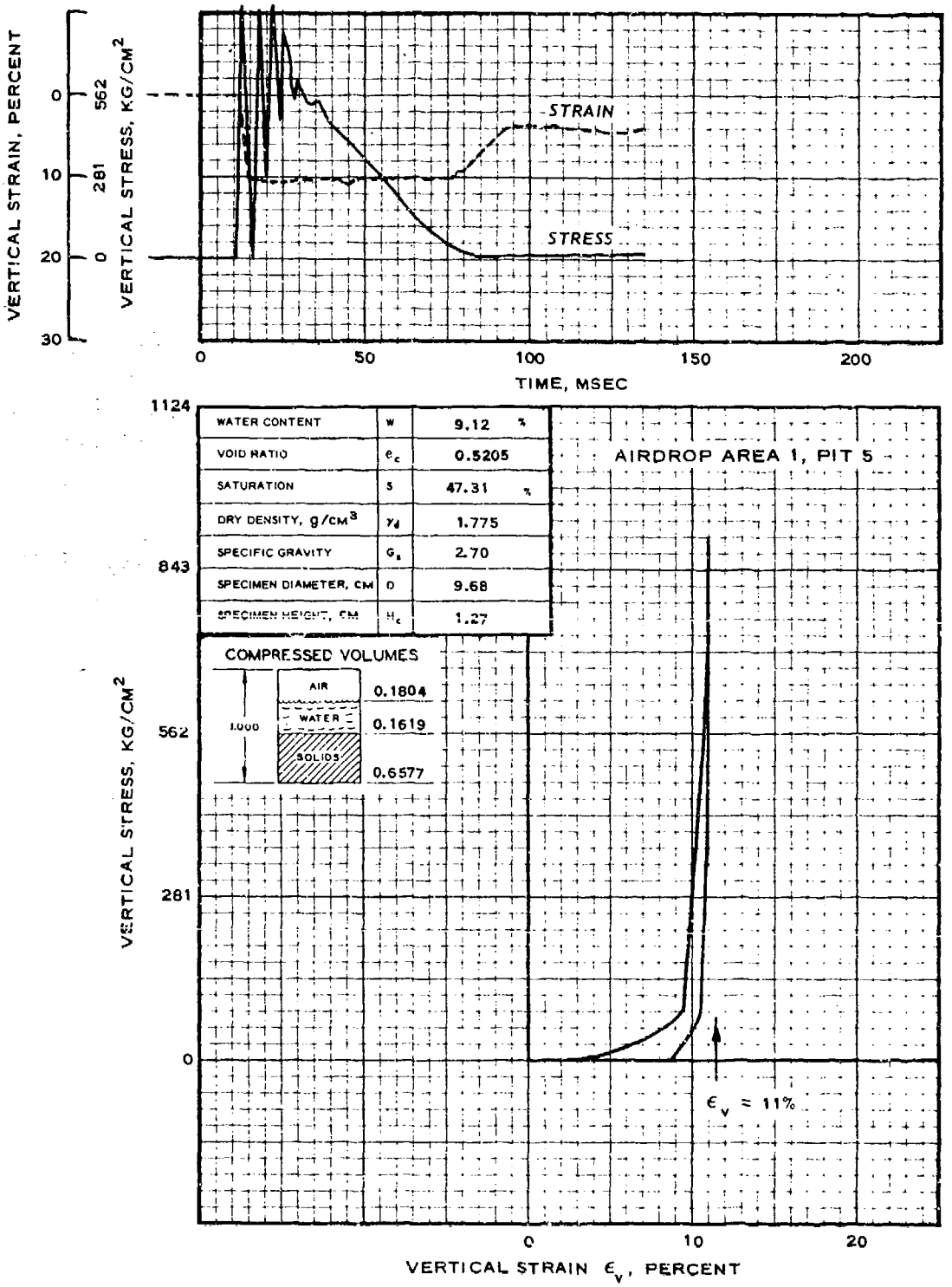

Fig. 17. Results of a uniaxial test

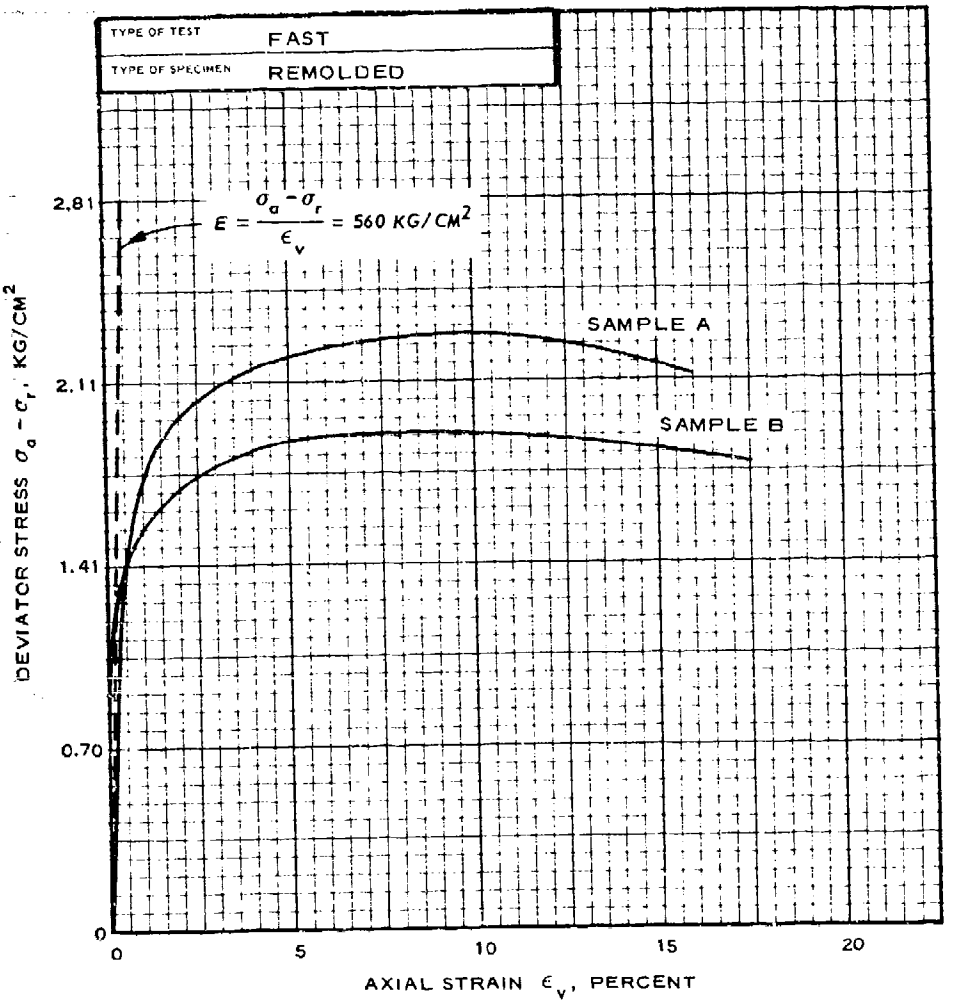

AIRDROP AREA 1, PIT 5			SAMPLE A	SAMPLE B		
INITIAL	WATER CONTENT	w	9.47 %	9.87 %	%	%
	DIAMETER, CM	D	5.34	5.35		
	HEIGHT, CM	H	12.57	12.47		
	VOID RATIO	e	0.457	0.484		
	SATURATION	S	53.38 %	55.05 %	%	%
	DRY DENSITY, g/cm^3	ρ_d	1.83	1.85		
	WET DENSITY, g/cm^3	ρ	2.00	2.00		
MINOR PRINCIPAL STRESS, PSI		σ_3	10.55	21.09		

Fig. 18. Triaxial compression test results, airdrop area 1, test pit 5

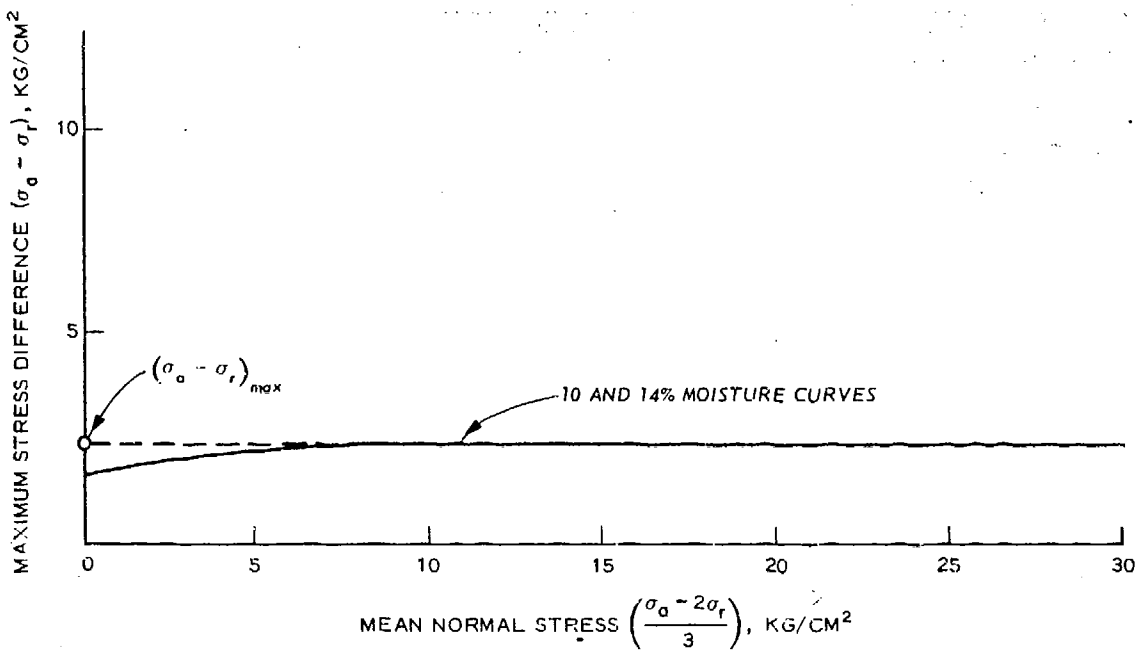

Fig. 19. Dynamic yield surface from triaxial compression test, airdrop area 1, test pit 5

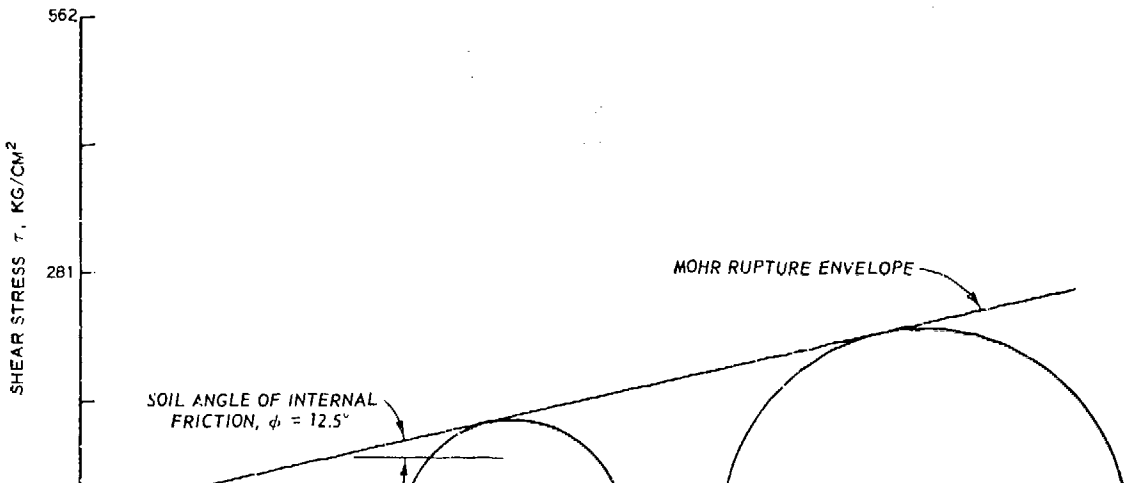

Fig. 20. Mohr's diagram, airdrop area 1, test pit 6, dry season

The experimental values of ϵ_v were determined from the uniaxial strain-stress strain data as shown in the example in fig. 17.

91. Ultimate shear strength. The ultimate shear strength (σ_u) was computed by the equation

$$\sigma_u = \frac{\left(\sigma_a - \sigma_r\right)_{max}}{\sqrt{3}} \qquad (2)$$

where

σ_u = ultimate shear strength of soil

σ_a = axial stress used in the triaxial compression test

σ_r = radial stress or confining pressure used in triaxial compression test

$\left(\sigma_a - \sigma_r\right)_{max}$ = stress difference at failure

The maximum stress difference $\left(\sigma_a - \sigma_r\right)_{max}$ used in eq 2 was determined from the dynamic yield surface as illustrated in fig. 19. The maximum stress difference of the soil is assumed to be the maximum soil stress that would be experienced by the substrate material and the ADSID/S during a penetration event.

92. Drag coefficient. The drag coefficient was computed using eq C2 (Appendix C), the ADSID/S dimension, and the computed coefficient of friction (μ) between the projectile and the soil. The coefficient μ was obtained as follows: The dynamic angle of internal friction of the soil ϕ was determined from the Mohr diagram (i.e. shear stress versus normal stress) shown in fig. 20. The relation shown in fig. 21 was then entered using the relative amounts of sand and clay in the soil sample as portrayed by the grain-size curve for the site and a value of δ/ϕ was determined for the dynamic case, where δ is the angle of friction between the projectile and the soil. Since the angle of internal friction ϕ is known (fig. 20), δ can be computed and the tangent of δ is the coefficient of friction μ. The values of μ and the ADSID/S dimension in conjunction with eq C2 (Appendix C) were then used to compute the drag coefficient C_D for each airdrop area. The values of μ and the data used to obtain them are listed in table 7.

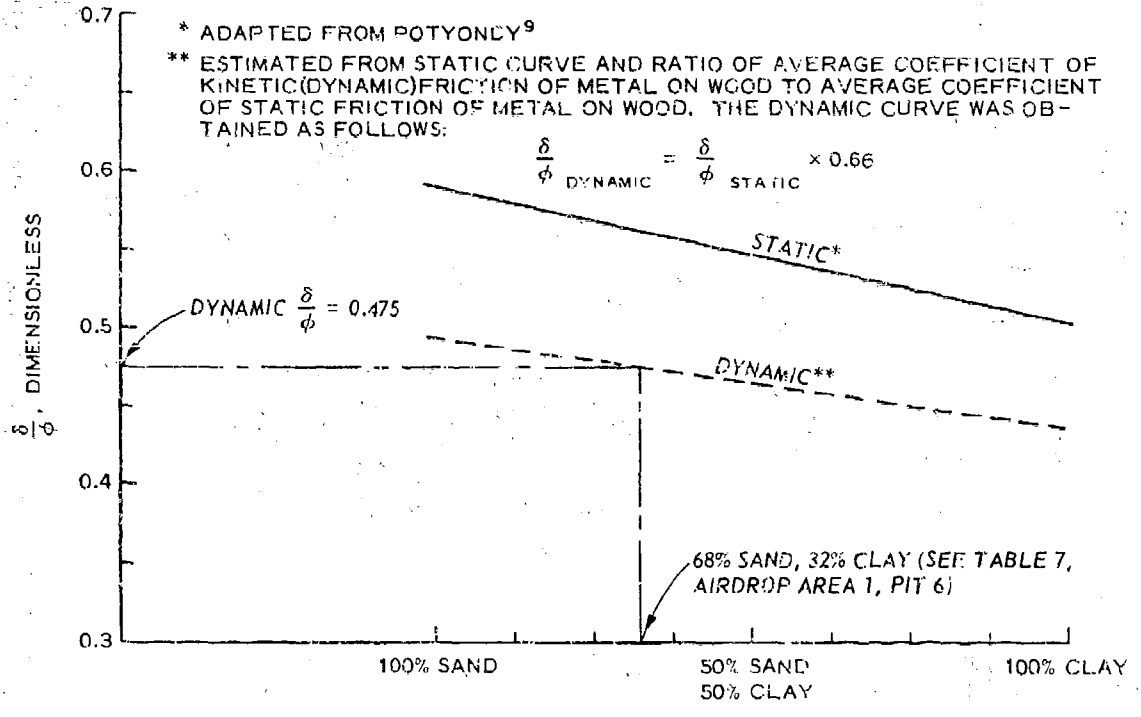

Fig. 21. Skin friction between smooth steel and soil (static and dynamic)

PART III: ANALYSIS OF DATA

93. To reach the objectives identified in paragraph 37, the analysis of the data was directed toward answering the following specific questions.

a. What are the seismic response characteristics of the SID test areas at Fort Huachuca? How do these characteristics vary in time and space?

b. What environmental factors should be measured in support of SID testing, i.e. both sensor detection performance and implantation performance, to provide a basis for the interpretation of the results? What are the temporal and spatial variations in terrain factors at Fort Huachuca?

c. Do the airdrop test sites at Fort Huachuca provide test environments that will allow evaluation of ADSID/S implantation over a wide range of soil conditions? What are the impact stresses imposed on ADSID/S's at the Fort Huachuca airdrop test areas?

d. What analytical schemes can be used to extrapolate SID test results (both sensor detection performance and sensor implantation performance) from one set of terrain (site) conditions to another?

94. This part of the report is directed toward the analysis of the data on a site-to-site basis; whereas Part IV addresses the mapping, i.e. the spatial variation of the relevant environmental, seismic response, and SID performance (detection distance) data.

Seismic Response Data

Selection of seismic response descriptors

95. As previously stated, the seismic response is the ground motion resulting from the propagation of seismic waves generated by a target or some background disturbance. The seismic waves generated by various targets (drop hammer, walking man, moving vehicle, etc.) used

in this study were measured with scientific geophones and recorded in analog format. Since the analog seismic signals proved unwieldy for site-to-site comparison and mapping, descriptors of the signal meaningful to SID detection performance testing were selected for analysis. These descriptors have been used in nearly all the seismic response studies conducted at WES including those conducted for TECOM, i.e. studies conducted for the Tropic Test Center and the Airborne Communication and Electronics Board in the Panama Canal Zone[10-13] and at Fort Bragg, North Carolina.[14,15] The descriptors selected for analysis are PPV, PSPV, and f_s; all are defined in paragraph 43.

96. As used herein, PPV is the maximum (peak) positive particle velocity (or amplitude) that occurred in the seismic wave for each respective distance. PSPV (peak summed particle velocity) can best be described by the techniques used to obtain it. A fast Fourier computer program was used to convert the digital data for each record from the time domain to the frequency domain, resulting in a curve of particle velocity versus frequency (f). A curve of summed particle velocity (SPV) versus f was obtained by applying a simulated 7-Hz filter band to the fast Fourier output data. The simulated filter used the equation

$$SPV_i = 7\left(\frac{X_{i-2} + X_{i-1} + X_i + X_{i+1} + X_{i+2}}{5}\right)$$

where X_i is the particle velocity at a frequency i, to average the particle velocity amplitudes occurring within the band and to determine the total response that occurred within the band. This process for obtaining PSPV is illustrated in fig. 22. The PSPV is the maximum value (amplitude) of SPV that occurs on the SPV-f curve. The frequency used was that at which PSPV occurred; this is the frequency at which most of the energy from the seismic wave is propagated at a given distance from the signal source.

97. In addition to PPV, PSPV, and f two other seismic descriptors, rms velocity (amplitude) and span were used. They are also defined in paragraph 43.

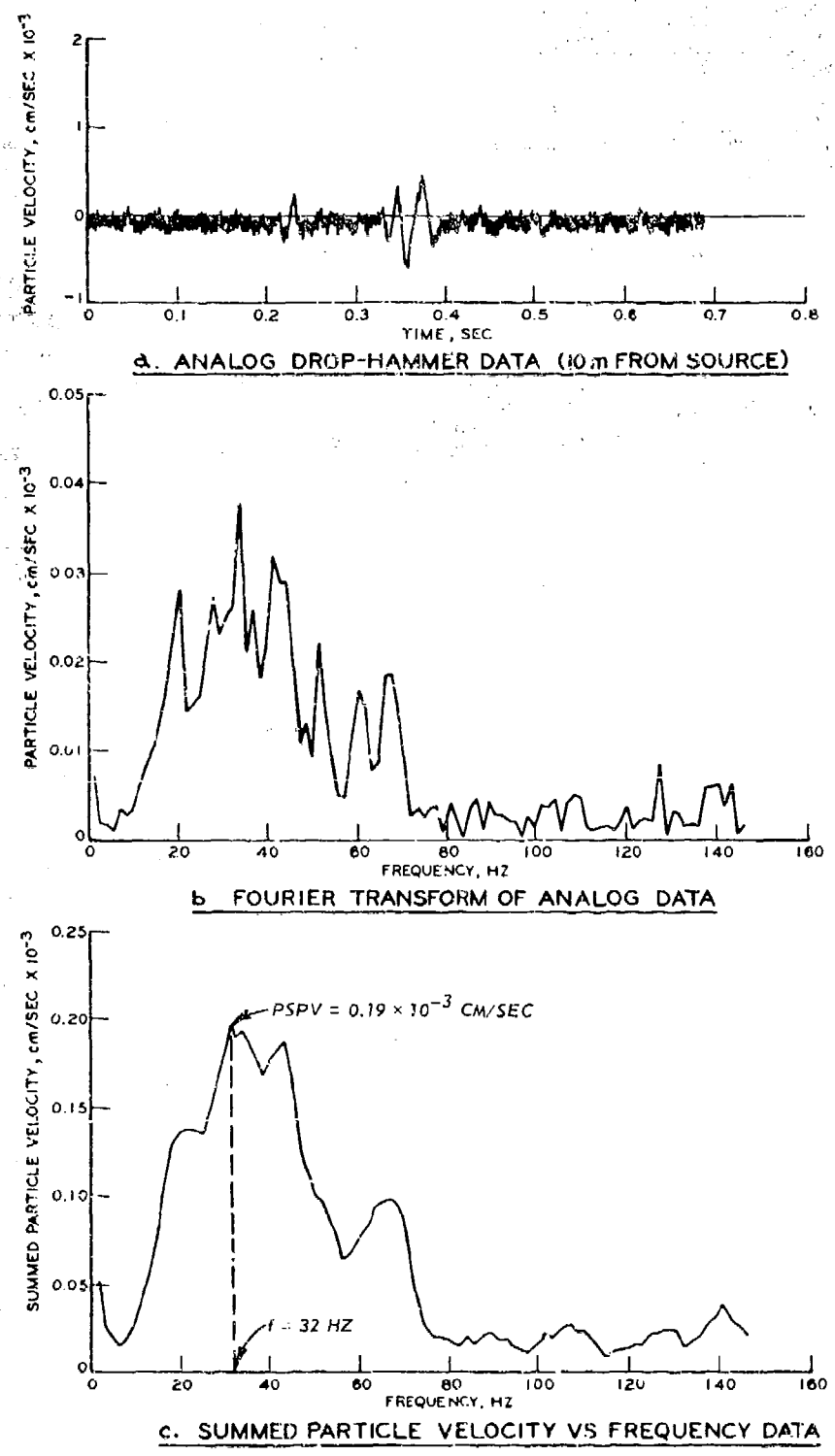

Fig. 22. Process for obtaining summed particle velocity-frequency data from analog data

Reproducibility of seismic descriptors

98. A prerequisite to a meaningful comparison of the seismic characteristics of a specific site at different times, such as in wet and dry seasons, or of the seismic responses of different sites is the inherent variability in the signal generator, measurement and reduction equipment, and procedures used to obtain the seismic descriptors (i.e. PPV, PSPV, and f). The controlled source, or drop hammer, has been used consistently as the signal generator for all TECOM seismic sensor studies. The variability of the equipment and procedures has been studied for selected sites in the Panama Canal Zone and at Fort Bragg (paragraph 95).

99. The results of the studies in Panama show that values of the three seismic response parameters (i.e. PPV, PSPV, and f), measured at all distances tested (10, 20, 30, 40, and 60 m), could be reproduced 85 percent of the time within ±10 percent of their mean values. The results of the drop-hammer reproducibility tests at Fort Bragg have been summarized and are included in fig. 23. These results, especially the PPV and PSPV values, show a decrease in variation with distance. To illustrate the percentage of variation in these data, the same three sites (sites 381, 492, and 493) were selected for determining the standard deviation/mean (SD/m) values. These SD/m percentages are tabulated below.

	Site 381			Site 492			Site 493		
Distance	PPV	PSPV	f	PPV	PSPV	f	PPV	PSPV	f
10	11	10	0	29	26	6	6	8	26
20	14	18	2	23	27	4	11	6	6
30	14	26	7	7	8	5	14	17	24
40	6	10	11	11	10	2	13	14	14
60				15	22	37	18	17	20

100. The variations in the Fort Bragg data are slightly greater than those in the Panama data. In summary, it appears the data obtained with the drop hammer are reproducible within about 15 percent of the mean, most of the time; therefore, the drop-hammer data should provide a

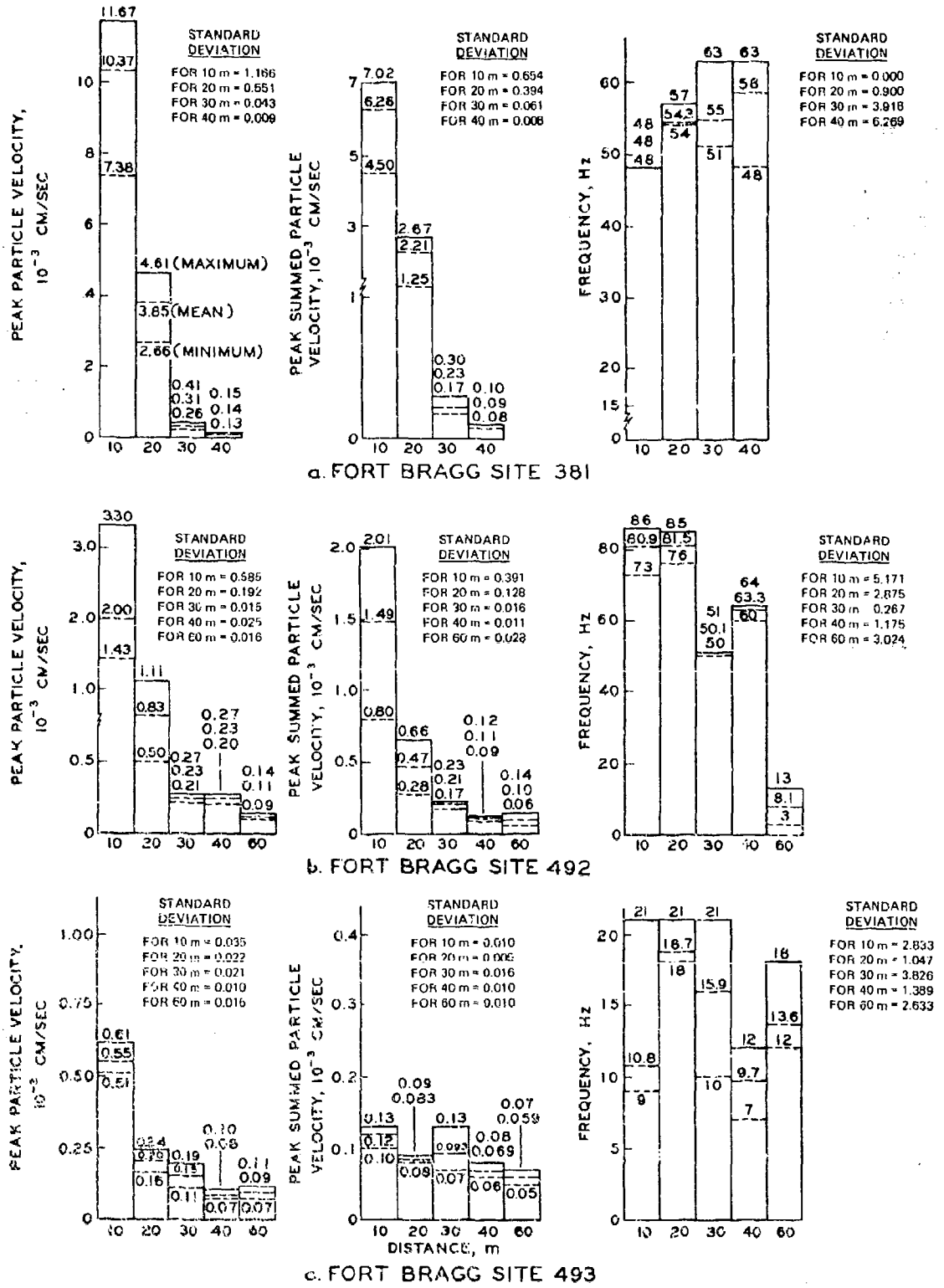

Fig. 23. Comparison of minimum values, maximum values, arithmetic means, and standard deviations for the general seismic descriptors (PPV, PSPV, and f), Fort Bragg repeatability tests (wet-season conditions)

useful basis for comparing the seismic response of one site with that of another and also for comparing the seismic responses at the same site under varying terrain conditions. Since the variability in the seismic response data is an important consideration in SID testing, at least three repetitions of each seismic measurement should be made in future seismic sensor studies.

Reduction of dry-season seismic response data

101. Field-data-collection programs were conducted in August 1971 (wet season) and March 1972 (dry season). Seismic response data resulting from drop-hammer, man-walking, and vehicle targets were obtained during both periods. The data collected in the wet season are believed to be in error as a result of an undetected instrumentation calibration problem and are not suitable for analysis; however, the wet-season drop-hammer data were reduced and are presented in table 8. The values of PPV and PSPV are consistently lower than expected and no further analysis was performed.

102. From the dry-season seismic response data, typical records for each site were selected as follows:

a. Drop hammer and man walking. Records at distances of 5, 10, 20, 30, 40, and 60 m from the energy source.

b. M151 vehicle. Records at distances of 50, 100, 150, 200, 250, 300, and 400 m from the energy source.

c. M577 vehicle. Records at distances of 100, 200, 300, 400, and 500 m from the energy source.

d. Ambient and induced noise. One sample record (0.682 sec).

103. The dry-season field-measured seismic response (analog signature) data obtained from the man-walking, drop-hammer, vehicle, and background- (ambient and induced) noise tests were converted to digital form by computer at 1500 points per second. The digitized records were then processed through a fast Fourier transform program to convert the digital data from the time domain to the frequency domain. PPV, PSPV, f, and rms velocity were then computed and tabulated for the

drop-hammer, man-walking, and vehicle energy sources (tables 8-10, respectively). Plots of SPV-f relations were derived for selected records from the vehicle and background-noise tests. These data and their analyses are discussed in the following paragraphs.

Site-to-site variation in
dry-season seismic response data

104. Graphs portraying the seismic response parameters PPV, PSPV, and f as a function of distance from the energy source are presented in figs. 24-26, respectively. The relations are discussed below.

105. PPV-distance data. The PPV data (fig. 24), in general, show a fairly good correspondence among sites within the hand-emplacement area (i.e. sites 335-342, 348, and 349). An exception to this trend is the curve for site 342, which shows a very small peak amplitude of 0.01×10^{-3} cm/sec at a distance of 60 m. The curves for sites within the airdrop areas (i.e. sites 347 and 410-413) show considerable data variation. The curve for Willcox Playa site (site 413) is a great deal different from those for sites within the four other airdrop areas.

106. PSPV-distance data. The PSPV data (fig. 25) vary considerably for distances less than approximately 40 m, and somewhat less for distances of 40-60 m. Data for the 10 sites within the hand-emplacement area and airdrop sites 410-412 show a fairly good correspondence. The Willcox Playa site (site 413) shows considerable variation from the other sites and also shows very little attenuation in the seismic wave between 5 and 60 m.

107. f-distance data. The sum-frequency data (fig. 26) portrayed for the sites within the hand-emplacement area vary considerably (20-50 Hz) at close distances, but are in relatively good agreement for distances of 30 m and greater. Sum-frequency data for airdrop sites 410-412 are not too much different from the data for the sites within the hand-emplacement area; however, there is more variation for certain frequencies (i.e. 30 and 40 Hz). The Willcox Playa site again is quite different from the other sites and shows a low and constant predominant sum frequency of 7-9 Hz. In addition to the variation of

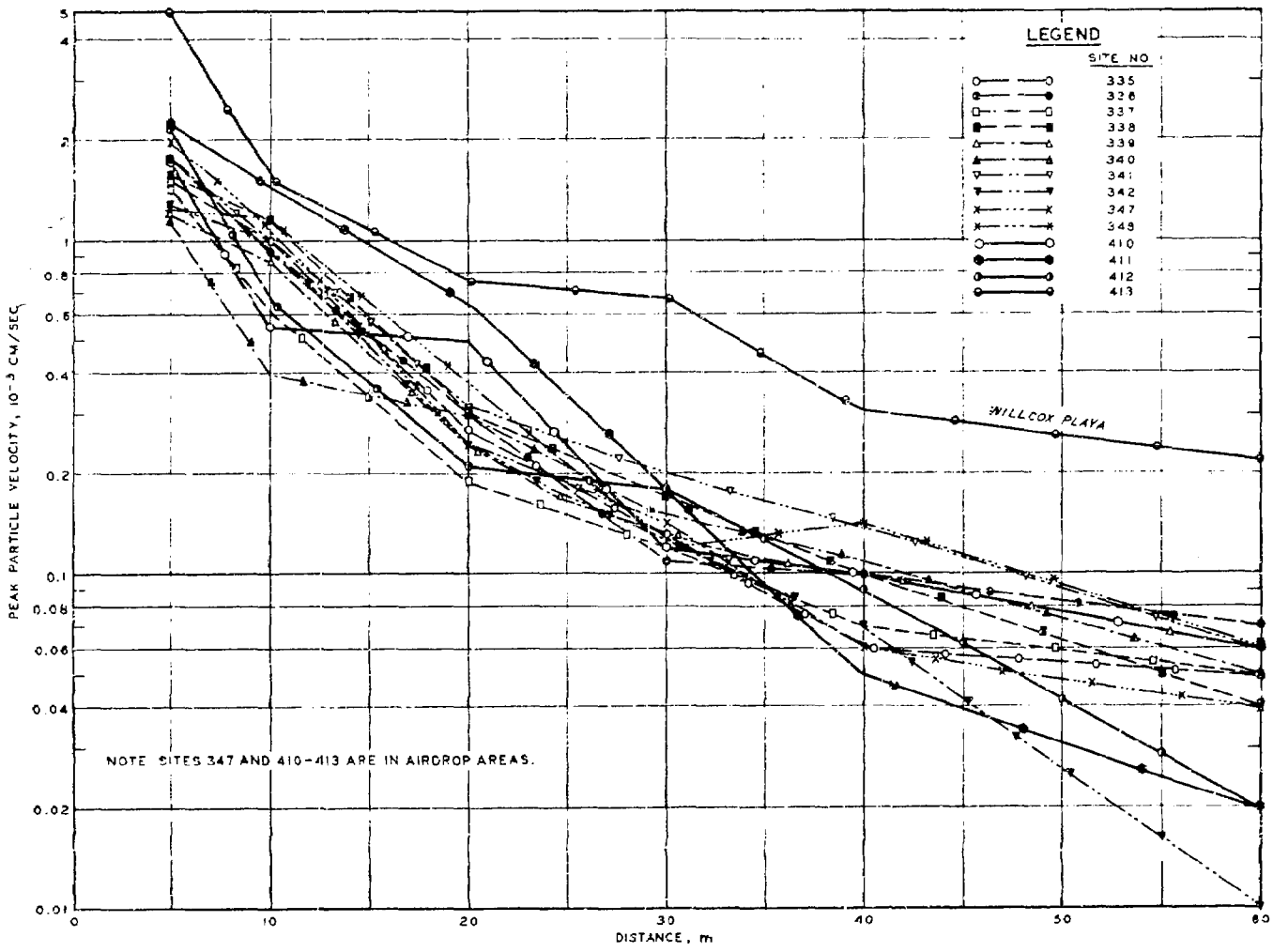

Fig. 24. Site-to-site variation in PPV at various distances from the drop-hammer energy source, dry-season conditions

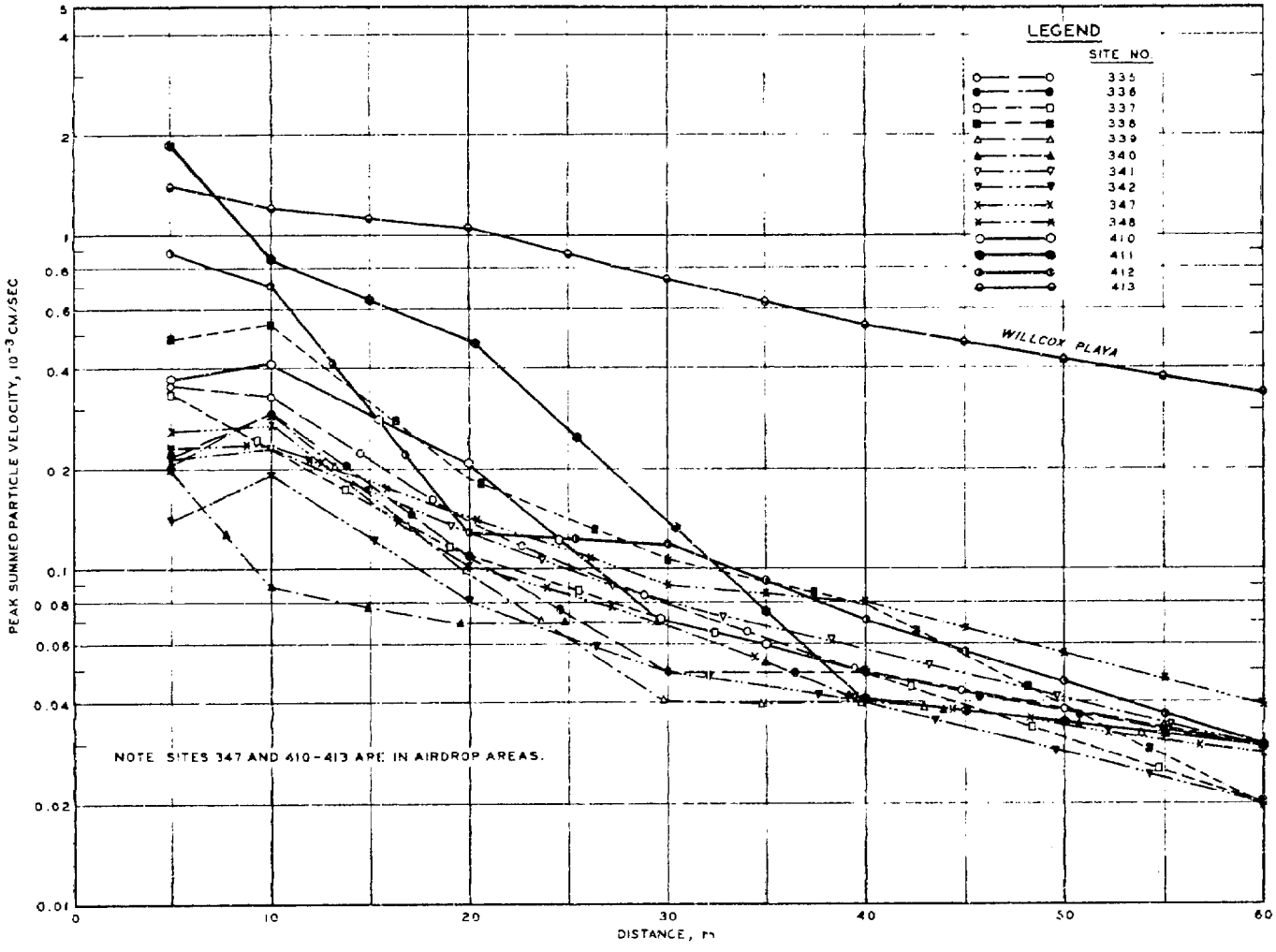

Fig. 25. Site-to-site variation in PSPV at various distances from the drop-hammer energy source, dry-season conditions

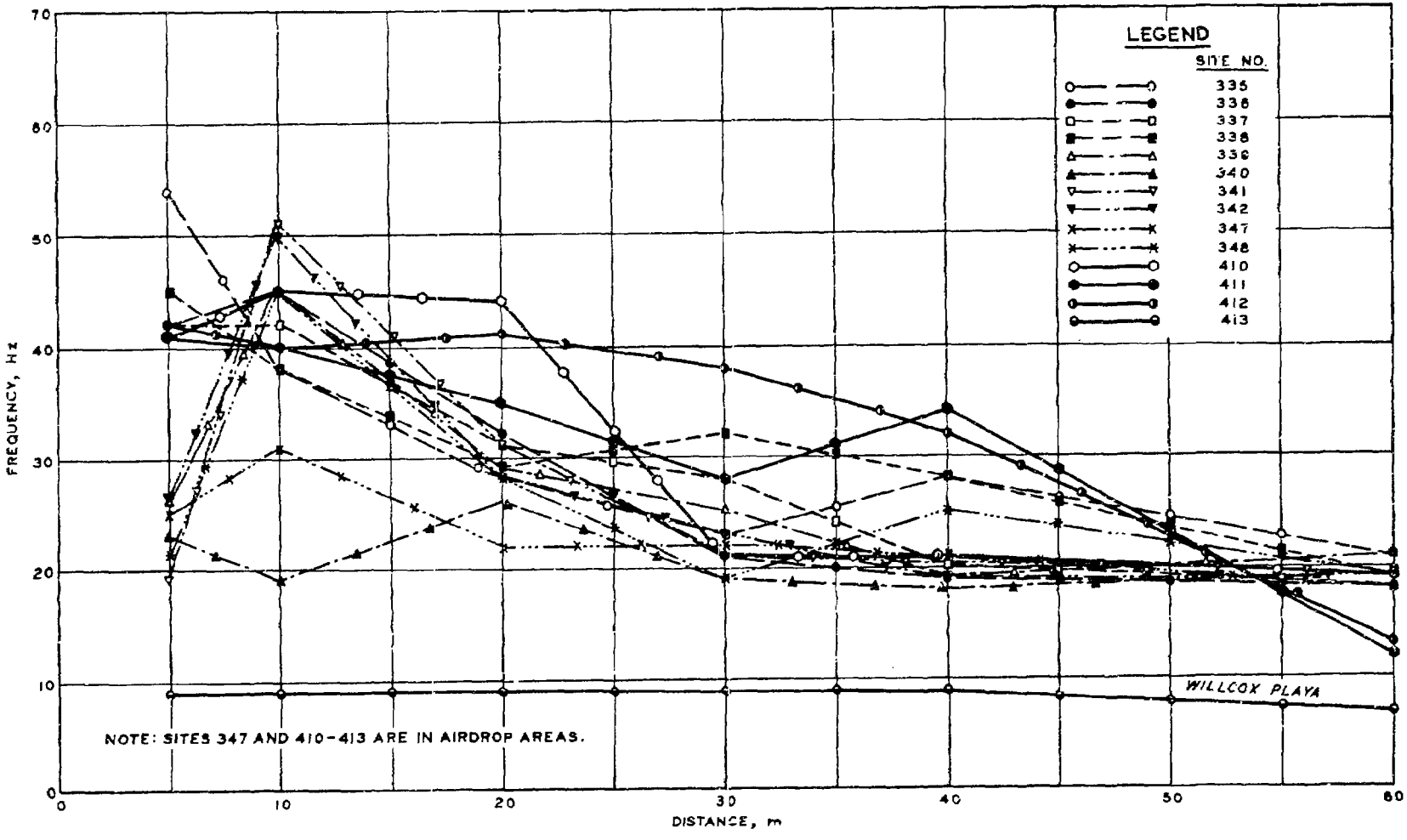

Fig. 26. Site-to-site variation in f at various distances from the drop-hammer energy source, dry-season conditions

sum-frequency data among the sites, there is also considerable variation in sum-frequency data within each site, with the exception of site 413.

Variation in dry-season ambient-noise data

108. The seismic response resulting from ambient (background) noise was recorded during normal working hours at each site as discussed in paragraph 74. One sample record (0.682 sec) each was selected for sites 335-337, 339, 341, 342, and 349 to study the range of variation in ambient noise found in the hand-emplacement test area. These records were used to generate SPV-f relations (fig. 27) to depict the amplitude and frequency content of the ambient seismic noise. The ambient noise present within the hand-emplacement area varied between 0.008×10^{-3} and 0.09×10^{-3} cm/sec in SPV amplitude with the maximum amplitudes generally falling within a low-frequency (1-20 Hz) bandwidth. Although the background noise was measured in diverse locations in the hand-emplacement area under various wind conditions and at different times of the day, the SPV-f data are quite similar in that they show relatively low background noise levels. Wind conditions observed at site 341 (see fig. 27e) were the highest measured (4.4-6.6 m/sec) during the background-noise tests, and the ambient-noise level at all frequencies is higher for that site than for the other six sites. Even so, the noise level is well below that which would cause difficulty in testing sensors with threshold levels and a frequency response similar to those of the Phase III MINISID. In summary, it appears that the hand-emplacement area should provide a seismically quiet area for SID testing, insofar as ambient noise is concerned.

Variation in dry-season induced-noise data

109. SID testing will always be affected by seismic noises induced by activities extraneous to the test. During the field program, seismic responses caused by aircraft (a Huey helicopter and a single- and a double-engine light aircraft) and by a freight train traveling across Willcox Playa were measured. The SPV-f relations derived from a selected number of measurements are presented in fig. 28. The data

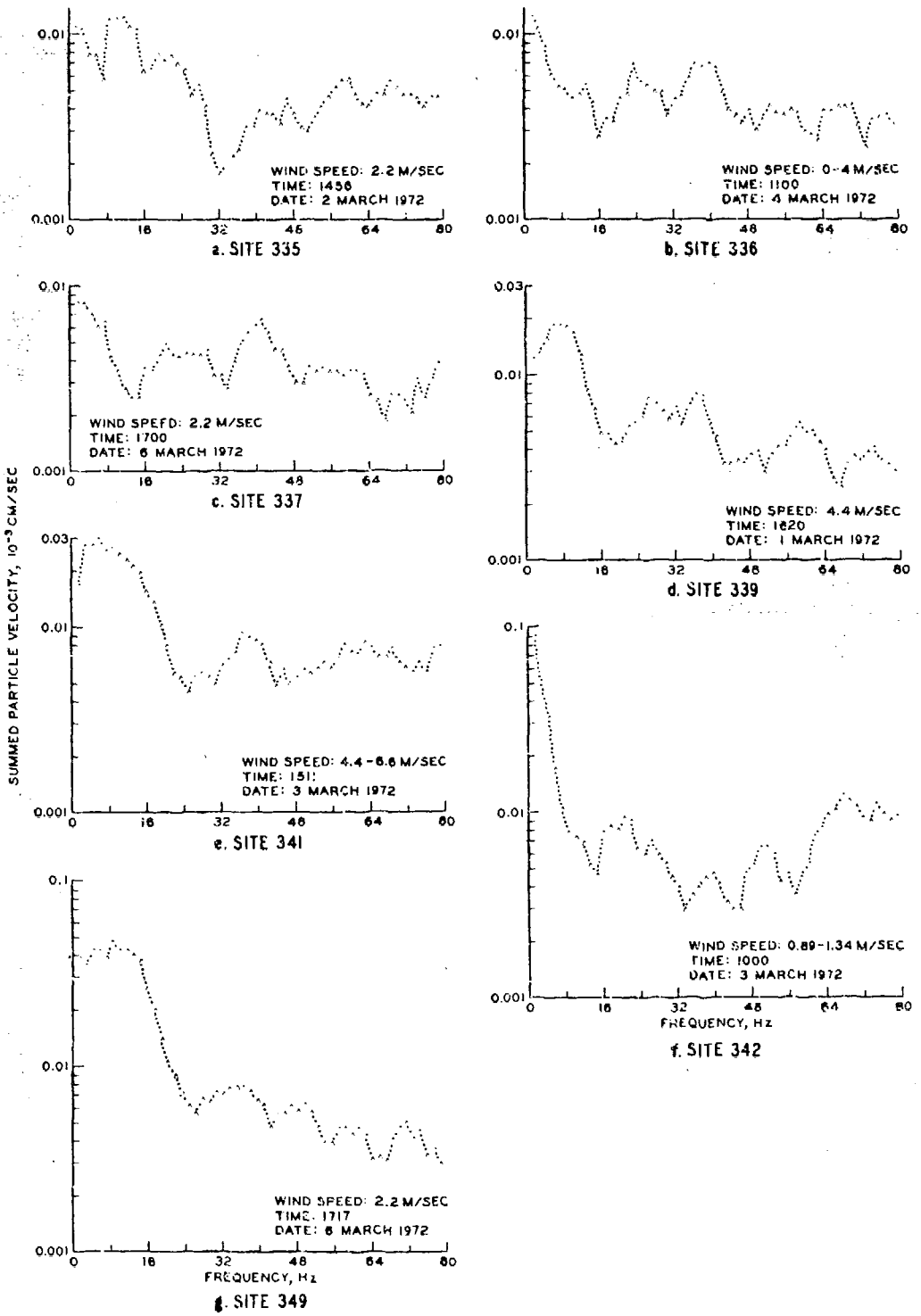

Fig. 27. Dry-season ambient-noise data

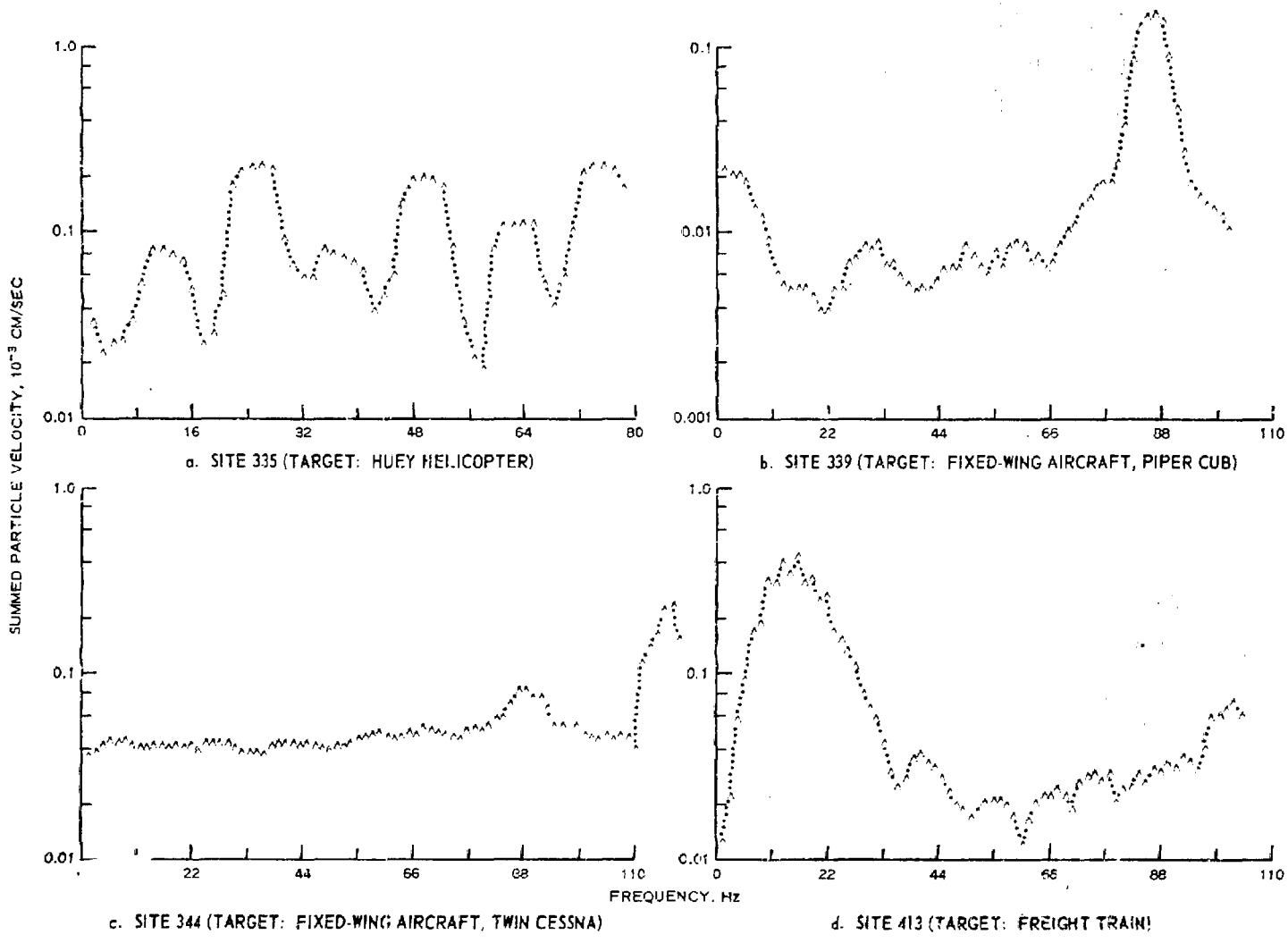

Fig. 28. Dry-season induced-noise data

displayed in fig. 28 were obtained on an opportunity basis; therefore, altitudes and distances from the energy source were not measured. As expected, the results show that the induced noises increase the general level of background noise and, in some cases, increase it markedly as a function of frequency. For example, the curve for the helicopter (fig. 28a) shows several peaks in amplitude occurring at frequency intervals of about 12 Hz. The Piper Cub (fig. 28b) did not appear to materially affect the noise level at frequencies below about 70 Hz (compare figs. 28a and 28b), but increased it sharply at 88 Hz. The noise level of the Twin Cessna (fig. 28c) showed a near constant amplitude (0.03×10^{-3} cm/sec) for frequencies between 0 and 100 Hz, with the exception of the small peak at approximately 88 Hz. At about 115 Hz an abrupt change in SPV amplitude occurred. The train traveling across Willcox Playa (fig. 28d) caused a large increase in seismic noise (0.3×10^{-3} cm/sec) from 0 to 16 Hz, and considerable variation in noise levels for frequencies between 16 and 110 Hz.

110. In summary, induced background noise will most likely occur during SID testing at Fort Huachuca. While the induced noise data presented herein are representative of only selected cases and do not necessarily reflect the maximum amplitude and predominant frequencies that might be encountered at Fort Huachuca, the amplitudes of the induced noises will be above those of the ambient noise, and the frequencies and amplitudes of induced noise will span a wide range of values. Since the ambient and induced background noises increase or, in some cases, decrease the sensitivity of certain types of SID's, it is recommended that the background noises be measured during the times of SID testing.

Seismic response from vehicles

111. Seismic response relations in terms of SPV versus f were obtained for the two vehicles (M151 and M577) that were tested at the two cross-country sites (344 and 345) in the hand-emplacement area. The vehicles were run at two speeds, 8 and 32 km/hr. These data are presented in fig. 29. The M577 traveling at 32 km/hr generated the highest SPV values for the frequencies shown. Also, except for some frequencies from 70 to 78 Hz for site 345 (fig. 29b), the M151 traveling at 8 km/hr

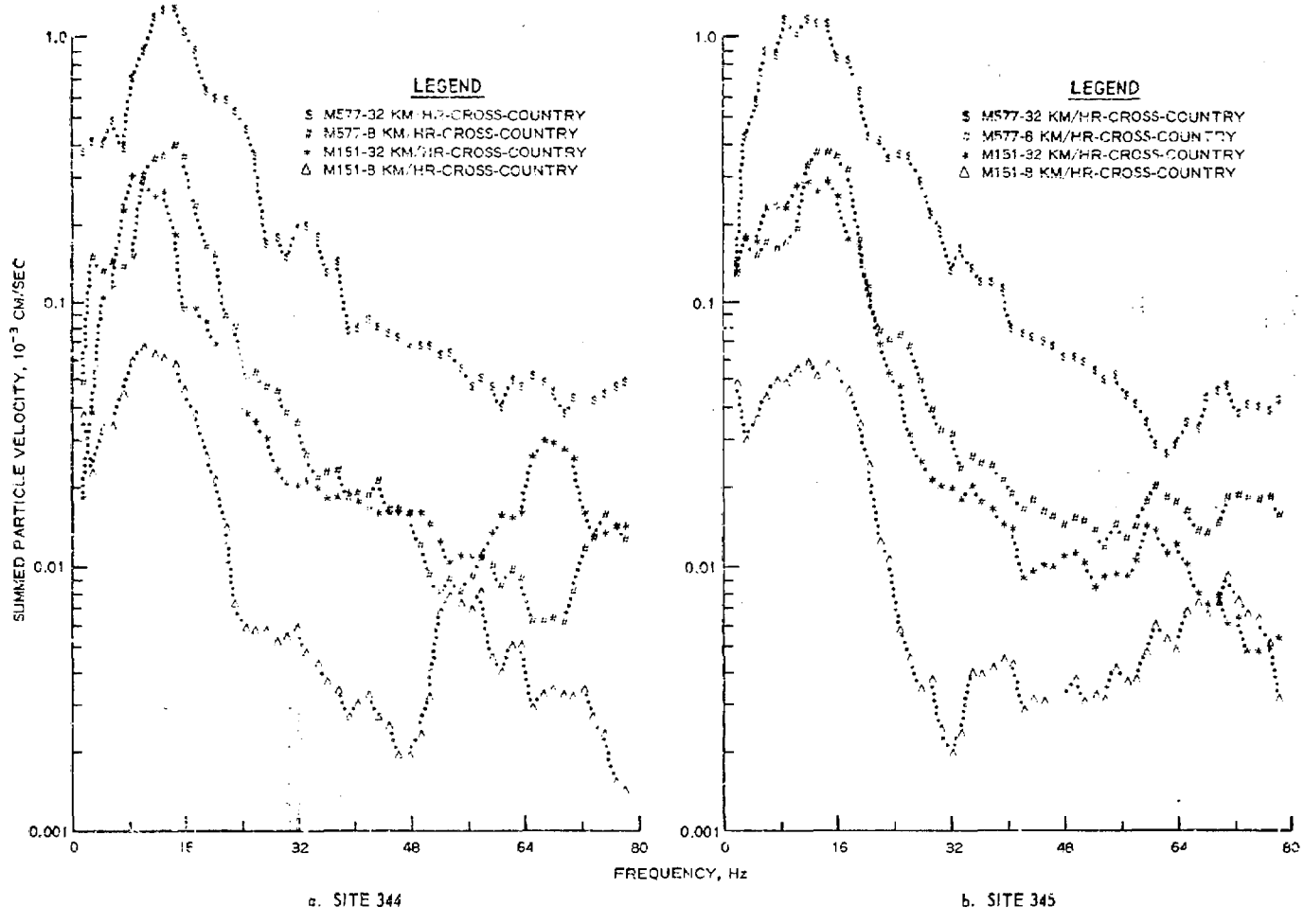

Fig. 29. Comparison of dry-season response data for the M151 and M577 vehicles at a distance of 200 m from sensor

generated the least amount of seismic response. It is interesting to note that for both sites, there is a good deal of similarity between the response generated by the M577 traveling at 8 km/hr and the M151 traveling at 32 km/hr. The general similarity in the SPV-f data for sites 344 and 345 for each of the two vehicles suggests that the terrain conditions at both sites are quite similar. Some of the more subtle differences noted among the SPV-f curves for the two sites cannot be fully explained, e.g. the lowest SPV value for the M151 traveling at 8 km/hr occurs at 48 Hz at site 344, and at 32 Hz at site 345. However, differences in the roughness of the surface over which the vehicles traveled could have accounted for differences of this kind and magnitude.

112. The results illustrate clearly that the seismic responses emanating from vehicles are a function of both vehicle type and speed. In addition, it is well known that the type of terrain, i.e. both surface and substrate conditions, also affects the seismic responses of vehicles, although in this case the two sites were quite similar. The implication of this is that if SID results from vehicle tests are to be extrapolated to conditions other than those occurring during the tests, the effects of vehicle speed and terrain must be quantitatively known.

Experimental MINISID and ADSID/S Test Data

MINISID data

113. Detection distances obtained at low-, medium-, and high-gain settings of a Phase III MINISID are presented in table 11. Fig. 30 shows graphically the wet- and dry-season MINISID detection values at medium gain. A point especially worthy of mention is that two different men made the walking tests in the wet and dry seasons; therefore, the data for these tests for the two seasons may or may not be directly comparable.

114. The detection distances presented in fig. 30 show a difference of 1-3 m for five sites (337-339, 342, and 345), a difference of 5-7 m for two sites (341 and 347), and a difference of 18-20 m for two sites (336 and 348). For the nine cases, there seems to be no

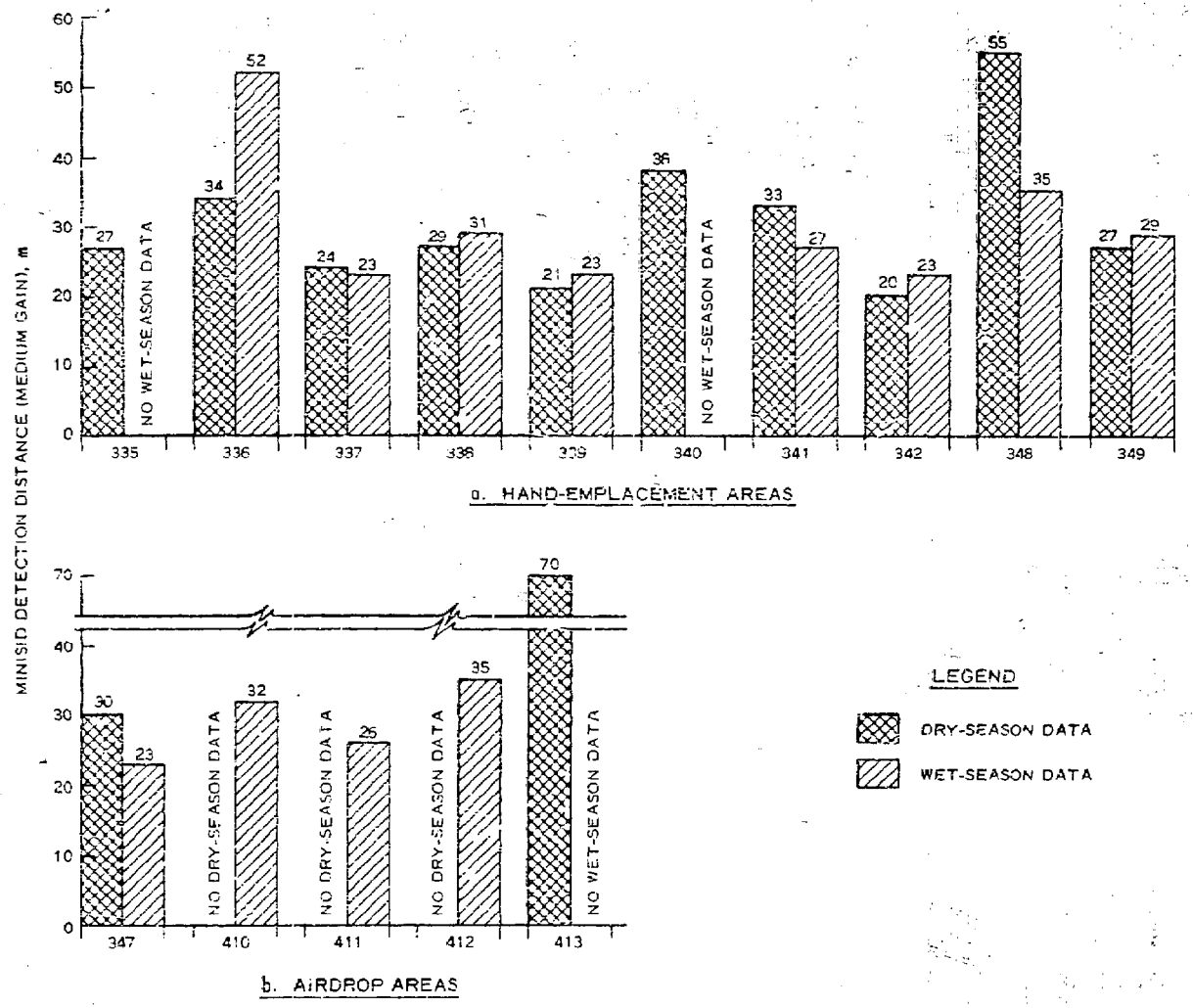

Fig. 30. Comparison of measured MINISID III detection performance data for dry- and wet-season conditions

particular trend toward either season's allowing a consistently greater or lesser detecti[illegible]age.

ADSID/S data

115. The results of the experimental ADSID/S tests conducted by CSEWS are presented in table 12. These tests were conducted during August 1972 and should be representative of wet-season conditions at the CSEWS test site.

116. The results, in general, show that most penetration lengths (i.e. depth of penetration measured along the longitudinal axis of the sensor) ranged between 20 and 35 cm, although penetrations as deep as 50 cm and as shallow as 15 cm were obtained. The emplacement configurations of two of the air-implanted ADSID/S's at the CSEWS test area are shown in fig. 31.

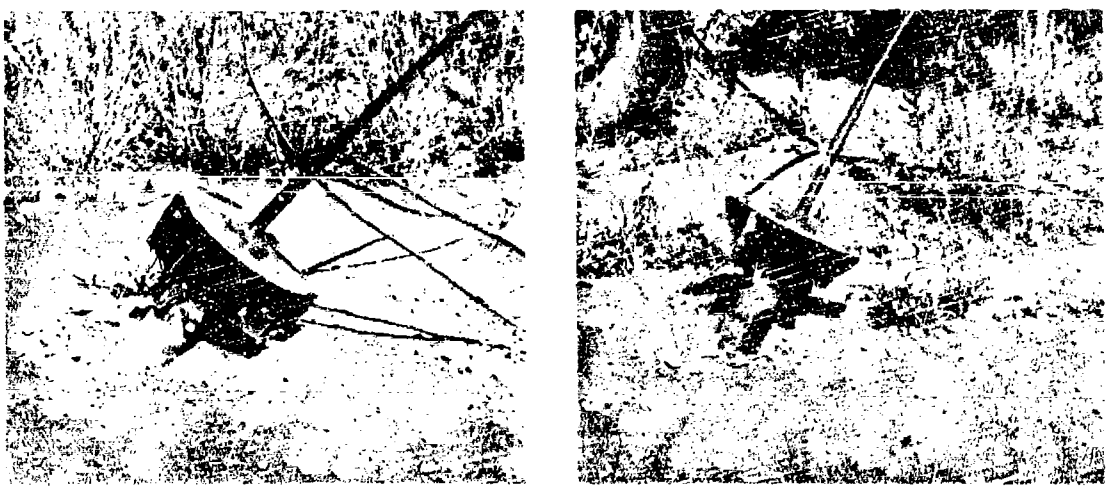

a. Impact angle 50 deg (off vertical)

b. Impact angle 40 deg

Fig. 31. ADSID/S implanted in CSEWS airdrop test area

Environmental Data

117. The environmental data obtained at Fort Huachuca test sites were those directly applicable to the prediction of SID detection performance and sensor-implantation performance as discussed previously. The data, along with the theoretical models (developed or in development

at WES), provide the input and analytical tools needs for interpretation and extrapolation of SID test results from site to site and from region to region. The environmental data collected for input to SID detection performance and air-implantation performance models are discussed below.

Data for SID detection performance predictions and evaluations

118. The environmental data measured in support of SID detection performance testing and prediction were obtained during August 1971 (wet season) and March 1972 (dry season). So that these data could be input directly into the SID detection performance prediction model, they were reduced and summarized by soil layers: surface, refraction layer 1, and refraction layer 2.

119. Surface layer. The surface, or uppermost, layer of soil is the thin zone of material that comes in contact with the seismic energy source (drop hammer, footstep, vehicle track or wheel, and so on) and the SID geophone. Although the phenomena dealing with the interaction of the energy source and the substrate have not been adequately quantified, the surface terrain factors considered important in the transfer of seismic energy from the source to the ground and from the ground to the SID geophone are:

a. Soil type (USCS).
b. Soil particle size, percent finer by weight.
c. Moisture content, percent.
d. Soil wet density, g/cm^3.
e. Cone penetration resistance, CPR (a measure of soil strength, kPa.
f. Height (cm) and density of vegetation ground cover.
g. Geometry of ground surface (roughness).

120. The data for the factors listed above with the exception of surface geometry data are given in tables 2-6. Of the factors listed, only soil type, soil particle size, and surface geometry can be considered static or constant with time. Moisture content, wet density, CPR, and height and density of vegetation change as a function of site and

weather conditions. From table 2, it can be seen that the majority of surface soils at the various sites, in general, exhibit the same characteristic gradation and most are classified SC. Exceptions to this trend are sites 339, 340, and 349, where the surface soils are classified SM, and sites 410 and 411, which contain 53.5 and 64.4 percent silt and clay, respectively, and are classified CL. Particle-size distributions for surface soils at Fort Huachuca sites generally are quite similar; however, there were considerably more small surface rocks at sites 338, 410, and 411 than at the other sites. The surface rocks contained in the substrate material at these sites were not included in the samples used to determine the particle-size distributions of the materials. (See ground photographs in figs. B2b, B7b, and B8a, respectively, Appendix B.)

121. Site-to-site and season-to-season comparisons of surface moisture content and CPR are shown in figs. 32 and 33, respectively. Similar comparisons for wet density are not presented herein since wet density is directly related to moisture content, i.e. $\rho = (1 + W)\gamma_d$, where ρ = soil wet density, W = soil moisture content (percent), and γ_d = soil dry density. The dry-season site-to-site moisture values within the hand-emplacement area ranged from a low of 0.9 percent (site 341) to a high of 5 percent (site 338). The next highest moisture contents were 2.8 percent (site 342) and 2.2 percent (site 336); for 7 of the 10 sites, the dry-season moisture content was less than 2 percent.

122. As expected, the moisture values within the hand-emplacement area were higher during the wet season, ranging from 5.2 percent (site 336) to 11.7 percent (site 338). In general, the surface moisture data (fig. 32) show that there was more variation from season-to-season than from site-to-site.

123. The dry-season surface CPR values (fig. 33) ranged from 100 to 1990 kPa, with considerable variation among the sites. The season-to-season variation was large for sites 335, 336, and 340; moderate for sites 338, 342, and 349; and insignificant for sites 337, 339, 341, and 348. In some cases the wet-season data exhibited greater CPR values than the dry-season data (e.g. sites 335, 336, 339, 342, and 349), which

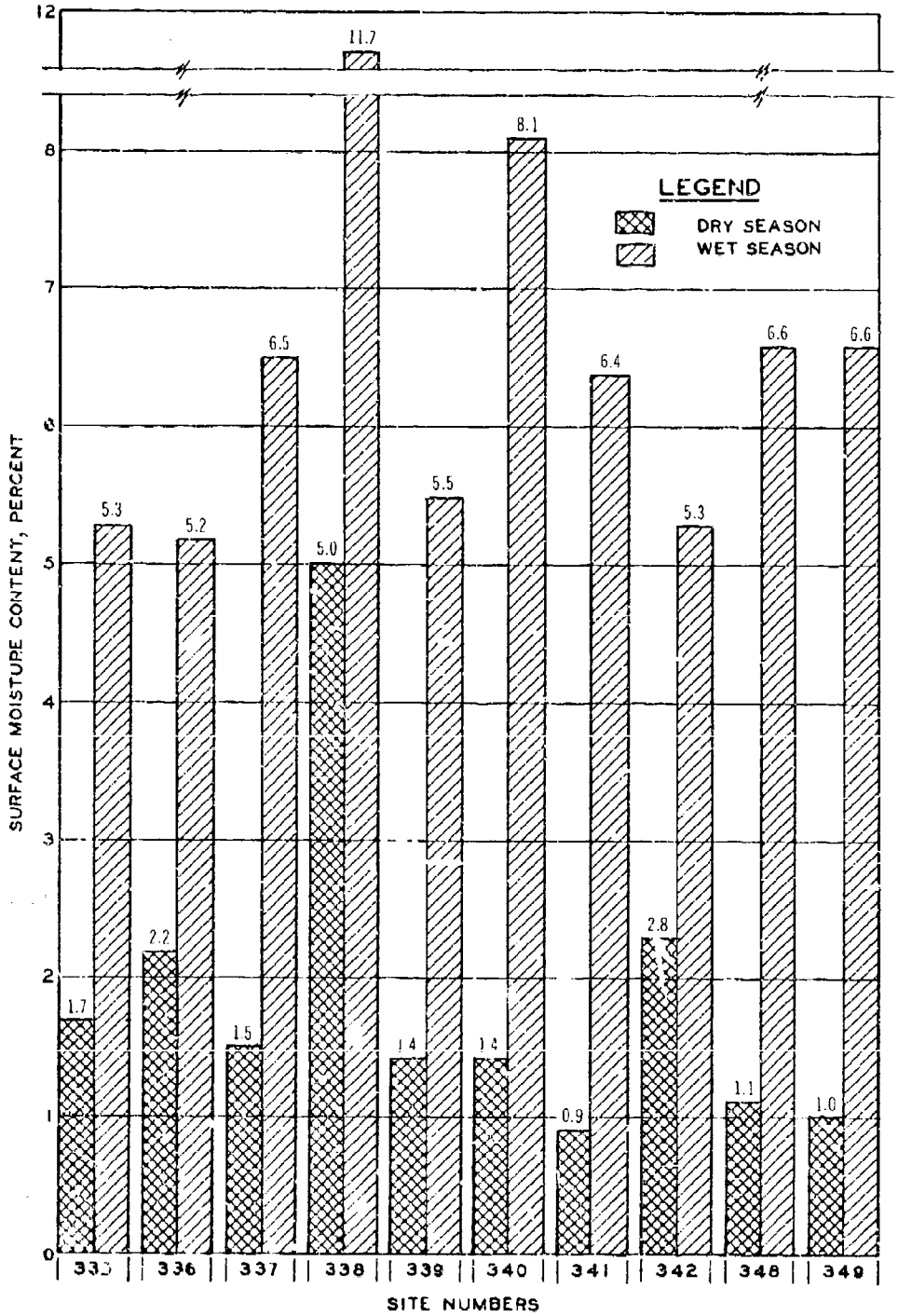

Fig. 32. Comparison of surface moisture contents for wet and dry seasons

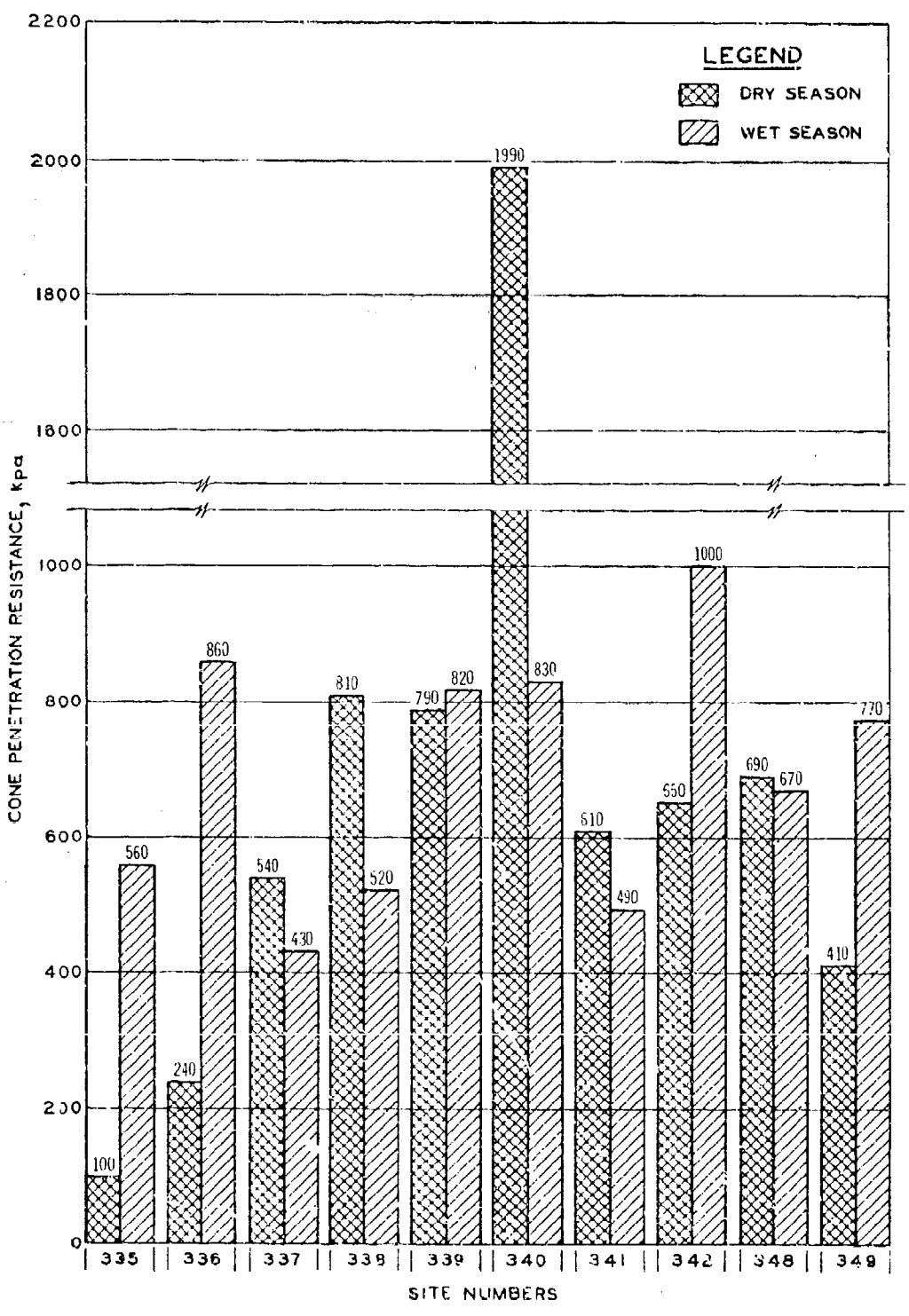

Fig. 33. Comparison of surface cone penetration resistance values for the wet and dry seasons

seems to indicate that the addition of moisture created some cohesion in the surface soil.

124. The vegetation ground cover (see table 6) occupying the sites within the hand-emplacement area was quite uniform in terms of density, height, and percent of ground covered. Only a few isolated areas (near the arroyos) were without some type of ground cover (sites 335, 337, and 339). As a result of this homogeneity, the relative effects of ground cover on SID testing were approximately the same for all sites within the hand-emplacement area.

125. The geometry of the ground surface had very little effect on SID detection performance because of the minor irregularities in surface configurations of the test sites (see paragraph 83).

126. Subsurface refraction layers 1 and 2. Refraction layers 1 and 2 are the first two subsurface layers containing different primary (or compression) wave velocities. These two layers are determined by techniques of refraction seismology and often, but do not necessarily, correspond to the apparent stratification in the soil profile, as stated in paragraphs 16-18.

127. Values of four terrain factors pertaining to refraction layers 1 and 2 are required as input to the WES Theoretical Seismic Propagation Model.[16] The four factors are listed below; their wet- and dry-seasons values are contained in table 2.

a. Compression wave velocity of layer 1 (V_{P1}) and layer 2 (V_{P2}), m/sec.

b. Shear wave velocity of layer 1 (V_{S1}) and layer 2 (V_{S2}), m/sec.

c. Thickness of layer 1 (T_1) and layer 2 (T_2), cm.

d. Wet density of layer 1 (ρ_1) and layer 2 (ρ_2), g/cm^3.

128. Site-to-site and season-to-season comparisons of compression wave velocities in refraction layers 1 and 2 are presented in fig. 34. For layer 1, the dry-season velocities ranged from 250 to 500 m/sec, whereas the wet-season velocities ranged from 230 to 455 m/sec, indicating that the range of variation does not change appreciably from the dry to the wet season. Fig. 34 also shows that the site-to-site

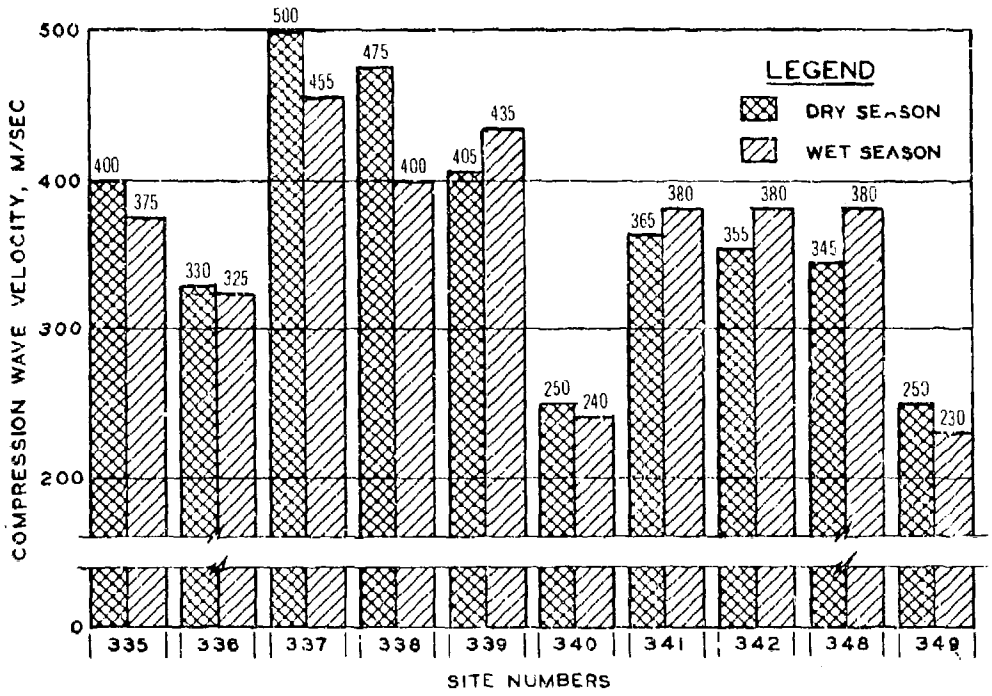

a. LAYER 1

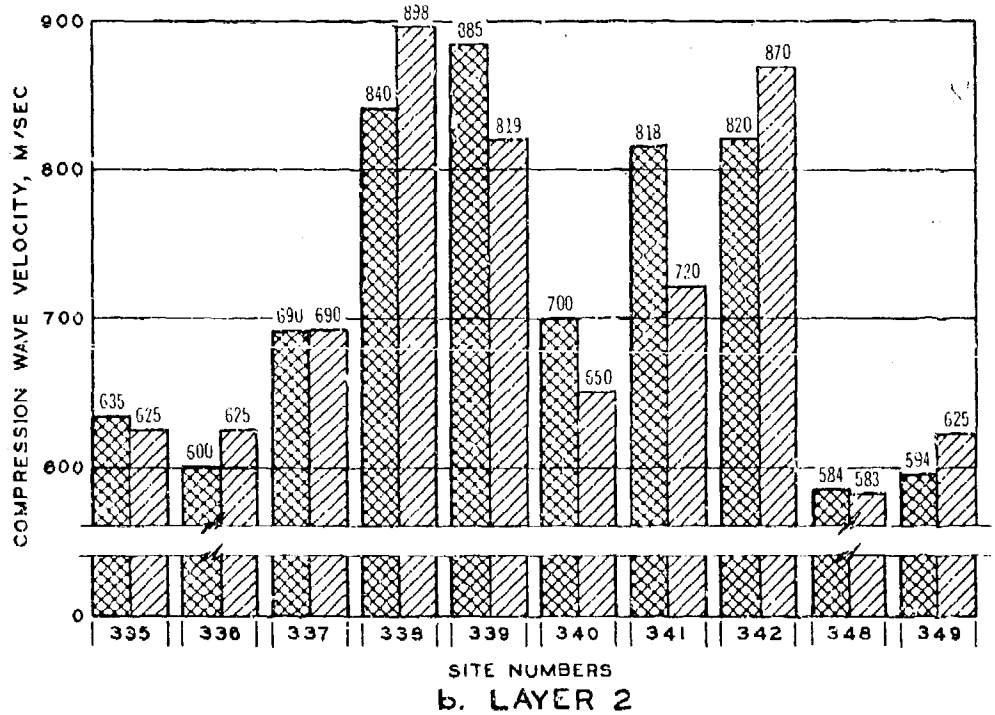

b. LAYER 2

Fig. 34. Comparison of compression wave velocities for layers 1 and 2 for the wet and dry seasons

variation for layer 1 was greater than the season-to-season variation. The same trends hold for the layer 2 compression wave velocities, i.e., the site-to-site variation was greater than the season-to-season. For all sites for which data are presented, the compression wave velocity of the second layer was greater than the compression wave velocity of the first layer. The maximum season-to-season variation was 75 m/sec (site 338) for layer 1 and 98 m/sec (site 341) for layer 2.

129. The wet- and dry-season values of shear wave velocities in layers 1 and 2 are portrayed in fig. 35. From these data it can be seen that the shear wave velocity in the first layer was consistently less than that in the second layer. For layer 1 the dry-season site-to-site shear wave velocities ranged from 129 to 207 m/sec (sites 336 and 338, respectively), whereas the wet-season shear wave velocities ranged from 137 to 182 m/sec (sites 339 and 348, respectively). For layer 2 the dry-season site-to-site variation ranged from 256 to 371 m/sec (sites 337 and 349, respectively) and the wet-season variation ranged from 245 to 346 m/sec (sites 336 and 342, respectively). The maximum measured season-to-season variation (40 m/sec) occurred at site 336, and the minimum (12 m/sec) occurred at site 335. In general, the season-to-season shear wave velocity data are greater in layer 2 than in layer 1.

130. The layer thicknesses of refraction layers 1 and 2 during the wet and dry seasons are compared in fig. 36. The data for layer 1 show a site-to-site thickness range of 50-140 cm for dry-season conditions and a site-to-site thickness range of 55-150 cm for wet-season conditions. These extremes occurred at sites 340 and 339, respectively. The maximum season-to-season thickness variation for layer 1 was 25 cm at site 349, and the minimum thickness variation was 5 cm at sites 337 and 340. The site-to-site thickness variation for layer 2 was much greater than for layer 1 with values for layer 2 ranging from 135 to >1575 cm and 110 to >1555 cm for the dry and wet seasons, respectively. These extremes occurred at sites 336 and 338, respectively. Sites 338, 339, 341, and 342 had very thick second layers (i.e. >1500 cm) in both seasons. (Values shown for these sites were limited by the length of the refraction line; therefore, they were not used to determine maximum

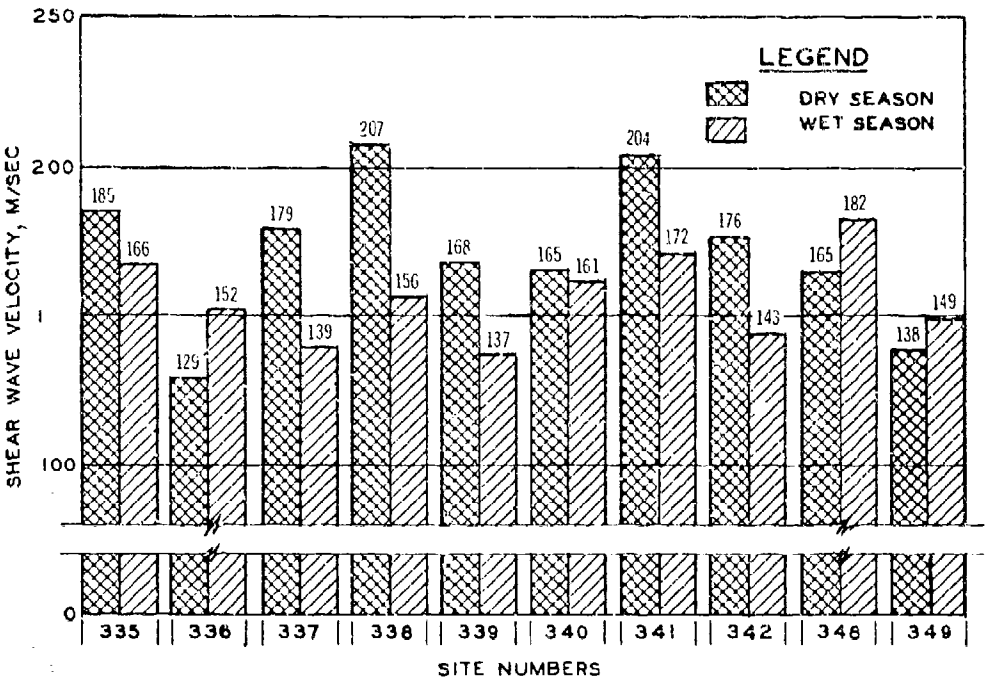

a. LAYER 1

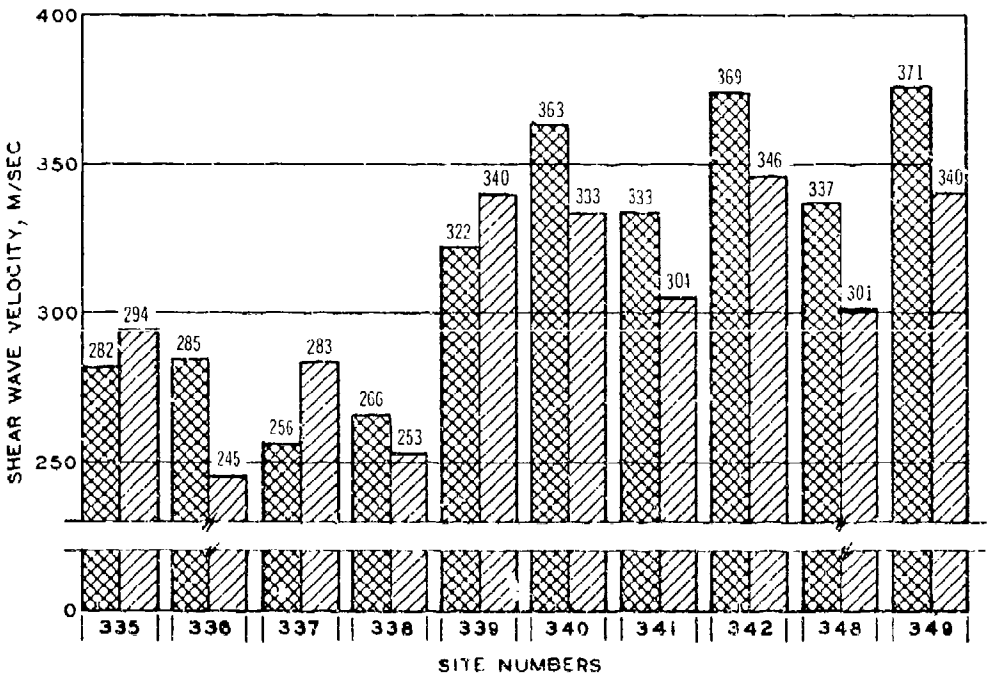

b. LAYER 2

Fig. 35. Comparison of shear wave velocities for layers 1 and 2 for the wet and dry seasons

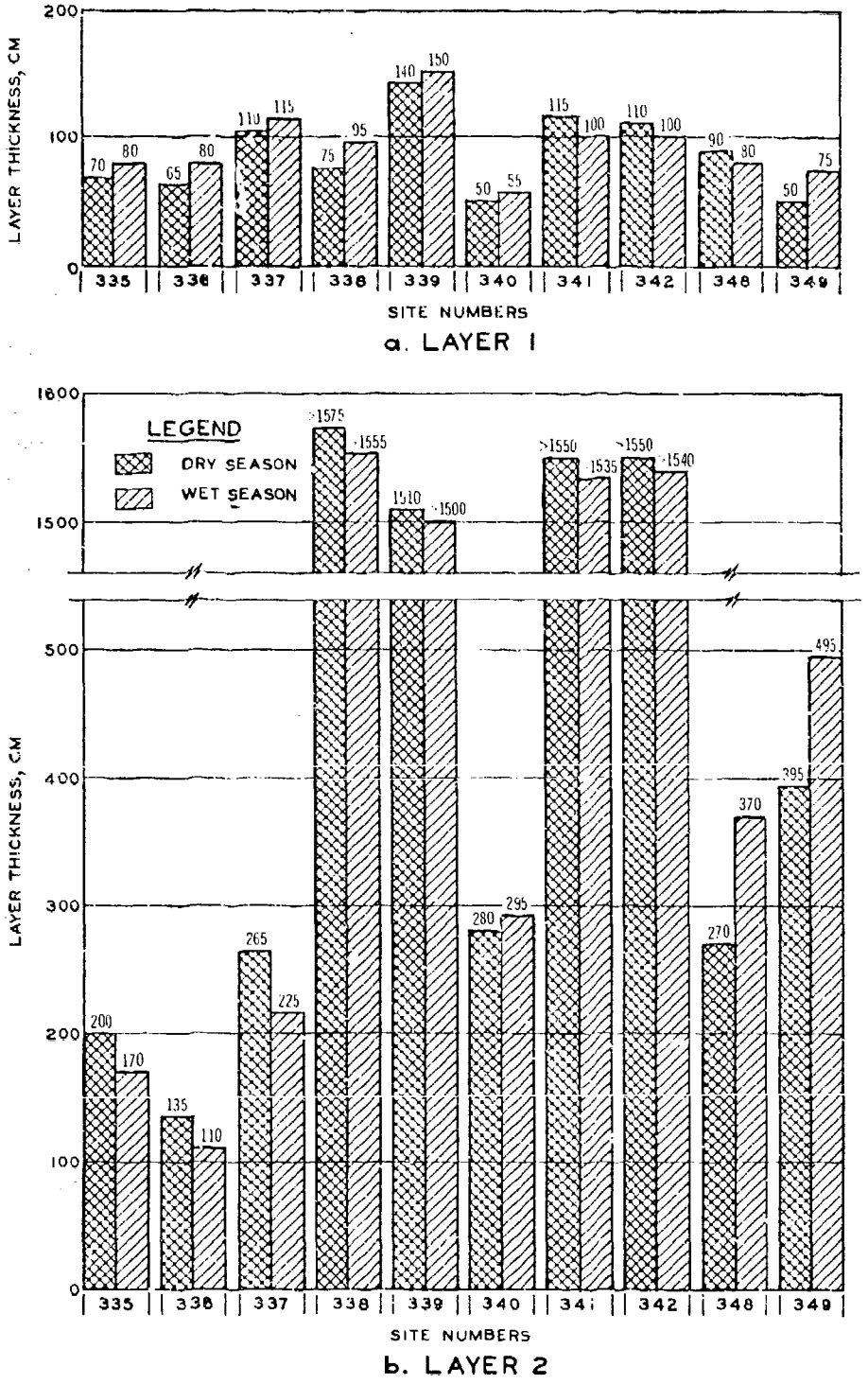

Fig. 36. Comparison of layer thicknesses for layers 1 and 2 for the wet and dry seasons

and minimum thicknesses.) The maximum season-to-season thickness variation in layer 2 was 100 cm at sites 348 and 349. The minimum season-to-season layer thickness variation (15 cm) also occurred in layer 2 at site 340.

131. A review of the wet densities in table 2 shows very little site-to-site variation in the first and second layers, i.e. values ranged from about 1.7 to 2.0 g/cm^3. As stated previously, the wet density varies as a function of moisture content, and the maximum seasonal variation in measured moisture content was 4.8 percent (site 349, layer 1). The rest of the moisture content values varied less than 3 percent. Therefore, the seasonal variation in wet density for the majority of sites was quite small.

132. Summary. The preceding paragraphs have discussed the temporal and spatial variation of the terrain factor either known (modeled) or assumed to have some effect on SID detection performance. The relative effects of terrain factors (and changes in them) cannot be specified in simple terms, because the propagating medium-seismic response interactions are exceedingly complex, and a practical and general theoretical solution requires extensive computer modeling. A general solution to this problem is being sought at WES, and a first-generation model has been developed (see reference 17). It is recommended that this model be used to perform sensitivity analyses on the Fort Huachuca data to establish the relative effects of the various terrain factors on seismic wave generation and propagation. Once this is accomplished, only those factors causing significant changes in SID detection ranges would require measurement in support of SID testing.

Data for sensor air-implantation performance predictions and evaluations

133. Data derived for use as input to equations (Appendix C) that predict implantation performance of air-delivered SID's are: the initial Young's modulus of elasticity, ultimate shear strength, compressibility parameter, soil mass density, and drag coefficient. The methods for deriving these factors from the uniaxial strain and triaxial compression tests are presented in paragraphs 87-92. The laboratory-obtained

data on these factors for airdrop areas 1, 4, and 5 are listed in table 13. Airdrop areas 2, 3, and 6 (see fig. 4 for location of areas 2 and 3 and fig. 5 for the location of area 6) were also selected for study of penetration characteristics of air-delivered SID's, but time and funding constraints prohibited any work on these areas. Airdrop area 2 had been selected to provide an area that would be impenetrable because of the numerous rock outcrops and shallow soil. Airdrop area 6 had been selected to present a target of soft material to study the effects of deep implantation of air-delivered SID's; and area 3 had been selected as a target of intermediate difficulty, along with airdrop areas 1, 4, and 5. The following paragraphs briefly discuss the input data obtained for airdrop areas 1, 4, and 5 for use with equations (Appendix C) that predict penetration depths of air-implanted SID's.

134. Average initial Young's modulus. The average initial Young's modulus E was obtained by taking an average E value from the deviator stress-axial strain relations, such as those illustrated by the example in fig. 18. The E values for airdrop areas 1, 4, and 5 are given in table 13. The dry-season E values varied from 560 to 1400 kg/cm^2 with test pit 5 in airdrop area 1 having the lowest value and test pit 6 in airdrop area 1 and test pit 2 in airdrop area 5 having the highest values. The wet-season E values are considerably lower, especially for airdrop areas 1 and 5.

135. Ultimate shear strength. The ultimate shear strength σ_u was obtained from the relations of maximum stress difference $(\sigma_a - \sigma_r)$ versus mean normal stress $(\sigma_a + 2\sigma_r)/3$ presented in fig. 37. The value of σ_u was determined by the procedure given in paragraph 91. For the dynamic yield envelopes (fig. 37) corresponding to wet-season conditions (i.e. high moisture values) for all airdrop areas and dry-season conditions (i.e. low moisture values) for airdrop area 5, pit 2, the ultimate shear strengths were determined from the maximum obtainable values of $\sigma_a - \sigma_r$ portrayed in fig. 37, utilizing equation 2. For the dynamic yield envelopes corresponding to dry-season conditions for airdrop area 1, pit 6, airdrop area 4, pits 3 and 4, and airdrop area 5, pit 1, a different procedure was used. The dynamic yield envelopes portrayed

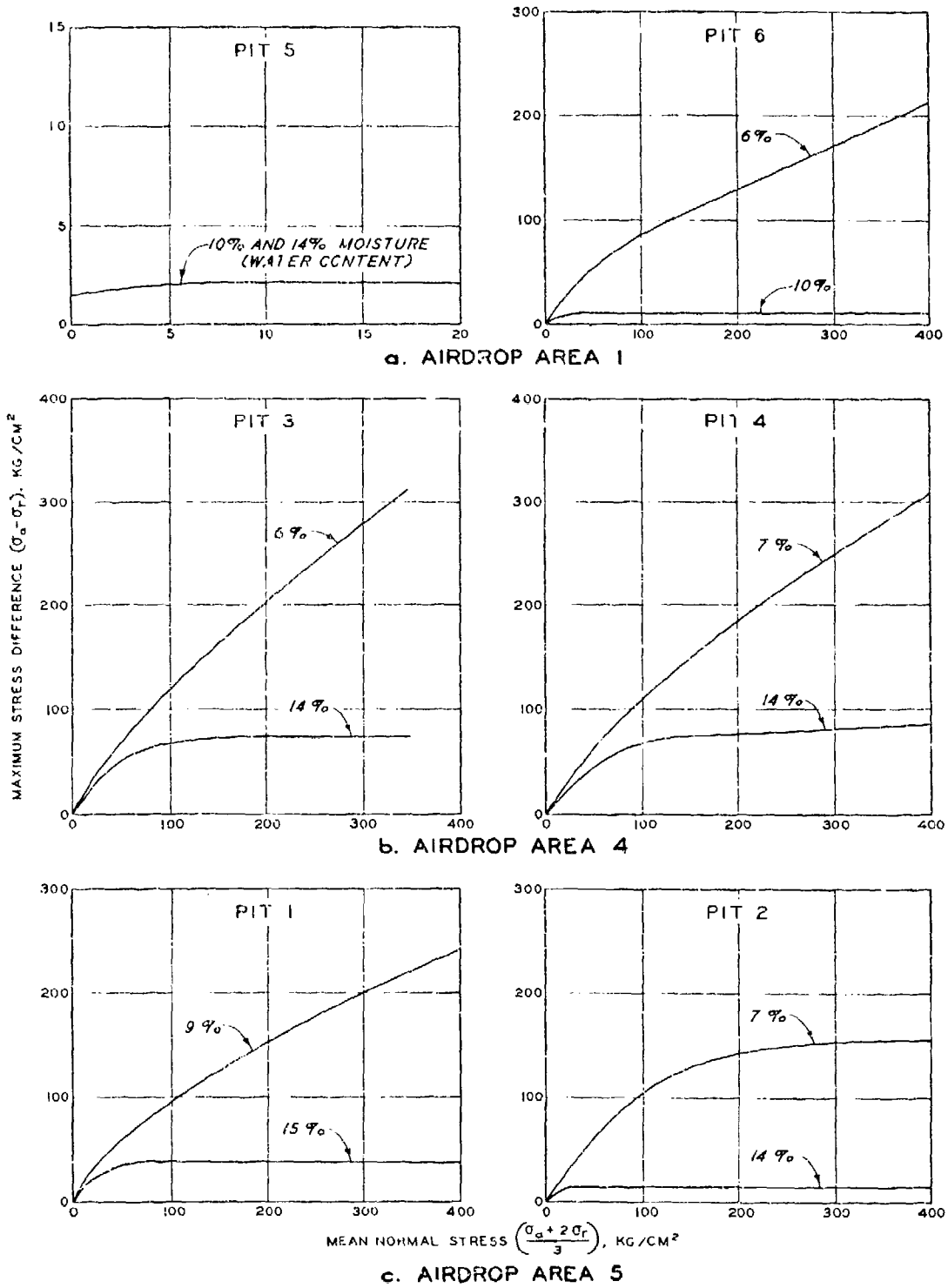

Fig. 37. Dynamic yield surfaces from triaxial compression test, airdrop areas 1, 4, and 5

by these airdrop areas did not reach a maximum value of $\sigma_a - \sigma_r$ (i.e. the slopes of the curves did not approach zero) for the range of mean normal stresses considered in the triaxial test. Since additional high pressure (i.e. mean normal stress) stress-strain data would have been required to obtain a maximum value of $\sigma_a - \sigma_r$ for these soil materials, and since the system of equations used to predict the depth of penetration of the ADSID/S was determined to be very insensitive to ultimate shear strengths larger than approximately 85 kg/cm^2 for the velocity range considered in this study, it was decided that $\sigma_a - \sigma_r$ values corresponding to a mean normal stress of about 300 kg/cm^2 would be sufficient for use in computing the ultimate shear strength of each of these airdrop areas (i.e. airdrop area 1, pit 6, airdrop area 4, pits 3 and 4, and airdrop area 5, pit 1, during dry-season conditions). The σ_u values used to determine penetration depths for the various airdrop areas are given in table 13.

136. The largest value of σ_u was obtained at airdrop area 4 and the lowest at airdrop area 1 during both the wet and dry seasons. Increase in soil moisture reduced the value of σ_u significantly. For the three airdrop areas for which ultimate shear strength data were obtained, the wet-season to dry-season variations were greater than the variations among airdrop areas 1, 4, and 5.

137. Compressibility parameter. The compressibility parameter ρ_p/ρ was computed using the uniaxial strain data summarized in fig. 38 and the following field-measured values for ρ. The computation procedure is given in paragraph 90.

Drop Area	Test Pit	Initial Soil Density (ρ), g/cm^3 Dry Season	Wet Season
1	5	1.99	2.14
	6	1.73	1.84
4	3	1.61	1.73
	4	1.63	1.76
5	1	1.60	1.70
	2	1.70	1.81

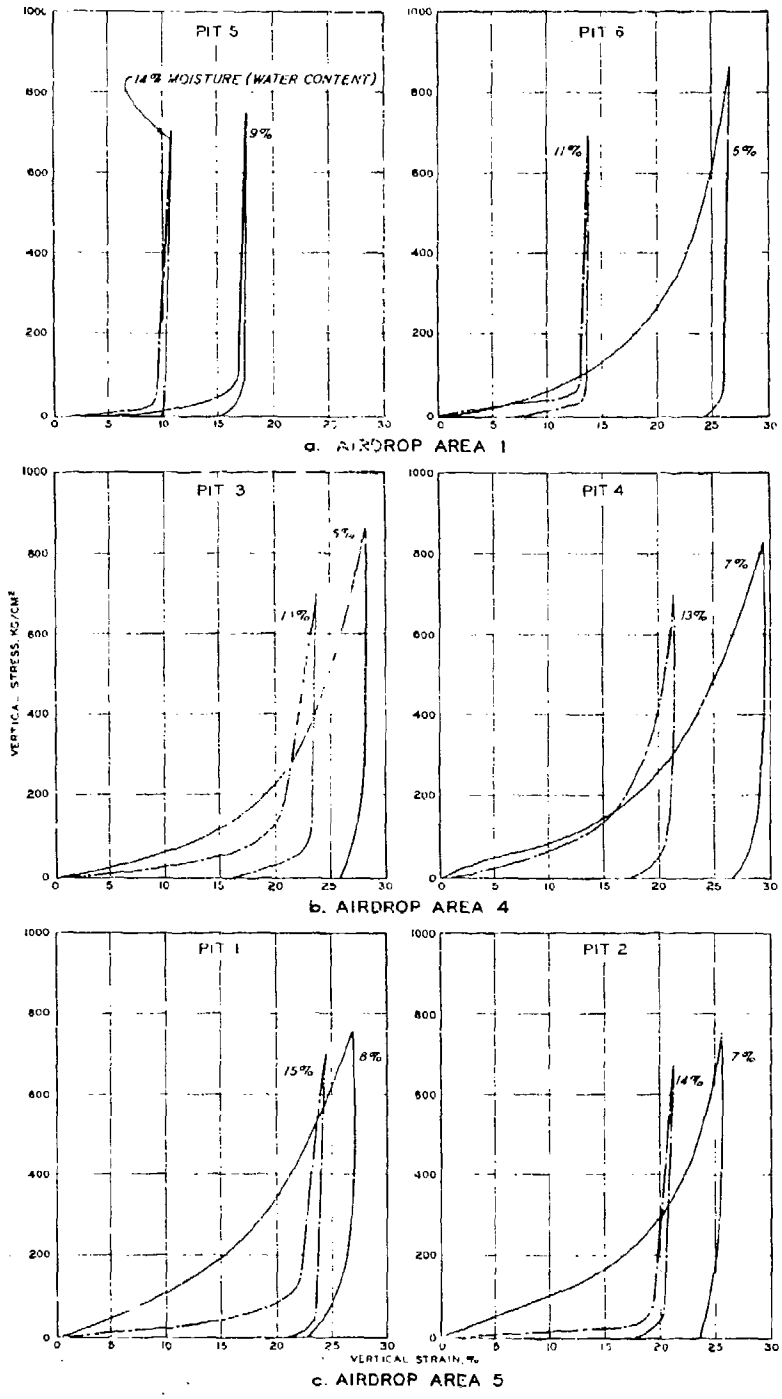

Fig. 38. Uniaxial strain data, airdrop areas 1, 4, and 5

The computed values in table 13 for the dry season vary from 1.18 to 1.33 and follow the same ranking trend as the ultimate shear strength data, in that the lowest values are for airdrop areas 1 and 5 and the highest values are for airdrop area 4. The season-to-season variation in the compressibility parameter data is smallest for airdrop area 5 and greatest for airdrop area 1.

138. Drag coefficient. The drag coefficient C_D computed as discussed in paragraph 92 resulted in a value of 0.2 for all sites and conditions, as shown in table 13.

139. Supplementary information. In addition to the information discussed in the previous paragraphs, soil profiles for airdrop areas 1 and 4-6 were prepared (fig. 39). Also some additional descriptive information taken in support of the seismic response tests is presented in table 2 for airdrop areas 1 and 3-6.

Prediction and Evaluation of MINISID Detection Performance

SID detection performance model

140. A theoretical simulation of the phenomena involved in sensor detection performance as depicted in fig. 1 is a complex mathematical problem, and a practical solution will require extensive use of the computer. As stated in paragraph 39, the detection problem has been divided into four component parts as follows:

a. The development of a forcing function that simulates transfer of energy from the seismic signal source to the substrate material.

b. The development of a seismic wave propagation model to simulate the propagation of microseismic waves within the substrate materials.

c. The development of functions that simulate the transfer of energy from the vibrating medium (substrate) to the sensor.

d. The development of functions that simulate the logic response of the sensor to the vibrating medium.

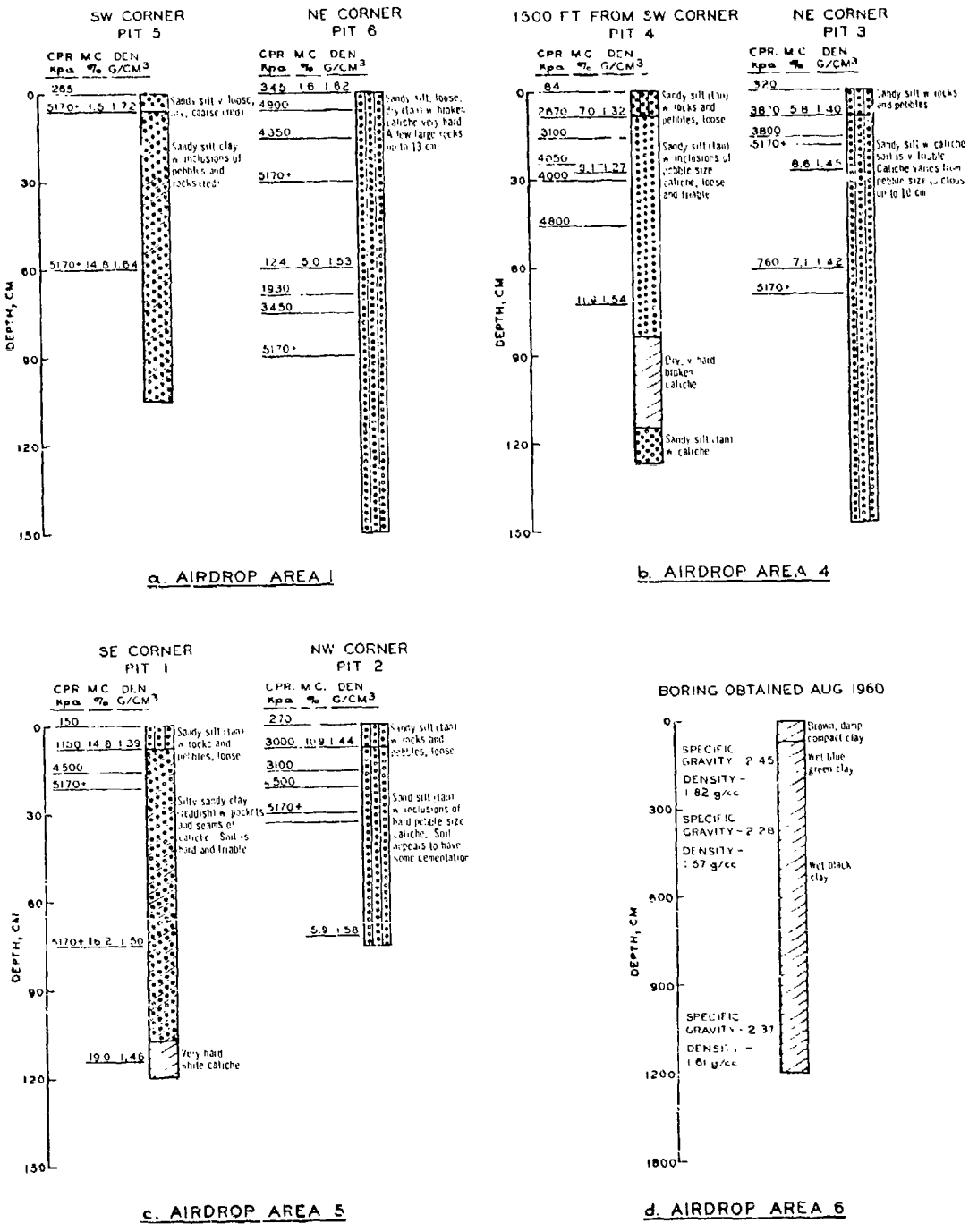

Fig. 39. Soil profiles for airdrop areas 1 and 4-6

141. Significant progress has been made to date on each component part of the overall sensor detection model. It is felt that once two serious omissions are incorporated into parts a and b above, the performance (i.e. detection range) of a SID system for both man-walking and moving-vehicle targets can be predicted realistically and quantitatively by utilizing the characteristics of the energy source and the input terrain surface and subsurface factor data. The omissions in parts a and b, respectively, are:

a. Component part a. A simulation of the stress applied to the ground from the source (i.e. a realistic force-time history of the source moving over the ground) has not been modeled.

b. Component part b. Macrogeometry coefficients representing local site conditions have not been available.

142. Functions describing the force-time histories of the energy sources are presently being developed by WES and will, hopefully, account for the transfer of energy from specified sources (i.e. drop hammer, footstep, vehicle, etc.) into the propagating substrate material. In support of b above, a literature review has been completed, and considerable information on the effects of macrogeometry on Rayleigh wave propagation has been compiled. However, these data have not been verified, and at the time of this report, they had not been incorporated into the overall detection prediction scheme.

SID detection distance predictions and evaluations

143. Forcing function and seismic wave propagation submodel predictions. To demonstrate the applicability of the forcing function and seismic wave submodels (i.e. component parts a and b of the overall detection model presented in paragraph 140), predictions of the analog signal as a function of distance from the source were derived for the drop-hammer energy source. These predictions are discussed briefly in the following paragraphs.

144. Laboratory measurements indicate that the restoring force associated with the drop hammer-soil system is a nonlinear function of

the displacement of the drop-hammer weight. The time-dependent forces exerted on the ground were calculated by using the Runge-Kutta method to numerically solve the differential equation of motion of the drop-hammer weight subject to a nonlinear restoring force. The calculations indicate that the forcing function can be approximated by a cosine squared pulse whose amplitude and pulse width are controlled by site conditions. To illustrate the effects of using a cosine squared pulse to simulate the force-time history of the drop-hammer energy source, it was experimentally determined (see reference 16) that a pulse width of 0.016 sec and a peak amplitude of 71.7×10^6 dynes were appropriate for the conditions for a selected site (site 341) at the time of test. (The cosine squared pulse obtained for site 341 is approximately equivalent to the stress produced by a footstep of a man weighing 73 kg and wearing size 9 boots.) This information was then used in conjunction with the field-measured properties listed below to obtain estimates of the span, peak amplitude, and rms amplitude within the predicted analog signal.

a. P-wave velocity of first refraction layer = 365 m/sec.
b. S-wave velocity of first refraction layer = 204 m/sec.
c. Wet density of first refraction layer = 1.75 g/cm^3.
d. Thickness of first refraction layer = 1.15 m.
e. P-wave velocity of infinite half-space (i.e. no second layer was encountered) = 818 m/sec.
f. S-wave velocity of infinite half-space = 333 m/sec.
g. Wet density of infinite half-space = 1.9 g/cm^3.
h. Soil damping coefficient $\zeta = 0.03$.

145. The resulting predictions of span, peak amplitude, and rms amplitude are plotted along with the measured values in fig. 40. As can be seen, the measured and predicted signals compare well in amplitude, frequency content, and duration. The frequency content of the cosine squared pulse appears to simulate the force-time history of the drop-hammer energy source, as indicated by the close agreement between the predicted and measured rms amplitudes.

146. The results presented (fig. 40) are for one site only, but similar results have been derived for other sites using similarly

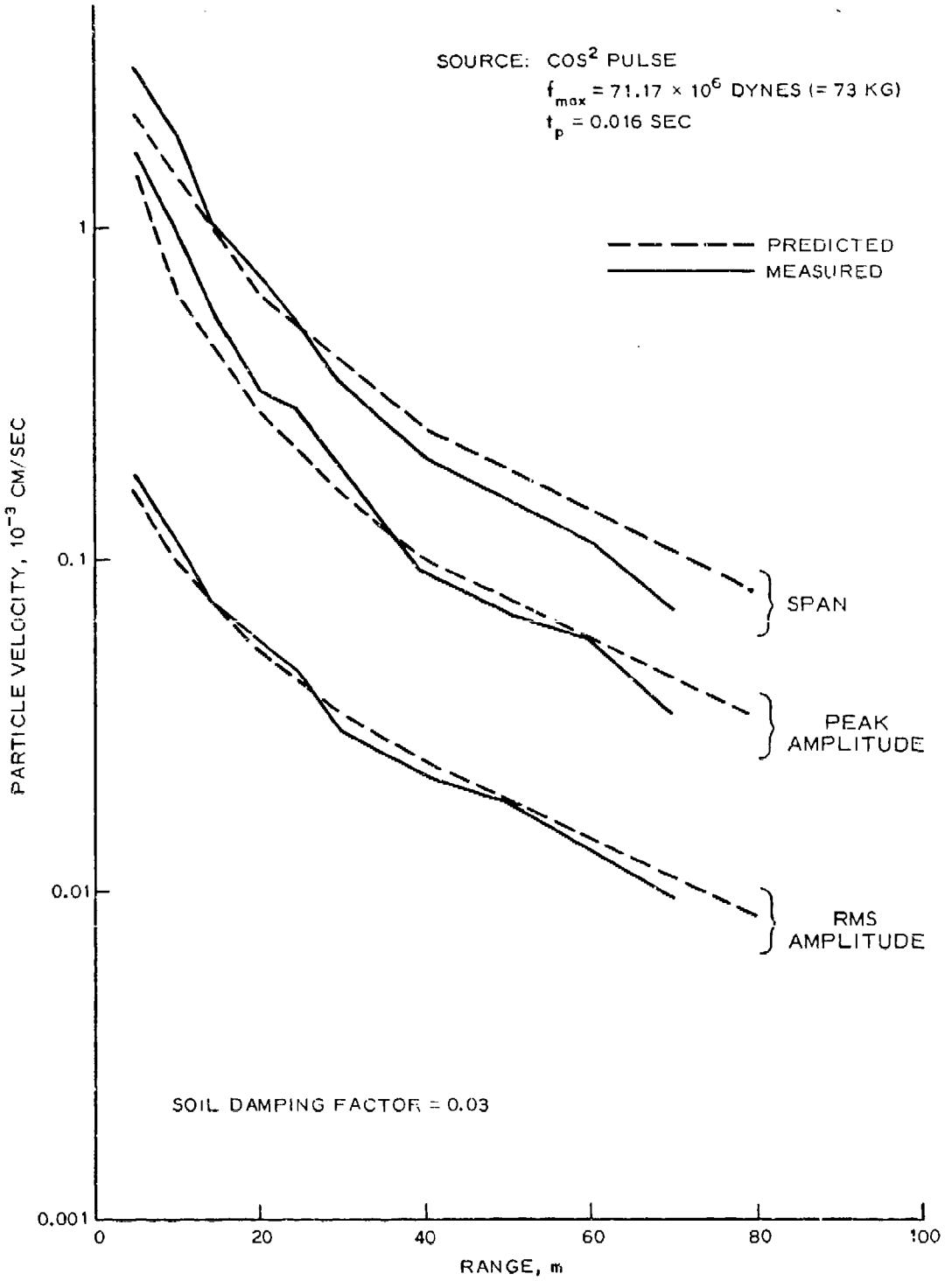

Fig. 40. Measured and computed signal characteristics for a simulated footstep, site 341

derived forcing functions. In addition, some predictions using forcing functions derived for the M151 and M113 vehicles have been made and compared with measured values. From the results obtained to date at WES, it seems reasonable to assume that current research will result in useful and workable solutions to the problems identified as component parts a and b in paragraph 140.

147. SID logic modeling. To study the problems associated with simulation of the transfer of energy from the vibrating medium to the SID and the logic response of the SID (component parts c and d in paragraph 140), use was made of the Phase III MINISID and analog man-walking test results. To derive a medium-gain detection distance, the field-measured analog recordings of the seismic response from a man-walking test were analyzed by an analog computer programmed to duplicate (model) the functioning logic of the MINISID. (A description of the analog computer model is given in Appendix D.)

148. Measured MINISID detection distances, the detection distances predicted by the analog computer model, and the differences between the two are presented in table 14. A plus sign (+) indicates that the model-predicted distance was greater than the measured distance, and a minus sign (-) indicates that it was less. Also presented are the mean difference, standard deviation, and the number of sites underpredicted and overpredicted for each geographical area (i.e. Fort Bragg, wet and dry seasons; Fort Huachuca, dry season; and several sites in West Germany).

149. From table 14, it can be seen that the measured and predicted values from the Fort Huachuca test sites were extremely close, with the mean and standard deviation of the differences being 3.1 and 4.4 m, respectively. Also, little bias toward overprediction or underprediction was observed, since eight sites were overpredicted and seven were underpredicted. The data from West Germany show a strong bias for overprediction and a relatively poor comparison, i.e. mean and standard deviation of 12 and 7.5, respectively. The Fort Bragg results were intermediate between the Fort Huachuca and the West Germany data.

150. The measured and predicted (modeled) detection distances

(table 14) for sites at each of the three geographical areas are quite close, especially when the following items are considered. The predicted distances were derived from one test (or, in some cases, two), whereas the MINISID detection distances were averages of from 5 to 15 tests. Also, the MINISID's used were production line items and were not the same in each area; the relative performances of the devices are not known. Further the background noise from one test to another could not be controlled, and as the wind or cultural activity changed, the background noise changed from test to test, and this induced significant effects on the test results (see paragraph 110).

151. Summary. The implication of these tentative analog computer results is that component parts c and d (paragraph 140) can be solved analytically. The transfer functions for any particular sensor can be readily derived and programmed on an analog or digital computer, thus giving a means for predicting SID performance if the analog wave train is available. The effect of geophone coupling was not adequately tested in these experiments because good coupling can usually be accomplished with the external geophone of the MINISID. Further study is needed to determine coupling efficiency as a function of sensor mass and geometry.

Prediction and Evaluation of Penetration Depths and Impact Deceleration Values for the ADSID/S

152. To derive an estimate of the range of air-implantation difficulty and the amount of deceleration that a typical air-delivered SID (Phase III ADSID/S, MA37) would experience at airdrop areas 1, 4, and 5, a theoretical study was performed using the system of equations in Appendix C. The depth of penetration for vertical (normal) impact and for an angle of 45 deg (oblique impact) and peak deceleration values for normal-impact conditions were predicted and are discussed in the following paragraphs. For both the normal and oblique impact configurations, the penetration calculations were terminated when the fin assembly (see fig. 13) of the ADSID/S sensor came in contact with the surface of the soil. This was done since no information was available on the behavior of the fin assembly and the tailplate to determine whether the assembly

would break, bend, or shear off when it came in contact with the substrate material during the penetration event.

Prediction of depth of penetration

153. Normal-impact predictions. Theoretical predictions of depth of penetration and deceleration were obtained for a normal-impact configuration of the ADSID/S for each of the six sites (i.e. six soil pits) within airdrop areas 1, 4, and 5. Two moisture contents were used that were assumed to be representative of the wet and dry seasons, respectively. The predicted depths are presented as a function of impact velocity in fig. 41. These relations reflect the terrain variations encountered within each of the areas. The location of the test pits represented by these predictions is shown in fig. 16.

154. Oblique-impact predictions. Theoretical predictions were also made for oblique (off-normal) impact configurations for each of the six sites within airdrop areas 1, 4, and 5, again with two moisture contents used. A theoretical solution for predicting the penetration of a projectile striking the soil at an oblique angle has not been adequately formulated. However, experience at WES has shown that for shallow penetrations a reasonable approximation of the depth of penetration for oblique impacts can be obtained by resolving the velocity vector (i.e. velocity along the trajectory of the projectile) into its horizontal and vertical components and then determining the vertical penetration (i.e. the vertical distance from the surface of the ground to the tip of the nose of the projectile) corresponding to the vertical component of the velocity vector. In order to obtain the penetration path length, the vertical penetration depth must be divided by $\cos \theta$, where θ is the angle of impact off vertical. Mathematically, the vertical (normal) impact velocity is expressed as

$$V_v = V_a \cos \theta$$

where

V_v = normal component of impact velocity vector

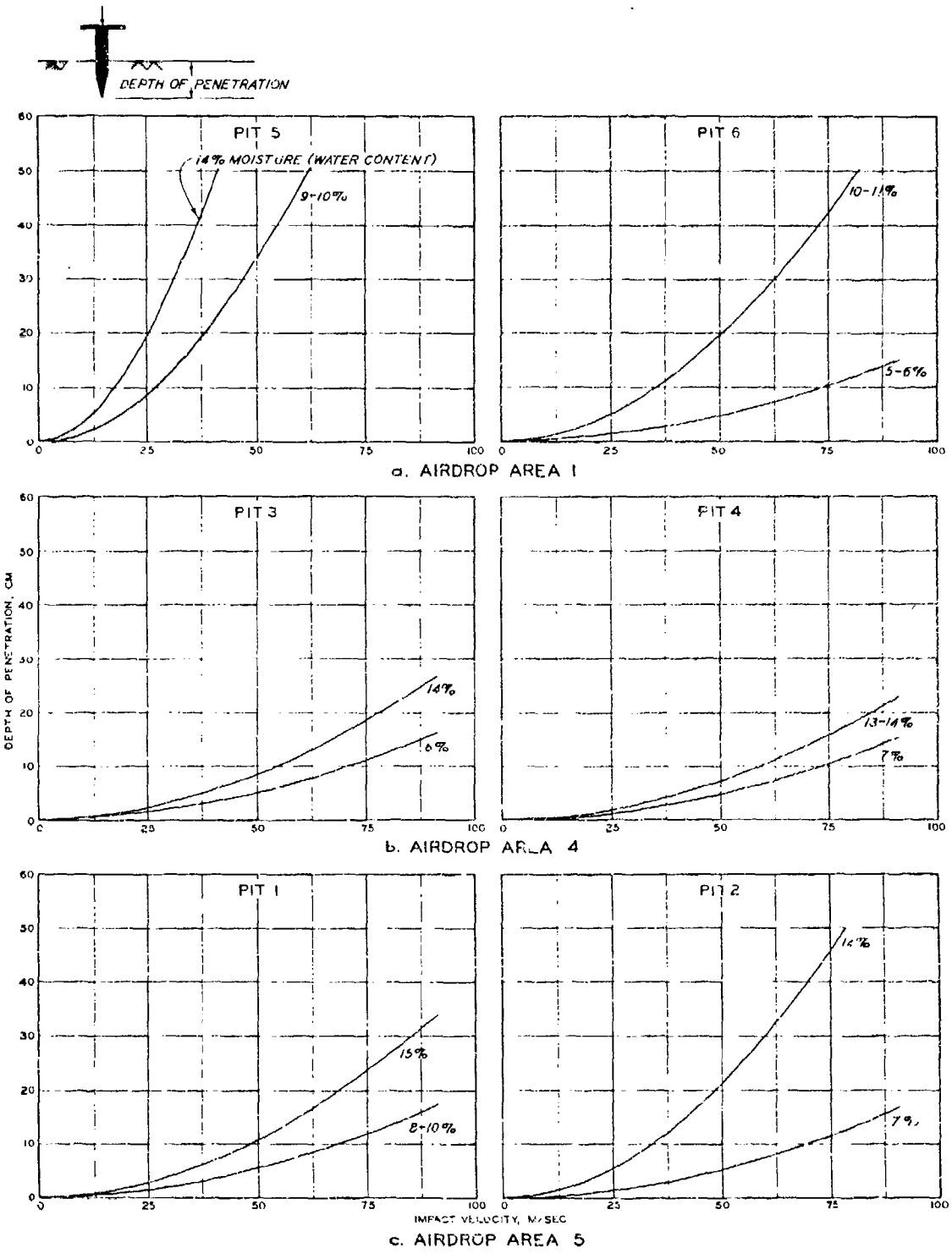

Fig. 41. Prediction of normal-impact penetration curves for ADSID/S, airdrop areas 1, 4, and 5

V_a = velocity vector along longitudinal axis of the ADSID/S (i.e. along the projectile trajectory)

θ = angle of impact (off vertical)

155. This technique was used to compute the depth-of-penetration predictions for an impact angle of 45 deg (fig. 42). The impact velocity portrayed in fig. 42 is the velocity vector along the 45-deg trajectory.

156. From the data (fig. 41) relating depth of penetration to impact velocity for vertically impacting ADSID/S's, it is noted that there is considerable variation in the penetration depths within and between the drop areas, and that the penetration depths are very dependent upon the amount of soil moisture. To illustrate the effects of moisture on the prediction depths, let it be assumed that 20 cm of penetration are required to ensure that the ADSID/S is emplaced sufficiently deep to operate as designed. From fig. 41, the impact velocities required to obtain a 20-cm depth of penetration for each airdrop area are as follows:

Area	Pit	Impact Velocity (m/sec) for 20-cm Penetration	
		Wet	Dry
1	5	25	38
	6	50	>100
4	3	78	>100
	4	89	>100
5	1	68	>100
	2	48	>100

157. The wet-season impact velocities for a depth of penetration of 20 cm vary from 25 m/sec (area 1, pit 5) to 89 m/sec (area 4, pit 4); whereas the dry-season velocities vary from 38 m/sec (area 1, pit 5) to >100 m/sec (all other five pits). The data tabulated above suggest that during the wet season, area 1 offers the least penetration resistance; whereas during the dry season only that portion of area 1 represented by pit 5 offers the least resistance. During the dry season, area 1, pit 6, and areas 4 and 5 require impact velocities greater than 100 m/sec to obtain a 20-cm penetration. The impact velocity normally used (i.e. the

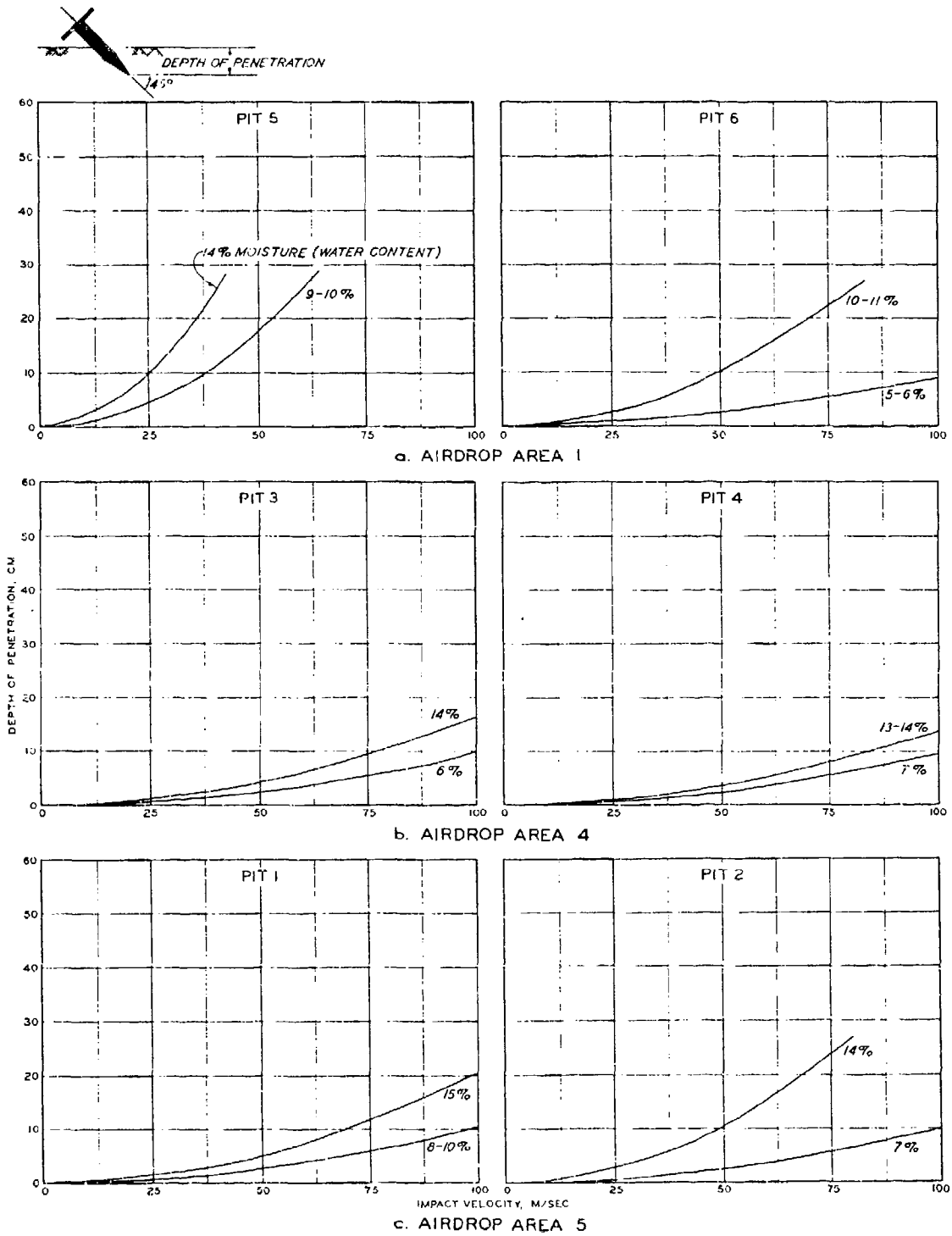

Fig. 42. Prediction of oblique-impact penetration curves for ADSID/S, airdrop areas 1, 4, and 5

anticipated velocity) for air-implantation of the ADSID/S is approximately 50 m/sec. The predicted depth-of-penetration curves show that at an anticipated optimum impact velocity of 50 m/sec, a depth of penetration of 20 m would occur only within area 1, pit 5, in both wet and dry seasons, and within area 1, pit 6, and area 5, pit 2, during the wet season.

158. In general, the ADSID/S impacts the ground at some angle off the vertical. Therefore, the results shown in fig. 41 show the highest value of penetration that could be expected at each drop area. Fig. 42 shows similar results for impact angles at 45 deg off the vertical. Normally, the impact angles are less than 45 deg off the vertical (see table 12 for experimental data); therefore, these curves should represent the minimum amount of penetration expected. As can be seen from the predicted curves, the impact velocity to allow a penetration of 20 cm would be greater than 100 m/sec for all sites (except area 1, pit 5) during the dry season and less than 100 m/sec for area 1 and pit 2 of area 5 during the wet season. If the impact velocity is assumed to be 50 m/sec, a 20-cm penetration path length would occur only at airdrop area 1, pit 5.

Prediction of maximum deceleration

159. The maximum rigid-body decelerations calculated for impact velocities of 50 m/sec for airdrop areas 1, 4, and 5 are listed in table 15. These calculations are for normal impacts of the ADSID/S. The specified maximum allowable deceleration for a workable Phase III ADISD/S, MA37, is approximately 9.85×10^3 m/sec^2. All computed deceleration values (see table 15) were over the maximum allowable deceleration value for a workable (i.e. operational) ADSID/S, except those for area 1, pit 5, during the wet and dry seasons, and area 1, pit 6, and area 5, pit 2, during the wet season.

Evaluation of theoretical depth-of-penetration predictions for oblique impacts

160. Since, as stated in paragraph 154, an adequate theory for predicting penetration of obliquely impacting projectiles is not

available, it was desired that the theoretical depth-of-penetration predictions made herein be experimentally verified. The ADSID/S tests conducted by CSEWS at Fort Huachuca provided a limited amount of data that could be used to estimate how well the theoretically predicted values, for obliquely impacting projectiles, matched the measured ones. To determine the terrain factor data in the CSEWS airdrop area, i.e. E, σ_u, ρ_p/ρ, μ, and C_D, laboratory tests were conducted on one bulk surface soil sample obtained from the area. Because of the small amount of soil available on the CSEWS area, laboratory tests (uniaxial and triaxial) were conducted at only one moisture content, i.e. 10 percent. These results, along with the results from two standard laboratory tests, grain-size distribution and Atterberg limits, were compared with corresponding data from all the sites in drop areas 1, 4, and 5. It was determined that the terrain conditions at the CSEWS airdrop area were similar to terrain conditions at area 1, pit 5, during the wet season (i.e. 14 percent moisture). This can be seen in fig. 43, where grain-size distributions for the two sites correspond quite closely, and in fig. 44, where the plasticity index and liquid limit data correspond quite closely. More significant is the similarity of the dynamic yield surfaces from the triaxial compression tests for the two sites as shown in fig. 45.

161. Based on the similarity between the test site conditions and the results of the triaxial compression tests, it was assumed that the depth of penetration-impact velocity relations generated for airdrop area 1, pit 5 (fig. 41), could be extrapolated to the CSEWS area, once they were corrected for moisture conditions at the time of test. From fig. 45 it can be seen that the dynamic yield surfaces derived from the triaxial tests were nearly identical for the soils at the CSEWS airdrop area at 10 percent moisture content and at airdrop area 1, pit 5, at 10-14 percent moisture content. For this reason it was assumed that penetration-impact velocity relations generated at 14 percent moisture content for area 1, pit 5, would correspond to the penetration-impact velocity relations at the CSEWS airdrop area at 10 percent moisture content. The relation for the CSEWS area is shown as a solid line in

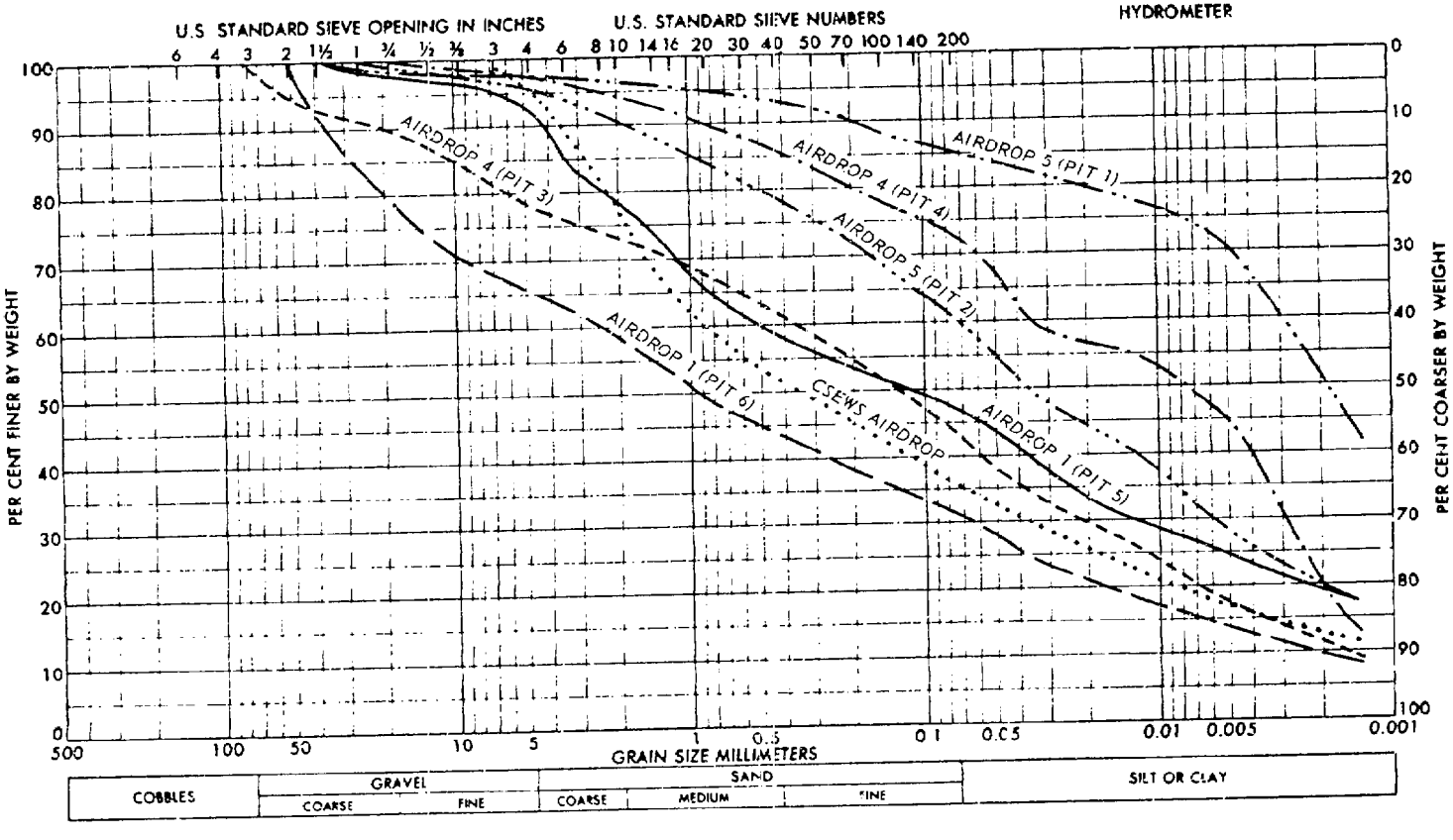

Fig. 13. Grain-size distributions in airdrop areas 1 and 4-6 and the CSEWS area

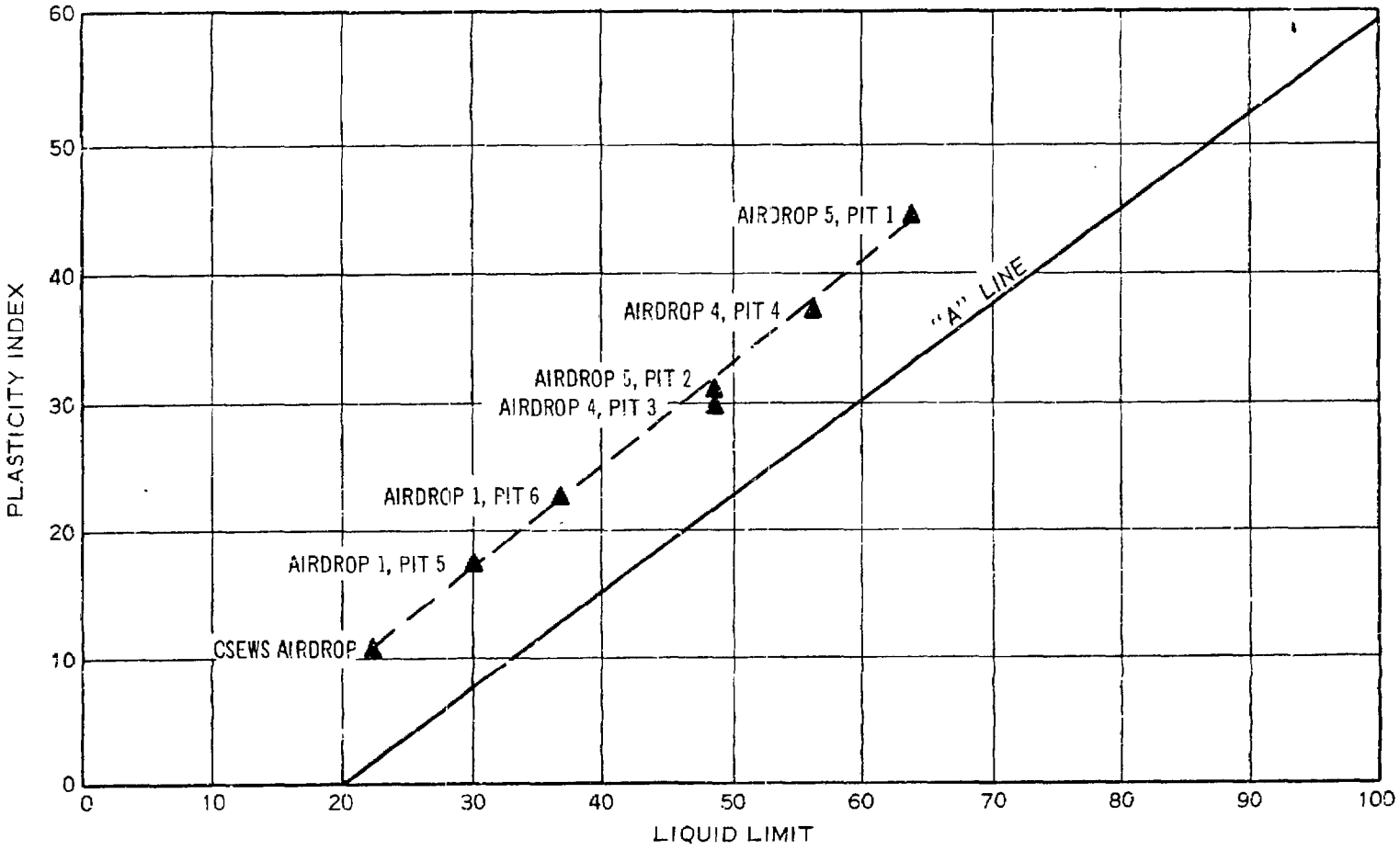

Fig. 44. Plasticity and liquid limit data for airdrop areas 1, 4, and 5 and the CSEWS area

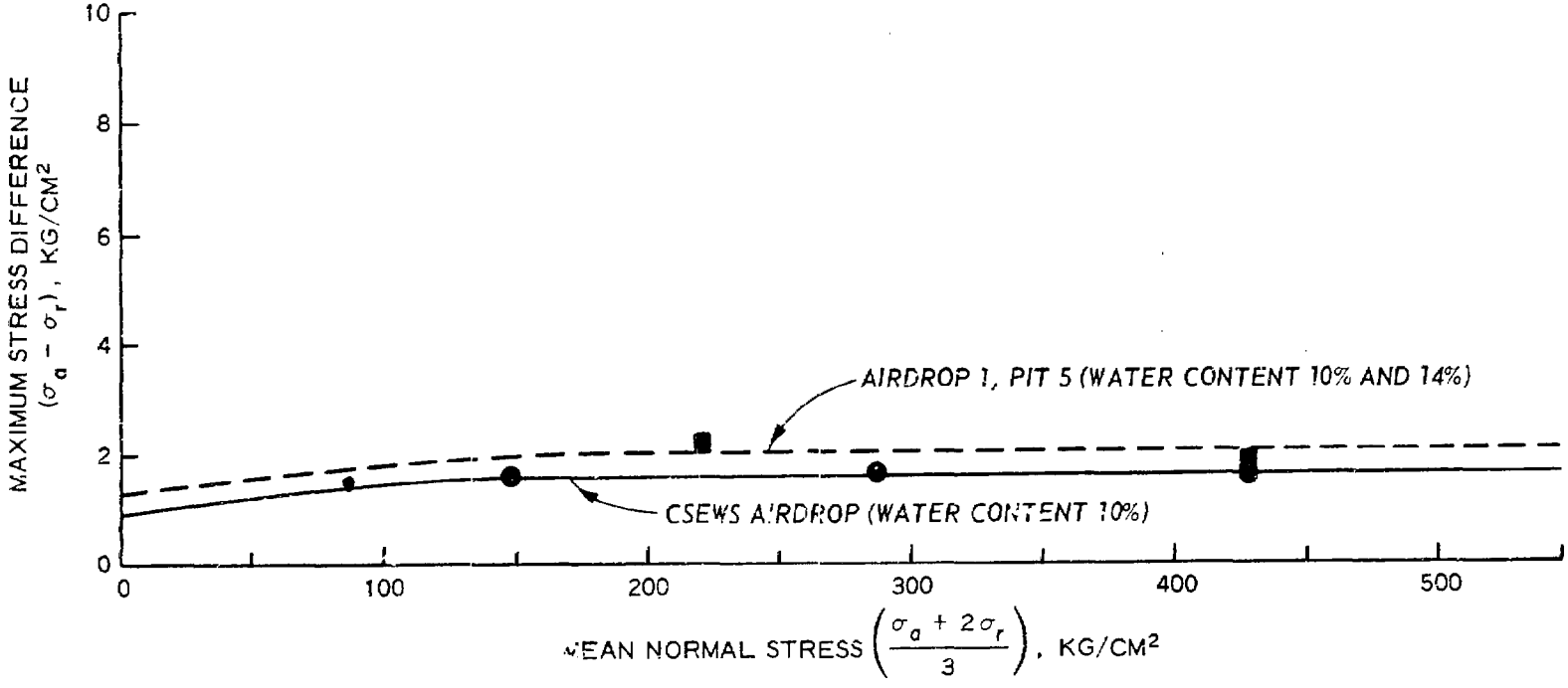

Fig. 45. Comparison of dynamic yield surfaces from triaxial compression tests for airdrop area 1 (pit 5) and CSEWS airdrop area

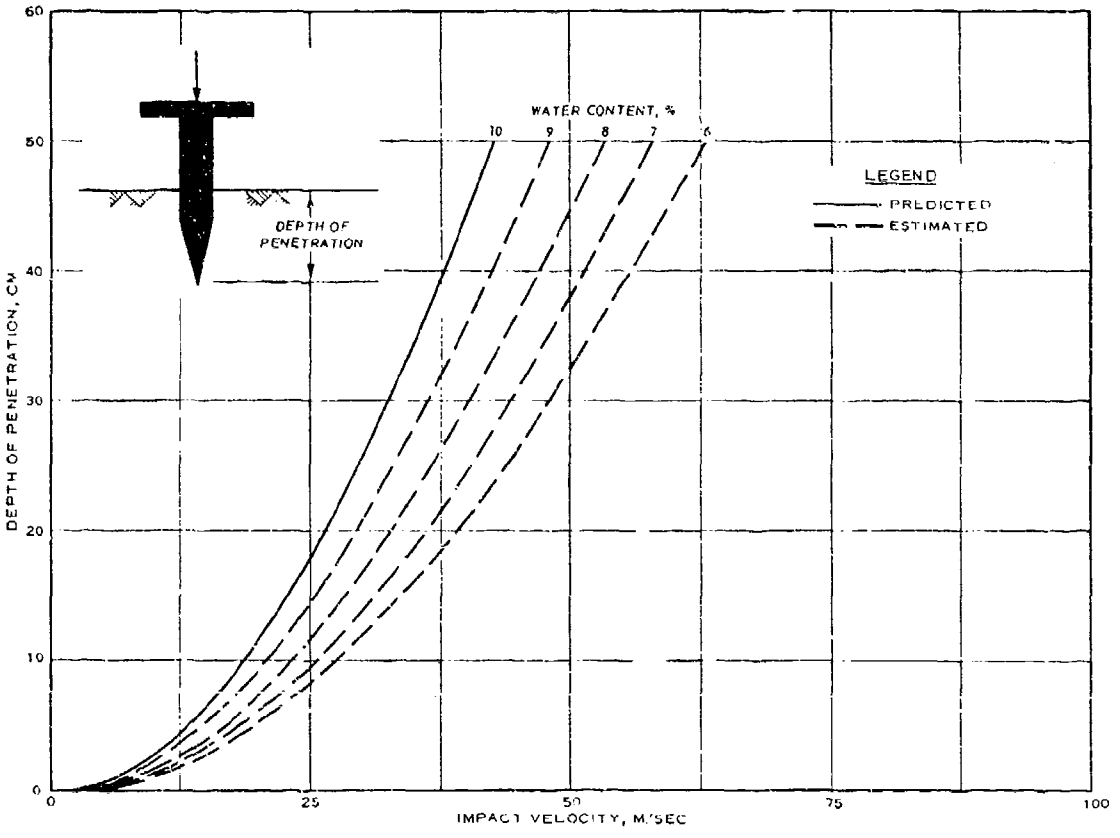

Fig. 46. Prediction of normal-impact penetration curves for various moisture contents, CSEWS airdrop area

fig. 46. Table 16 shows that the experimental ADSID/S tests (where impact velocities were measured) were conducted in soils whose moisture values ranged from 5.5 to 8.6 percent. To provide a basis for estimating the depth of penetration at these moisture contents, the penetration-impact velocity data shown as the solid line in fig. 46 were extrapolated to cover moisture contents at the time of the experimental ADSID/S tests. These extrapolated penetration impact relations are shown as dashed lines in fig. 46. The extrapolation was linear based on the spread of the 10 and 14 percent moisture curves shown in fig. 41 for area 1, pit 5.

162. Near-surface impact velocities were measured for 11 tests (i.e. tests 5, 9, 11, 12, 34, 36, 75, 76, and 78-80) at the CSEWS airdrop area. These tests were used as a basis for comparing the predicted

penetration values. The test data obtained at the CSEWS area include: (a) impact velocity vector along the trajectory of the ADSID/S, (b) ADSID/S impact angle, and (c) surface soil moisture content and strength. The predicted depth of penetration derived from the graphs shown in fig. 46 were compared with the field-measured depth of penetration values (table 16). Because all the test sensors (i.e. ADSID/S) impacted the ground at an angle off the vertical, the predicted length of penetration (as opposed to vertical depth of penetration) is used so that the predicted and measured values will be more directly comparable.

163. The method used to predict the depth of penetration was identical with that described in paragraph 154 and involved determining the vertical impact velocity (see bottom of table 16) from the impact velocity vector. Next, this velocity was used to enter the curves in fig. 46 at the appropriate field moisture content to determine the corresponding depth of penetration from which the length of penetration was calculated. This method of obtaining a prediction of the length of penetration does not adequately simulate the penetration phenomena for oblique impacts, but experience has shown that it yields relatively good approximation of penetration lengths, especially for shallow penetrations.

164. The results of this study appear to confirm this also because it can be seen that the deviations from measured penetration lengths range from an underprediction of 12 cm (test 75, table 16) to an overprediction of 8 cm (test 34, table 16). When the nonrigorous analytical procedures used to derive the penetration estimates are considered, the predicted results are surprisingly compatible with the measured values. Although this comparison cannot be interpreted as a verification of the theoretical depth-of-penetration predictions (figs. 41 and 42) it does increase confidence in the predicted penetration depths of the air-implanted SID's.

Summary

165. The airdrop areas (areas 1-6 and the CSEWS area) provided terrains covering a wide range of penetration characteristics. This variation in terrain conditions allows the testing of air-implanted

SID's under varying stress conditions (i.e. high to low rigid-body deceleration values) and under a variety of soil strength conditions.

Extrapolation of SID Performance Values

166. The WES concept for the extrapolation of SID test results is based on the assumption that adequate simulation models describing the phenomena under test can be formulated. In the case of SID detection performance, this involves simulating the generation, propagation, and coupling of the seismic energy from the source to the sensor. In the case of air-implantation of sensors, it involves simulating the penetration event of an air-delivered SID and the coupling of the SID to the soil. The extrapolation concept also requires that the terrain inputs to the simulation models be constitutive and measurable properties of the terrain, such that they can be classified and portrayed on an areal basis. Based on the data presented in this part of the report, it is felt that adequate simulation models required to implement the concept can be derived. For a discussion of the mapping of terrain factors on an areal basis see Part IV of this report.

PART IV: MAPPING OF TERRAIN AND SEISMIC RESPONSE FACTORS AND SID PERFORMANCE VALUES

167. The theoretical detection prediction scheme and/or concepts presented in this report provide an analytical framework for obtaining SID performance predictions for man-walking targets in various world terrains. A point worthy of reemphasizing is that the prediction scheme requires specific terrain and seismic input data for execution. In pursuit of a general SID detection prediction capability, as illustrated in fig. 2, this portion of the report pertains to the development of procedures for preparing terrain factor maps that will delineate the geographical distribution of the individual factors describing the relative seismic response of the area and those factors required or hypothesized as being required as input to the SID detection performance model (i.e. forcing function and seismic wave propagation submodels).

168. The terrain and seismic factor mapping discussed herein pertains to the Fort Huachuca hand-emplacement test area and consists of preparing four types of maps: (a) a terrain factor complex map for subsurface layers 1 and 2 to provide inputs to the theoretical seismic wave propagation model, (b) surface condition maps to be used with the forcing function model under development, (c) seismic response factor complex maps to show the relative seismic response of the hand-emplacement area, and (d) SID performance maps. The terrain and seismic response factor complex maps and the SID performance maps are based on data obtained by WES field teams during August 1971 and March 1972 and are assumed to be representative of the wet- and dry-season conditions at the test sites.

169. The terrain and seismic factors and the SID performance values (i.e. detection distances) mapped for the hand-emplacement area at Fort Huachuca provide a direct basis for comparing (i.e. correlating) the terrain and/or seismic factor conditions in other geographic regions, including the test areas at Fort Bragg[14,15] and in the Panama Canal Zone.[10,13] The following paragraphs describe the detailed procedures used in preparing the terrain and seismic factor maps and the SID performance map for the Fort Huachuca hand-emplacement area.

Terrain Factor Mapping for Subsurface Soil Layers

170. The four terrain factors that have been mapped are:

a. Thickness of layer 1 (T_1) and layer 2 (T_2).

b. Compression wave velocity for layer 1 (V_{P1}) and layer 2 (V_{P2}).

c. Shear wave velocity for layer 1 (V_{S1}) and layer 2 (V_{S2}).

d. Wet density for layer 1 (ρ_1) and layer 2 (ρ_2).

Terrain factor mapping classes

171. Since classification is a prerequisite to any mapping process, and the adequacy of the proposed map depends upon its class intervals, considerable effort was devoted to determining appropriate terrain mapping classes. Consideration also was given to selecting classes that could be used in comparing terrain conditions at Fort Huachuca with other TECOM SID test areas. The class intervals or class ranges of each of the terrain factors were chosen to minimize the effect of stratification. This was accomplished by selecting class ranges that would minimize the error when midpoint values on which to make predictions of SID detection performance are used; however, class intervals too small to be mapped adequately were avoided.

172. Two sets of terrain factor classes were established prior to mapping, one set for layer 1 and the other for layer 2. Before any mapping was accomplished, the midpoint values of the tentatively selected class ranges were input to the theoretical seismic wave propagation model to determine the adequacy of the selected ranges. If the PPV and rms amplitudes of the predicted signal obtained using the theoretical model compared closely with the PPV and rms amplitudes resulting from the field-measured drop-hammer signal, the mapping class ranges were considered adequate. If the comparison showed differences greater than 15 percent (for distances greater than 20 m), smaller mapping class ranges were selected, and the above-mentioned process was repeated until adequate classes were established for all terrain factors (V_P,V_S,T, and ρ). The four terrain factors and their selected mapping classes are listed in table 17.

Mapping of terrain
factors for layers 1 and 2

173. The terrain factors for layers 1 and 2 of the test area were mapped by using the environmental data collected during the field program, air-photo interpretation techniques, a topographic map of the area, and the interpreter's personal knowledge of the mapped area.

174. The air-photo interpretation was accomplished through a series of steps, the first being to obtain the necessary overlapping (stereo) photos of the hand-emplacement area. This was followed by a stereoscopic examination of the overlapping prints, whereby various photographic terrain patterns were identified, according to tone and texture, together with their topographic relations. For the photographic patterns within which ground truth (i.e. site) data were available, the class range as portrayed by the data for that particular site was used. In those patterns without ground truth data, the class ranges for each terrain factor were assigned by extrapolation from the points of known ground truth data, through associations of similar patterns and through the interpreter's knowledge of the area. After all the identified patterns had been outlined on the air photos, a map unit symbol representing a factor value class was assigned to each respective pattern. In effect, the resulting map portrayed the four factor value classes (table 17) for one terrain factor, such as wet density (ρ). Similar maps were then prepared for V_P, V_S, and T, respectively.

175. After the four terrain factors (V_P,V_S,T, and ρ) for each of the two layers had been mapped, they were combined into a factor complex map (fig. 47) by superimposing each of the individual maps on a common base map. To simplify the identification of each delineated area on the factor complex map, the areas were identified by numbers from 1 to 40. These numbers represent discrete combinations of classes of each of the four terrain factors for the two soil layers in the hand-emplacement area, and are contained in the factor complex map legend shown in table 18.

Evaluation of mapping classes

176. To determine the adequacy of the selected factor map class

NOTE: FOR LEGEND SEE TABLE 18.

Fig. 47. Terrain factor complex map for layers 1 and 2, hand-emplacement area. (For a larger print of this figure, see map 2 in pocket inside back cover)

ranges, a check was made by comparing the theoretical predicted results (using 20-m measured seismic (analog) signals and the prediction models described in Appendix D) for sites 335-342, 348, and 349 with the predicted values obtained using midpoint values of the class ranges from map units 1, 3, 10, 45, 51, 64, 89, 96, 103, and 115, respectively. The factor values used in the model to obtain the predictions for the site and mapped conditions are given in table 19. The results of this comparison are shown in table 20. Excellent correlation of results was obtained with the 20-m reference signals, the largest difference being 2 m observed at site 337, and map unit 103. In general, these results indicate that the selection of the factor mapping classes was a good compromise between prediction accuracy and mapping practicality.

Mapping of Surface Terrain Factors

177. The relative effect of surface terrain factors on the transfer of seismic energy from the source to the substrate has not been quantitatively determined. Nevertheless, surface moisture content, soil type, and surface CPR almost surely control the transfer of seismic energy for man-walking energy sources. For this reason, these terrain factors will almost certainly be required as inputs to the forcing function model under development. These three surface terrain factors have been mapped for the hand-emplacement area, and are discussed in the following paragraphs.

Surface soil moisture content

178. Six factor classes of soil moisture content for the dry and wet seasons were established for the mapping of the hand-emplacement area, as follows:

Factor Class	Surface Soil Moisture Factor Value Range percent
1	1-3
2	4-8
3	9-12

(Continued)

Factor Class	Surface Soil Moisture Factor Value Range percent
4	13-16
5	17-20
6	21-40

Soil moisture classes 4-6 did not occur in the hand-emplacement area during either the wet or dry season, but were established to provide the class ranges necessary for comparison of the Fort Huachuca SID hand-emplacement area with other TECOM SID test areas. The wet- and dry-season surface soil moisture content factor map for the SID hand-emplacement area is shown in fig. 48. The units on this map represent factor classes of each moisture factor class (1-3) range for the dry and wet seasons.

Surface soil type (or classification)

179. Five factor classes of surface soil type (i.e. soil classification by USCS) were established as follows:

Factor Class	Surface Soil Type Factor Value Range USCS Classification
1	SP
2	SC
3	OL
4	SM
5	GM

The SP material consisted of a relatively clean sand with little or no fines, the SC material consisted of a sand with an appreciable amount of fines (i.e. a sand-clay mixture), the OL soil was primarily an organic silt, the SM was a sand-silt mixture with low plasticity, and the GM was a gravel-sand-silt mixture. (Soil type class 3 (OL) did not occur in the hand-emplacement area.) The soil type map for the hand-emplacement area is presented as fig. 49.

Surface cone penetration resistance (CPR)

180. Six factor classes of surface CPR were also established for

MAP UNIT	MOISTURE FACTOR CLASS	
	DRY SEASON	WET SEASON
1	1	2
2	2	3
3	1	3

FACTOR CLASS	MOISTURE FACTOR CLASS RANGE, %
1	1-3
2	4-8
3	9-12

Fig. 48. Surface moisture content factor map, hand-emplacement area

MAP UNIT	SOIL TYPE
1	SP
2	SC
4	SM
5	CM

Fig. 49. Surface soil type map, hand-emplacement area

the mapping of the hand-emplacement area as follows:

Factor Class	Surface Cone Penetration Resistance (CPR) Factor Value Range, kPa
1	0-200
2	200-400
3	400-600
4	600-900
5	900-1200
6	1200-1800

The mapping units portrayed by the various patches on the surface CPR map (fig. 50) include the factor classes for both the wet- and dry-season conditions.

Mapping of Dry-Season General Seismic Response Factors

181. The three dry-season general descriptors (i.e. PPV, PSPV, and f as functions of distance) as determined by the seismic signal generated by the drop-hammer (controlled) energy source were used for mapping the seismic response of the hand-emplacement area. (Wet-season data could not be used, as discussed in paragraph 101.) Prior to mapping, best-fit curves representing the field-measured drop-hammer PPV, PSPV, and f data (table 8) were generated. The PPV, PSPV, and f data for selected distances were then obtained from the best-fit curves (table 8) and these data were used as a basis for constructing the seismic response complex map (fig. 51). The factor classes established for the mapping of the three descriptors were designed to be responsive to the operational logic of Phase III SID's (see fig. A3, Appendix A) and the distribution of the factor classes that occurred within the hand-emplacement area.

Seismic response factor mapping classes

182. PPV and PSPV mapping classes. The factor mapping classes (table 21) were selected such that classes 1, 2, and 3 would generally

SCALE IN METERS
200 0 200 400

MAP UNIT	SURFACE CPR FACTOR CLASS DRY SEASON	WET SEASON
1	3	1
2	3	2
3	3	3
4	3	4
5	4	4
6	4	6
7	6	4

FACTOR CLASS	CPR FACTOR CLASS RANGE - kPa
1	0 - 200
2	200 - 400
3	400 - 600
4	600 - 900
5	900 - 1200
6	1200 - 1800

Fig. 50. Surface cone penetration resistance factor map, hand-emplacement area

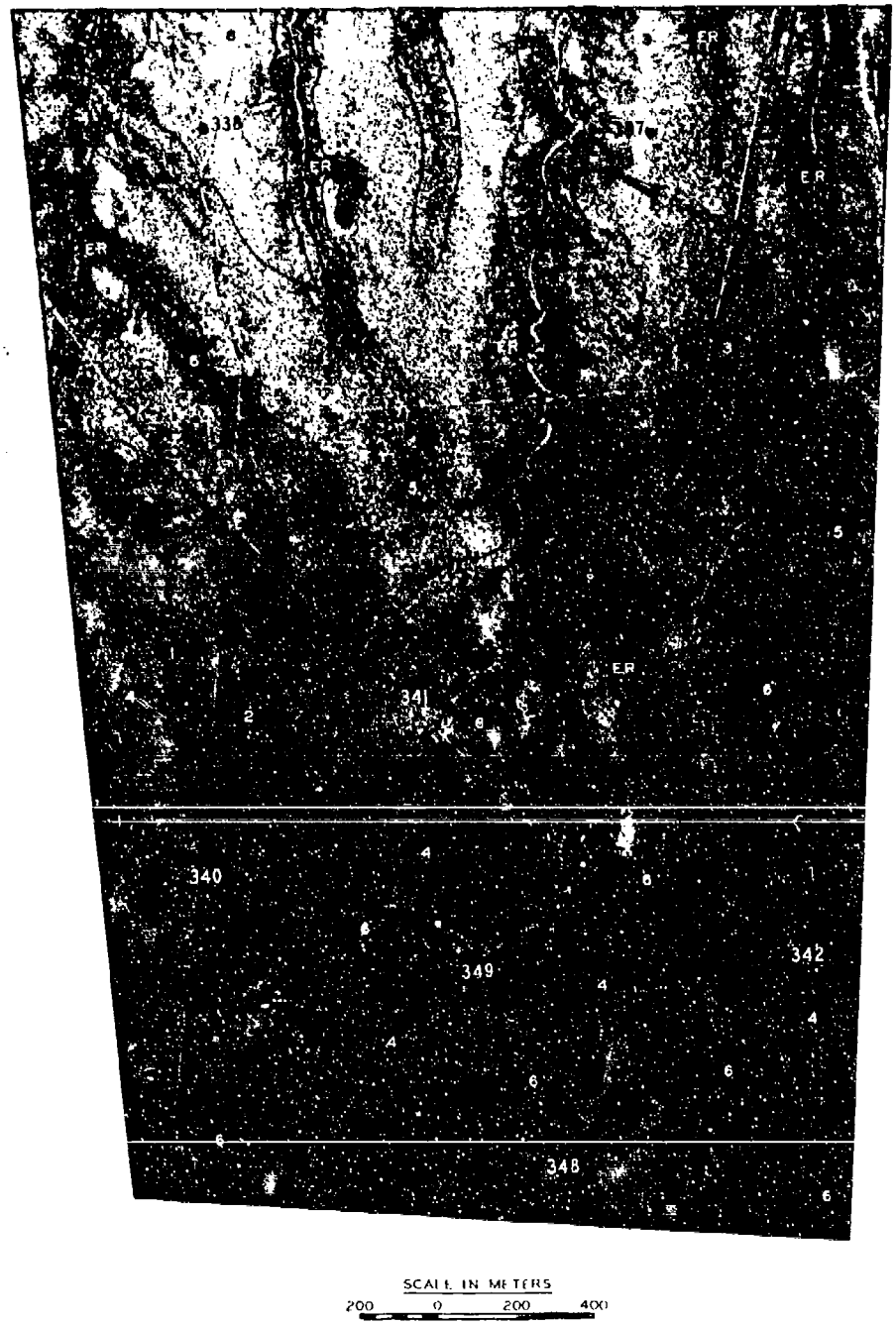

NOTE: FOR LEGEND SEE TABLE 21.

Fig. 51. Dry-season drop-hammer seismic response map, hand-emplacement area. (For a larger print of this figure, see map 3 in pocket inside back cover)

correspond to the Phase III SID threshold values on high, medium, and low gain, respectively. The threshold values at 30 Hz are approximately 0.08×10^{-3}, 0.18×10^{-3}, and 0.50×10^{-3} cm/sec, respectively (see fig. A3, Appendix A). These values are relatively conservative, since they offer a reasonable compromise between a frequency bandwidth at 9-45 Hz and peak values at approximately 14 Hz. Classes 4-8 for PPV and classes 4-10 for PSPV were selected to encompass the drop-hammer field-measured values (table 21).

183. f mapping classes. The mapping classes for f were selected such that they would encompass the frequency response of the Phase III SID and also the field-measured values. These factor class ranges also are listed in table 21.

Mapping of seismic response factors

184. The seismic response factor complex map (fig. 51) was generated by first preparing individual factor maps for PPV, PSPV, and f for distances of 5, 10, 20, 30, 40, and 60 m, respectively. This was accomplished by examining the drop-hammer best-fit data (table 8) for PPV, PSPV, and f at the various distances and selecting a factor class for each corresponding distance (i.e. a factor class for 5, 10, 20, 30, 40, and 60 m, respectively). The factor class for each distance was then noted on a base map. At this stage, boundaries were drawn delineating zones or patches in which all the class numbers were the same. In effect, the map differentiated the area in terms of PPV, PSPV, and f for a selected distance, such as 20 m.

185. All the individual PPV, PSPV, and f maps for each of the selected distances (i.e. 5, 10, 20, 30, 40, and 60 m) were consolidated into a single map (i.e. a factor complex map). All factor class ranges identified on the map in the order of PPV, PSPV, and f factors were tabulated, and each array (i.e. unique combinations of values of PPV, PSPV, and f) was assigned a map unit number. The resulting tabulation (table 21) is the legend for the seismic response factor complex map (fig. 51); a unit on this map represents an array of class ranges as identified in the legend, and delineates areas exhibiting similar

combinations of seismic conditions, at least insofar as PPV, PSPV, and I' are concerned.

Mapping of MINISID III Detection Performance Values

186. A MINISID III performance (detection distance) map of the hand-emplacement area (fig. 52) was constructed using the experimental detection range data (table 9) obtained during wet- and dry-season conditions at the ten sites (sites 335-342, 348, and 349), air-photo interpretation techniques, terrain data obtained within the area, and the interpreter's personal knowledge of the hand-emplacement area. The mapping classes were selected to minimize the difference between the mapped values and those portrayed by the experimental detection range data. The legend for the MINISID III performance map is given in table 22. The legend for the SID performance map (table 22) does not differentiate between wet- and dry-season conditions. As can be seen in fig. 30 (a bargraph showing a comparison of the wet- and dry-season detection distances at medium gain), there appears to be no trend toward any one season giving a consistently greater or lesser detection range. For example, the detection distance data presented for the wet and dry seasons in fig. 30 show a difference of 1-3 m for five sites (337-339, 342, and 349), a difference of 5-7 m for two sites (341 and 347), and a difference of 18 and 20 m for two sites (336 and 348, respectively). A more distinct trend may have been observed if the same man had been used for the walk tests during both seasons. As this was not the case, the experimental MINISID III data for the two seasons' conditions cannot be considered absolutely compatible. The characteristics of the two personnel used for these tests were: The wet-season MINISID III data are based on a man weighing 79.2 kg, wearing boots size 11, and walking an average pace of 1 m/step; whereas, the dry-season MINISID III data are based on a man weighing 65.8 kg, wearing boots size 9, and walking an average pace of 1 m/step.

187. To illustrate the effects of personnel characteristics on the MINISID III detection ranges, the results of a few selected tests

NOTE: MAP BASED ON MAN WEIGHING 66-79 KG, WEARING BOOT SIZE 9-11, WALKING AN AVERAGE STRIDE OF 1 M/STEP.

FOR LEGEND SEE TABLE 22.

Fig. 52. SID detection performance map, hand-emplacement area. (For a larger print of this figure, see map 4 inside back cover)

were conducted at Fort Huachuca and are summarized below:

Site No.	Personnel Characteristics: Weight kg	Boot Size	Avg Stride m	Dry-Season Detection Range (Avg of 3 Tests)
335	65.8	9	1.0	27
335	79.2	11	1.0	33
336	65.8	9	1.0	34
336	70.2	7-1/2	0.83	27

PART V: SUMMARY OF RESULTS, CONCLUSIONS, AND RECOMMENDATIONS

Results and Conclusions

188. As stated in paragraph 37, the overall objective of this seismic and environmental study was to improve procedures for conducting engineering tests to evaluate various SID systems. The following discussion will show how well the specific objectives were achieved.

Significant terrain and seismic response factors and their variation

189. The significant terrain factors required to determine sensor detection performance are:

a. Surface terrain factors (paragraph 119):
   (1) Soil type
   (2) Soil particle size
   (3) Soil moisture content
   (4) Soil wet density
   (5) Soil strength (cone penetration resistance)
   (6) Height and density of vegetation ground cover
   (7) Geometry of ground surface (roughness)

b. Subsurface terrain factors (paragraph 127):
   (1) Compression wave velocity (each layer)
   (2) Shear wave velocity (each layer)
   (3) Thickness of each layer
   (4) Soil wet density of each layer

190. The relative effects of terrain factors (and changes in them) cannot be specified in simple terms. However, it is felt that a sensitivity analysis performed on the Fort Huachuca data by a first-generation model developed at WES would indicate those factors that cause significant changes in SID detection ranges. As a result, only those factors indicated by the analysis would have to be measured in future studies (paragraph 132).

191. To improve the overall procedures for prediction, extrapolation, and comparison of SID performances (detection and implantation),

meteorological and vegetation data should also be obtained within the general area of SID testing as follows:

a. Meteorology factors (paragraph 76):
   (1) Wind speed
   (2) Wind direction
   (3) Precipitation (rainfall and snowfall)

b. Vegetation factors (description of plants within a radius of ≈ 100 m of the SID test site) (paragraph 78):
   (1) Average plant base diameter and number of stems per plant
   (2) Average plant height
   (3) Average dominant plant spacing
   (4) Plant crown characteristics (average diameter and depth)

192. The seismic response parameters (i.e. PPV, PSPV, and f as a function of distance) resulting from the drop-hammer energy source (which is assumed to be comparable to that resulting from a footstep source) indicate that the hand-emplacement area provides terrain conditions that are somewhat ideal for performing engineering tests of hand-emplaced SID's (paragraphs 105-107). The seismic responses as measured at the 10 test sites (see Appendix B) show some site-to-site variation, and this variation should be considered in SID engineering testing; however, it is believed that this variation can be accounted for analytically and therefore will not necessarily result in any erratic or inconsistent results in engineering tests performed on the hand-emplaced SID's. The variations in seismic response parameters portrayed by air-drop areas 1 and 4-6, as measured in the dry season, indicate, in general, that the detection performance of air-implanted SID's can be evaluated for a large range of terrain conditions (paragraphs 105-107). The variation in these conditions allows the testing of air-implanted SID's under varying stress conditions (i.e. high to low rigid-body deceleration values) and under a variety of soil strength conditions (paragraph 165).

193. The seismic responses resulting from induced background

noises created by low-flying fixed-wing and rotary-wing aircraft are of sufficient frequency and duration within the East Range to have significant effects upon certain types of SID testing; therefore, measurements of the induced-noise level must be made during SID testing (paragraph 110). The seismic response resulting from wind action on plant structures within the hand-emplacement area and the airdrop areas did not produce seismic waves of sufficient magnitude that were considered significant to the engineering testing of most SID systems employing a Phase III type or similar logic (paragraph 108).

194. Based on the surface and subsurface terrain data (and, in some cases, seismic data) obtained during wet- and dry-season conditions at Fort Huachuca, it was determined that the selected SID test sites portrayed significant variation from site to site, but, in general, very little variation between wet- and dry-season conditions (paragraphs 121-125, 128-131, 134-138 and figs. 32-38).

Data collection procedures

195. The procedures used by WES for acquisition and recording of the significant terrain and seismic response data listed in paragraphs 189 and 191 are being documented in a separate loose-leaf report and will be provided to Fort Huachuca upon completion.

Factor maps of hand-emplacement area

196. The terrain factor complex maps (figs. 47-50) prepared for the hand-emplacement area provide surface and subsurface factor data on an areal basis for use with the forcing function and seismic wave propagation submodels to estimate SID performance (i.e. detection distances) for man-walking energy sources (paragraph 167). The seismic response factor complex map (fig. 51) prepared for the hand-emplacement area provides seismic data on an areal basis on PPV, PSPV, and f as a function of distance, and will be useful in selecting representative areas (i.e. areas that will provide the least amount of terrain variation) for conducting SID engineering tests.

Extrapolating SID test results

197. Based on the WES concept (fig. 2) for the extrapolation of SID test results, adequate simulation models describing the phenomena

under test are being formulated (paragraphs 151 and 166). In the case of SID detection performance, this involves simulating the generation, propagation, and coupling of the seismic energy from the source to the sensor. In the case of implantation of air-delivered SID's, this involves simulating the terrain-penetration event of an air-delivered SID and the coupling of the SID to the soil. The extrapolation concept also requires that the terrain inputs to the simulation models be constitutive and measurable properties of the terrain such that they can be classified and portrayed on an areal basis.

Depth of penetration and deceleration of air-implanted sensors

198. The predicted (and unvalidated) depth-of-penetration results for airdrop areas 1, 4, and 5 indicate that the ADSID/S air-delivered sensor will implant satisfactorily (i.e. it will obtain a penetration depth sufficient for detections of a seismic disturbance) within airdrop area 1 (test pit 5) during both the wet and dry seasons; and within airdrop area 1 (test pit 6) and airdrop area 5 (test pit 2), it will implant satisfactorily only during the wet season (paragraph 157). These predictions are based on the assumption that the anticipated impact velocity of the ADSID/S will be approximately 50 m/sec. For airdrop area 1 (test pit 6) and airdrop areas 4 and 5 during the dry season, the penetration results indicate that the ADSID/S at 50 m/sec impact velocity will penetrate the soil only a few centimeters and then probably fall down (paragraph 157). All computed deceleration values were over the maximum allowable for a workable ADSID/S, except those for area 1 (pit 5) during the wet and dry seasons, area 1 (pit 6) during the wet season, and area 5 (pit 2) during the wet season (paragraph 159).

199. The very limited experimental penetration data obtained at the CSEWS airdrop area compared reasonably well with theoretical predictions of penetrations (paragraph 164). The comparison of these data also shows that the depth of penetration of a typical air-implanted SID (i.e. ADSID/S) is very dependent upon terrain moisture conditions (at the time of test) (paragraph 161).

200. The input parameter data required by the equations

(presented in Appendix C) used to provide theoretical estimates for the depth of penetration and impact deceleration of air-implanted SID's are obtained from special laboratory tests on undisturbed soil samples. The inputs to the equations are:

a. Initial Young's modulus of elasticity, E .

b. Ultimate shear strength, σ_u .

c. Compressibility parameter, ρ_p/ρ .

d. Soil wet density, ρ .

e. Coefficient of friction between the projectile and the soil, μ .

f. Drag coefficient, C_D .

Recommendations

201. Since the Fort Huachuca hand-emplacement area exhibited rather small differences in the four subsurface terrain factors (i.e. V_P,V_S,T, and ρ) between the wet- and dry-season conditions, it is recommended that measurements of these factors be made only for new sites established for engineering testing of a SID system. It is further recommended that soil moisture content and cone penetration resistance (soil strength) be measured at all sites (including the ones sampled by WES) that are to be used for engineering tests. To obtain moisture and strength data on-site in the proper form for use, a calcium carbide gas pressure moisture tester (i.e. Speedy Moisture Tester) and the WES cone penetrometer are recommended. (The procedures for using this equipment are being documented as noted in paragraph 195 and will be furnished to Fort Huachuca upon completion.)

202. WES has a mathematical computer model (see reference 3) that provides estimates of moisture content and strength of the 0- to 15-cm and 15- to 30-cm soil layers. It is recommended that this model be utilized to estimate daily moisture contents and strengths for specific areas to be used for wet-season testing at Fort Huachuca, since local rainfall records are available for the hand-emplacement and the airdrop areas, and these data are required as the basic input to the prediction

model. It is also recommended that measurements of wind speed, wind direction, and precipitation (rainfall and snowfall) be obtained during SID testing for use in interpreting test results (paragraph 77).

203. The input parameter data for use with the sensor implantation equations, which provide penetration depths and impact stresses of air-delivered SID's, are presently obtained from the results of special uniaxial strain and triaxial compression tests performed in the laboratory on undisturbed soil samples. This procedure for obtaining the necessary parameter data is very time-consuming and too costly for practical application, such as for use in day-to-day sensor testing. Therefore, it is recommended that research be continued to determine better and faster methods for obtaining input data required by the sensor implantation equations, as well as by all other models being developed at WES to estimate and extrapolate SID performances for world terrain conditions.

204. It is recommended that a WES type drop-hammer apparatus be used by Fort Huachuca personnel to calibrate a test site for SID engineering evaluation. It is also recommended that at least three successive drops of the hammer be made at each data collection site, and the average of the resulting seismic response data be used for comparing SID performance at one site with that of another site (paragraph 100).

205. Since the theoretical procedures briefly presented in this report appear to offer a rational basis for interpreting and extrapolating SID test results, it is recommended that work be continued on the further development of the WES theoretical seismic wave propagation model to allow for the following considerations:

a. Forcing function to account for the transfer of seismic energy from the source to the propagating medium.

b. Viscous damping coefficients that better approximate site conditions.

c. Forcing function that more adequately describes near-field wave propagation.

d. Coefficients that describe the geometry of the ground surface.

e. Special studies to determine the effects of sensor mass, sensor attitude or configuration, and terrain coupling on SID performance.

LITERATURE CITED

1. Richard, F. E., Hall, J. R., Jr., and Woods, R. D., Vibrations of Soils and Foundations, Prentice-Hall, Englewood Cliffs, N. J., 1970.

2. Devine, J. C., "The Fort Huachuca, Arizona, 15-Year Base Climate Calendar, 1956-1970," Technical Report ECOM 6057, Feb 1971, U. S. Army Electronics Command, Atmospheric Sciences Laboratory, Meteorological Support Activity, Fort Huachuca, Ariz.

3. Smith, M. and Meyer, M. M., "Automation of a Model for Predicting Soil Moisture and Soil Strength (SMSP Model)," Miscellaneous Paper M-73-1, Jan 1973, U. S. Army Engineer Waterways Experiment Station, CE, Vicksburg, Miss.

4. Schindler, L., "Design and Evaluation of a Device for Determining the One-Dimensional Compression Characteristics of Soils Subjected to Impulse-Type Loads," Technical Report S-68-9, Nov 1968, U. S. Army Engineer Waterways Experiment Station, CE, Vicksburg, Miss.

5. Ehrgott, J. Q., "Calculation of Stress and Strain from Triaxial Test Data on Undrained Soil Specimens," Miscellaneous Paper S-71-9, May 1971, U. S. Army Engineer Waterways Experiment Station, CE, Vicksburg, Miss.

6. Sowers, G. F., "Strength Testing of Soils, Laboratory Shear Testing of Soils," Special Technical Publication No. 361, pp 3-5, 9-14, 1964, American Society for Testing and Materials, Philadelphia, Pa.

7. Bishop, A. W. and Henkle, D. V., The Measurement of Soil Properties in the Triaxial Test, 2d ed., Edward Arnold, London, 1962.

8. Ehrgott, J. W. and Sloan, R. C., "Development of a Dynamic High-Pressure Triaxial Test Device," Technical Report S-71-15, Nov 1971, U. S. Army Engineer Waterways Experiment Station, CE, Vicksburg, Miss.

9. Potyondy, J. G., "Skin Friction Between Various Soils and Construction Materials," Geotechnique, Vol XI, No. 4, Dec 1961, pp 339-353.

10. Link, L. E., West, H. W., and Benn, B. O., "Seismic and Environmental Characteristics of the Sensor Test Areas in the Panama Canal Zone; Dry-Season Conditions," Technical Report M-72-2, Report 1, Jun 1972, U. S. Army Engineer Waterways Experiment Station, CE, Vicksburg, Miss.

11. U. S. Army Engineer Waterways Experiment Station, CE, "Report of Conference on Seismic Propagation Study," Aug 1971, Vicksburg, Miss.; conference held 22 Jun 1971 at the U. S. Army Waterways Experiment Station.

12. _____, "Report of Second Conference on Seismic Propagation Study," May 1972, Vicksburg, Miss.; conference held 15 Dec 1971 at the U. S. Army Research Office, Washington, D. C.

13. Marcuson, W. F. III and Leach, R. E., "Seismic and Environmental Characteristics of the Sensor Test Areas in the Panama Canal Zone; Wet-Season Conditions," Technical Report M-72-2, Report 2, May 1972, U. S. Army Engineer Waterways Experiment Station, CE, Vicksburg, Miss.

14. West, H. W. "Effects of Environment on Microseismic Wave Propagation Characteristics in Support of SID Testing at Fort Bragg, N. C.; Dry-Season Conditions," Technical Report M-73-2, Report 1, June 1973, U. S. Army Engineer Waterways Experiment Station, CE, Vicksburg, Miss.

15. West, H. W. and Engdahl, T., "Effects of Environment on Microseismic Wave Propagation Characteristics in Support of SID Testing at Fort Bragg, N. C.; Wet- and Dry-Season Conditions," Report 2 (in preparation), U. S. Army Engineer Waterways Experiment Station, CE, Vicksburg, Miss.

16. Lundien, J. R. and Nikodem, H., "A Mathematical Model for Predicting Seismic Signals in Terrain Materials," Technical Report M-73-4, June 1973, U. S. Army Engineer Waterways Experiment Station, CE, Vicksburg, Miss.

17. Benn, B. O. and Link, L. E., "A System for Predicting Seismic Sensor Performance," Technical Report (in preparation), U. S. Army Engineer Waterways Experiment Station, CE, Vicksburg, Miss.

18. Ross, B. and Hanagud, S., "Penetration Studies of Ice with Application to Arctic and Subarctic Warfare," Final Report, SRI Project 7000-452, Sep 1969, Stanford Research Institute, Menlo Park, Calif.; prepared under Contract N00014-68-A-0243, NR 274-008 for Submarine Arctic Warfare and Scientific Program, Naval Ordnance Laboratory, Silver Spring, Md., and Office of Naval Research, Washington, D. C.

19. Brooks, W. B. and Reis, G. E., "Soil Penetration Theory," Technical Report SC-4950(RR), Sep 1963, Sandia Corporation, Albuquerque, N. Mex.

20. Rohani, B., "High-Velocity Fragment Penetration of Soils Targets," Proceedings of the Conference on Rapid Penetration of Terrestrial Material, Texas A&M University, College Station, Tex., Feb 1972.

21. _____, "Theoretical Study of the Penetration of an Antipersonnel Mine Projectile into Earth Materials," Miscellaneous Paper S-72-33, Aug 1972, U. S. Army Engineer Waterways Experiment Station, CE, Vicksburg, Miss.

22. _____, "Fragment and Projectile Penetration Resistance of Soils; High-Velocity Fragment Penetration into Laboratory-Prepared Soils Targets," Miscellaneous Paper S-71-12, Report 2 (in preparation), U. S. Army Engineer Waterways Experiment Station, CE, Vicksburg, Miss.

Table 1

Summary of Meteorological Data During Times of Seismic Tests

Area	Site	Date of Test		Air Temperature °C		Daily Air Temperature Range, °C		Wind Speed m/sec		Wind Direction deg		Rainfall		
												Wet Season		Dry Season
		Wet Season	Dry Season	Wet Season	Dry Season	Wet Season	Dry Season	Wet Season	Dry Season	Wet Season	Dry Season	Amt cm	Time hr	Amt cm
Hand-emplacement	335	18 Aug 71	2 Mar 72	23	18	17-27	3-22	15	2	10	225	None	--	None
	336	21 Aug 71	4 Mar 72	22	22	16-28	3-28	6	1	5	225	None	--	None
	337	21 Aug 71	7 Mar 72	22	21	16-28	4-28	6	3	5	270	None	--	None
	338	19 Aug 71	4 Mar 72	27	28	16-28	3-28	7	2	8	225	0.43	0450	None
	339	24 Aug 71	1 Mar 72	28	20	17-29	7-19	4	5	5	270	0.25	0450	None
	340	19 Aug 71	6 Mar 72	25	22	16-28	7-30	6	3	6	270	0.43	0450	None
	341	20 Aug 71	3 Mar 72	29	22	17-27	2-24	9	8	8	270	Trace	1650	None
	342	26 Aug 71	3 Mar 72	22	18	17-30	2-24	5	1	4	270	None	--	None
	348	27 Aug 71	7 Mar 72	26	26	17-30	4-28	3	2	4	270	None	--	None
	349	27 Aug 71	6 Mar 72	28	28	17-30	7-30	5	2	6	270	None	--	None
Airdrop 1	347	26 Aug 71	10 Mar 72	22	15	17-30	7-29	5	2	12	220	None	--	--
Airdrop 4	410	--	10 Mar 72	--	32	--	7-30	--	4	--	240	--	--	None
Airdrop 5	411	--	11 Mar 72	--	33	--	--	--	--	--	--	--	--	--
Airdrop 3	412	--	11 Mar 72	--	26	--	--	--	--	--	--	--	--	--
Airdrop 6	413	--	--	--	--	--	--	--	--	--	--	--	--	--

Table 2

Summary of Seismic Refraction and Environmental Data

Area	Site	Layer Thickness* m		Compressional Wave Velocity m/sec		Shear Wave Velocity m/sec		Wet Density g/cm³		Moisture Content %		Soil Type USCS	Atterberg Limits			Soil Grain Size, Percent Finer by Weight						Cone Penetration Resistance kPa	
		Wet Season	Dry Season	Wet Season	Dry Season	Wet Season	Dry Season	Wet Season	Dry Season	Wet Season	Dry Season		LL	PL	PI							Wet Season	Dry Season
Hand-emplace-ment	345	Surface	Surface	--	--	--	--	[illegible]	[illegible]	5.3	[illegible]	SM	15.0	[illegible].0	6.0	100	[illegible].2	[illegible].2	[illegible].4	[illegible].4	12.4	660	100
		60	70	370	420	166	178	[illegible].70	[illegible].77	13.2	10.5	SM	NP	NP	NP	100	97.2	85.9	59.4	32.5	12.4	5.70	5.70
		170	200	685	695	254	252	--	--	7.6	7.4	SM	NP	NP	NP	100	76.4	73.9	59.7	[illegible].5	[illegible].9	--	--
	346	Surface	Surface	--	--	--	--	1.60	1.60	5.2	2.2	SM	15.0	10.0	5.0	100	94.2	89.3	65.1	49.9	12.6	860	240
		50	65	325	415	119	123	--	2.01	6.4	6.0	SM	15.0	10.0	5.0	100	94.2	89.2	65.1	55.9	12.6	5.70	5.70
		110	135	425	600	245	285	--	2.04	10.8	9.2	CL	39.0	19.0	20.0	100	98.3	96.1	80.3	73.4	24.5	--	--
	347	Surface	Surface	--	--	--	--	1.70	1.62	6.5	1.5	SM	14.0	10.0	4.0	100	87.2	77.7	51.9	39.6	8.4	430	540
		115	105	465	520	191	177	--	1.62	7.7	7.2	SM	31.0	11.0	20.0	100	99.7	98.1	62.1	43.3	19.7	5.70	5.70
		225	265	690	690	265	254	--	--	9.5	4.2	SM	--	--	--	--	--	--	--	--	--	--	--
	348	Surface	Surface	--	--	--	--	1.45	1.45	11.7	5.0	SM	27.0	14.0	13.0	100	95.8	86.4	69.6	47.1	15.9	520	810
		95	75	400	410	144	20	--	1.40	10.1	7.1	SM	30.0	12.0	18.0	--	--	--	--	--	--	5.70	5.70
		>1535	>1575	595	640	254	256	--	--	9.4	--	SM	--	--	--	100	94.5	95.0	71.6	44.6	13.2	--	--
	349	Surface	Surface	--	--	--	--	1.77	1.70	5.5	1.4	SM	NP	NP	NP	100	89.1	86.4	56.9	30.0	6.1	820	790
		150	145	470	485	172	172	--	--	7.6	5.0	SM	31.0	13.0	18.0	100	95.0	84.9	56.2	41.3	21.7	5.70	5.70
		>1530	>1510	815	815	349	322	--	--	--	--	SM	22.0	11.0	11.0	100	96.7	88.6	59.5	43.7	10.7	--	--
	340	Surface	Surface	--	--	--	--	1.71	1.67	6.1	1.4	SM	NP	NP	NP	100	90.6	93.9	68.1	50.1	8.3	830	1990
		55	50	240	250	101	102	--	1.60	3.0	4.5	SM	--	--	--	100	90.5	93.9	68.1	50.1	8.3	5.70	5.70
		245	240	650	720	334	348	--	2.00	5.7	4.5	SM	28.0	14.0	13.0	100	90.5	93.5	65.6	44.2	20.1	--	--
	341	Surface	Surface	--	--	--	--	1.71	1.75	6.4	0.9	SM	14.0	10.0	4.0	100	96.6	85.0	59.5	33.2	9.6	490	610
		100	115	310	345	142	201	--	--	7.1	8.3	SM	24.0	12.0	12.0	100	93.5	90.5	66.0	44.7	15.5	5.70	5.70
		>1550	>1535	720	710	404	339	--	--	--	--	SM	--	--	--	--	--	--	--	--	--	--	--
	342	Surface	Surface	--	--	--	--	1.65	2.04	5.3	2.8	SM	12.0	10.0	2.0	100	98.3	86.4	57.6	34.6	8.0	1000	650
		100	110	370	355	144	174	1.70	1.84	8.9	8.9	SM	34.0	15.0	19.0	100	99.[illegible]	84.6	59.5	45.[illegible]	23.0	5.70	5.70
		>1550	>1540	870	820	340	367	--	--	--	--	SM	--	--	--	--	--	--	--	--	--	--	--
	388	Surface	Surface	--	--	--	--	1.60	1.72	6.6	1.1	SM	11.0	10.0	1.0	100	96.1	86.3	51.6	40.3	7.6	670	690
		60	90	350	405	142	165	1.96	1.79	7.9	5.2	SM	36.0	19.0	17.0	100	89.9	81.9	48.[illegible]	35.[illegible]	20.[illegible]	5.70	5.70
		370	270	583	514	301	337	--	--	--	--	SM	--	--	--	--	--	--	--	--	--	--	--
	349	Surface	Surface	--	--	--	--	1.78	1.69	6.6	1.0	SM	11.0	9.0	2.0	100	96.[illegible]	89.5	51.6	31.[illegible]	7.2	770	410
		45	50	240	230	103	101	1.78	1.70	7.2	2.4	SM	26.0	14.0	12.0	100	97.3	85.7	48.7	31.[illegible]	17.[illegible]	5.70	5.70
		495	395	625	594	340	371	1.75	1.72	5.7	3.7	--	--	--	--	--	--	--	--	--	--	--	--
Airdrop 1	347	Surface	Surface	--	--	--	--	1.74	1.75	7.2	1.4	SM	13.0	9.0	4.0	100	87.9	83.[illegible]	50.[illegible]	33.2	7.[illegible]	370	330
		55	55	230	230	114	129	1.85	[illegible].82	13.[illegible]	[illegible].4	SM	30.0	15.0	15.0	100	84.1	77.2	44.[illegible]	31.[illegible]	22.[illegible]	5.70	5.70
		>245	>255	695	703	337	352	--	1.72	[illegible].0	5.2	--	--	--	--	--	--	--	--	--	--	--	--
Airdrop 4	410	Surface	Surface	--	--	--	--	--	1.37	--	6.0	CL	24.0	11.0	13.0	100	88.6	85.9	75.0	53.5	[illegible].8	--	360*
		--	140	--	3.2	--	121	--	1.74	--	8.5	CL	38.0	19.0	19.0	100	98.7	97.1	91.7	80.1	25.5	--	5.70
		--	>245	--	720	--	312	--	--	--	--	--	--	--	--	--	--	--	--	--	--	--	--
Airdrop 5	411	Surface	Surface	--	--	--	--	--	1.46	--	1.1	CL	30.0	13.0	12.0	100	95.6	92.4	79.3	64.4	15.3	--	330
		--	235	--	35	--	1[illegible]	--	1.70	--	15.1	CL	45.0	27.0	18.0	100	97.4	97.0	96.2	89.5	37.4	--	5.70
		--	510	--	229	--	[illegible]2	--	--	--	--	--	--	--	--	--	--	--	--	--	--	--	--
Airdrop 3	412	Surface	Surface	--	--	--	--	--	1.64	--	2.[illegible]	SM	NP	[illegible]	NP	100	90.[illegible]	93.1	79.[illegible]	20.9	4.1	--	100
		--	250	--	340	--	151	--	1.86	--	4.4	--	20.0	15.0	5.0	100	96.[illegible]	92.4	78.6	47.4	4.9	--	--
		--	120	--	1148	--	412	--	--	--	--	--	--	--	--	--	--	--	--	--	--	--	--
Airdrop 6	413	Surface	Surface	--	--	--	--	--	1.26	--	10.1	SC	--	--	--	--	--	--	--	--	--	--	540
		--	335	--	39	--	134	--	--	--	51.6	CL	--	--	--	--	--	--	--	--	--	--	--
		--	405	--	1650	--	435	--	--	--	--	--	--	--	--	--	--	--	--	--	--	--	--

Note: Maximum reading of cone penetrometer is 6[illegible]. Data are for three soil layers as follows: line 1, surface soil; line 2, first refraction layer; line 3, second refraction layer. Wet-season data obtained in August 1971; dry-season data obtained in March 1972.

* Thickness for layers 1 and 2 determined by refraction seismic techniques.

Table 3

Summary of Moisture Data

Site No.	Depth cm	Moisture Content, % Wet* Season	Dry** Season	Difference†
335	Surface	5.3	1.7	+3.6
	50	13.2	10.5	+2.7
	100	7.6	7.4	+0.2
336	Surface	5.2	2.2	+3.0
	50	6.4	6.0	+0.4
	100	10.8	9.3	+1.5
337	Surface	6.5	1.5	+5.0
	50	7.7	7.2	+0.5
	100	5.5	4.2	+1.3
338	Surface	11.7	5.0	+6.7
	50	10.1	7.1	+3.0
	100	9.3	6.1	+3.2
339	Surface	5.5	1.4	+4.1
	50	9.1	7.4	+1.7
	100	7.2	6.1	+1.1
340	Surface	8.1	1.4	+6.7
	50	3.0	4.5	-1.5
	100	5.6	6.5	-0.9
341	Surface	6.4	0.9	+5.5
	50	5.9	9.7	-3.8
	100	7.9	8.3	-0.4
342	Surface	5.3	2.8	+2.5
	50	7.0	5.0	+2.0
	100	8.2	8.3	-0.1
348	Surface	6.6	1.1	+5.5
	50	8.4	4.4	+4.0
	85	7.3	5.2	+2.1
349	Surface	6.6	1.0	+5.6
	50	7.2	2.4	+4.8
	85	5.7	3.7	+2.0
347	Surface	7.2	1.4	+5.8
	50	13.4	6.4	+7.0
	85	8.4	5.2	+3.2
410	Surface	26.4	6.0	+20.4
	50	10.2	8.5	+1.7
	80	--	8.8	--
411	Surface	32.6	7.4	+25.2
	50	18.2	10.5	+7.7
	100	--	15.1	--
412	Surface	11.4	2.6	+8.8
	50	5.3	3.8	+1.5
	100	--	4.4	--
413	Surface	††	10.1	--
	50	††	46.0	--
	100	††	52.0	--
	200	††	76.0	--

* Data obtained March 1972.
** Data obtained August 1971.
† Difference obtained by subtracting dry-season data from wet-season data.
†† Area inundated during wet season (August-October).

Table 4

Summary of Cone-Penetration Resistance (Soil Strength) Data

Site No.	Season	Cone-Penetration Resistance, kPa, by Various Depths, cm						
		Surface	2.5	5.0	7.5	10.0	12.5	15.0
335	Wet season	560	2300	3590	3540	3410	4000	3630
	Dry season	100	1210	4090	5170+			
	Difference	+460	+1090	- 500	-1630			
336	Wet season	860	2470	3220	2790	2530	2460	2700
	Dry season	240	3710	5170+				
	Difference	+620	-1240	-1950				
337	Wet season	430	1500	2300	2480	2340	2520	3070
	Dry season	540	3580	4710	5170+			
	Difference	-110	-2080	-2410	-2690			
338	Wet season	520	1090	1630	1800	1920	2200	2710
	Dry season	810	2800	5170+				
	Difference	-290	-1110	-3540				
339	Wet season	820	2400	3070	3720	2940	2500	2290
	Dry season	790	4760	5170+				
	Difference	+ 30	-2360	-1500				
340	Wet season	830	2130	3230	3210	3140	3060	3100
	Dry season	1990	4500	5170+				
	Difference	-1160	-2370	-1940				
341	Wet season	490	1720	2590	2770	2830	2680	2700
	Dry season	610	4240	4900	4940	5170+		
	Difference	-120	-2520	-2310	-2170	-2340		
342	Wet season	1000	3000	4440	4480	4450	4390	4350
	Dry season	650	5000	5170+				
	Difference	+ 350	-1400	- 730				
348	Wet season	670	2110	2940	3250	3080	2880	2750
	Dry season	690	4250	5170+				
	Difference	- 20	-2140	-2230				
349	Wet season	770	2220	3030	3010	2810	2940	3370
	Dry season	410	3680	5120	5170+			
	Difference	+360	-1420	-2090	-2160			
347	Wet season	370	760	1140	1450	1940	2450	3280
(Airdrop 1)	Dry season	330	2650	4910	5170+			
	Difference	+ 40	-1890	-3770	-3720			
410	Wet season*	--	--	--	--	--	--	--
(Airdrop 4)	Dry season	30	370	1200	1800	2010	2010	2700
	Difference	--	--	--	--	--	--	--
411	Wet season*	--	--	--	--	--	--	--
(Airdrop 5)	Dry season	320	1290	1900	1950	2350	2540	2590
	Difference	--	--	--	--	--	--	--
412	Wet season*	--	--	--	--	--	--	--
(Airdrop 3)	Dry season	80	470	1230	2010	2400	2810	3190
	Difference	--	--	--	--	--	--	--
413	Wet season*	--	--	--	--	--	--	--
(Airdrop 6)	Dry season	940	1660	1940	1810	1810	1360	1290
	Difference	--	--	--	--	--	--	--

Note: Wet-season data obtained during August 1971; dry-season data obtained during March 1972. Maximum reading of cone penetrometer is 5170; values presented are averages of 15 individual penetration readings.

* No data obtained during wet season.

Table 5

Soil Data for Special CSLWS Airdrop Area*

Airdrop Test No.	Moisture Content, %	Cone Penetration Resistance, kPa**	Airdrop Test No.	Moisture Content, %	Cone Penetration Resistance, kPa
1	6.0	3630	61	6.5	5170+
2	--	--	62	5.8	5170+
3	--	--	63	4.2	5170+
4	8.8	4400	64	4.4	5170+
5	6.3	4980	65	5.4	4980
6	7.6	4340	66	6.7	3900
7	5.6	3930	67	3.9	5170
8	6.1	5140	68	7.1	2900
9	5.6	4920	69	4.8	1860
10	6.1	--	70	6.4	4740
11	6.4	5130	71	8.6	2590
12	8.6	3710	72	6.5	3240
13	4.7	4220	73	5.8	4830
14	8.7	2960	74	9.4	4230
15	9.0	1550	75	7.6	5170+
16	5.1	4690	76	6.4	4790
17	8.6	4670	77	6.9	4210
18	9.9	4030	78	7.9	4850
19	8.3	4770	79	5.5	4900
20	4.2	5140	80	6.5	4510
21	4.2	5150	81	--	--
22	4.6	5170	82	7.1	4600
23	5.3	5120	83	6.4	5080
24	6.5	4620	84	8.7	5080
25	--	--	85	8.4	5000
26	--	2010	86	8.0	4940
27	7.1	3400	87	8.6	4420
28	10.2	1670	88	6.4	4300
29	11.2	1030	89	16.5	920
30	10.7	5170+	90	13.0	2380
31	--	5120	91	7.7	4670
32	--	--	92	8.3	4830
33	6.7	4670	93	9.5	4010
34	8.2	5050	94	5.6	5170+
35	5.7	5170+	95	5.5	5170+
36	8.0	5170+	96	10.9	4680
37	--	5030	97	7.4	5170+
38	4.2	5170+	98	12.1	2250
39	7.9	3310	99	9.0	3600
40	4.3	5170+	100	4.4	5170+
41	5.4	5170+	101	4.3	5170+
42	5.6	4030	102	3.2	5170+
43	3.5	4420	103	4.5	5170+
44	9.0	4310	104	5.6	5170+
45	6.7	5170+	105	4.1	5170+
46	7.9	4960	106	4.9	4970
47	5.8	5170+	107	--	--
48	9.6	2630	108	6.9	5170+
49	8.6	5170+	109	6.0	5170+
50	5.1	5110	110	5.2	5170+
51	3.3	5170+	111	--	--
52	5.0	4650	112	7.5	5170+
53	3.7	5170+	113	6.4	5170+
54	4.6	5170+	114	3.8	5170+
55	3.5	5100	115	3.6	5090
56	4.8	4910	116	3.2	5170+
57	5.2	5170+	117	3.1	5170+
58	7.1	4100	118	6.5	5170+
59	6.5	5170+	119	8.3	5170+
60	4.6	5110	120	4.5	5170+

* Soil type: a gravel-sand-silty mixture classified as SC according to Unified Soil Classification System; surface wet density 1.7 to 1.9 g/cm^3 (based on 10 samples).

** A plus sign (+) denotes maximum penetrometer reading.

Table 6

Summary of Vegetation Data

Area	Site	Plant Type (Species)	Area of Plant Coverage, %	Plant Height cm	Stem Base Diam mm	No. of Stems per Plant	Crown Diam cm	Crown Depth cm	Avg Plant Spacing cm	Vegetation Ground Cover Type, Height, and Percent of Coverage
Hand-emplacement	335	Acacia	50	130	20	8	120	80	260	No ground cover
		Mesquite	20	130	60	3	150	60	1040	
	336	Desert grass	80	60	2	14	30	20	40	Grass, 60 cm in height and 80 percent coverage
	337	Acacia	45	100	30	10	110	90	300	No ground cover
		Mesquite	30	130	12	4	220	110	570	
	333	Desert grass	58	50	2	20	30	10	104	Grass 50 cm in height and 55 percent coverage
		Acacia	47	90	20	6	60	50	218	
	339	Acacia	28	160	8	6	130	90	417	No ground cover
		Mesquite	56	140	8	7	140	90	115	
	340	Desert grass	80	60	2	15	45	30	42	Grass 60 cm in height and 80 percent coverage
		Mesquite	25	200	150	3	300	175	870	
	341	Desert grass	65	60	2	25	40	20	73	Grass 60 cm in height and 65 percent coverage
		Mesquite	25	170	100	5	200	120	800	
	342	Desert grass	75	60	2	18	30	20	48	Grass 60 cm in height and 75 percent coverage
	348	Desert grass	60	60	2	35	45	20	72	Grass 60 cm in height and 60 percent coverage
	349	Desert grass	80	60	2	18	30	20	43	Grass 60 cm in height and 80 percent coverage
Airdrop 1	347	Desert grass	80	60	2	18	40	20	42	Grass 60 cm in height and 80 percent coverage
		Cressote	30	130	12	4	130	110	540	
Airdrop 4	410	Mesquite	32	100	60	4	140	60	500	No ground cover
Airdrop 5	411	Desert grass	58	50	2	20	40	20	100	Grass 50 cm in height and 58 percent coverage
		Cressote	40	100	15	3	150	75	350	
Airdrop 3	412	Reeds	85	150	2	30	40	20	35	Grass 60 cm in height and 85 percent coverage
Airdrop 6	413	--	--	--	--	--	--	--	--	No ground cover - Willcox Playa

Table 7

Summary of Soils Data, Airdrop Areas

Air Drop Area	Test Pit	Season	Relative Amount, % Sand	Clay	δ/ϕ	ϕ, deg	δ, deg	Tan δ
1	5	Dry	53	47	0.465	0	0	0
1	5	Wet	53	47	0.465	0	0	0
1	6	Dry	68	32	0.475	12.5	5.94	0.103
1	6	Wet	68	32	0.475	0	0	0
4	3	Dry	56	44	0.468	0	0	0
4	3	Wet	56	44	0.468	0	0	0
4	4	Dry	28	72	0.450	8.5	3.83	0.067
4	4	Wet	28	72	0.450	2.0	0.90	0.016
5	1	Dry	14	86	0.443	8.0	3.54	0.061
5	1	Wet	14	86	0.443	0	0	0
5	2	Dry	40	60	0.458	2.5	1.15	0.020
5	2	Wet	40	60	0.458	0	0	0

Note: ϕ = angle of internal friction, deg.
δ = angle of friction between projectile and soil, deg.
tan δ = coefficient of friction μ.

Table 9

Summary of Drop Hammer Seismic Response Data

Area	Site	Distance from Energy Source m	Seismic Response Measurements											
			PPV, 10^{-3} cm/sec				PSPV, 10^{-3} cm/sec				f_r, Hz			
			Field Measured		Best-Fit Curve		Field Measured		Best-Fit Curve		Field Measured		Best-Fit Curve	
			Wet Season	Dry Season	Wet Season	Dry Season	Wet Season	Dry Season	Wet Season	Dry Season	Wet Season	Dry Season	Wet Season	Dry Season
Hand-emplacement	335	5	0.99	1.50	0.52	1.14	0.13	0.37	0.17	0.42	31	54	34	39
		10	0.53	0.97	0.35	0.67	0.16	0.34	0.11	0.26	47	38	33	37
		20	0.17	0.27	0.21	0.32	0.06	0.14	0.06	0.14	29	28	31	34
		30	0.16	0.13	0.15	0.18	0.04	0.08	0.04	0.09	31	23	29	30
		40	0.10	0.06	0.12	0.11	0.01	0.05	0.02	0.06	22	28	27	26
		60	0.06	0.05	0.07	0.04	0.01	0.03	0.01	0.03	18	21	24	18
	336	5	1.56	1.75	0.68	1.05	0.11	0.21	0.14	0.27	31	42	37	40
		10	0.27	0.92	0.39	0.64	0.10	0.30	0.09	0.18	47	45	36	38
		20	0.14	0.30	0.18	0.34	0.05	0.11	0.05	0.11	34	32	33	33
		30	0.06	0.11	0.10	0.21	0.03	0.05	0.03	0.07	26	21	31	29
		40	0.04	0.10	0.05	0.14	0.02	0.05	0.02	0.05	22	19	29	25
		60	0.02	0.07	0.02	0.06	0.01	0.03	0.01	0.03	31	18	24	16
	337	5	0.75	1.48	0.60	0.90	0.13	0.34	0.15	0.42	31	42	38	41
		10	0.33	0.63	0.35	0.53	0.10	0.23	0.10	0.29	44	42	36	38
		20	0.16	0.19	0.17	0.26	0.06	0.11	0.05	0.20	31	31	31	33
		30	0.09	0.12	0.10	0.14	0.04	0.07	0.04	0.16	28	28	27	29
		40	0.07	0.07	0.06	0.09	0.02	0.05	0.02	0.13	22	21	23	24
		60	0.07	0.05	0.02	0.03	0.01	0.02	0.01	0.10	15	18	15	15
	338	5	1.30	1.56	0.70	1.41	0.21	0.50	0.36	0.64	32	45	33	39
		10	0.48	1.14	0.46	0.80	0.23	0.55	0.21	0.38	38	38	33	38
		20	0.23	0.30	0.28	0.37	0.11	0.19	0.10	0.19	31	29	32	34
		30	0.17	0.17	0.19	0.20	0.06	0.11	0.05	0.11	25	32	31	30
		40	0.12	0.10	0.14	0.11	0.04	0.08	0.03	0.07	28	28	29	27
		60	0.09	0.04	0.09	0.04	0.01	0.02	0.01	0.03	31	19	27	20
	339	5	0.46	1.20	0.42	0.85	0.10	0.22	[illegible]	0.29	31	26	38	34
		10	0.32	0.87	0.26	0.53	0.09	0.30		0.18	47	45	36	33
		20	0.11	0.24	0.16	0.29	0.05	0.10	[illegible]	0.10	31	29	33	30
		30	0.07	0.16	0.09	0.18	0.03	0.04	0.0[illegible]	0.06	23	25	29	28
		40	0.05	0.10	0.06	0.12	0.02	0.04	0.	0.04	21	19	26	25
		60	0.03	0.06	0.03	0.06	0.01	0.02	0.01	0.02	23	22	19	20

(Continued)

Note: Wet-season data obtained August 1971; dry-season data obtained March 1972.

Table 8 (Continued)

Area	Site	Distance from Energy Source m	Seismic Response Measurements											
			PPV, 10^{-3} cm/sec				PSPV, 10^{-3} cm/sec				f, Hz			
			Field Measured		Best-Fit Curve		Field Measured		Best-Fit Curve		Field Measured		Best-Fit Curve	
			Wet Season	Dry Season	Wet Season	Dry Season	Wet Season	Dry Season	Wet Season	Dry Season	Wet Season	Dry Season	Wet Season	Dry Season
Hand-emplacement (continued)	340	5	--	1.15	--	0.81	--	0.20	--	0.17	--	23	--	24
		10	--	0.40	--	0.49	--	0.09	--	0.12	--	19	--	23
		20	--	0.30	--	0.26	--	0.07	--	0.07	--	26	--	22
		30	--	0.15	--	0.16	--	0.07	--	0.05	--	19	--	21
		40	--	0.11	--	0.10	--	0.04	--	0.04	--	18	--	20
		60	--	0.05	--	0.05	--	0.03	--	0.03	--	19	--	18
	341	5	0.79	1.73	0.65	1.69	0.11	0.22	0.13	0.27	23	19	28	36
		10	0.40	1.03	0.36	0.92	0.06	0.23	0.08	0.18	26	51	27	33
		20	0.20	0.33	0.16	0.39	0.05	0.13	0.05	0.12	29	31	27	29
		30	0.09	0.20	0.08	0.19	0.04	0.08	0.03	0.09	23	21	26	25
		40	0.05	--	0.04	0.10	0.02	--	0.02	0.07	22	--	25	--
		60	0.03	0.06	0.01	0.03	0.01	0.03	0.01	0.05	31	19	24	--
	342	5	0.73	1.30	0.33	1.24	0.06	0.14	0.08	0.21	5	26	35	34
		10	0.25	1.00	0.22	0.67	0.06	0.19	0.05	0.14	42	50	33	33
		20	0.10	0.24	0.15	0.27	0.03	0.08	0.03	0.08	31	28	29	30
		30	0.10	0.12	0.11	0.13	0.02	0.05	0.02	0.05	22	23	24	27
		40	0.06	0.07	0.09	0.06	0.02	0.04	0.02	0.04	19	19	20	24
		60	0.11	0.01	0.06	0.02	0.02	0.02	0.01	0.02	10	19	12	17
	348	5	0.58	1.25	0.42	1.17	0.10	0.23	0.12	0.32	22	21	26	30
		10	0.33	1.17	0.28	0.71	--	0.23	0.08	0.21	--	45	26	29
		20	0.11	0.37	0.17	0.36	0.06	0.14	0.05	0.13	26	28	25	27
		30	0.11	0.12	0.12	0.21	0.04	0.09	0.04	0.09	20	19	24	25
		40	0.08	0.14	0.08	0.13	0.03	0.08	0.03	0.07	25	25	23	23
		60	0.06	0.06	0.05	0.06	0.01	0.04	0.03	0.04	21	19	22	19
	349	5	0.34	--	0.33	1.14	0.11	--	0.08	0.30	25	--	28	--
		10	0.15	--	0.22	0.62	0.03	--	0.05	0.19	25	--	28	32
		20	0.14	--	0.15	0.26	0.05	--	0.03	0.10	28	--	27	29
		30	0.12	--	0.11	0.12	0.04	--	0.02	0.06	25	--	27	27
		40	0.05	--	0.09	0.06	0.02	--	0.02	0.04	19	--	26	24
		60	0.06	--	0.06	0.02	0.01	--	0.01	0.02	29	--	24	19

(Continued)

Table 8 (Concluded)

Area	Site	Distance from Energy Source m	Seismic Response Measurements											
			PPV, 10^{-3} cm/sec				PSPV, 10^{-3} cm/sec				f, Hz			
			Field Measured		Best-Fit Curve		Field Measured		Best-Fit Curve		Field Measured		Best-Fit Curve	
			Wet Season	Dry Season	Wet Season	Dry Season	Wet Season	Dry Season	Wet Season	Dry Season	Wet Season	Dry Season	Wet Season	Dry Season
Airdrop 1	347	5	1.05	1.96	0.61	1.35	0.15	0.26	0.18	0.32	23	25	25	27
		10	0.40	1.10	0.38	0.75	0.12	0.27	0.10	0.20	31	31	25	26
		20	0.17	0.25	0.21	0.33	0.05	0.10	0.05	0.11	22	22	25	25
		30	0.08	0.14	0.14	0.17	0.03	0.07	0.03	0.07	23	22	25	23
		40	0.10	0.06	0.09	0.09	0.02	0.04	0.02	0.05	23	21	25	22
		60	0.07	0.04	0.05	0.03	0.01	0.03	0.01	0.03	31	18	25	18
Airdrop 4*	410	5	--	1.72	--	1.81	--	0.37	--	0.50	--	41	--	39
		10	--	1.56	--	0.99	--	0.42	--	0.30	--	45	--	38
		20	--	0.50	--	0.41	--	0.21	--	0.15	--	44	--	36
		30	--	0.12	--	0.20	--	0.07	--	0.09	--	21	--	34
		40	--	0.10	--	0.10	--	0.05	--	0.06	--	21	--	30
		60	--	--	--	0.03	--	--	--	0.02	--	--	--	--
Airdrop 5*	411	5	--	2.30	--	3.24	--	1.91	--	2.17	--	41	--	45
		10	--	1.46	--	1.55	--	0.87	--	1.08	--	40	--	42
		20	--	0.65	--	0.51	--	0.50	--	0.38	--	35	--	35
		30	--	0.18	--	0.19	--	0.14	--	0.15	--	28	--	29
		40	--	0.05	--	0.08	--	0.04	--	0.07	--	34	--	23
		60	--	0.02	--	0.01	--	0.02	--	0.01	--	12	--	11
Airdrop 3*	412	5	--	2.15	--	1.66	--	0.90	--	0.78	--	42	--	44
		10	--	1.69	--	0.91	--	0.72	--	0.45	--	40	--	42
		20	--	0.21	--	0.39	--	0.13	--	0.21	--	41	--	38
		30	--	0.18	--	0.19	--	0.12	--	0.12	--	38	--	33
		40	--	0.09	--	0.10	--	0.07	--	0.07	--	32	--	29
		60	--	0.02	--	0.03	--	0.02	--	0.02	--	13	--	21
Airdrop 6*	413	5	--	4.66	--	2.47	--	1.43	--	1.98	--	9	--	9
		10	--	1.56	--	1.59	--	1.23	--	1.35	--	9	--	9
		20	--	0.77	--	0.94	--	1.06	--	0.89	--	9	--	9
		30	--	0.67	--	0.64	--	0.74	--	0.68	--	9	--	9
		40	--	0.31	--	0.46	--	0.54	--	0.55	--	9	--	9
		60	--	0.22	--	0.26	--	0.33	--	0.39	--	7	--	9

* No seismic data obtained during wet season.

Table 9

Summary of Dry-Season Man-Walking Seismic Response Data

Area	Site	Distance from Energy Source ft	Peak Particle Velocity 10^{-3} cm/sec Field Measured	Peak Particle Velocity 10^{-3} cm/sec Fit Curve	Dominant Frequency, Hz Field Measured	Dominant Frequency, Hz Fit Curve	Root Mean Square Velocity 10^{-3} cm/sec Field Measured
Wood-emplacement	306	5	1.29	1.36	0.62	0.69	40	36.0	0.09
		10	1.04	0.84	0.64	0.40	39	35.1	0.10
		20	0.47	0.37	0.31	0.20	39	31.7	0.06
		30	0.20	0.20	0.17	0.13	37	29.9	0.04
		40	0.19	0.11	0.07	0.08	8	26.0	0.02
		60	0.06	0.04	0.04	0.04	16	18.0	0.01
Wood-emplacement	306	5	1.27	1.40	0.69	0.44	46	41.5	0.07
		10	0.7	0.81	0.60	0.31	44	34.0	0.14
		20	0.31	0.39	0.17	0.17	24	33.1	0.07
		30	0.20	0.21	0.11	0.11	26	28.0	0.05
		40	0.11	0.14	0.06	0.07	20	23.4	0.03
		60	0.05	0.05	0.04	0.04	13	13.5	0.01
Wood-emplacement	337	5	1.47	0.85	0.46	0.35	37	30.3	0.01
		10	0.71	0.37	0.18	0.09	32	31.1	0.07
		20	0.28	0.07	0.15	0.13	20	28.4	0.03
		30	0.10	0.07	0.09	0.08	28	25.9	0.02
		40	0.09	0.10	0.06	0.06	16	23.2	0.01
		60	0.05	0.03	0.04	0.03	23	16.1	0.00
Wood-emplacement	338	5	1.26	1.77	0.56	0.87	46	34.0	0.07
		10	1.41	0.96	0.41	0.43	25	37.3	0.01
		20	0.26	0.17	0.21	0.18	26	33.7	0.04
		30	0.19	0.06	0.10	0.07	30	29.7	0.07
		40	0.13	0.15	0.10	0.11	28	26.8	0.04
		60	0.06	0.04	0.04	0.03	19	13.8	0.00
Wood-emplacement	339	5	1.10	0.85	0.47	0.31	48	42.1	0.13
		10	0.64	0.61	0.40	0.21	41	39.0	0.10
		20	0.23	0.26	0.16	0.11	24	33.4	0.06
		30	0.11	0.15	0.07	0.07	28	27.3	0.03
		40	0.07	0.09	0.05	0.05	19	20.9	0.02
		60	0.05	0.04	0.03	0.03	16	11.9	0.00
Wood-emplacement	340	5	0.58	0.62	0.39	0.05	10	21.5	0.16
		10	0.31	0.30	0.15	0.17	31	28.4	0.07
		20	0.23	0.24	0.09	0.12	21	19.7	0.04
		30	0.21	0.18	0.09	0.07	19	18.5	0.03
		40	0.15	0.15	0.08	0.08	19	17.4	0.03
		60	0.11	0.11	0.06	0.04	14	15.1	0.00
Wood-emplacement	341	5	1.49	1.82	0.42	0.50	10	26.1	0.24
		10	1.57	1.10	0.38	0.30	19	26.1	0.01
		20	0.47	0.58	0.20	0.19	31	26.2	0.11
		30	0.31	0.25	0.12	0.13	23	25.0	0.05
		40	0.17	0.23	0.08	0.09	28	20.2	0.03
		60	0.10	0.12	0.05	0.05	25	16.0	0.01
Wood-emplacement	342	5	1.60	0.95	0.31	0.20	28	29.7	0.23
		10	0.40	0.57	0.21	0.20	29	28.4	0.08
		20	0.19	0.20	0.11	0.11	25	25.9	0.04
		30	0.18	0.13	0.08	0.08	20	23.4	0.03
		40	0.12	0.11	0.05	0.05	24	20.6	0.02
		60	0.06	0.05	0.03	0.03	19	16.7	0.02

Area	Site	Distance from Energy Source ft	Peak Particle Velocity 10^{-3} cm/sec Field Measured	Peak Particle Velocity 10^{-3} cm/sec Fit Curve	Dominant Frequency, Hz Field Measured	Dominant Frequency, Hz Fit Curve	Root Mean Square Velocity 10^{-3} cm/sec Field Measured
Wood-emplacement	343	5	1.08	1.08	0.47	0.50	23	24.0	0.13
		10	0.91	0.81	0.31	0.25	23	23.7	0.14
		20	0.45	0.47	0.24	0.20	19	23.1	0.09
		30	0.24	0.21	0.13	0.16	23	22.1	0.05
		40	0.20	0.12	0.10	0.10	22	21.2	0.05
		60	0.11	0.10	0.07	0.07	25	20.7	0.02
Wood-emplacement	345	5	0.89	0.84	0.34	0.23	32	31.6	0.10
		10	0.34	0.62	0.24	0.19	28	29.8	0.13
		20	0.17	0.24	0.09	0.12	31	26.4	0.04
		30	0.14	0.15	0.11	0.09	32	23.2	0.05
		40	0.08	0.11	0.06	0.07	15	19.6	0.02
		60	0.03	0.07	0.05	0.04	15	12.7	0.02
Airdrop 1	347	5	1.31	1.07	0.35	0.37	38	33.7	0.23
		10	0.58	0.64	0.29	0.24	36	30.1	0.15
		20	0.41	0.33	0.17	0.14	19	28.8	0.07
		30	0.19	0.19	0.08	0.09	25	25.5	0.03
		40	0.10	0.13	0.07	0.07	21	23.2	0.01
		60	0.06	0.05	0.04	0.04	13	15.7	0.02
Airdrop 4	410	5	1.79	1.09	1.08	0.77	08	27.4	0.41
		10	0.96	0.78	0.61	0.48	03	00.9	0.21
		20	0.06	0.40	0.17	0.26	26	25.6	0.07
		30	0.16	0.24	0.14	0.16	23	24.4	0.06
		40	0.13	0.15	0.11	0.11	21	23.7	0.04
		60	0.08	0.07	0.06	0.05	20	20.8	0.02
Airdrop 5	411	5	2.26	1.95	1.26	1.26	40	32.0	0.62
		10	1.18	1.09	0.66	0.72	26	30.9	0.25
		20	0.45	0.50	0.25	0.32	15	28.5	0.11
		30	0.21	0.26	0.11	0.16	27	27.1	0.05
		40	0.19	0.15	0.07	0.09	28	22.7	0.03
		60	0.06	0.05	0.04	0.03	16	15.7	0.02
Airdrop 3	412	5	1.69	1.45	0.99	0.67	44	41.3	0.41
		10	1.05	0.88	0.30	0.35	46	38.8	0.19
		20	0.24	0.37	0.10	0.18	26	31.0	0.04
		30	0.16	0.19	0.14	0.11	18	29.1	0.05
		40	0.10	0.11	0.07	0.07	34	24.3	0.03
		60	0.05	0.04	0.04	0.03	15	14.5	0.07
Airdrop 6	413	5	4.67	3.46	1.38	1.05	9	8.4	0.84
		10	0.11	0.40	0.08	1.05	9	8.6	0.68
		20	1.10	1.06	0.95	0.73	7	8.3	0.29
		30	0.65	0.77	1.10	0.49	9	7.6	0.28
		40	0.41	0.50	0.46	0.35	7	7.6	0.17
		60	0.04	0.22	0.49	0.19	7	6.8	0.12

Table 10

Summary of Vehicle Seismic Response Test Data, Hand-Emplacement Area

Cross-Country Site	Vehicle	Speed km/hr	Distance from Energy Source m	Seismic Response Measurements (Dry Season)						
				Peak Particle Velocity 10^{-3} cm/sec		Peak Summed Particle Velocity 10^{-3} cm/sec		Frequency, Hz		Root Mean Square Velocity 10^{-3} cm/sec
				Field Measured	Best-Fit Curve	Field Measured	Best-Fit Curve	Field Measured	Best-Fit Curve	Field Measured
344	M151	8	50	0.14	0.15	0.11	0.14	13	13.3	0.04
			100	0.06	0.10	0.06	0.07	15	13.3	0.02
			150	0.09	0.07	0.07	0.04	13	13.3	0.02
			200	0.08	0.06	0.07	0.03	10	13.3	0.02
			250	0.04	0.05	0.01	0.02	16	13.3	0.01
			300	0.04	0.04	0.01	0.01	13	13.3	0.01
			400	--	0.03	--	0.01	--	--	--
			500	--	0.02	--	0.00	--	--	--
	M151	32	50	0.51	0.54	0.46	0.53	18	18.5	0.18
			100	0.28	0.31	0.26	0.30	21	17.1	0.10
			150	--	0.21	--	0.20	--	--	--
			200	0.23	0.14	0.31	0.14	9	14.3	0.09
			250	--	0.10	--	0.10	--	--	--
			300	0.05	0.08	0.04	0.08	12	11.5	0.02
			400	0.05	0.04	0.05	0.04	10	8.7	0.02
			500	--	0.03	--	0.03	--	--	--
	M577	8	50	--	1.10	--	1.69	--	--	--
			100	0.63	0.68	1.35	0.90	15	15.4	0.38
			150	--	0.48	--	0.58	--	--	--
			200	0.33	0.36	0.40	0.39	15	14.3	0.12
			250	--	0.28	--	0.27	--	--	--
			300	0.21	0.23	0.13	0.19	13	13.1	0.05
			400	0.22	0.15	0.08	0.10	12	11.6	0.04
			500	0.12	0.10	0.06	0.05	16	10.7	0.03
	M577	32	50	--	2.95	--	4.97	--	--	--
			100	1.43	1.66	1.26	2.37	15	12.1	0.50
			150	--	1.08	--	1.31	--	--	--
			200	1.00	0.74	1.34	0.77	15	14.2	0.40
			250	--	0.53	--	0.46	--	--	--
			300	0.32	0.39	0.29	0.29	12	16.3	0.12
			400	0.24	0.21	0.27	0.11	12	18.4	0.09
			500	0.11	0.12	0.02	0.05	28	20.5	0.05
345	M151	8	50	0.22	0.18	0.20	0.16	21	17.4	0.07
			100	0.09	0.12	0.05	0.09	13	16.1	0.02
			150	0.08	0.08	0.06	0.06	13	14.8	0.02
			200	0.07	0.06	0.06	0.04	12	13.5	0.02
			250	0.05	0.05	0.02	0.03	15	12.2	0.01
			300	--	0.04	--	0.02	--	--	--
			400	--	0.03	--	0.01	--	--	--
			500	--	0.02	--	0.01	--	--	--
	M151	32	50	--	0.61	--	0.61	--	--	--
			100	0.26	0.35	0.37	0.35	13	14.5	0.10
			150	--	0.23	--	0.23	--	--	--
			200	0.29	0.16	0.29	0.16	15	13.0	0.09
			250	--	0.12	--	0.12	--	--	--
			300	0.07	0.09	0.05	0.09	12	11.5	0.02
			400	0.05	0.05	0.02	0.05	9	10.0	0.01
			500	--	0.03	--	0.03	--	--	--
	M577	8	50	--	1.24	--	2.14	--	--	--
			100	1.24	0.72	1.82	1.15	13	14.8	0.42
			150	--	0.48	--	0.71	--	--	--
			200	0.25	0.35	0.37	0.47	15	13.0	0.12
			250	--	0.26	--	0.32	--	--	--
			300	0.16	0.19	0.17	0.22	12	11.2	0.07
			400	0.08	0.11	0.07	0.11	9	9.4	0.02
			500	0.07	0.07	0.07	0.06	7	7.6	0.05
	M577	32	50	1.70	2.35	1.58	2.68	25	22.5	0.98
			100	1.69	1.36	2.44	1.59	12	16.3	0.29
			150	0.90	0.90	0.90	1.09	12	11.5	0.36
			200	0.91	0.61	1.19	0.79	9	8.0	0.16
			250	--	0.47	--	0.59	--	--	--
			300	0.30	0.35	0.45	0.45	6	5.1	0.13
			400	0.17	0.20	0.30	0.27	7	7.6	0.08
			500	0.13	0.12	0.14	0.17	7	--	0.04

Table 11

Summary of MINISID Data for Man-Walking and Vehicle Tests

Area	Site	No. of Test	MINISID Detection Distance, m: Low Gain* Dry Season	Medium Gain Wet Season	Medium Gain Dry Season	High Gain* Dry Season
Man-Walking Data						
Hand-emplacement	335	1	9.0**	--	28.0**	63.0**
		2	10.0	--	26.5	63.0
		3	10.0	--	28.0	68.0
		4	10.0	--	27.5	65.0
		5	--	--	27.0	67.5
		Avg	9.8	--	27.4	65.3
	336	1	11.0**	47.0†	28.0**	60.0**
		2	12.0	47.0	36.0	66.0
		3	12.0	58.0	34.0	66.0
		4	13.0	55.0	35.0	68.0
		5	--	52.0	35.0	--
		Avg	12.0	51.8	34.2	66.0
	337	1	3.0**	25.0†	24.0**	48.0**
		2	5.0	21.0	23.0	52.0
		3	5.0	23.0	23.0	52.0
		4	6.0	22.0	25.0	55.0
		Avg	4.8	23.0	23.6	51.8
	338	1	13.0**	22.0†	30.0**	49.0**
		2	12.0	30.0	33.0	50.0
		3	12.0	30.0	28.0	50.0
		4	12.0	34.0	29.0	51.0
		5	--	35.0	--	--
		Avg	12.3	31.4	29.0	50.0
	339	1	--	18.0†	21.5**	40.0**
		2	--	26.0	20.0	41.5
		3	--	22.0	22.5	42.5
		4	--	24.0	23.0	44.0
		5	--	25.0	20.0	41.0
		Avg	--	23.0	21.4	41.6
	340	1	11.0**	--	38.0**	89.0**
		2	9.0	--	40.0	84.0
		3	11.0	--	38.0	89.0
		4	9.0	--	38.0	76.0
		5	--	--	37.0	89.0
		Avg	10.0	--	38.2	86.0
	341	1	8.0**	28.0†	33.0**	76.0**
		2	8.0	26.0	35.0	71.0
		3	8.0	26.0	35.0	80.0
		4	--	29.0	29.0	80.0
		5	--	--	33.0	69.0
		Avg	8.0	27.2	33.0	75.2
	342	1	4.0**	19.0†	20.0**	34.0**
		2	3.0	24.0	20.0	40.0
		3	1.0	22.0	20.0	38.0
		4	5.0	25.0	19.0	34.0
		5	3.0	22.0	--	35.0
		Avg	3.2	22.4	19.8	36.2
	348	1	14.0**	35.0†	55.0**	79.0**
		2	14.0	36.0	54.0	81.0
		3	17.0	33.0	56.0	79.0
		4	14.0	35.0	56.0	76.0
		5	18.0	--	--	89.0
		Avg	15.8	34.5	55.3	80.0
	349	1	7.0**	27.0†	27.0**	53.0**
		2	6.0	30.0	25.0	56.0
		3	5.0	30.0	27.0	55.0
		4	--	27.0	27.0	55.0
		5	--	30.0	--	--
		Avg	6.0	28.8	26.5	54.8
Man-Walking Data (Continued)						
Airdrop 1	347	1	10.0**	29.0†	23.0**	56.0**
		2	9.0	--	24.0	60.0
		3	10.0	--	23.0	60.0
		4	12.0	--	22.0	59.0
		5	13.0	--	--	--
		Avg	10.8	29.0	23.0	58.8
Airdrop 4	410	1	16.0**	--	30.0**	62.0**
		2	13.0	--	30.0	60.0
		3	13.0	--	35.0	61.0
		4	16.0	--	31.0	61.0
		5	12.0	--	--	--
		Avg	14.0	--	31.5	61.0
Airdrop 5	411	1	17.0**	--	25.0**	64.0**
		2	17.0	--	25.0	45.0
		3	17.0	--	29.0	45.0
		4	20.0	--	28.0	45.0
		5	--	--	27.0	45.0
		Avg	17.8	--	26.0	48.8
Airdrop 3	412	1	13.0**	--	33.0**	50.0**
		2	14.0	--	40.0	51.0
		3	13.0	--	34.0	54.0
		4	11.0	--	37.0	54.0
		5	--	--	31.0	51.0
		Avg	12.8	--	35.0	52.0
Airdrop 6	413	1	40.0††	--	71.0††	101.0††
		2	42.0	--	69.0	98.0
		3	45.0	--	71.0	105.0
		4	45.0	--	69.0	104.0
		5	44.0	--	--	105.0
		Avg	43.2	--	70.0	102.0
Vehicle Data						
Hand-emplacement: CC	344‡	1	200.0	330.0	310.0	400.0
		2	--	330.0	--	450.0
		Avg	200.0	330.0	310.0	425.0
CC	344‡‡	1	190.0	298.0	280.0	475.0
		2	260.0	300.0	325.0	500.0
		Avg	225.0	299.0	302.5	487.5
CC	344§	1	60.0	120.0	175.0	265.0
		2	60.0	115.0	150.0	275.0
		Avg	60.0	117.5	162.5	270.0
CC	344§§	1	10.0	75.0	90.0	125.0
		2	15.0	85.0	75.0	135.0
		Avg	12.5	80.0	82.5	130.0
CC	345§	1	60.0	--	210.0	250.0
CC	345§§	1	15.0	--	45.0	125.0
		2	--	--	--	--
		Avg	15.0	--	45.0	125.0
CC	345‡	1	225.0	--	350.0	390.0
		2	225.0	--	300.0	411.0
		Avg	225.0	--	300.0	403.0
	345‡‡	1	238.0	--	333.0	457.0
		2	222.0	--	258.0	400.0
		Avg	230.0	--	295.5	428.5

Note: Wet-season data obtained in August 1971; dry-season data obtained in March 1972.

* No test conducted in the wet season.

** Detection distance for a man weighing 69.8 kg (wearing boots, size 9) and walking an average of one step per meter.

† Detection distance for a man weighing 79.2 kg (wearing boots, size 11) and walking an average of one step per meter.

†† Detection distance for a man weighing 70.3 kg (wearing boots, size 7-1/2) and walking an average of one step per 0.83 m.

‡ M-77 vehicle, speed 32 km/hr.

‡‡ M-77 vehicle, speed 8 km/hr.

§ M-151 vehicle, speed 32 km/hr.

§§ M-151 vehicle, speed 8 km/hr.

Table 12

AFSWP/S Test Data for Special CSEWS Airdrop Area

Test No.	Length of Penetration Along Sensor Impact Trajectory, cm	Sensor Impact Angle deg	Aircraft* Speed m/sec	Aircraft* Altitude m	Wind Speed, m/sec, and Direction
1	29.2	36	87.5	183	0.0
2	49.7	51			
3	31.8	22			
4	30.5	46			
5**	25.4	37			
6	31.8	36			
7	29.2	40			
8	25.4	32			
9**	24.1	39			
10	28.6	40			
11**	27.9	35			
12**	27.9	28			
13	35.6	33			2.6 S
14	33.0	42			
15	48.3	41			
16	27.9	20			
17	36.8	29			
18	31.8	19			
19	26.7	35		122	
20	27.9	33			
21	22.9	36			
22	20.3	46			1.0 S
23	27.9	50			
24	27.9	40			
25	--	--			
26	--	--			
27	33.0	30		183	
28	41.9	45			
29	50.8	33			
30	24.1	40			
31	24.1	35			
32	--	--			
33	24.1	42			
34**	22.9	52			
35	24.1	46			
36**	26.7	60			
37	33.0	22			0.0
38	27.9	41			
39	30.5	49			
40	20.3	31			
41	27.9	29			
42	30.5	35			
43	27.9	24			
44	35.6	31			
45	27.9	40			
46	33.0	28			
47	25.4	20			
48	20.3	58			
49	25.4	54		1[illegible]2	1.5 E
50	21.6	30		172	
51	20.3	26		172	
52	25.4	40		183	
53	24.1	33		183	
54	22.9	21		183	
55	25.4	24		237	
56	29.2	26		238	
57	27.9	23		236	
58	50.8	30		241	
59	29.2	18		241	
60	22.9	26		241	
61	22.9	41	87.5	244	1.5 S
62	25.4	33			
63	21.6	18			
64	20.3	15			
65	25.4	30			
66	31.8	30			
67	17.8	16			
68	40.6	32			
69	50.8	49			
70	33.0	18		250	
71	50.8	28		250	
72	33.0	33		250	
73	25.4	62		91	1.0 S
74	29.2	55			
75**	30.5	59			
76**	24.1	62			
77	29.2	55			
78**	22.9	55			
79**	22.9	55			
80**	27.9	46			
81	--	--			
82	30.5	50			
83	20.3	62			
84	17.8	61			
85	25.4	30		183	1.5 S
86	38.5	28			
87	33.0	35			
88	35.6	46			
89	43.2	36			
90	45.7	38			
91	30.5	31		244	
92	30.5	19			
93	20.3	24			
94	22.9	36			
95	20.3	25			
96	33.0	40			
97	20.3	31			0.0
98	40.6	29			
99	38.1	25			
100	25.4	24			
101	20.3	51			
102	24.1	17			
103	15.2	26			
104	24.1	42			
105	22.9	39			
106	29.2	31			
107	--	--			
108	29.2	12			
109	22.9	51		183	
110	26.7	46			
111	--	--			
112	20.3	35			
113	17.8	35			
114	22.9	36			
115	34.3	18		244	
116	20.3	30			
117	27.9	26			
118	25.4	32			
119	26.7	36			
120	22.9	30			

Note: For soil moisture and strength data corresponding to each test number, see table 4.

* Direction of aircraft, west to east.

** Near-surface impact velocity measurements obtained using high-speed ground photography (see table 16).

Table 13

Summary of Input Parameters Used in Penetration Predictions of ADSID/S Sensor

Airdrop Area	Test Pit	Water Content, %		Average Initial Young's Modulus E, kg/cm^2		Ultimate Shear Strength σ_u, kg/cm^2		Compressibility Parameter* ρ_p/ρ		Drag Coefficient, C_D	
		Dry Season	Wet Season	Dry Season	Wet Season	Dry Season	Wet Season	Dry Season	Wet Season	Dry Season	Wet Season
1	5	9-10	14	560	147	1.22	1.22	1.18	1.11	0.2	0.2
	6	5-6	10-11	1400	560	119.00	6.06	1.29	1.14	0.2	0.2
4	3	6	14	1120	910	162.00	44.00	1.32	1.26	0.2	0.2
	4	7	13-14	1220	1120	162.00	43.60	1.33	1.23	0.2	0.2
5	1	8-10	15	1120	840	120.00	24.20	1.29	1.27	0.2	0.2
	2	7	14	1400	490	80.00	7.95	1.28	1.23	0.2	0.2

* For an imcompressible material $\rho_p/\rho = 1$.

Table 14

Comparison of Measured and Predicted Detection Distances (Medium Gain)
Using Analog Computer Models and Man-Walking Data

Site No.	Detection Distance, m: Measured by MINISID	Predicted	Difference	Remarks
		Wet-Season Conditions (Aug 1972), Fort Bragg, N. C.*		
370	64	60	-4	
371	106	97	-8	High background noise during MINISID tests
372	93	87	-6	
373	56	74	+18	High background noise during analog man-walking tests
374	85	86	+1	
375	43	41	-2	
376	81	73	-8	Wind gusting during MINISID tests
377	73	63	-10	
378	37	36	-1	
379	41	55	+14	
380	40	27	-13	Wind gusting during MINISID tests
381	29	28	+1	
382	85	77	-8	
383	19	24	+5	
492	81	81	0	
493	36	64	+28	
		Dry-Season Conditions (Mar 1972), Fort Bragg, N. C.**		
373	46	40	-6	
374	44	54	+10	
375	28	31	+3	
376	69	73	+4	
377	64	62	-2	
378	26	65	+39	
379	24	29	+5	
380	22	23	+1	
381	25	29	+4	
382	26	52	+26	
383	12	12	0	
		Dry-Season Conditions (Mar 1971), Fort Huachuca, Ariz.†		
335	27	24	-3	
336	34	29	-5	
337	24	20	-4	
338	29	27	-2	
339	21	22	+1	
340	38	34	-4	
341	33	35	+1	
342	20	22	+2	
347	23	24	+1	
348	55	52	-3	
349	26	28	+2	
410	32	33	-1	
411	26	39	+13	High background noise during analog man-walking tests (backhoe machine digging hole)
412	35	38	+3	
413	70	72	+2	
		Wet-Season Conditions (Jan 1973), Germany††		
414	0	5	+5	
416	26	40	+14	High background noise during analog man-walking tests (factory, road traffic)
417	17	31	+14	
419	14	23	+9	
426	1	7	+6	High wind noise during analog man-walking tests
431	40	53	+14	
432	0	4	+4	
445	18	30	+12	High background noise during analog man-walking tests
448	14	33	+19	High background noise during analog man-walking tests
461	22	51	+29	High background noise during analog man-walking tests
462	31	39	+8	
468	3	5	+2	

* Mean difference, 7.7; std dev, ±11.0; number of sites overpredicted, 6; number of sites underpredicted, 8.
** Mean difference, 9.1; std dev, ±13.2; number of sites overpredicted, 8; number of sites underpredicted, 2.
† Mean difference, 3.1 m; std dev, ±4.4 m; number of sites overpredicted, 8; number of sites underpredicted, 7.
†† Mean difference, 12.0; std dev, 7.5; number of sites overpredicted, 12; number of sites underpredicted, 0.

Table 15

Prediction of Maximum Deceleration of ADSID/S at 50-m/sec Impact Velocity

Airdrop Area	Test Pit	Maximum Deceleration of ADSID/S at 50-m/sec Impact Velocity, m/sec^2	
		Wet Season	Dry Season
1	5	1.927×10^3	3.769×10^3
	6	6.420×10^3	2.730×10^4
4	3	1.519×10^4	2.555×10^4
	4	1.771×10^4	2.687×10^4
5	1	1.175×10^4	2.355×10^4
	2	5.968×10^3	2.408×10^4

Note: Maximum allowable deceleration for ADSID/S is approximately 9.85×10^3 m/sec^2 .

Table 16

Comparison of Measured and Predicted Penetration Depths of Air-Delivered (ADSID/S) Sensors at CSEWS Airdrop Test Area

Test No.*	Impact Velocity Vector m/sec	Impact Angle (Off Vertical) deg	Moisture Content %	Length of Penetration, cm		
				Measured	Predicted	Difference, Measured from Predicted
5	47.795	37	6.3	25.4	24.4	-1.0
9	46.032	39	5.6	24.1	22.1	-2.0
11	51.227	35	6.4	28.0	27.4	-0.5
12	44.603	28	8.6	27.9	30.0	+2.1
34	52.962	52	8.2	22.9	30.9	+8.1
36	51.297	60	8.0	26.7	24.1	-2.6
75	45.129	59	7.6	30.0	18.5	-12.0
76	50.224	62	6.4	24.1	14.7	-9.4
78	49.104	55	7.9	22.9	25.9	+3.0
79	49.409	55	5.5	22.9	17.5	-5.4
80	47.809	46	6.5	27.9	20.3	-7.6

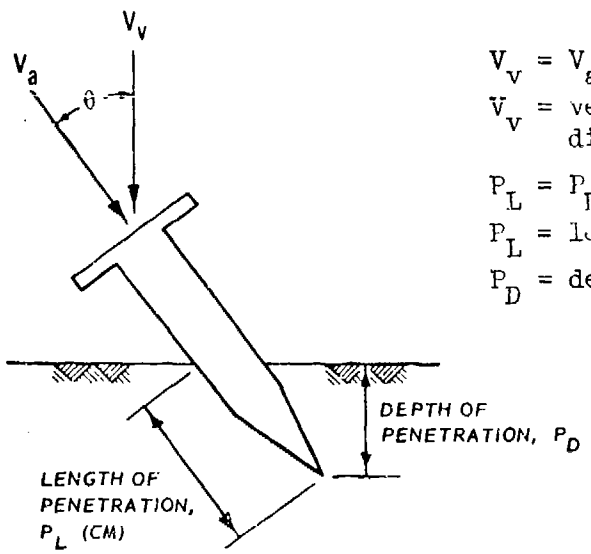

$V_v = V_a \cos \theta$

V_v = velocity in the vertical direction

$P_L = P_D / \cos \theta$

P_L = length of penetration

P_D = depth of penetration

* See table 2 for site descriptions.

Table 17

Factor Classes and Factor Value Ranges for Terrain Factor Complex Map, Hand-Emplacement Area, Wet and Dry Seasons

Factor Class	Layer Thickness T cm	Compression Wave Velocity V_P m/sec	Shear Wave Velocity V_S m/sec	Density ρ g/cm^3
		Layer 1		
1	40-65	220-260	75-115	1.00-1.45
2	66-95	261-290	116-135	1.46-1.60
3	96-125	291-320	136-155	1.61-1.80
4	126-165	321-360	156-175	1.81-2.10
5	166-200	361-400	176-190	2.11-2.30
6	201-240	401-460	191-220	
7	241-280	461-525		
8	281-320			
9	321-600			
		Layer 2		
1	100-150	470-570	235-285	1.61-1.80
2	151-240	571-645	286-335	1.81-2.10
3	241-330	646-750	336-385	2.11-2.30
4	331-480	751-950		
5	481-600	951-1100		
6	601-800	1101-1300		
7	801-1100	1301-1700		
8	1101-2000	1701-2100		

Table 18

Legend for Terrain Factor Complex Map, Hand-Emplacement Area, Wet and Dry Seasons

Map Unit	Factor Class: Layer 1 T_1	V_{P1}	V_{S1}	ρ_1	Layer 2 T_2	V_{P2}	V_{S2}	ρ_2
1	1	1	3	3	4	2	3	1
2	1	1	3	3	5	3	3	2
3	1	1	4	3	3	3	3	2
4	1	3	3	3	3	3	3	2
5	1	4	2	2	2	2	1	2
6	1	4	2	4	1	1	1	2
7	1	4	2	4	1	2	1	2
8	2	4	3	3	4	2	3	2
9	2	4	4	4	3	2	2	2
10	2	4	6	2	5	2	2	1
11	2	4	6	3	3	4	4	2
12	2	5	5	3	2	2	1	2
13	2	7	6	4	8	4	1	3
14	3	1	1	2	3	1	1	1
15	3	1	3	2	5	1	2	1
16	3	2	3	2	2	1	2	2
17	3	3	3	3	5	3	2	2
18	3	5	5	3	3	3	1	2
19	3	5	5	3	5	4	2	2
20	3	5	5	4	4	3	3	3

Map Unit	Factor Class: Layer 1 T_1	V_{P1}	V_{S1}	ρ_1	Layer 2 T_2	V_{P2}	V_{S2}	ρ_2
21	3	5	5	4	5	4	3	2
22	3	5	6	3	8	4	2	2
23	3	5	6	4	5	3	1	3
24	3	7	5	4	1	4	2	3
25	3	7	5	4	3	3	1	2
26	4	3	3	2	5	1	1	1
27	4	4	5	2	5	3	1	1
28	4	6	4	4	3	3	1	2
29	4	6	4	4	5	4	2	2
30	4	6	4	4	8	4	2	2
31	4	6	6	4	6	4	1	2
32	4	6	6	4	8	2	2	3
33	4	6	6	4	8	4	1	3
34	4	7	5	4	2	4	2	3
35	4	7	6	4	8	4	1	3
36	6	6	4	4	2	4	2	3
37	9	6	4	4	8	4	2	2
38	9	6	5	4	6	4	2	3
39	9	7	5	4	8	4	2	3
40	9	7	6	4	8	4	1	3

Table 19

Summary of Terrain Factor Map Data for Theoretical Model Predictions, Fort Huachuca, Arizona (Dry Season)

Test Area	Map Unit No.	First Layer				Second Layer			
		Layer Thickness T_1 cm	Compression Wave Velocity V_{P1} m/sec	Shear Wave Velocity V_{S1} m/sec	Wet Density ρ_1 g/cm^3	Layer Thickness* T_2 cm	Compression Wave Velocity V_{P2} m/sec	Shear Wave Velocity V_{S2} m/sec	Wet Density ρ_2 g/cm^3
Hand-emplacement	1	53	240	146	1.71	406	608	361	1.71
	3	53	240	166	1.71	286	698	361	1.96
	7	53	341	126	1.96	125	608	260	1.96
	9	81	341	166	1.96	286	608	311	1.96
	12	81	381	183	1.71	196	608	260	1.96
	13	81	493	206	1.96	1601	851	260	2.21
	21	111	381	183	1.96	1601	851	361	1.96
	22	111	381	206	1.71	1601	851	311	1.96
	25	111	493	183	1.96	286	698	260	1.96
	30	146	431	166	1.95	1601	851	311	1.96

* Second-layer thickness is assumed to be an infinite half-space for a two-layered case.

Table 20

Comparison of Theoretical Predictions Based on Site and Factor Complex Data

Site No.	Map Unit	Predictions Based on Site Data and 20-m Reference Signal	Predictions Based on Factor Complex Data and 20-m Reference Signal	Difference, m
335	12	27	27	0
336	7	25	24	+1
337	25	17	15	+2
338	13	28	28	0
339	30	17	16	+1
340	3	25	25	0
341	22	31	31	0
342	21	19	19	0
348	9	27	28	-1
349	1	22	21	+1

Table 21

Legend for Dry-Season Drop-Hammer Seismic Response Map, Hand-Emplacement Area

Map Unit	Drop-Hammer Seismic Response Factor Class																	
	PPV						PSPV						f					
	5 m	10 m	20 m	30 m	40 m	60 m	5 m	10 m	20 m	30 m	40 m	60 m	5 m	10 m	20 m	30 m	40 m	60 m
1	4	3	2	2	1	1	2	2	1	1	1	1	3	3	2	2	2	2
2	4	3	2	2	1	1	3	2	2	1	1	1	5	5	4	3	3	1
3	4	3	2	2	2	1	2	2	1	1	1	1	4	4	4	3	3	2
4	4	4	2	2	1	1	2	2	1	1	1	1	4	4	4	3	2	1
5	4	4	3	2	1	1	3	2	2	1	1	1	5	5	4	3	3	1
6	4	4	3	2	2	1	3	2	2	1	1	1	4	4	3	3	3	2
7	4	4	3	2	2	1	3	2	2	1	1	1	9	7	5	3	2	2
8	4	4	3	3	2	2	4	3	2	2	2	2	5	5	4	4	3	1

Seismic Response Factor Class	Seismic Response Factor Value Range		
	PPV	PSPV	f
	10^{-3} cm/sec	10^{-3} cm/sec	Hz
1	0.0 to 0.10	0.0 to 0.10	11 to 16
2	0.11 to 0.30	0.11 to 0.30	17 to 22
3	0.31 to 0.60	0.31 tp 0.60	23 to 29
4	0.61 to 1.50	0.61 to 1.00	30 to 36
5	1.51 to 3.50	1.01 to 1.50	37 to 43
6	3.51 to 7.00	1.51 to 2.50	44 to 50
7	7.01 to 13.00	2.51 to 3.50	51 to 56
8	13.01 to 28.00	3.51 to 6.00	57 to 62
9	--	6.01 to 13.00	63 to 68
10	--	13.01 to 28.00	69 to 74

Table 22

Legend for SID Performance Map, Hand-Emplacement Area

Wet and Dry Seasons

Map Unit	Detection Distance Class: Low Gain	Medium Gain	High Gain	Class	Detection Distance Class Range, m
1	1	3	5	1	1 to 4
2	1	3	6	2	5 to 10
3	1	4	5	3	11 to 20
4	1	4	6	4	21 to 30
5	1	5	8	5	31 to 40
6	2	3	5	6	41 to 50
7	2	4	5	7	51 to 60
8	2	4	6	8	61 to 80
9	2	4	8	9	81 to 110
10	2	5	6	10	111 to 140
11	2	5	8		
12	2	5	9		
13	3	4	5		
14	3	4	6		
15	3	5	6		
16	3	5	8		
17	3	5	9		
18	3	7	8		

APPENDIX A: MINISID AND ADSID/S DEVICES

1. The Phase III MINISID is a hand-emplaced, seismic intrusion detection device, whereas the Phase III ADSID/S (MA37) can either be hand-emplaced or emplaced by dropping from a fixed-wing or rotary-wing aircraft. The major components of the signal processing circuitry of the MINISID and ADSID/S are the geophone (MINISID contains an external cable-attached geophone and the ADSID/S contains an internal geophone), band-pass amplifier, and an integration circuit (i.e. a detection and alarm circuit). Both sensing devices can be disabled by the destruction of internal components. Such disabling of the MINISID can be caused by continuous transmission, tampering, battery run-down, end of programmed life, and improper recovery techniques. The disabling criteria for the ADSID/S are:

a. Tilting (i.e. improper implantation) or handling. The unit is disabled if the implantation angle is greater than 60-65 deg from the vertical.

b. End of programmed life. Time is preselected as 7, 14, 28, 45, 65, or 90 days, and an OFF position can be specified for its operational life.

c. End of battery life. Approximately 150 days.

d. Tampering. The unit is disabled by an antitamper circuit if disassembly is attempted after impact.

Since the ADSID/S is a ballistic penetration device, its impacting environment is critical to the survival of its internal components. The characteristics for survival of its interna components of the aircraft-delivered device are given below:

a. Shock. Half-size wave of 6-m/sec duration and less than 1000-g's peak deceleration.

b. Vibration. 20 to 2000 Hz with 20-g's peak.

c. Pressure. 5 to 35 psi or approximately 1/3 to 2-1/3 atmospheres.

2. The operational components of the signal processing circuitry of the MINISID and ADSID/S devices are discussed briefly below.

Geophone

3. The Phase III SID geophone consists of a coil of conducting wire and a magnet, one rigidly fixed with respect to the earth and the other suspended from a fixed support by a spring. Any relative motion between the coil and magnet produces a voltage across the coil terminals, which is proportional to the velocity of the motion. The geophone is considered to move as if it were part of the earth, and thus produces electrical signals whenever seismic oscillations are detected. The geophone sets the low-frequency operating point of the system and, in the case of a Phase III seismic sensor, has a resonant frequency of approximately 14 Hz as illustrated in fig. A1. The Phase III geophone is also

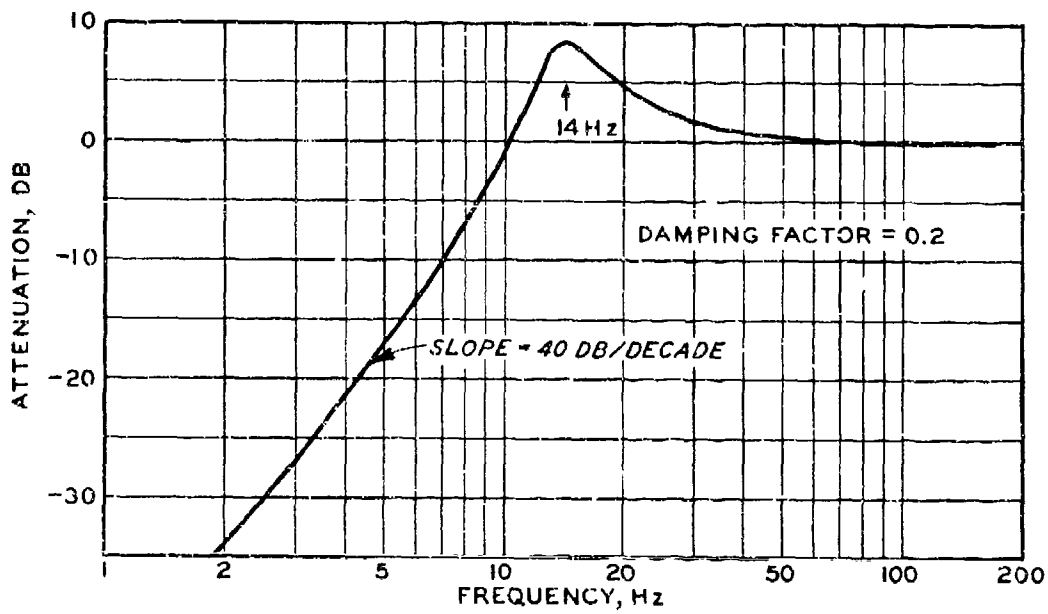

Fig. A1. Response at SID geophone

underdamped and has a damping factor of approximately 0.2 (i.e. 20 percent of critical damping).

Band-Pass Amplifier

4. The electrical signal from the geophone is of a very low level

and must be increased in the band-pass amplifier before further processing can take place. Most SID amplifiers can be set for various gains (low, medium, and high), which are separated by 8 db. The sensor amplifier reduces some of the background noise and enhances the seismic signal from the seismic sources by virtue of its limited bandwidth of from 9 to 45 Hz, as shown in fig. A2. These are the frequencies at which the

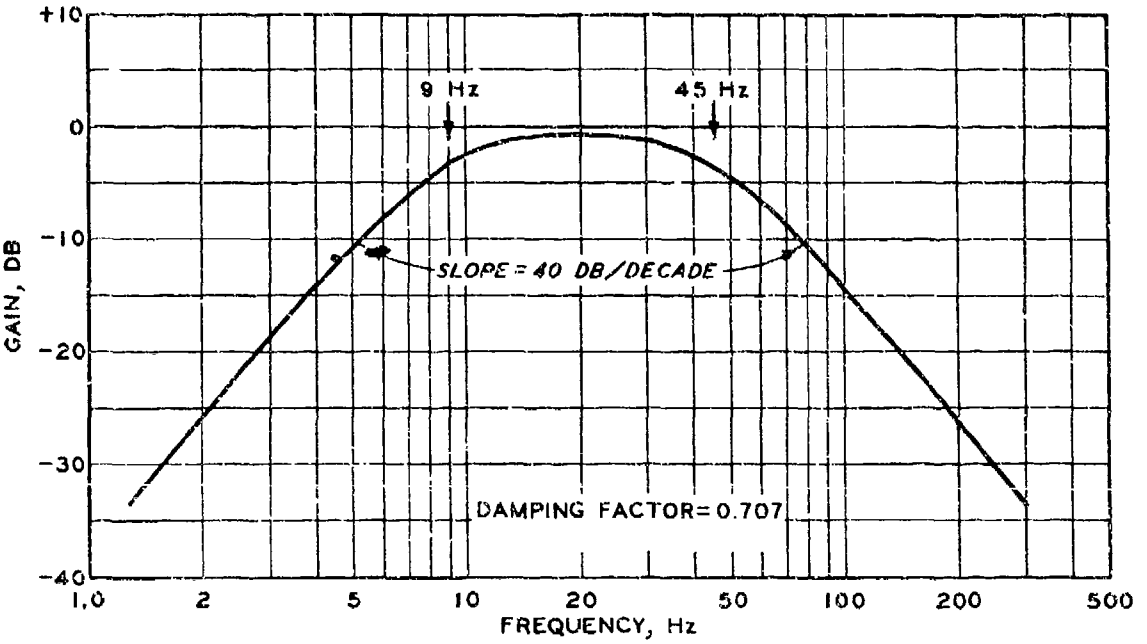

Fig. A2. Response of SID band-pass amplifier

gain is reduced by 3 db from that at the center frequency. The particle velocity-frequency logic for low, medium, and high gains of a Phase III SID is shown in fig. A3.

Integration Circuit

5. The integration circuit is designed to reduce false alarms caused by background noise. The signal is rectified, and only signals whose amplitude is 0.5 v or larger are allowed to be processed further. This corresponds to a particle velocity value of 38.1×10^{-6} cm/sec or larger at high gain at a frequency of 14 Hz, as indicated by fig. A3.

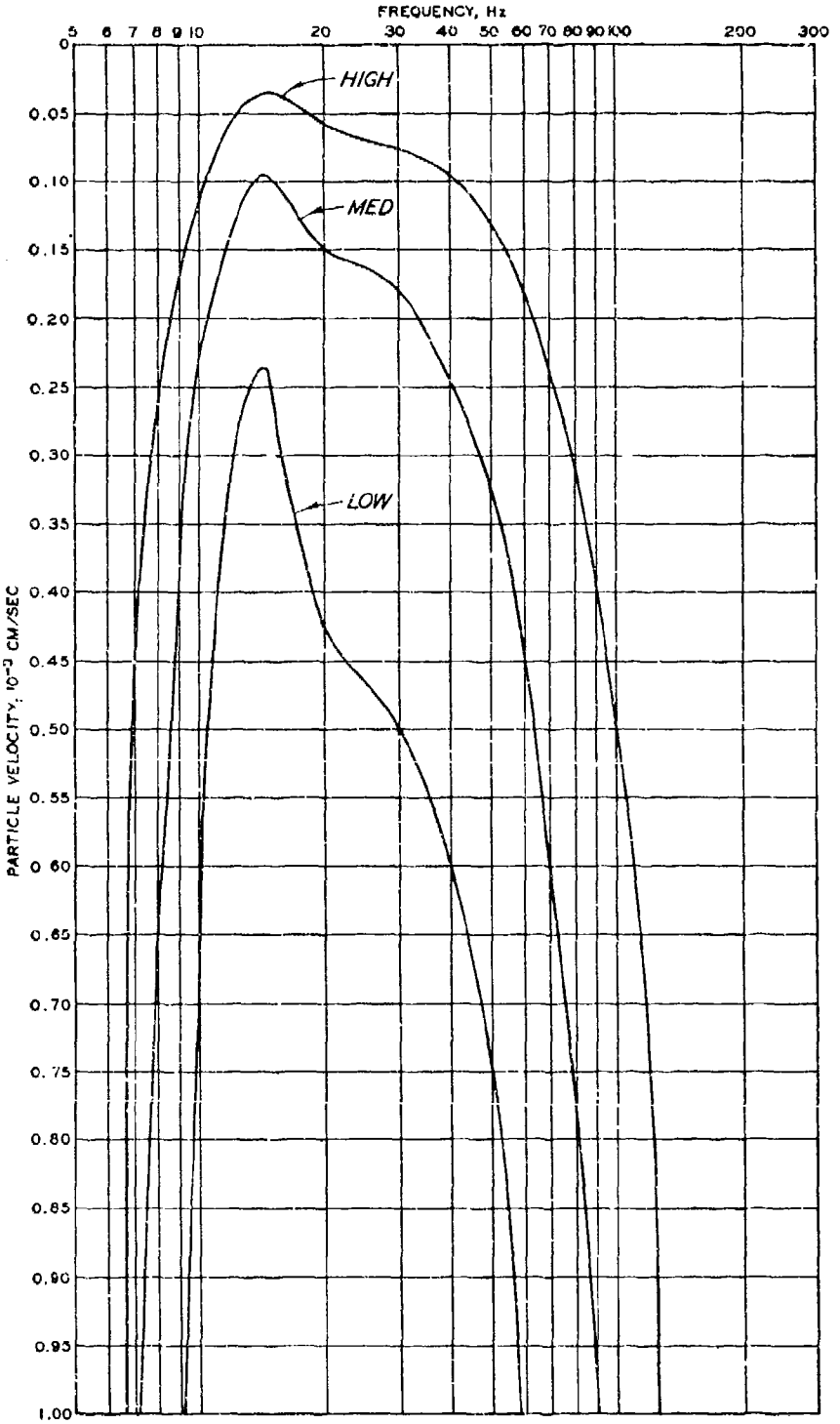

Fig. A3. Particle velocity-frequency response for a Phase III MINISID

At other frequencies or other gain settings, the value of particle velocity applied to the geophone would be correspondingly higher. The SID alarm system operates in one of two modes as follows: (a) the alarm is set if approximately four signals are detected within a 6-sec period; or (b) the alarm is set if a signal longer than 2 sec is detected (single seismic signals less than 2 sec long are ignored; multiple seismic signals less than 2 sec long are processed in the same manner as footstep-type signals). The maximum alarm rate for the SID is one alarm every 10 sec. This rate conserves battery life and still conveys the needed information to the monitoring point.

6. The SID alarms are recorded on an annunciator or display unit (portatale). These devices allow an operator to monitor a number of SID's at the same time and thereby assess the type of seismic disturbances in an area. In general, the alarm rate can be used to identify the source of the seismic disturbance and the direction of travel of the disturbance if proper emplacement is made. For example, consider an array of SID's emplaced along a trail. If the SID's alarm in sequence, the operator can identify the direction of travel as being in the direction of the SID alarms. The velocity of travel can be determined from the rate at which the alarms are recorded. If all the SID's alarmed simultaneously, the operator can probably identify the source as an aircraft (e.g. helicopter) or exploding shell. Unfortunately, with the SID's presently available, interpretation of the alarm pattern is an art rather than a science.

APPENDIX B: TERRAIN SITE DESCRIPTIONS AND SUPPLEMENTARY REFRACTION SEISMIC DATA

General Site Descriptions

1. The seismic and environmental data included in this report were collected by WES field teams at 12 sites within the hand-emplacement test area and 5 sites within the 6 airdrop areas. These sites are discussed briefly in the following paragraphs.

Hand-emplacement area (sites 335-342, 344, 345, 348, and 349)

2. Site 335 was situated on flat terrain and within an area where the vegetation consisted of acacia and mesquite that reached heights of 1 to 2 m. The substrate material was a loose, silty, coarse sand, classified SC by USCS in the surface layer (0-5 cm) and a reddish-brown sand-clay-silt mixture (GC) in the 5- to 100-cm layer. A view southwest along the 110-m line is shown in fig. B1a.

3. Site 336 was located on flat terrain with no surface irregularities. The vegetation surrounding it was composed of desert grass (species unknown) 20-30 cm in height and with stem diameters of 2-3 mm; a few very widely spaced mesquite bushes 1-2 m in height occurred near sta +80 (fig. B1b). The substrate material in the surface layer (0-7 cm) was a silty sand (SC) and in the subsurface layer (7-75 cm) was a reddish-brown sandy clay (CL).

4. Site 337, situated on flat terrain and within approximately 100 m of a major drainageway, was surrounded by closely spaced mesquite and acacia bushes that reached heights of 1 to 2 m (fig. B2a). The substrate material was a coarse, silty sand (SC) in the surface layer 0-5 cm) and a reddish-brown clayey sand (SC) in the 5- to 100-cm layer.

5. Site 338 was situated on terrain that had a slightly downward slope of approximately 3 percent (fig. B2b). The vegetation occupying the site was predominantly desert grass 50-75 cm in height, and occurred in clumps spaced approximately 50-75 cm apart. A few widely spaced acacia bushes, 1 m in height, surrounded the site. The substrate

a. Site 335

b. Site 336

Fig. B1. Sites 335 and 336, hand-emplacement area

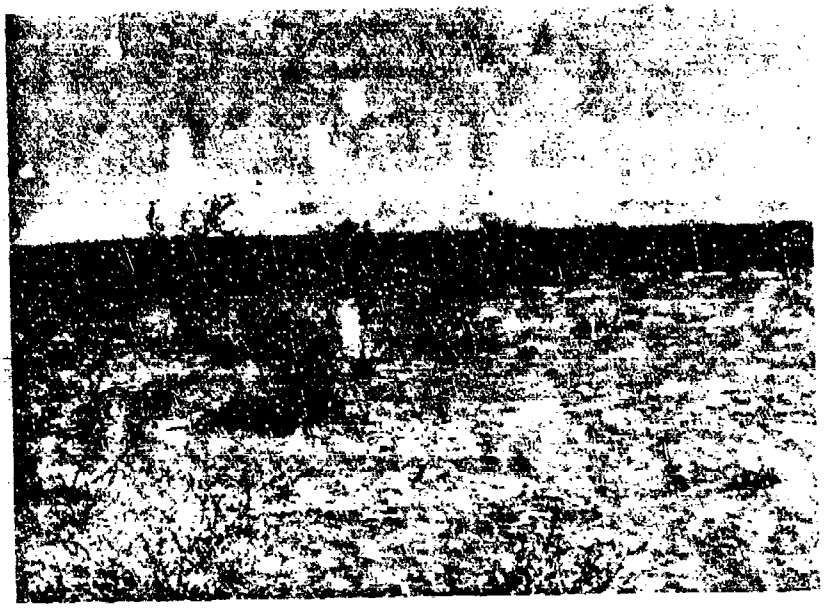

a. Site 337

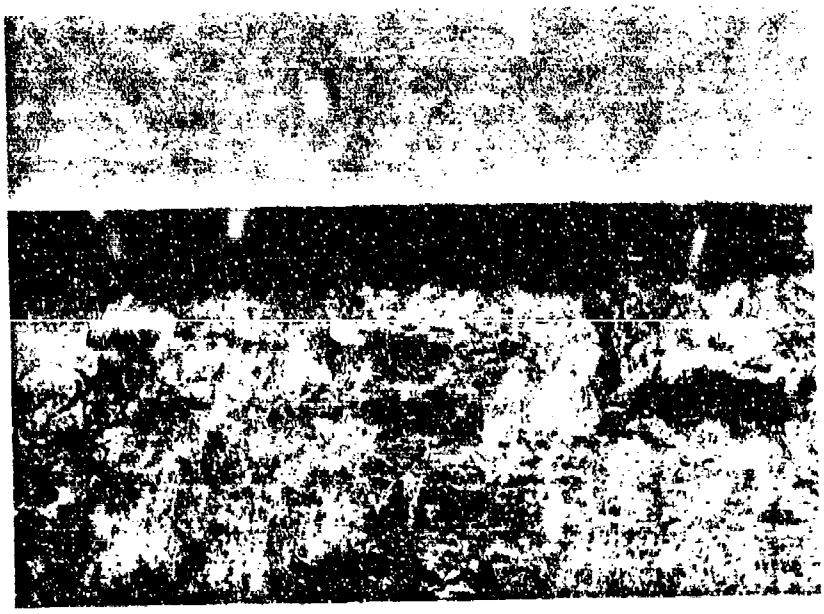

b. Site 338

Fig. B2. Sites 337 and 338, hand-emplacement area

material in the surface layer (0-5 cm) was a loose silty-sand and gravel mixture (SC). Several large stones (rocks) up to 5 cm in diameter were embedded in the ground surface. The material in the 5- to 80-cm layer was a hard, compact, reddish-brown clayey sand with small gravel (SC).

6. Site 339 (fig. B3a) was on flat terrain and within 200 m of a major drainageway. No surface rocks occurred at the site. The vegetation surrounding the 110-m line consisted of widely spaced acacia and mesquite that reached heights of 1-2 m. The substrate material was a silty sand (SM) in the 0- to 4-cm layer and a clayey sand (SC) in the 4- to 200-cm layer.

7. Site 340, located in grass-covered terrain and within the uppermost part of a drainageway, sloped slightly downward at about 2 percent in the direction of sta +100 (fig. B3b). In addition to the grass vegetation, some rather large mesquite trees 2 m in height surrounded the site. Substrate material was a silty sand (SM) in the 0- to 7-cm layer and a reddish-brown clayey sand (SC) in the 7- to 100-cm layer.

8. Site 341 (fig. B4a) had a relatively smooth ground surface and was approximately 30 percent covered with a low-growing (height 30 cm) desert grass. A few widely spaced mesquite trees surrounded the site. The substrate material was a coarse sand (SC) in the surface layer (0-7 cm) and a reddish-brown clayey sand with some gravel (SC) in the subsurface layer (7-100 cm).

9. Site 342 was also situated in an area covered with grass approximately 60 cm in height. The ground surface along the 110-m line portrayed no surface irregularities. The substrate material was a coarse sand (SC) in the 0- to 4-cm layer and a reddish-brown clayey sand (SC) in the 4- to 100-cm layer. A view of site 342 from sta 0 is shown in fig. B4b.

10. Site 348 was in an area where the topography was very flat and the vegetation consisted of a dense stand of grass (fig. B5a). A few widely spaced mesquite trees 1-2 m in height occurred within 75 m of the site. The substrate material was a loose, silty sand (SC) in the 0- to 7-cm layer and a reddish-brown clayey sand (SC) down to a depth of 100 cm.

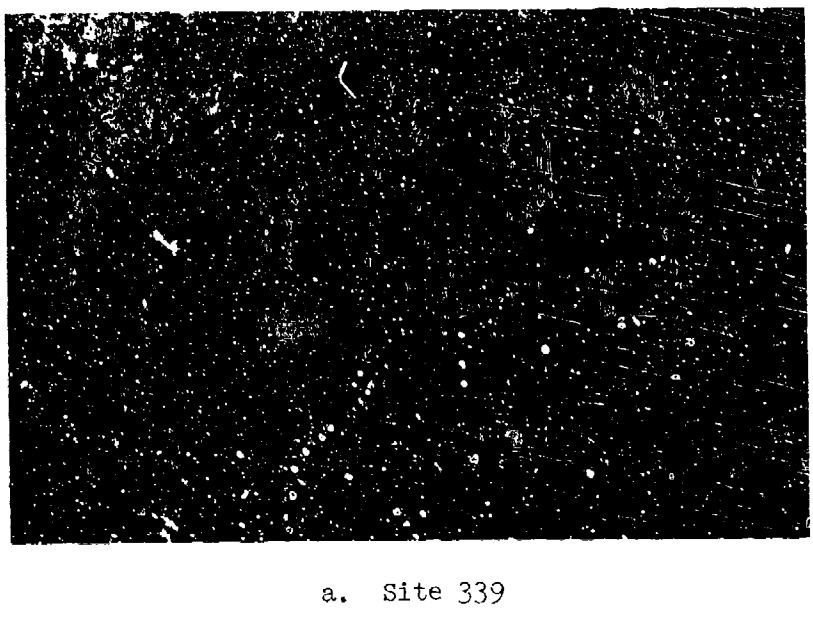

a. Site 339

b. Site 340

Fig. B3. Sites 339 and 340, hand-emplacement area

a. Site 341

b. Site 342

Fig. B4. Sites 341 and 342, hand-emplacement area

a. Site 348

b. Site 349

Fig. B5. Sites 348 and 349, hand-emplacement area

11. Site 349 was covered (approximately 90 percent) with a very dense grass (height approximately 60 cm) (fig. B5b). The ground surface along the line sloped slightly downward (approximately 2 percent) in the direction of sta +100, and there were a few large and widely spaced mesquite trees near sta +50. The substrate material was a coarse sand-silt mixture (SM) in the 0- to 7-cm layer and a reddish-brown clayey sand with small gravel (SC) in the 7- to 100-cm layer.

12. Cross-country site 344 covered an area 1000 m long and was positioned from about 400 m southwest of site 342 to 250 m southwest of site 339. The site sloped gently downward (approximately 5 percent) in the direction of sta +100 and contained very few surface irregularities. Grass approximately 30-60 cm in height occurred along the entire length of the line. The substrate material varied from a silty sand (SM) to a clayey sand (SC) in the surface layer (0-7 cm). The material below the surface layer and down to a depth of approximately 100 m was predominantly a clayey sand (SC). A general view of the site is shown in fig. B6a.

13. Cross-country site 345 extended from about 300 m north of site 348 to about 150 m west of site 336. The terrain, in general, sloped slightly downward toward sta +1000. The desert grass that occurred along the line varied in height from about 20 to 75 cm. A few scattered areas contained no vegetation. The substrate material in the surface layer (0-7 cm) was primarily a clayey sand (SC) and in the subsurface layer (7-100 cm) ranged from a sandy clay (CL) to clayey sand (SC). A general view of the cross-country site near sta +50 is shown in fig. B6b.

Airdrop area 1 (site 347)

14. Site 347 was situated in flat terrain and within an area containing a rather close spacing of large (3 m in height) mesquite trees (fig. B7a). The substrate material was a very loose, coarse, silty sand (SC) in the 0- to 5-cm layer and a red sandy clay (CL) in the 5- to 100-cm layer.

a. Cross-country site 344

b. Cross-country site 345

Fig. B6. Cross-country sites 344 and 345, hand-emplacement area

a. Airdrop area 1, site 347

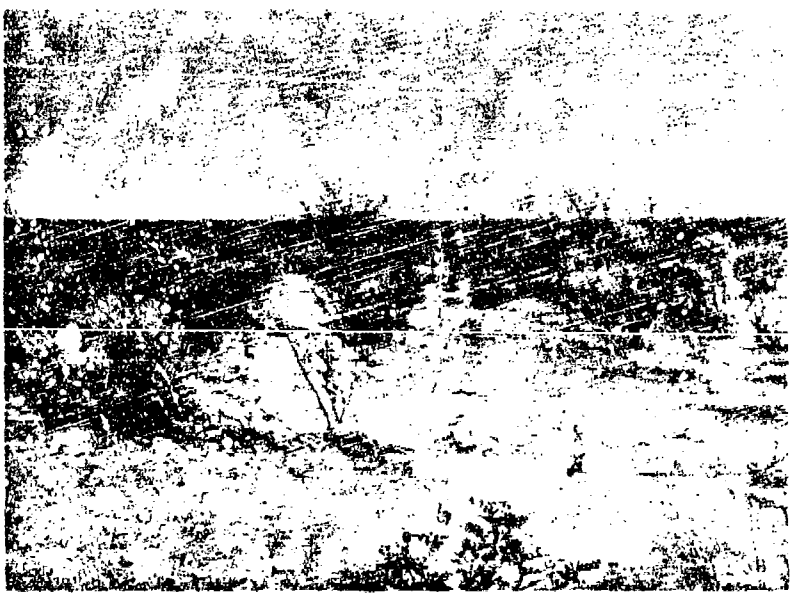

b. Airdrop area 4, site 410

Fig. B7. Sites 347 and 410

Airdrop area 2 (rock outcrop site; unnumbered)

15. Exposed bedrock and boulders covered the ground surface at this site. A few small areas (i.e. patches) contained a dark brown, coarse, gravelly sand material (GW). The vegetation occupying the site consisted of grass and scattered clumps of acacia.

Airdrop area 3 (site 412)

16. Site 412 (fig. B6b) was situated on flat terrain and within a large arroyo (a drainageway). A wash channel 2 m wide and 5 m deep occurred within the arroyo and paralleled the 110-m line. The vegetation was a dense stand of reeds (a type of grass) approximately 1-1.5 m in height. The substrate materials consisted of loose silty sand (SC) in the 0- to 20-cm layer, a coarse sand (SW) in the 20- to 45-cm layer, and a silty sand (SM) in the 45- to 100-cm layer.

Airdrop area 4 (site 410)

17. Site 410 (figs. B7b and B9a) was situated on a slope of approximately 2 percent. The vegetation was composed primarily of creosote bushes approximately 1-1.5 m in height; their average spacing varied from 1.5 to 3.0 m. The substrate material consisted of a gray, loose silty sand with pebbles (0- to 7-cm layer), and a firm, light-brown clay (CL) with scattered caliche down to a depth of 100 cm.

Airdrop area 5 (site 411)

18. The ground surface at site 411 varied from flat (from sta 0 to sta +50) to sloping (sta +50 to sta +100). The vegetation was composed of small woody plants (acacia) that reached heights of 1 to 2 m and had stem diameters of 1-2 cm. The acacia vegetation covered approximately 80 percent of the ground surface and made walking through the area very difficult. The substrate material in the surface layer (0-15 cm) was predominantly a silty sand with white caliche, and contained some rock fragments (figs. B8a and B9b). The material in the subsurface layer (15-100 cm) was a red clay (CH) and some white caliche.

Airdrop area 6 (site 413)

19. Site 413 (fig. B10) was situated in a rather large, flat lake bed (Willcox Playa). The substrate material in the surface layer

a. Airdrop area 5, site 411

b. Airdrop area 3, site 412

Fig. B8. Sites 411 and 412

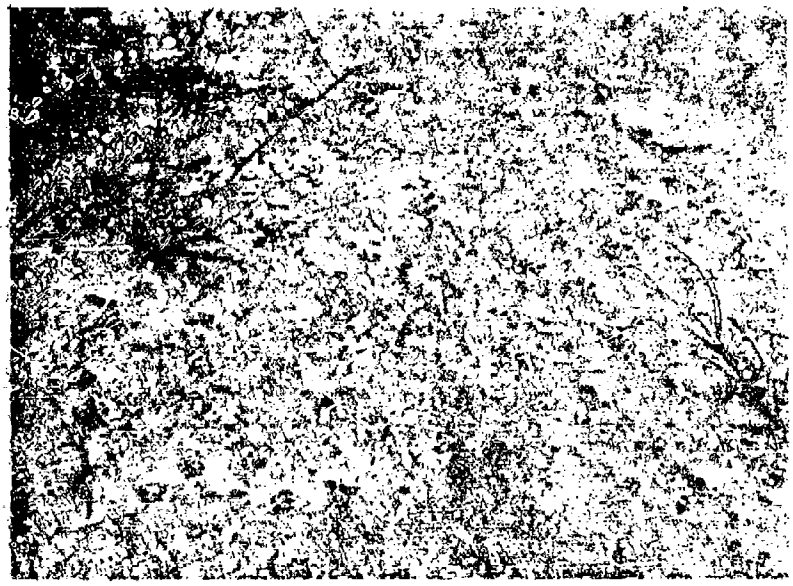

a. Airdrop area 4, site 410

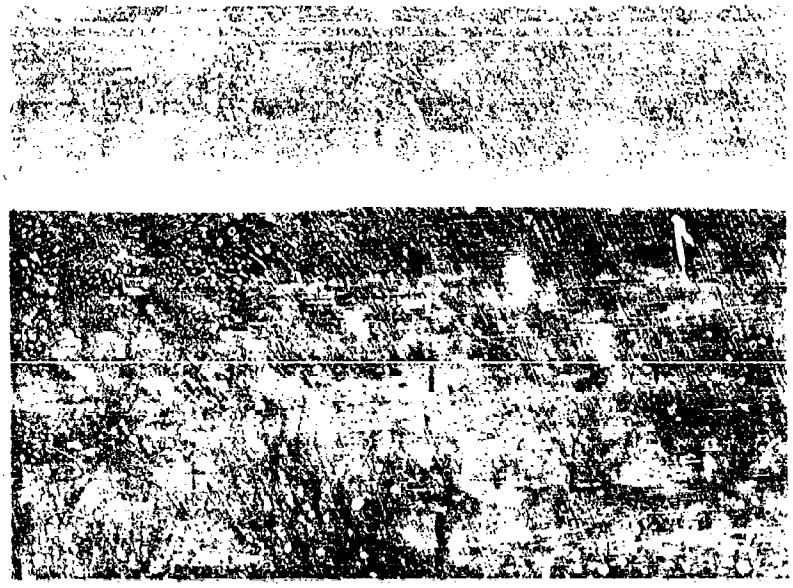

b. Airdrop area 5, site 411

Fig. 89. Sites 410 and 411

Fig. B10. Airdrop area 6, site 413

(0-20 cm) was a silty clay (CL) and in the subsurface layer (20-100 cm) was a dark gray clay (CH).

CSEWS airdrop area

20. The CSEWS airdrop area was situated on an unimproved airstrip (fig. B11). The substrate material consisted of a sandy silt to clayey sand (SC) with various amounts of gravel and small pebbles.

Refraction Seismic Data

21. Wet- and dry-season refraction seismic data for sites 335-342, 345 (wet season only), 347-349, and 410-412 (dry season only) within the hand-emplacement and airdrop test areas at Fort Huachuca are included as figs. B12-B37. These data are portrayed in the conventional time-versus-distance format.

a. View along airstrip used for CSEWS airdrop tests

b. Surface soil conditions

Fig. B11. CSEWS airdrop test area

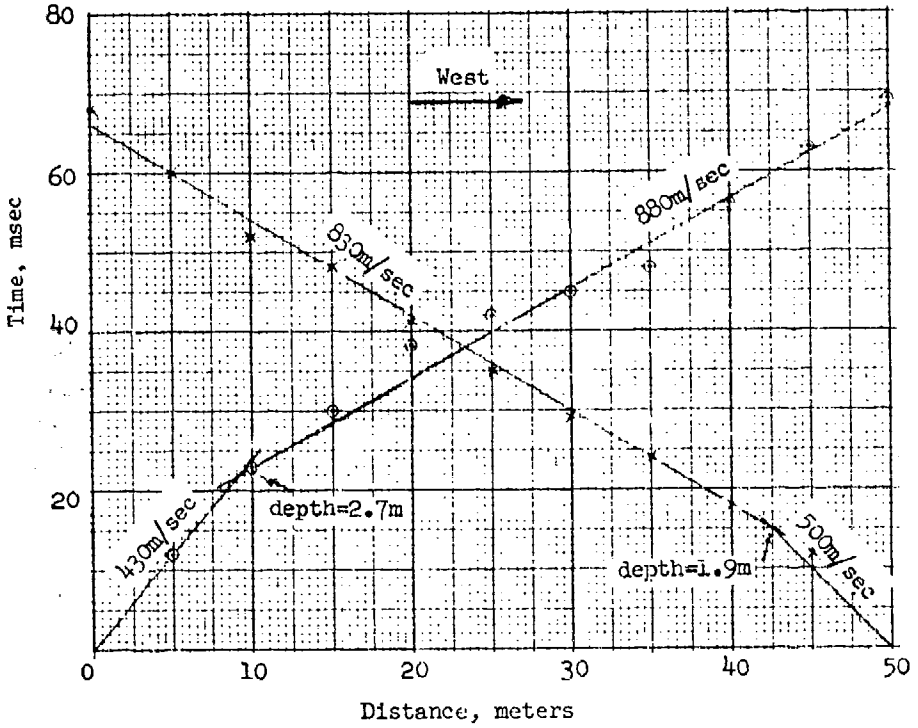

Fig. B12. Wet-season refraction seismic data, site 335

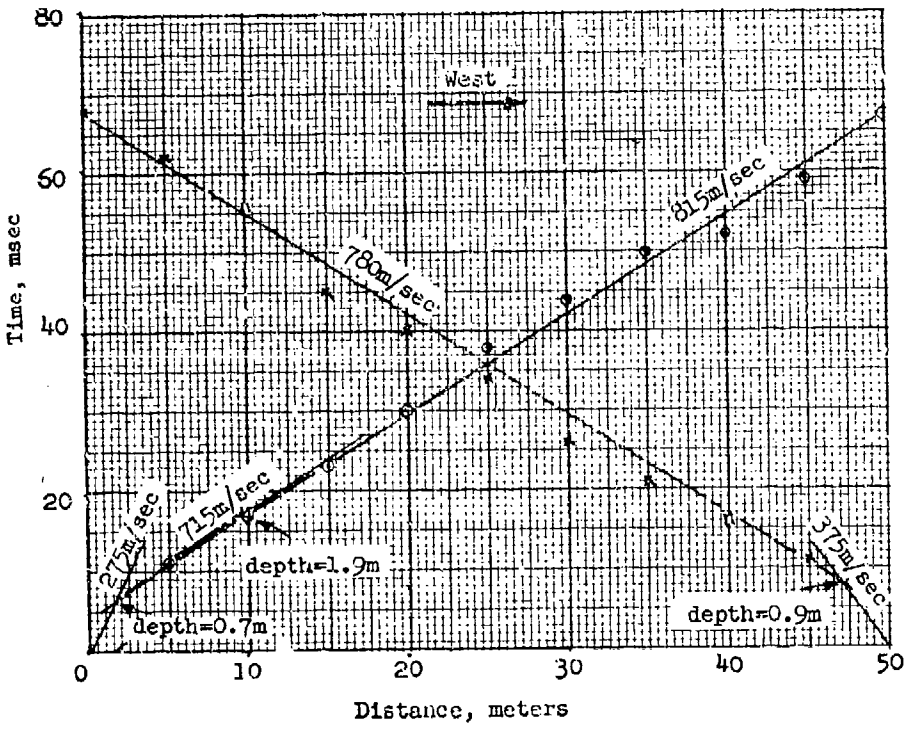

Fig. B13. Wet-season refraction seismic data, site 336

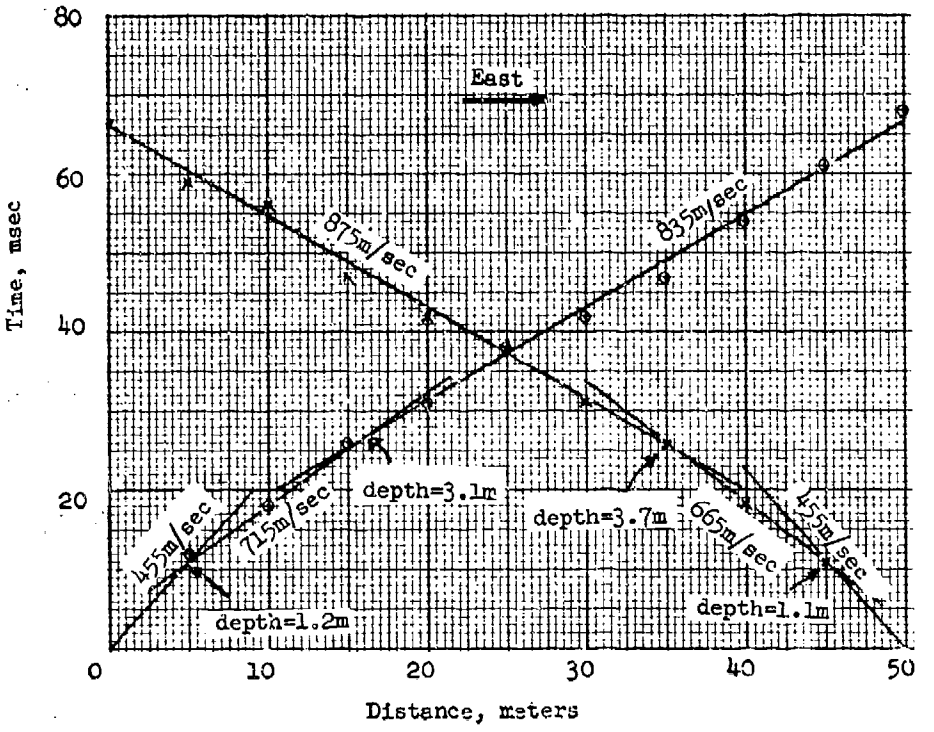

Fig. B14. Wet-season refraction seismic data, site 337

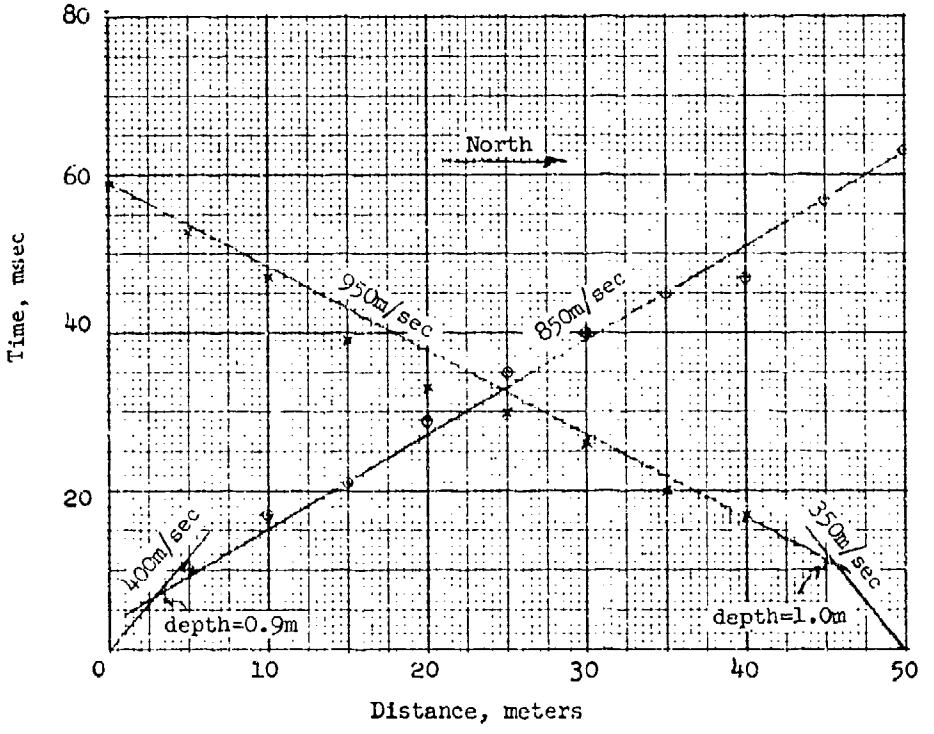

Fig. B15. Wet-season refraction seismic data, site 338

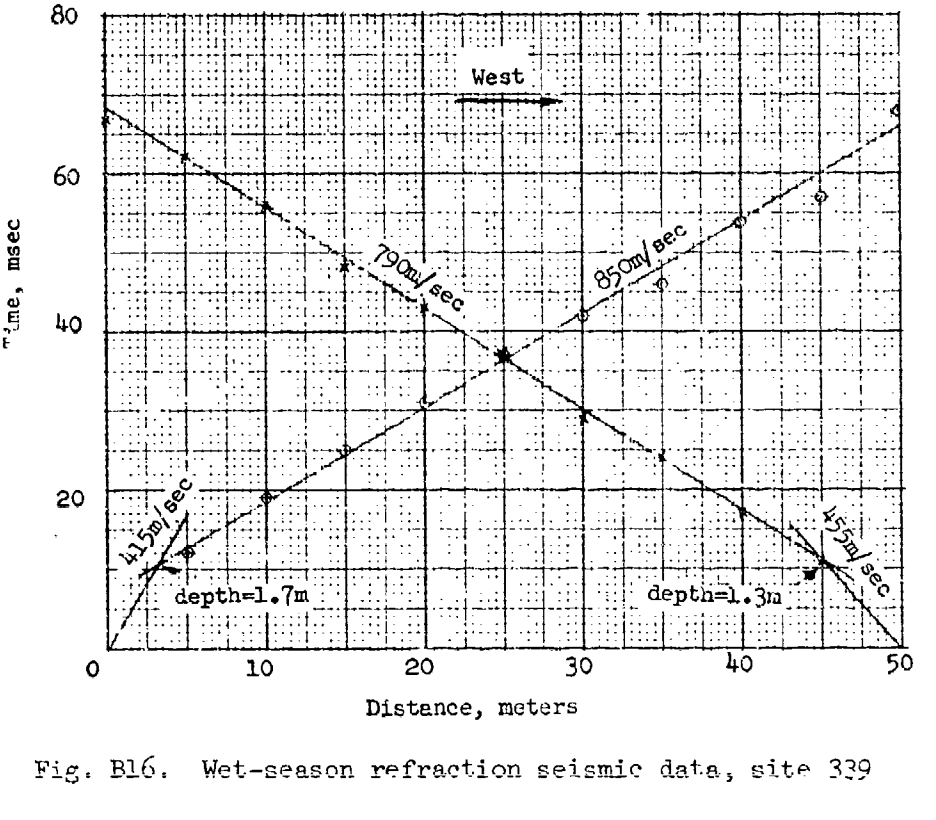

Fig. B16. Wet-season refraction seismic data, site 339

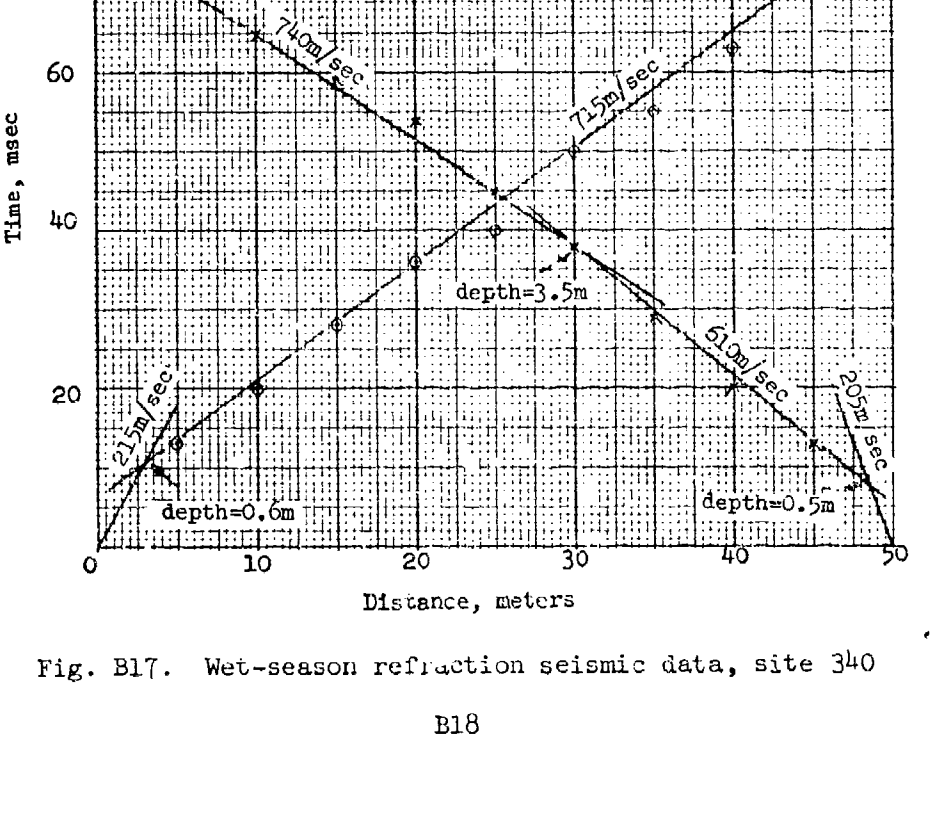

Fig. B17. Wet-season refraction seismic data, site 340

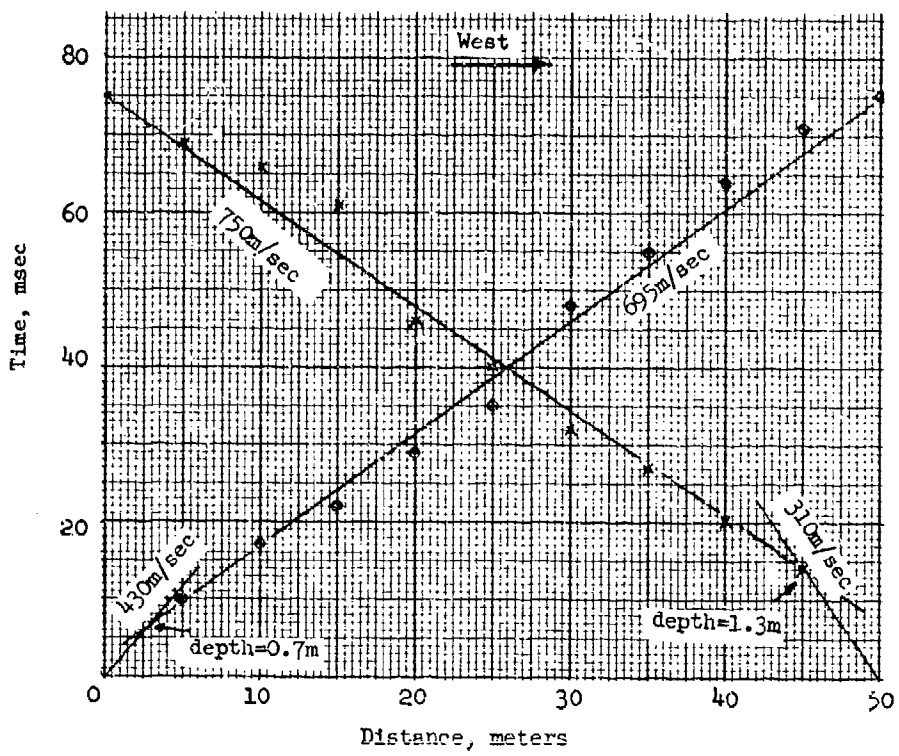

Fig. B18. Wet-season refraction seismic data, site 341

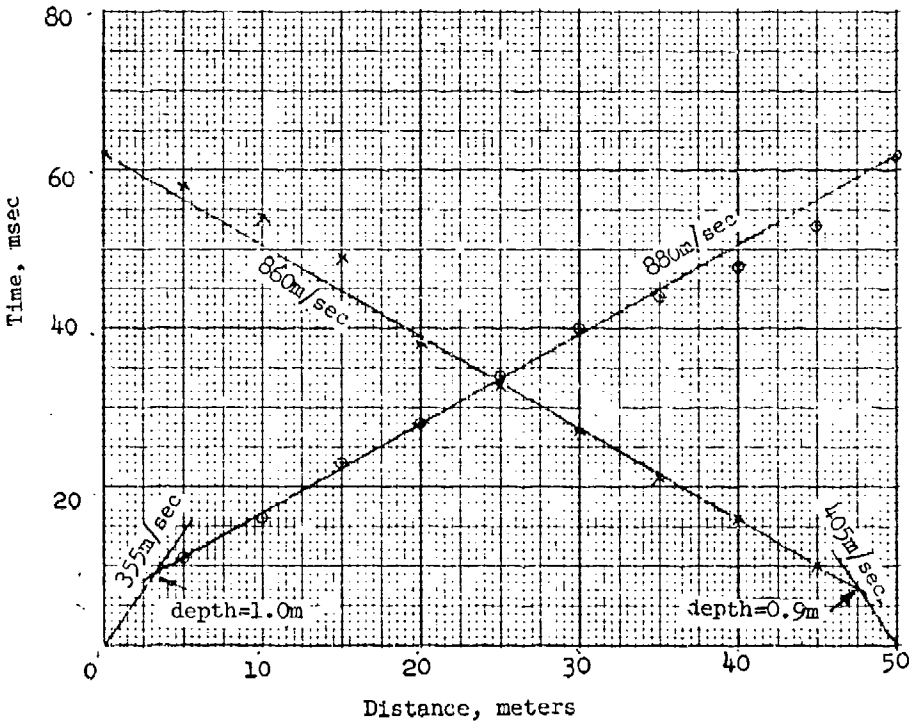

Fig. B19. Wet-season refraction seismic data, site 342

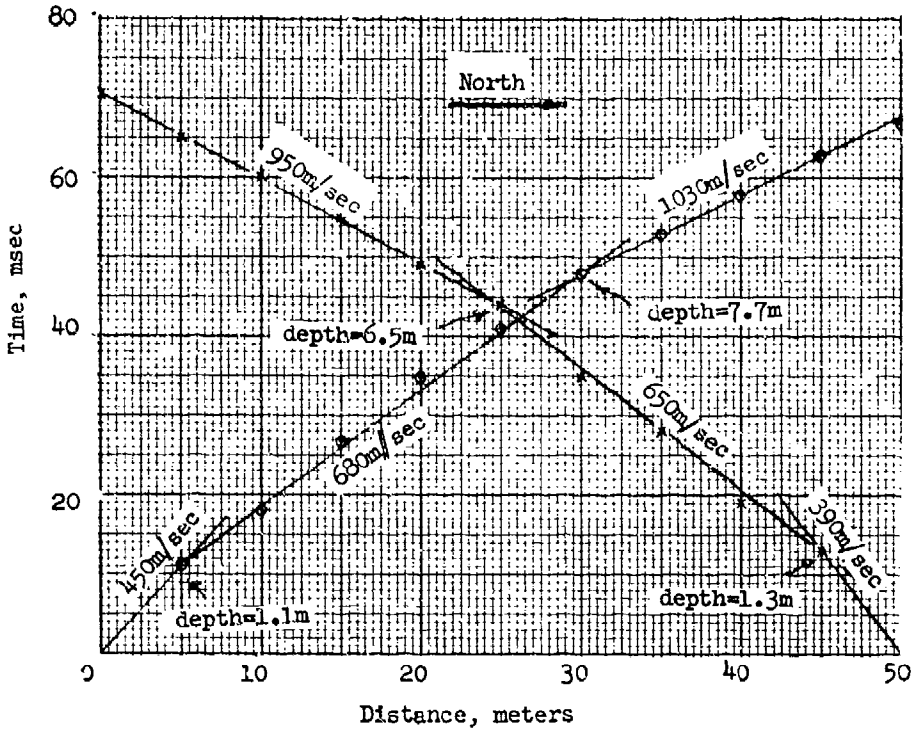

Fig. B20. Wet-season refraction seismic data, site 345

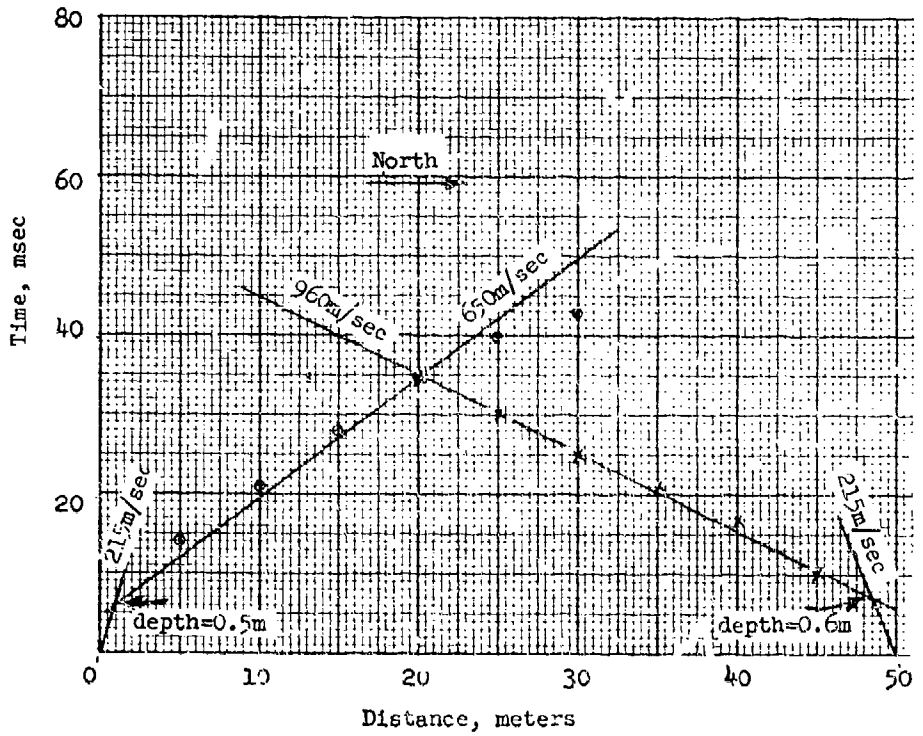

Fig. B21. Wet-season refraction seismic data, 347

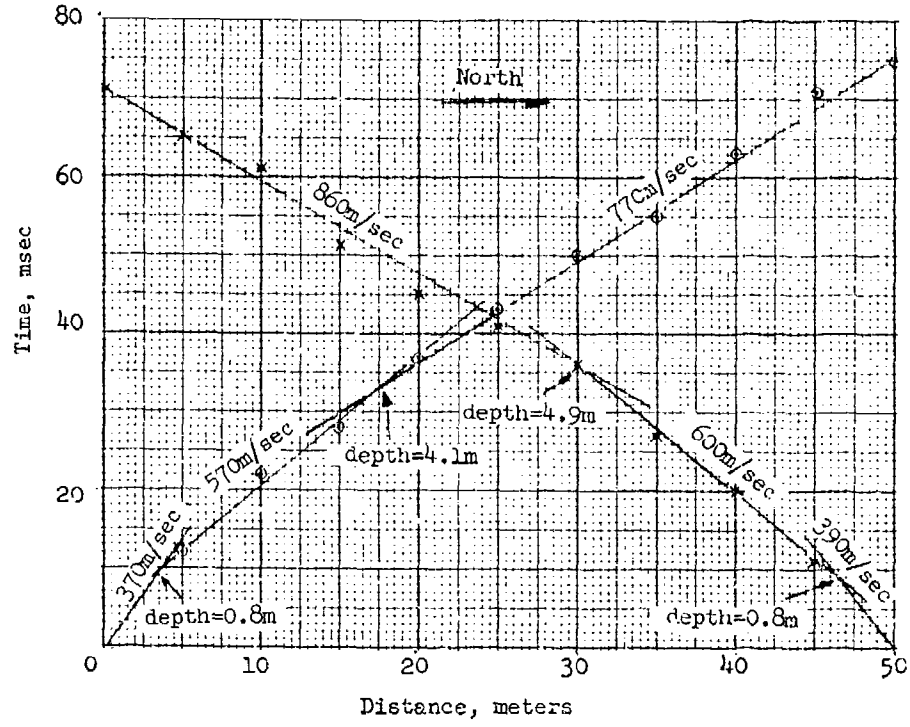

Fig. B22. Wet-season refraction seismic data, site 348

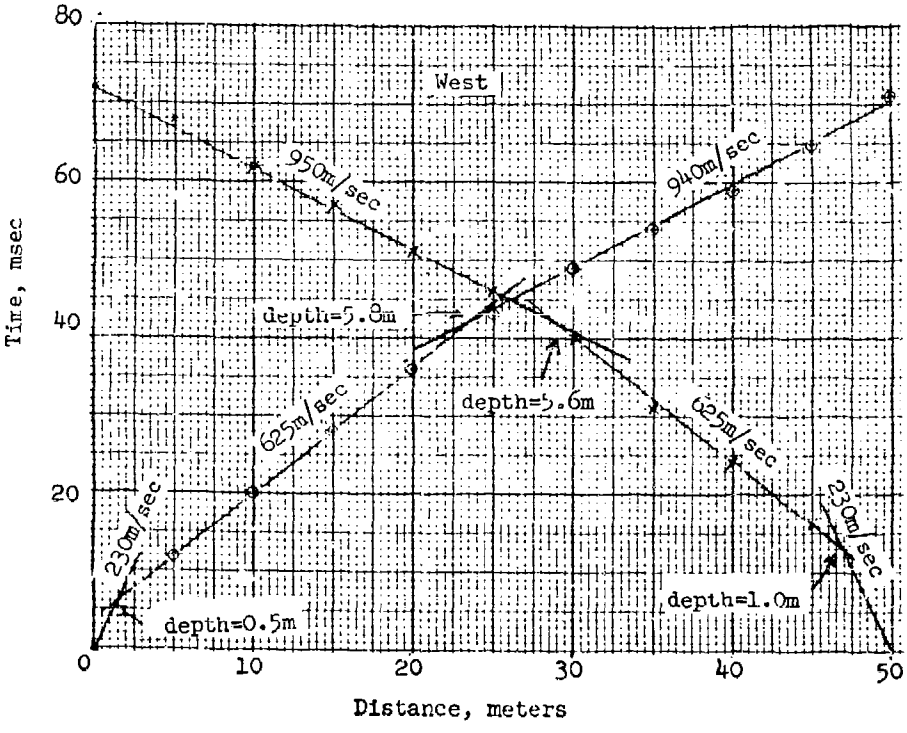

Fig. B23. Wet-season refraction seismic data, site 349

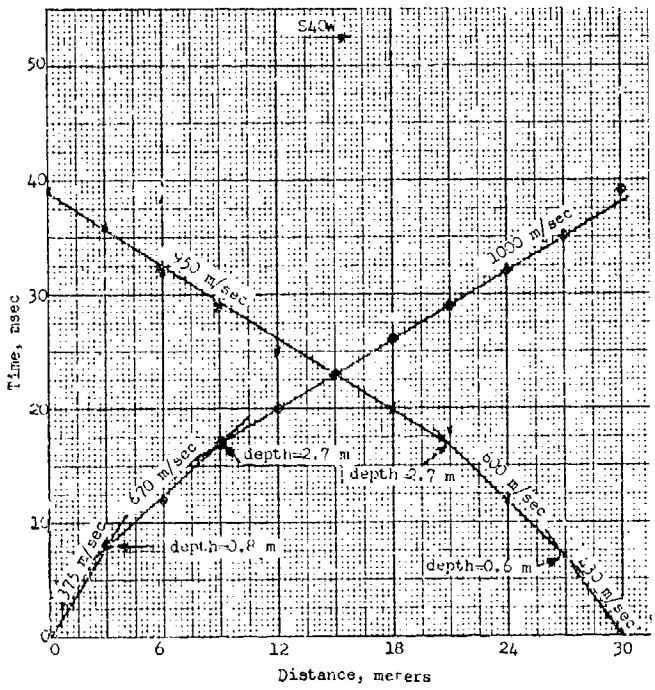

Fig. B24. Dry-season refraction seismic data, site 335

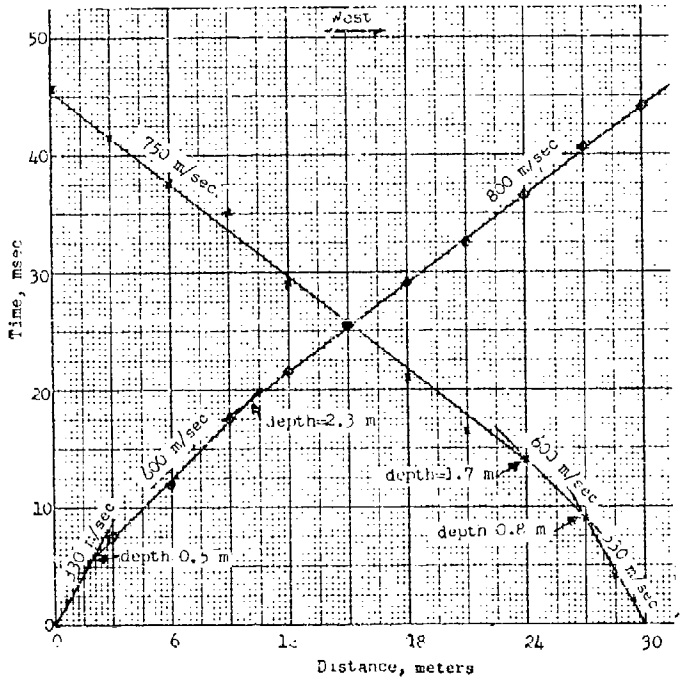

Fig. B25. Dry-season refraction seismic data, site 336

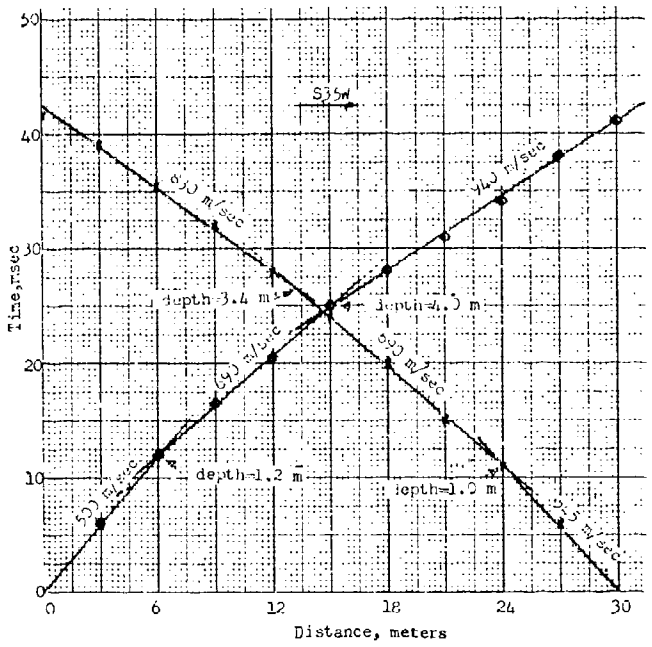

Fig. B26. Dry-season refraction seismic data, site 337

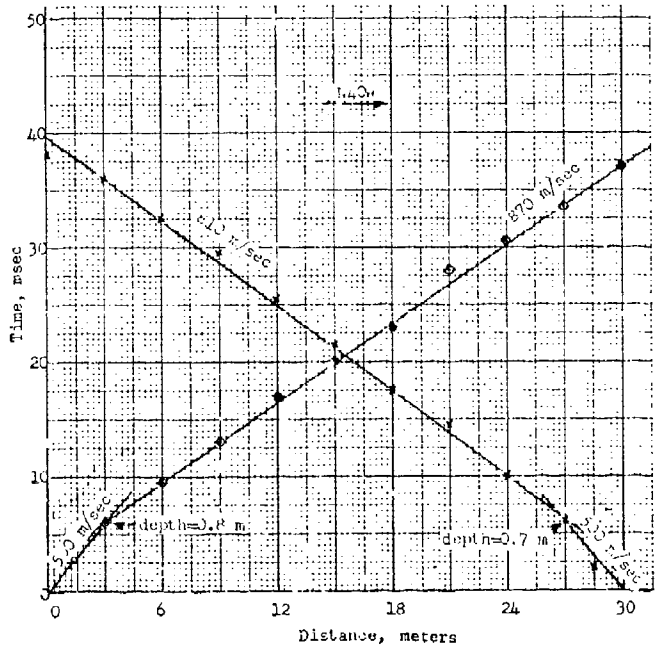

Fig. B27. Dry-season refraction seismic data, site 338

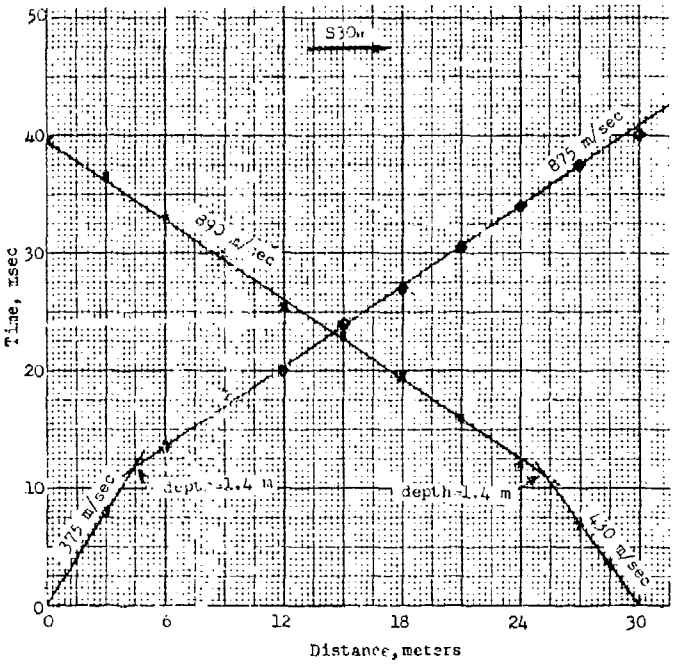

Fig. B23. Dry-season refraction seismic data, site 339

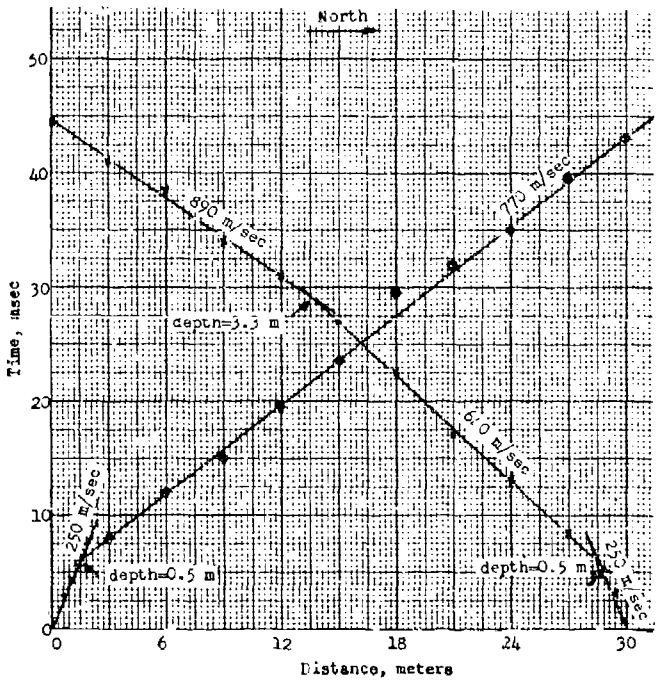

Fig. B29. Dry-season refraction seismic data, site 340

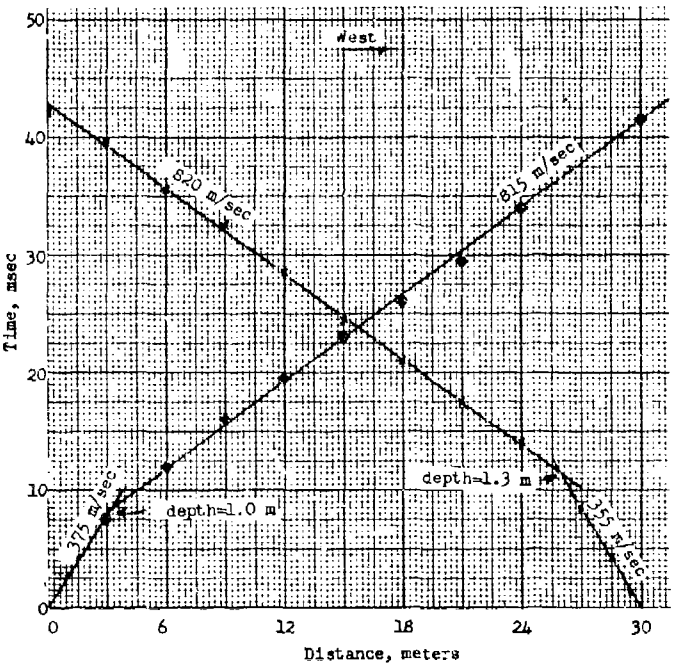

Fig. B30. Dry-season refraction seismic data, site 341

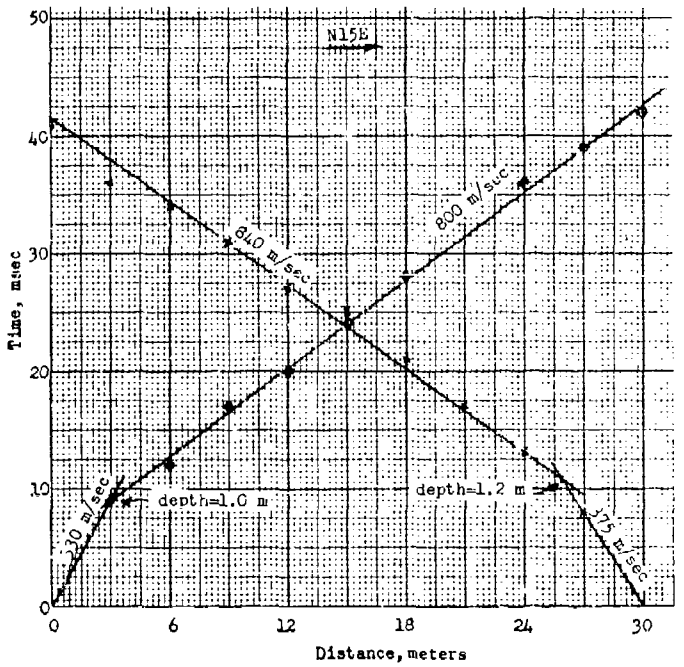

Fig. B31. Dry-season refraction seismic data, site 342

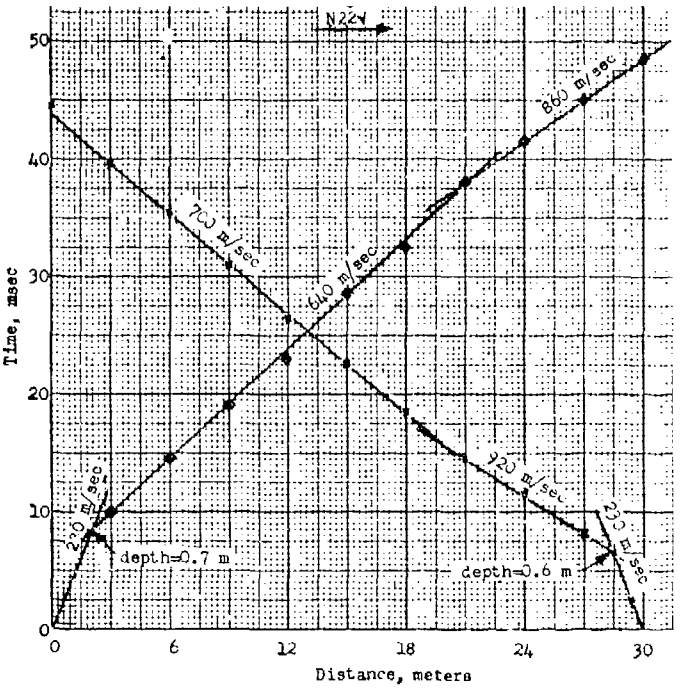

Fig. B32. Dry-season refraction seismic data, site 347

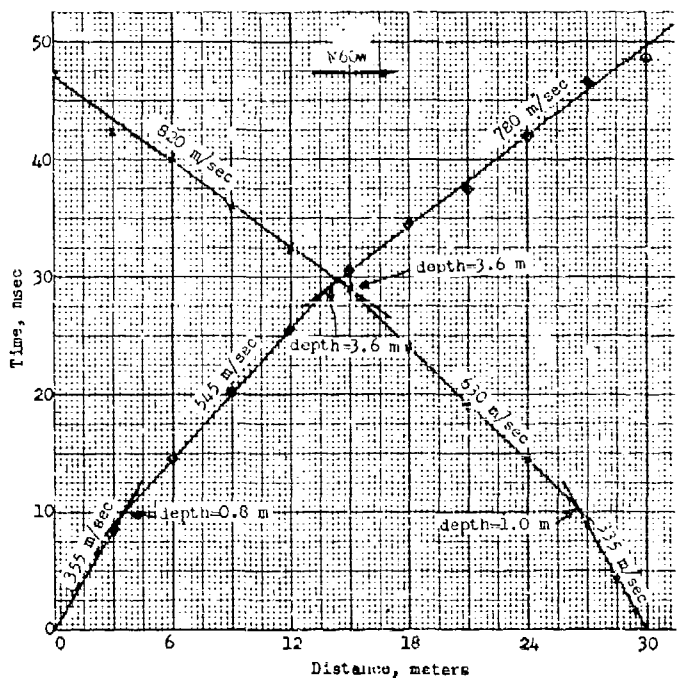

Fig. B33. Dry-season refraction seismic data, site 348

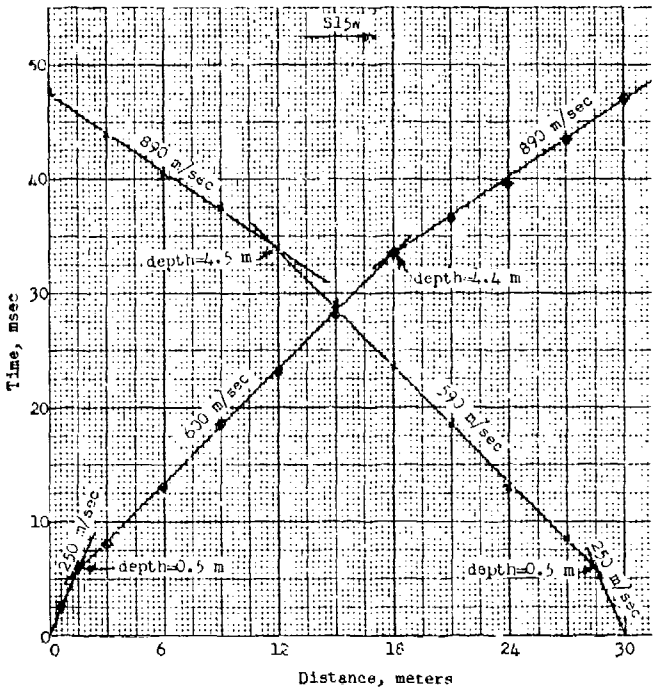

Fig. B34. Dry-season refraction seismic data, site 349

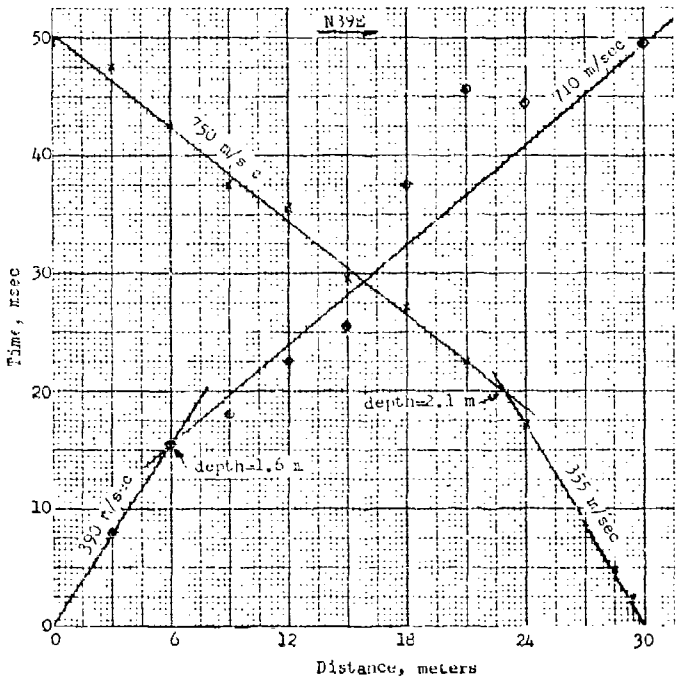

Fig. B35. Dry-season refraction seismic data, site 410

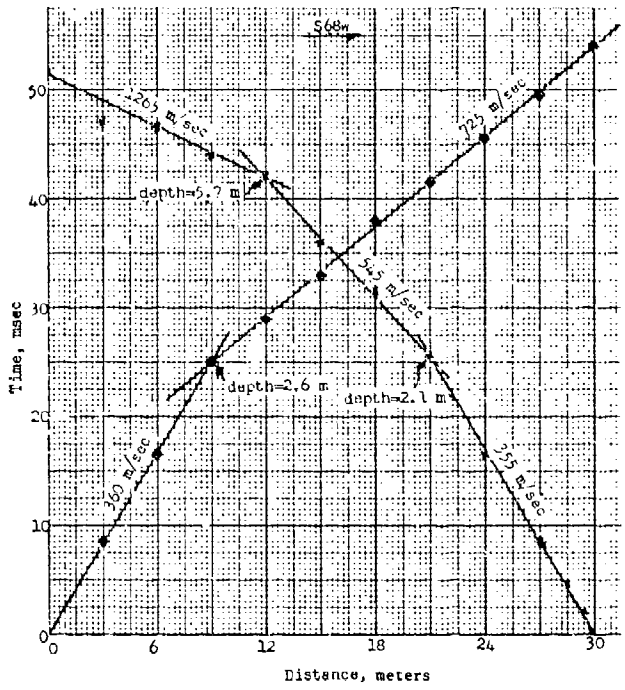

Fig. B36. Dry-season refraction seismic data, site 411

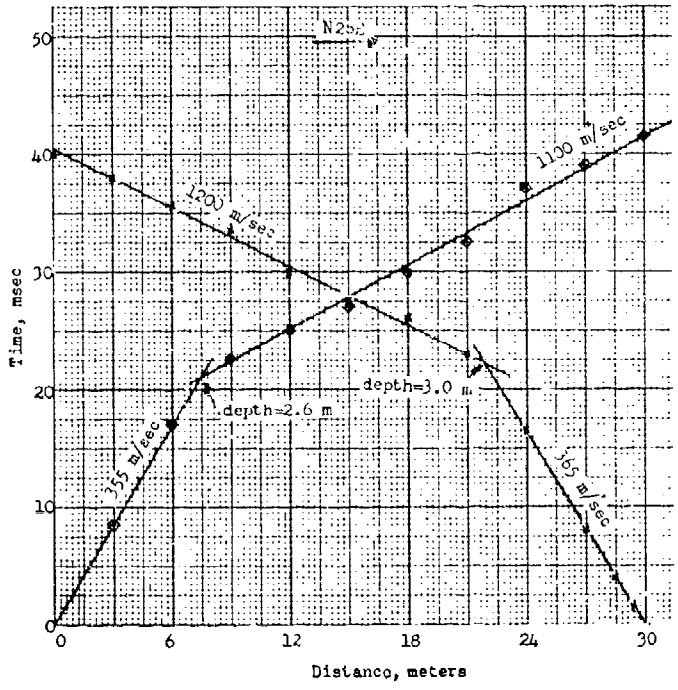

Fig. B37. Dry-season refraction seismic data, site 412

APPENDIX C: EQUATIONS FOR PREDICTING PENETRATION DEPTHS AND DECELERATION VALUES FOR AIR-IMPLANTED SENSORS

1. The fundamental concepts of the mathematical penetration model used to predict the depth of penetration of the ADSID/S sensor into the Fort Huachuca terrain materials are documented in this appendix. The penetration model is based on the dynamic cavity expansion theory for an elastic-plastic locking medium formulated by Ross and Hanagud,[18] and the soil penetration theory derived by Brooks and Reis.[19] The dynamic cavity expansion theory has been used successfully in penetration studies of ice, frozen ground, and various types of soils.[20-22] The soil penetration theory of Brooks and Reis, modified to account for the compressibility of the substrate materials by utilizing the expression for the dynamic pressure inside a spherical cavity as derived by Ross and Hanagud, was used in this study.

2. By assuming a simple elastic-plastic constitutive model for soil, Brooks and Reis derived the following differential equation of motion for an ogival projectile penetrating into a homogeneous soil medium in the vertical direction z.

$$\frac{m}{A}\frac{d^2z}{dt^2} + \sigma_u\left(\frac{2}{3}\frac{E}{\sigma_u}\right)^{2/3} + \frac{1}{2}C_D\bar{\rho}\left(\frac{dz}{dt}\right)^2 = 0 \qquad \text{(C1)}$$

where

m = mass of projectile

A = cross-sectional area of projectile

$\frac{d^2z}{dt^2}$ = acceleration of projectile at time t

σ_u = ultimate strength of substrate material (equivalent to Von Mises yield limit)

E = initial elastic modulus of substrate material (equivalent to Young's modulus)

C_D = drag coefficient

$\bar{\rho}$ = initial mass density of soil

$\frac{dz}{dt}$ = velocity of projectile at time t

3. Using the Newtonian form of aerodynamic drag, Brooks and Reis derived the following expression for the drag coefficient C_D in terms of the geometry of the frontal face (fig. C1) of the projectile and the

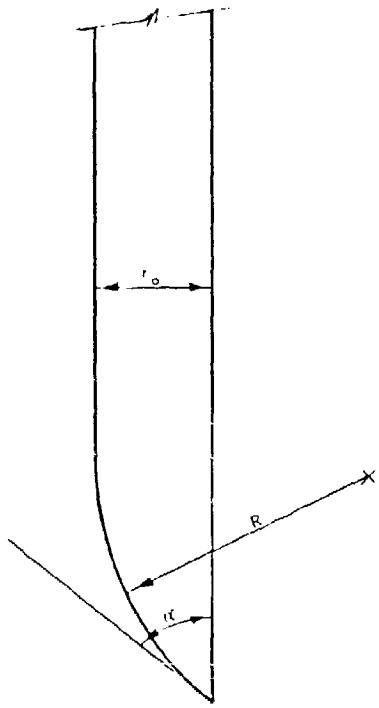

Fig. C1. Projectile parameters

frictional forces acting on it.

$$C_D = 4\left(\frac{R}{r_o}\right)^2 \left\{\frac{1}{4}\sin^4\alpha + \frac{R - r_o}{R}\left[\frac{1}{3}\cos\alpha(\sin^2\alpha + 2) - \frac{2}{3}\right]\right\} + 4\mu\left(\frac{R}{r_o}\right)^2 \left[-\frac{1}{8}\left(\frac{1}{4}\sin 4\alpha - \alpha\right) - \frac{R - r_o}{3R}\sin^3\alpha\right] \qquad (C2)$$

where

R = radius of ogive

$\frac{R}{2r_o}$ = the caliber ratio of the ogive

r_o = radius of projectile

α = ogive angle, see fig. C1

μ = coefficient of friction between the projectile and the soil

4. The differential eq C1, in conjunction with the expression for the drag coefficients C_D (eq C2), was used to predict the penetration of the ADSID/S into earth materials. The ultimate strength of the substrate material σ_u, however, was modified to account for the compressibility of the material. The following initial and end conditions were used to integrate eq C1:

$$\left.\begin{aligned} \frac{dz}{dt} &= V_i \qquad \text{when} \qquad z = 0 \\ \frac{dz}{dt} &= 0 \qquad \text{when} \qquad z = Z_{max} \end{aligned}\right\} \tag{C3}$$

where

V_i = impact velocity of projectile

Z_{max} = maximum depth of penetration

5. To account for the compressibility of the material, the ultimate strength was modified using the expression $\sigma_u[(2/3)(E/\sigma_u)]^{2/3}$ in eq C1. (This expression corresponds to the quasi-static pressure in a spherical failure zone at the interface of the projectile and the soil.) This was accomplished by equating the expression above to a corresponding expression derived by Ross and Hanagud for a compressible elastic-plastic material. Assuming an elastic-plastic material of the locking type characterized by the pressure-volumetric strain relation and shearing stress-shearing strain relation shown in fig. C2, Ross and Hanagud derived the following expression for the quasi-static pressure inside a spherical cavity.

$$P_s = \frac{4}{9} E[1 - \exp(-3\beta)] - \frac{2}{3} Y \ell n \delta + \frac{2}{27} \pi^2 E_t - \frac{4}{9} E_t \eta \tag{C4}$$

The parameters in eq C4 are as follows:

$$\delta = 1 - \frac{\rho}{\rho_p} \exp(-3\beta) \tag{C5}$$

$$\eta = \sum_{n=1}^{\infty} \frac{\delta^n}{n^2} \tag{C6}$$

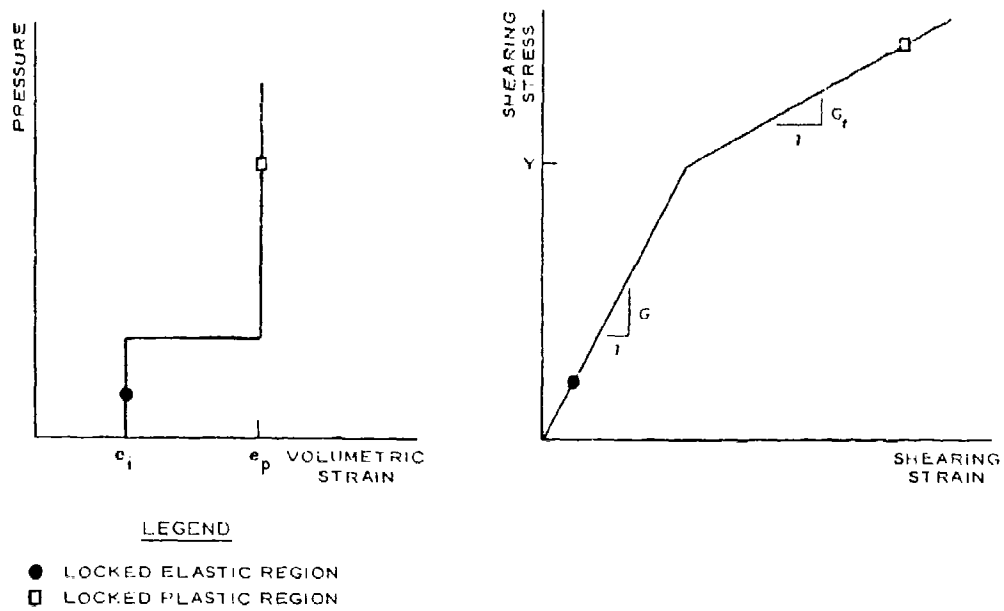

Fig. C2. Idealized stress-strain curves for a locking elastic-plastic material

$$\beta = \frac{Y}{2E} - \frac{e_i}{3} \tag{C7}$$

$$\rho_p = \rho \exp(e_p) \tag{C8}$$

where (for eq C4-C8)

E = Young's modulus of elasticity, corresponding to locked elastic region in fig. C2, = 3G, where G is the shear modulus

Y = yield strength of substrate material, shown in fig. C2

n = dummy variable

E_t = strain-hardening modulus, corresponding to locked plastic region in fig. C2, = $3G_t$

ρ = initial density of substrate material

e_i = volumetric strain related to the elastic region of the pressure-volumetric strain curve in fig. C2

e_p = volumetric strain related to plastic region of the pressure-volumetric strain curve in fig. C2

6. It is to be noted that due to the locking characteristic of

the volumetric-strain-pressure relation in fig. C2, the bulk modulus of the material in both the elastic and the plastic range is infinitely large, and the shear modulus G is equal to E/3 . If the parameters e_i and e_p in eq C4-C8 are taken to be zero, an incompressible material will be simulated. To simulate a perfectly elastic-plastic material, the strain-hardening parameter E_t should be equated to zero.

7. In order to be compatible with the Brooks and Reis assumption of perfectly elastic-plastic material in utilizing eq C4, the strain-hardening parameter E_t was taken to be zero. The system of eq C4, C5, C7, and C8 was then studied parametrically to determine the effects of compressibility of the material on the pressure P_s inside the cavity. It was found that for the range of variables considered in this study, the pressure P_s calculated for an incompressible material (i.e., $e_p = e_i = 0$) is approximately ρ_p/ρ times the corresponding value for the compressible material, i.e.

$$(P_s)\ \text{incompressible} \approx \frac{\rho_p}{\rho}\ (P_s)\ \text{compressible} \tag{C9}$$

Now equating the two expression for the quasi-static pressure P_s and $\sigma_u[(2/3)(E/\sigma_u)]^{2/3}$ and solving for σ_u yields

$$\sigma_u = \left(\frac{}{2E}\right)^2 P_s^3 \tag{C10}$$

In view of eq C9 and C10, the modified value of the ultimate strength of the material, denoted by (σ_u) compressible , then becomes

$$(\sigma_u)\ \text{compressible} = \frac{1}{(\rho_p/\rho)^3}\ (\sigma_u) \tag{C11}$$

For an incompressible material $\rho_p/\rho = 1$ and no modification of σ_u is necessary.

8. Eq C1, C2, and C11 contain eight parameters that define a terrain impact condition for a prediction: m , A , E , σ_u , ρ_p , ρ , μ , and C_D . The parameters E and σ_u for input to the equations were determined from the triaxial compression test data (fig. 18)

presented in Part III of the main text. The parameter ρ_p was determined from the uniaxial strain test results (fig. 17), also presented in Part III of the main text, by idealizing them with the locking model shown in fig. C2. The friction coefficient μ was determined from the triaxial test results using the procedure given by Potyondy.[9] The frontal face (nose) of the ADSID/S was approximated as a 4.35 caliber ogive, and the drag coefficient C_D was then calculated using eq C2 and the values of the friction coefficient μ for each drop area.

APPENDIX D: COMPUTER MODELS FOR PREDICTION OF SID DETECTION PERFORMANCE

Theoretical Detection Performance Computer Model

1. The overall theoretical detection performance computer model used in this study is composed of two submodels, the seismic wave propagation model and the sensor logic model. The detailed steps in the formulation of this model will not be presented in this report, since they have been documented in two other reports.[16,17] A brief description of the model, however, is presented in the following paragraphs.

Seismic wave propagation model

2. A general expression has been developed for predicting the characteristics of a seismic signal (i.e. particle velocity, particle acceleration, or particle displacement) at selected ranges from a specified energy source such as a walking man, moving vehicle, or other disturbances. The general equation is

$$A_{L,p}(R_m,t) = \sum_{n=1}^{\infty} \omega_n^{(p-1)} F\left[A_{L,p}(R_k,t)\right]\sqrt{\frac{R_m}{R_k}}\,|S_n|\, e^{-\xi \frac{\omega_n}{V_R}(R_m-R_k)} \cos\left[\omega_n t + \phi + \frac{\pi}{2}(p-1) - \frac{\omega_n}{V_R}(R_m - R_k) + \Theta_S\right] \quad \text{(D1)}$$

where

$A_{L,p}(R_m,t)$ = particle motion, in cm, at a selected range R_m and time t

L = vertical component of three-dimensional seismic wave

p = 0, 1, 2; 0 for particle displacement, 1 for particle velocity, and 2 for particle acceleration

R_m = range at which the new signal is desired. The range is assumed to be in the far field (i.e. farther than 2-1/2 wavelengths from the source).

t = time, sec

n = frequency numbers. A maximum of 1024 frequency data points are normally used to describe a particle velocity curve.

ω_n = circular frequency, radians/sec

$F\left[A_{L,p}(R_k,t)\right]$ = Fourier transform of a measured particle motion, in cm, at range R_k and time t

S_n = magnitude of surface geometry coefficient

e = base of natural logarithm

ξ = viscous damping coefficient; assumed to be equal to 0.03

V_R = Rayleigh wave velocity, m/sec

ϕ = phase factor associated with $F\left[A_{L,p}(R_k,t)\right]$

Θ_S = phase factor associated with S_n

3. The inputs required by the seismic wave propagation model (eq D1) are as follows:

a. Source signal of stress applied to the ground as a function of time for the specified energy source (walking man, moving venicle, etc.).

b. Terrain data on V_P, V_S, ρ, and T for each substrate soil layer.

c. The viscous damping coefficient ξ; the coefficient used in conjunction with the real Rayleigh wave number k (where $k = 2\pi/\lambda$, and λ = wavelength to account for viscous damping in the medium), i.e. $\vec{k} = k(1 - i\xi)$, where $\vec{k}$ is the complex k.

The output from the model is the particle velocity, particle acceleration, or particle displacement as a function of time for various selected distances from the energy source. Predictions are normally obtained for each 3-m distance to some maximum selected value. For the Fort Huachuca study, predictions of the vertical component of particle velocity as a function of time were made. The particle velocity-time data were then used as input to the seismic sensor logic model for predicting SID performance as discussed in the following paragraph.

Seismic sensor logic model

4. The seismic sensor logic model is composed of a series of subroutines that, in general, utilize transfer functions to simulate the effects of the frequency response of each of the electronic components of a SID on the seismic signal received by the geophone. (The outputs from the seismic wave propagation model are the inputs to this model.)

5. SID geophone transfer function. The equation for the transfer function for the SID geophone was developed from attenuation-phase plots (Bode diagrams). This method is based on the relation between phase and the rate of change of gain with frequency. The equation used for the Phase III SID geophones is

$$TF_1 = \frac{K_1(if)^2}{(if)^2 + 5.6(if) + 196}$$

where

TF_1 = transfer function for the Phase III SID geophone

K_1 = arbitrary constant associated with geophone calibration

$i = \sqrt{-1}$

f = frequency, Hz

6. SID band-pass amplifier transfer function. The equation developed for the transfer function for the band-pass amplifier is

$$TF_2 = \frac{K_2(if)^2}{[(if)^2 + 12.726(if) + 81][(if)^2 + 63.63(if) + 2025]}$$

where

TF_2 = transfer function for the Phase III SID band-pass amplifier

K_2 = arbitrary constant associated with the amplifier gain

7. Scientific geophone transfer function. Because the input seismic signal in the particle velocity-time relation was obtained with a scientific geophone, the response characteristics of the scientific geophone had to be taken into account. The transfer function for the scientific geophone is

$$TF_3 = \frac{K_3(if)^2}{(if)^2 + 7.07(if) + 25}$$

where

TF_3 = transfer function for the scientific geophone

K_3 = arbitrary constant associated with scientific geophone calibration

8. The theoretical combined transfer function for the geophone and band-pass amplifier of the Phase III SID and the scientific geophone is given below

$$TF = \frac{(TF_1)(TF_2)}{TF_3}$$

or

$$TF = \frac{K(if)^2[(if)^2 + 7.07(if) + 25]}{[(if)^2 + 5.6(if) + 196][(if)^2 + 12.726(if) + 81][(if)^2 + 63.63(if) + 2025]}$$

where

$$K = \frac{K_1 K_2}{K_3}$$

The value of K was determined to be compatible with the alarm amplitude threshold values for the Phase III SID. The alarm levels are 38.1×10^{-6}, 95.2×10^{-6}, and 238.1×10^{-6} cm/sec for high-, medium-, and low-gain settings, respectively (see fig. A3, Appendix A). A graphic presentation of the transfer functions describing the effects of geophones and the band-pass amplifier on the seismic analog signal is given in fig. D1.

9. The output from the seismic sensor performance model is the activation range for low-, medium-, and high-gain settings of the SID. The activation distance obtained may not be the distance at which the energy source is first detected. This results from the fact that the SID does not transmit a radio-frequency (RF) signal until the logic integrates a number of signals from succeeding energy sources. Thus, the actual detection distance may be 3 to 5 m less than the value for SID logic activation (that is, if the source is moving toward the SID). If the energy source is moving tangential to the SID, the distance at which the SID logic is activated will be approximately the distance at which the energy source would be detected.

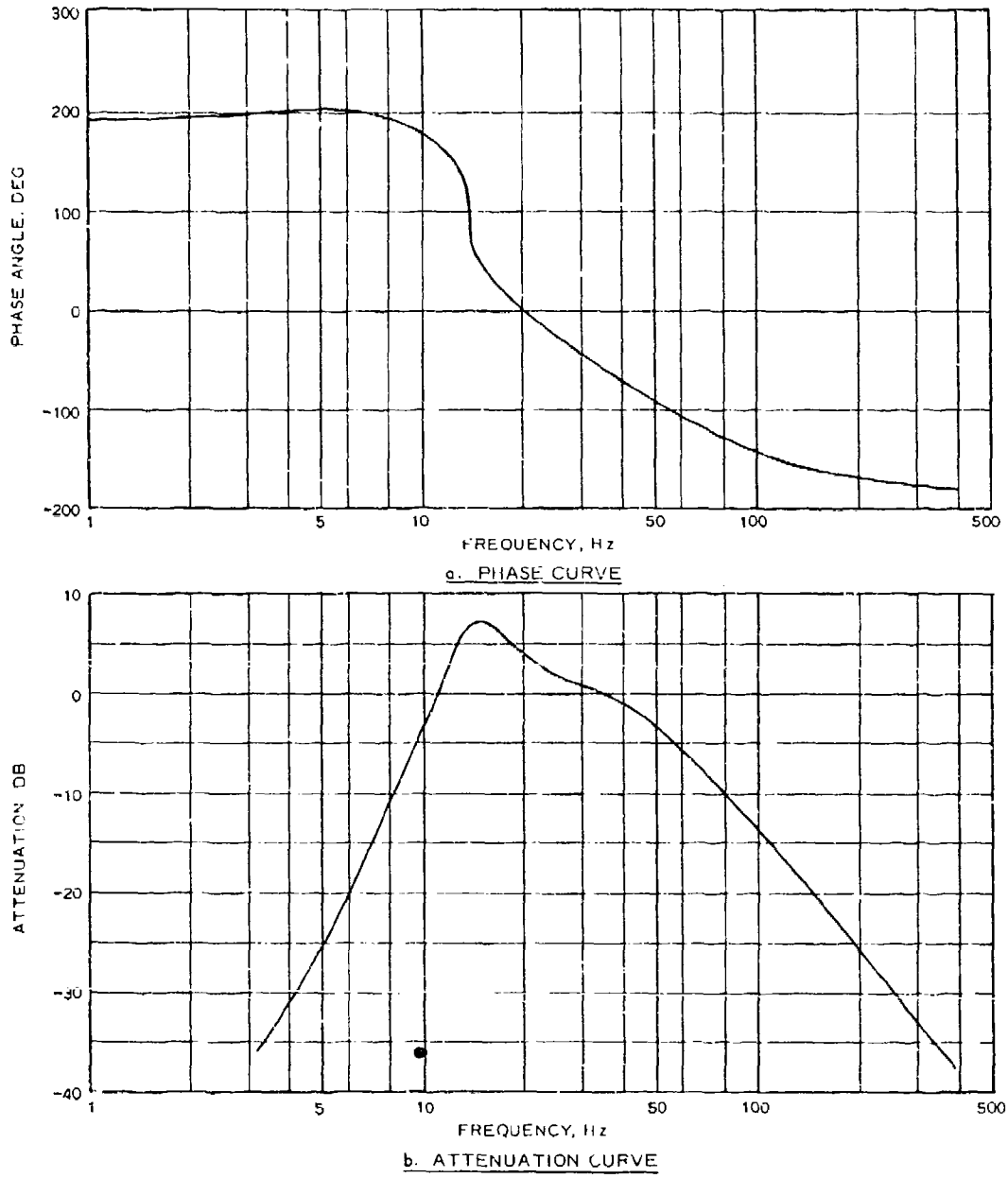

Fig. D1. Graphic presentation of transfer function describing effects of the SID geophone and band-pass amplifier

Analog Computer Model

10. The analog computer used to obtain predictions of SID detection performance was a Systron Donner Model SD/80. A schematic diagram of the computer system is shown in fig. D2.

11. The analog model was built to be flexible and to allow simulation of the wave shapes actually observed in a Phase III SID. The basic components of the analog computer model are as follows:

a. An input voltage comparator, with a trigger level corresponding to each respective SID gain setting (low, medium, or high).

b. A pulse-shaping network, which forms a pulse whose area is proportional to the seismic input signal.

c. A pulse-integrating circuit, which stores pulses from the shaping network for a preset time interval.

d. A second voltage comparator, with a trigger level corresponding to the detection resulting from four seismic signals in 6 sec.

12. The analog computer was calibrated with a damped 30-Hz sine wave whose peak positive value (amplitude) times the appropriate gain setting (low, medium, or high) equals the threshold level for the first comparator. This sine wave was programmed to cycle four times in a period of 6 sec to simulate the minimum signal that would trigger (i.e. activate) a Phase III SID logic circuit. The low- and medium-gain logics were programmed separately on the computer to facilitate calibration and system operation (the SID logic corresponding to high gain was not programmed at the time of this report).

13. The computer model was operated by inputting the FM analog tape recordings of the seismic response generated by a walking man or moving vehicle. The output (see example, fig. D3) was in the form of an x-y plot that displays the position of the energy source along the test line. Successive event markers on the plot indicated preselected distances, such as 1 m, 10 m, 50 m, and so on. A d-c voltage shift

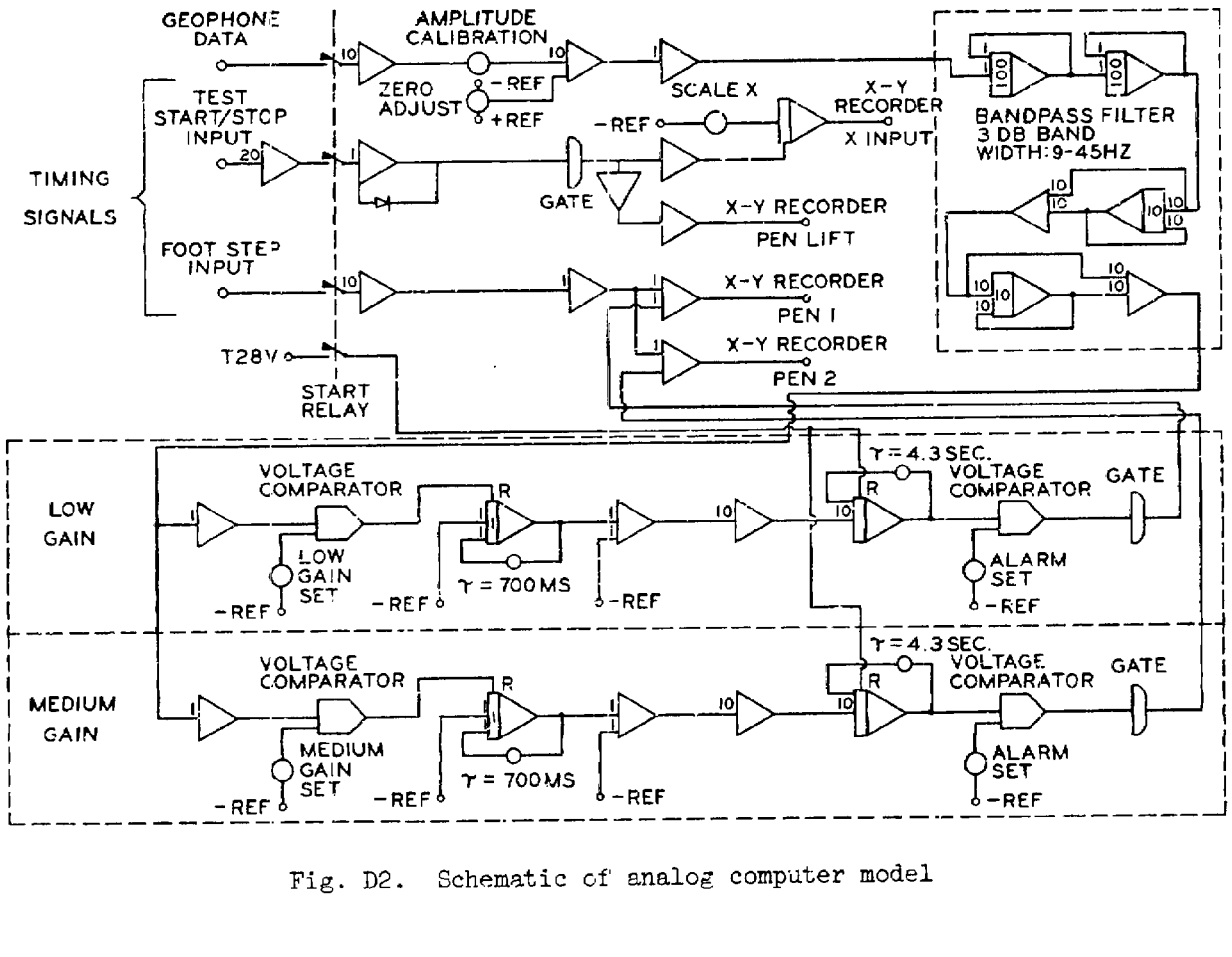

Fig. D2. Schematic of analog computer model

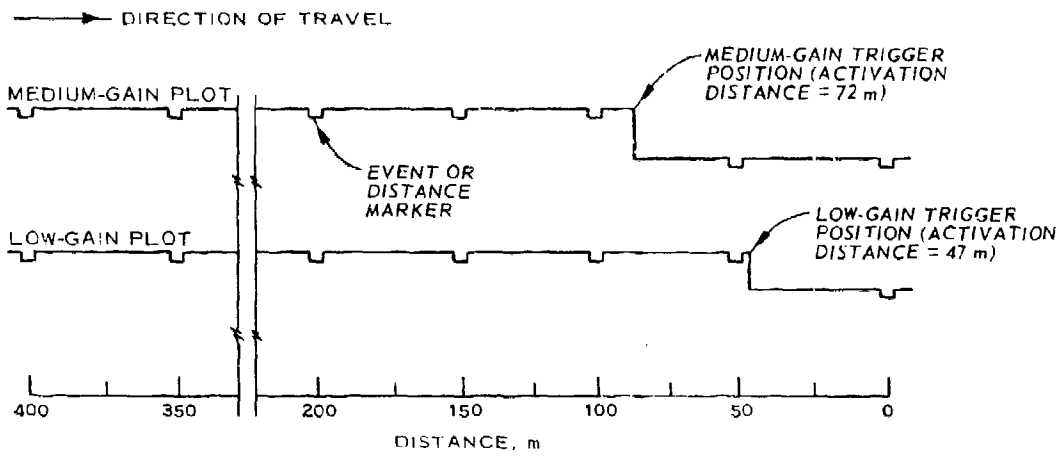

NOTE: PREDICTION SHOWN IS FOR M151 VEHICLE (SPEED 8 KM/HR)

Fig. D3. Example of output of analog computer model

(line displacement) on the plot indicated that the SID had triggered. The detection range was then determined by measuring the horizontal length from the start of the line to the point of displacement.

Unclassified

Security Classification

DOCUMENT CONTROL DATA - R & D

(Security classification of title, body of abstract and indexing annotation must be entered when the overall report is classified)

1 ORIGINATING ACTIVITY (Corporate author)

U. S. Army Engineer Waterways Experiment Station
Vicksburg, Mississippi

2a. REPORT SECURITY CLASSIFICATION

Unclassified

2b. GROUP

3 REPORT TITLE

EFFECTS OF TERRAIN ON THE PROPAGATION OF MICROSEISMIC WAVES AND IMPLANTATION CHARACTERISTICS OF AIR-DELIVERED SENSORS AT FORT HUACHUCA, ARIZONA; WET- AND DRY-SEASON CONDITIONS

4 DESCRIPTIVE NOTES (Type of report and inclusive dates)

Final report

5 AUTHOR(S) (First name, middle initial, last name)

Harold W. West
Behzad Rohani

6 REPORT DATE	7a. TOTAL NO. OF PAGES	7b. NO OF REFS
June 1973	213	22

8a. CONTRACT OR GRANT NO.	9a. ORIGINATOR'S REPORT NUMBER(S)
b. PROJECT NO. 9-CO-002-000-010	Technical Report M-73-3
c.	9b. OTHER REPORT NO(S) (Any other numbers that may be assigned this report)
d.	

10 DISTRIBUTION STATEMENT

Distribution limited to U. S. Government agencies only; test and evaluation; June 1973. Other requests for this document must be referred to U. S. Army Engineer Waterways Experiment Station.

11 SUPPLEMENTARY NOTES	12 SPONSORING MILITARY ACTIVITY
	U. S. Army Test and Evaluation Command U. S. Army Electronics Proving Ground Fort Huachuca, Arizona

13 ABSTRACT

To obtain a quantitative basis for experiment design decisions regarding evaluation of seismic intrusion detector (SID) systems, test areas were selected (one for hand-emplaced SID's and six for air-implanted SID's) and special seismic and environmental field experiments were conducted at Fort Huachuca during Aug 1971 and Mar 1972. Data obtained were assumed to be representative of wet- and dry-terrain conditions at the test sites. The selection of the SID test areas, their wet- and dry-terrain characteristics, and the procedures for collecting environmental data and conducting seismic response tests (i.e. man-walking, drop-hammer, M151 wheeled and M977 tracked vehicles, ambient and induced noises) are described. Also presented are experimental detection distance data on the hand-emplaced miniaturized SID (MIIDS), and experimental data on the depth of penetration and angle of impact of the air-delivered seismic intrusion detector/short (AFSID/S). A theoretical system for modeling the quantitative effects of the terrain on SID detection performance and methods by which SID test results can be extrapolated from one site condition to another are also presented. This system has been implemented on the Waterways Experiment Station computer and involves acquisition of terrain and seismic data for input to the model; exercising the model for each set of terrain factor data; and portraying the performance predictions for each set of terrain and seismic factor data. A system of equations for determining soil penetration and deceleration of air-delivered SID's is included. The system employs a series of computer routines which treat the soil as an elastic-plastic, strain-hardening, compressible medium. Inputs for the penetration equations are dynamic stress-strain data obtained from laboratory triaxial compression and unixial strain tests. The hand-emplacement area provided near-ideal terrain conditions for engineering tests of hand-emplaced SID's. Surface and subsurface terrain data therein varied more from site to site than between wet and dry seasons. Seismic responses measured at the 10 test sites within the hand-emplacement area show some site-to-site variation, which should be considered in SID engineering testing. This variation can be accounted for analytically; therefore it will not necessarily result in any erratic or inconsistent results in engineering testing of the hand-emplaced SID's. Variations in seismic response parameters portrayed by airdrop areas 1 and 3-6, measured in the dry season, generally indicate that the detection performance of air-implanted SID's can be evaluated for a large range of terrain conditions. The variations in these conditions allow the testing of air-implanted SID's under varying stress conditions (i.e. high to low rigid-body deceleration values) and various soil strength conditions. The theoretical detection prediction scheme and/or concepts provide an analytical framework for predicting the performance for man walking targets in various world

(Continued)

DD FORM 1 NOV 68 1473 REPLACES DD FORM 1473, 1 JAN 68, WHICH IS OBSOLETE FOR ARMY USE.

Unclassified

Security Classification

Unclassified
Security Classification

14 KEY WORDS	LINK A		LINK B		LINK C	
	ROLE	WT	ROLE	WT	ROLE	WT
Computers						
Fort Huachuca, Arizona						
Seismic intrusion detectors						
Seismic waves						
Sensors						
Terrain						

ABSTRACT (CONTINUED)

terrains. The scheme requires specific terrain and seismic input data for execution, and as a result, four types of maps were prepared: terrain factor complex maps for subsurface layers 1 and 2 to provide inputs to the theoretical seismic wave propagation model; surface condition maps to be used with the forcing function model under development; seismic response factor complex maps to show the relative seismic response of the hand-emplacement area; and SID one-man walking detection performance maps. The predicted depths of penetration [illegible] ADSID/2 compared reasonably well with the very limited experimental penetration data; they show the depth of penetrations to be very dependent upon near-surface moisture conditions. Operating principles of hand-emplaced miniaturized SID's and air-delivered SID's used in special tests to yield data for aiding in the evaluation of techniques for predicting SID performance are given in Appendix A. The test sites are described and supplementary refraction seismic data are given in Appendix B. The equations for predicting penetration depths and deceleration values for air-implanted SID's are presented in Appendix C, and the computer models used to predict SID detection performance are described in Appendix D.

Unclassified
Security Classification

EAST RANGE BOUND
AIRDROP AREA 2
BABOCOMARI RIVER
MET STATION 3
AIRDROP AREA 4(410)
AIRDROP AREA

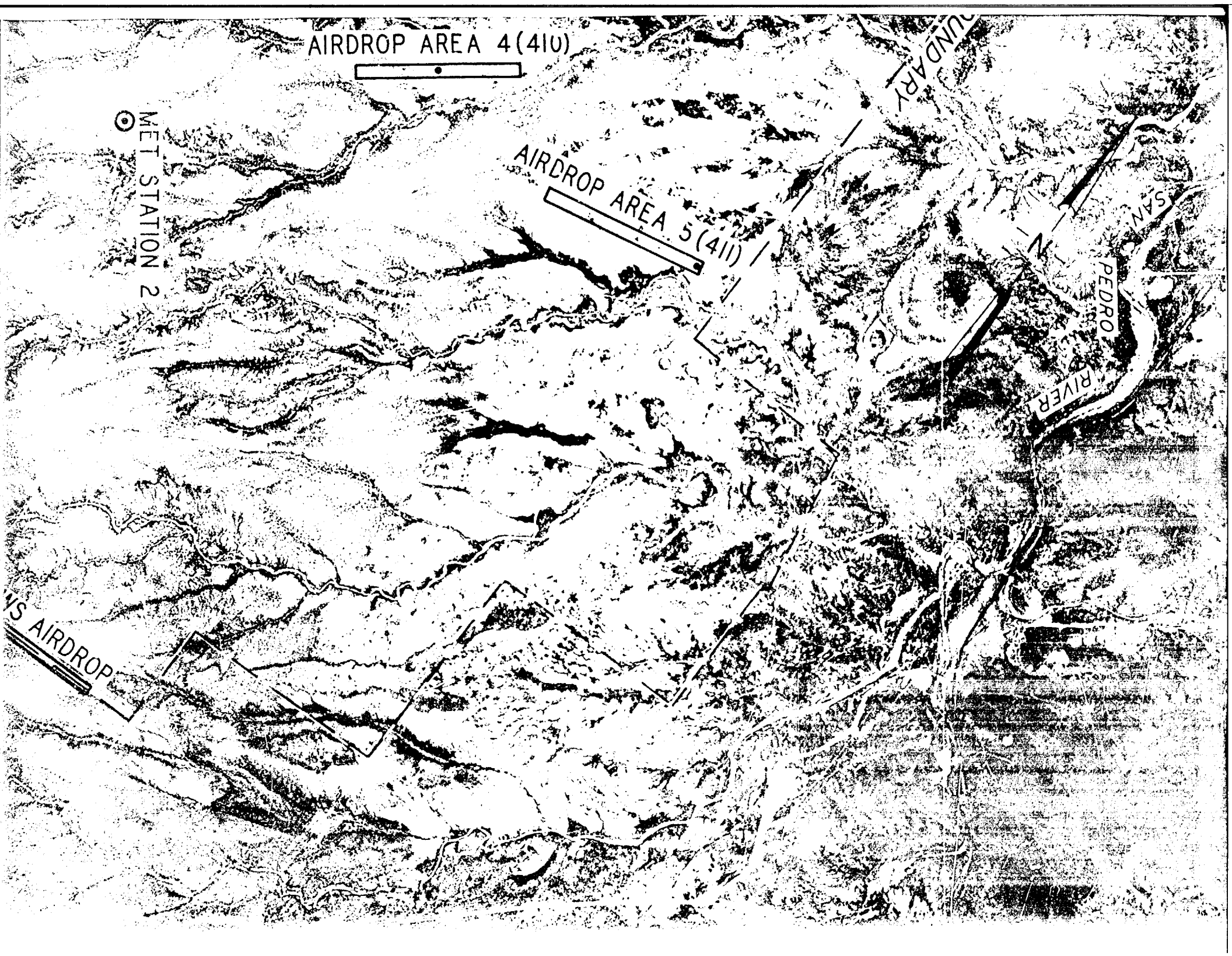
AIRDROP AREA 4 (410)
AIRDROP AREA 5 (411)
MET STATION 2
SAN PEDRO RIVER


AIRDROP AREA 1 (347)
AIRDROP AREA 3 (412)
ARIZONA STATE HWY 90

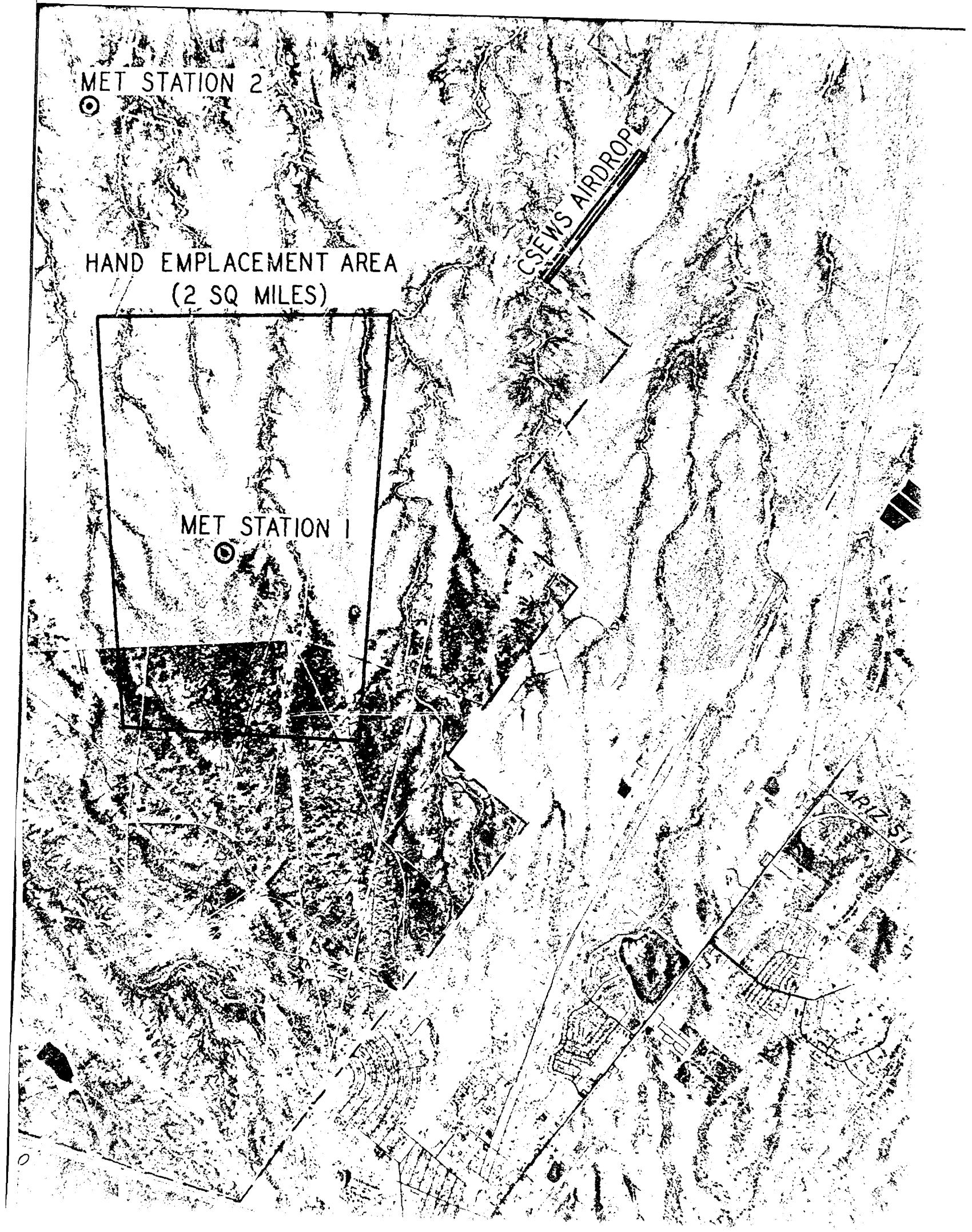
MET STATION 2
CSEWS AIRDROP
HAND EMPLACEMENT AREA
(2 SQ MILES)
MET STATION 1
ARIZ 51

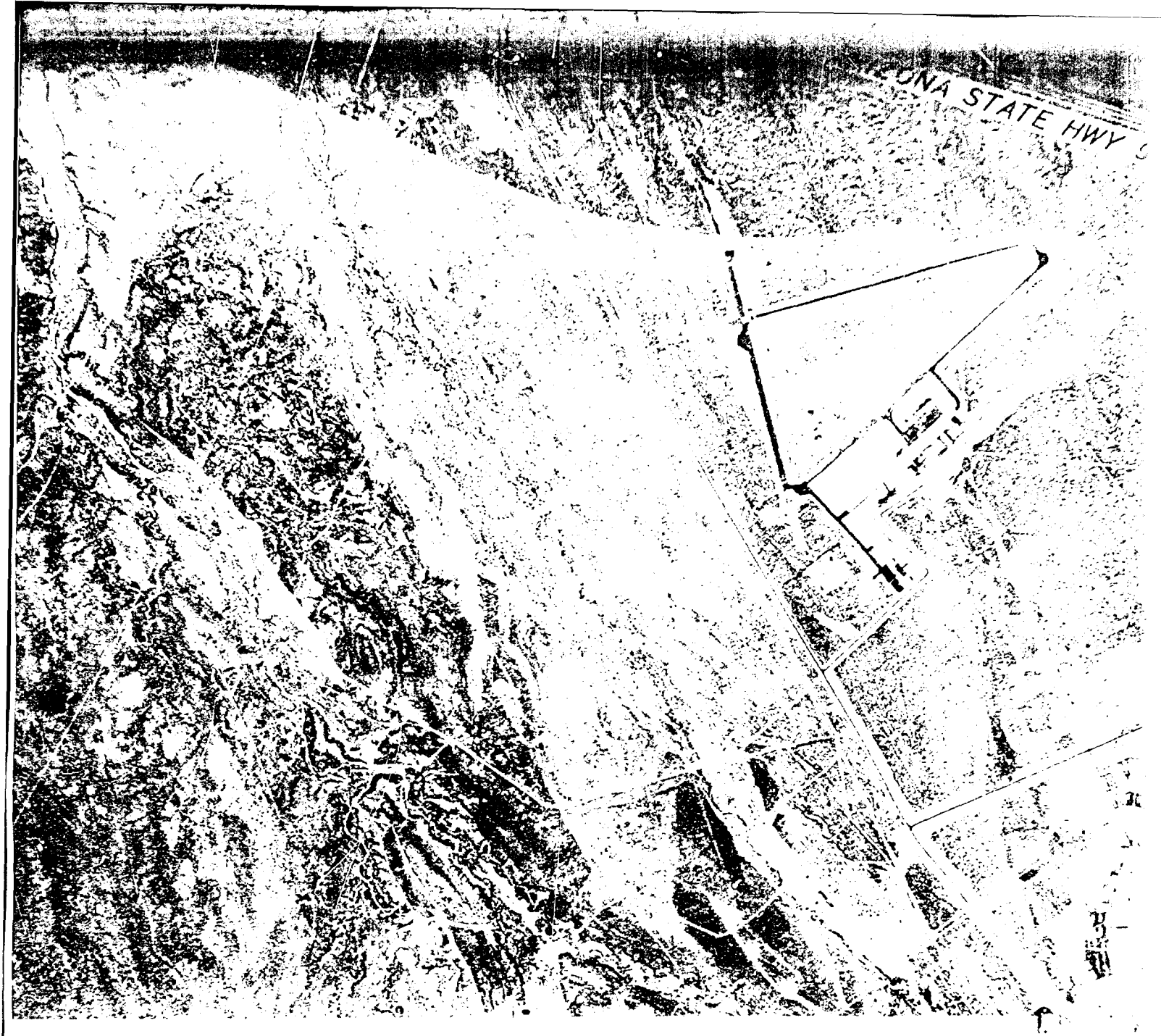

LOCATION OF HAND-EMPLAC
EAST RANGE, FOI

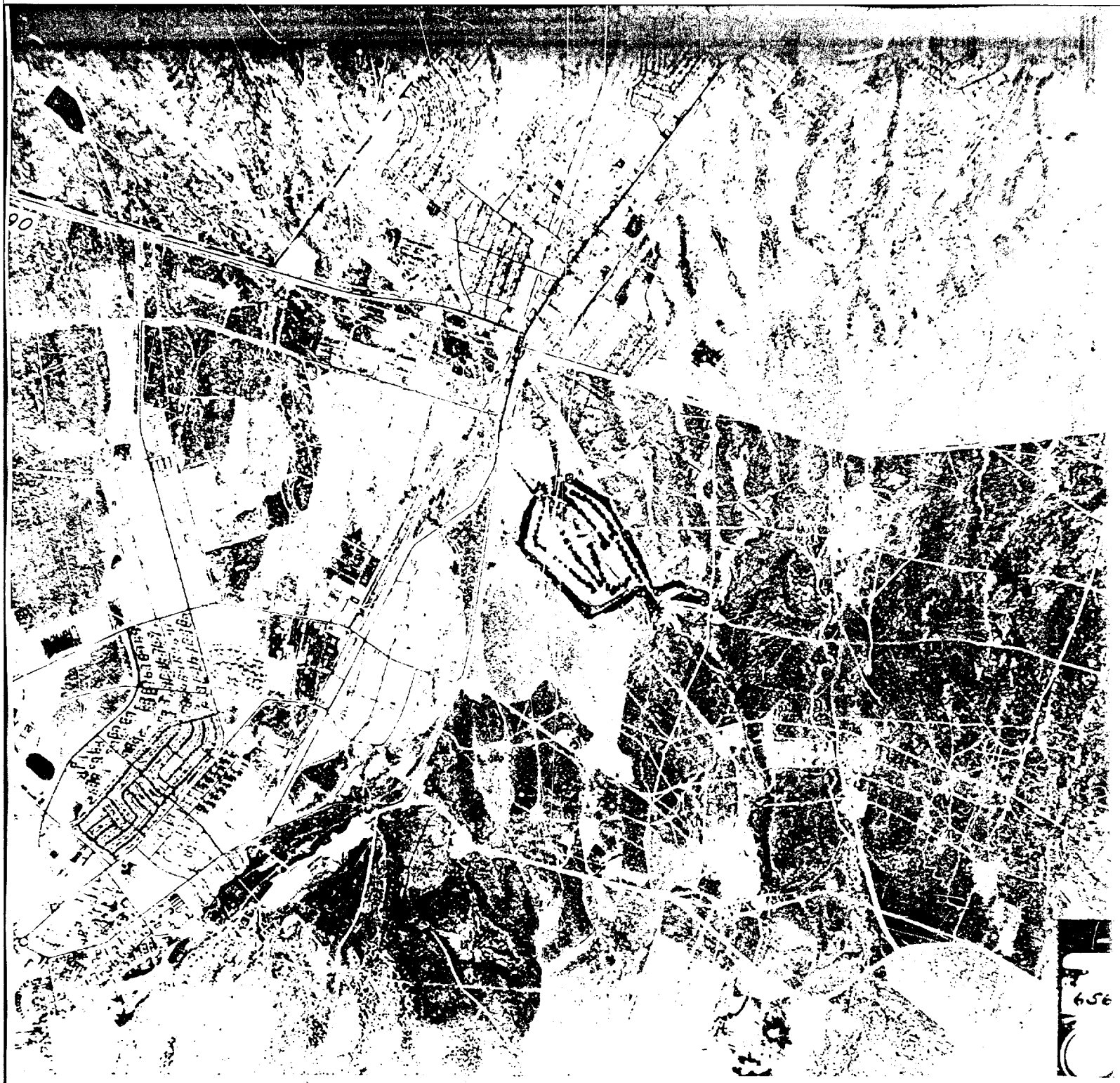

EMENT AND AIRDROP TEST AREAS,
RT HUACHUCA, ARIZONA

MAP

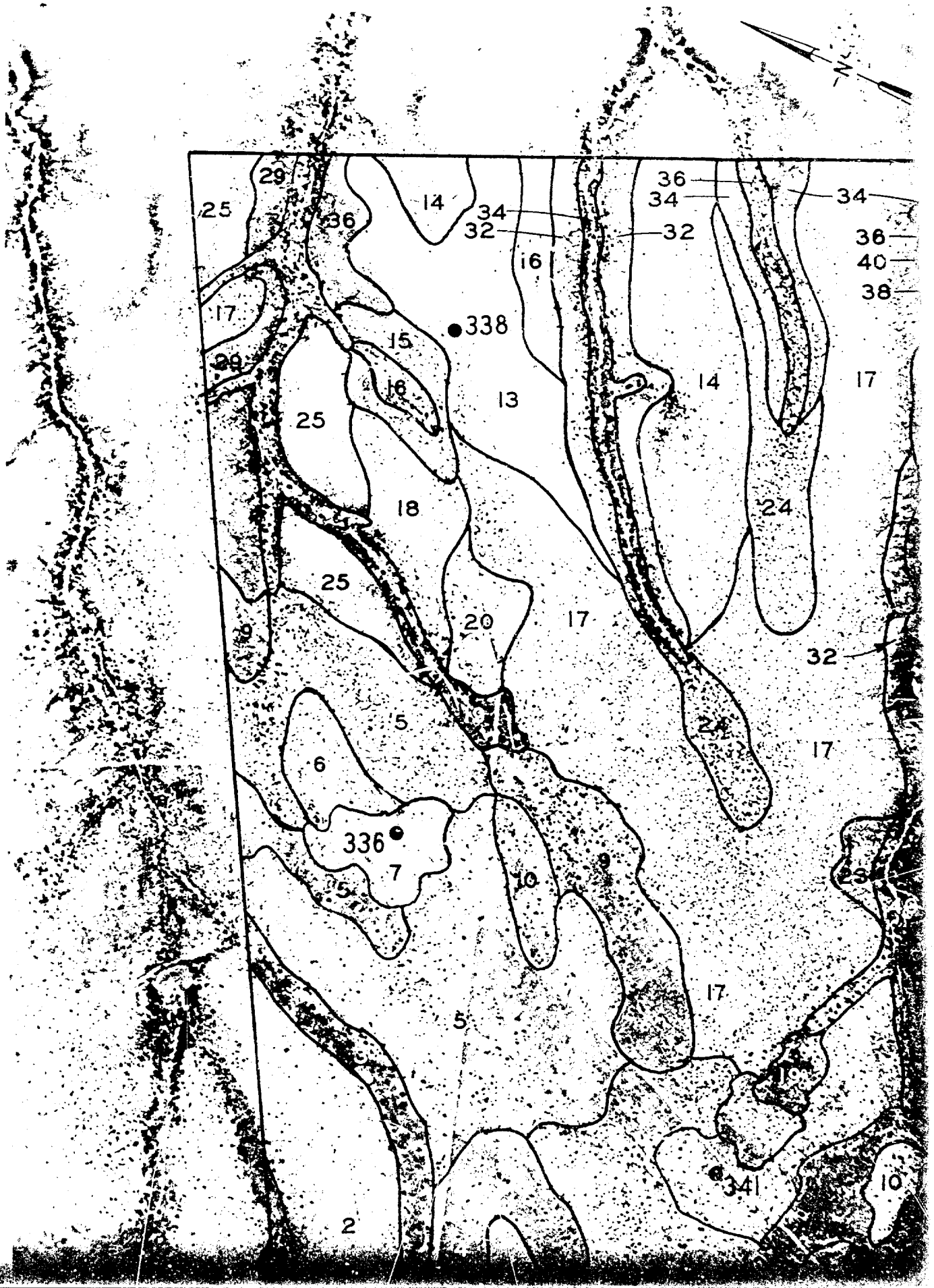
29
25
36
14
34
32
36
34
34
32
36
40
38
16
17
338
15
29
16
13
14
17
25
18
24
25
20
17
9
32
5
24
17
6
336
7
5
10
9
23
17
5
341
10
2

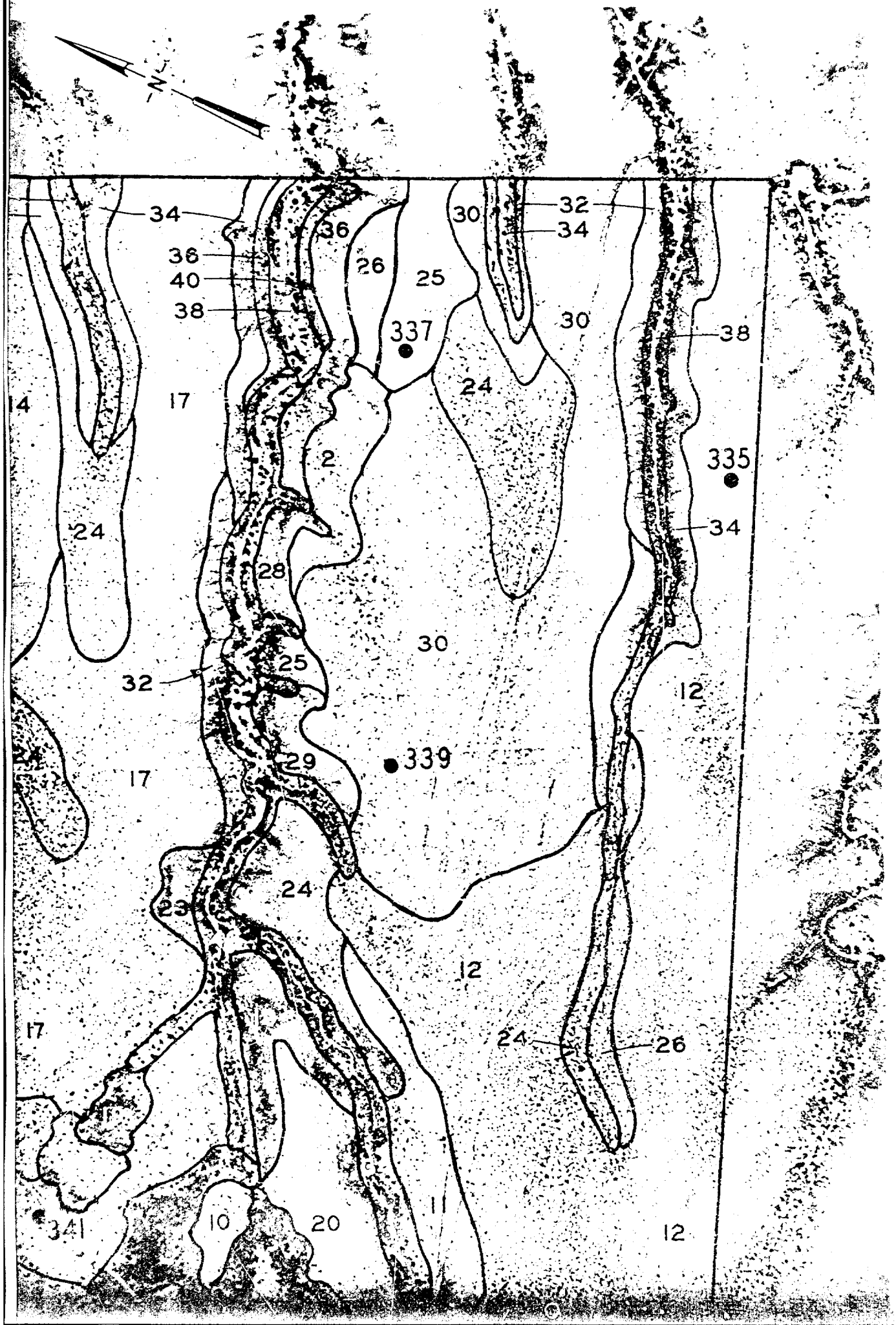
N
34
36
38
40
38
36
26
25
337
30
32
34
30
38
24
14
17
2
335
24
34
28
30
25
32
12
339
29
17
24
23
12
17
24
26
341
10
20
11
12

Map Unit	Factor Class							
	Layer 1				Layer 2			
	T_1	V_{P1}	V_{S1}	ρ_1	T_2	V_{P2}	V_{S2}	ρ_2
1	1	1	3	3	4	2	3	1
2	1	1	3	3	5	3	3	2
3	1	1	4	3	3	3	3	2
4	1	3	3	3	3	3	3	2
5	1	4	2	2	2	2	1	2
6	1	4	2	4	1	1	1	2
7	1	4	2	4	1	2	1	2
8	2	4	3	3	4	2	3	2
9	2	4	4	4	3	2	2	2
10	2	4	6	2	5	2	2	1
11	2	4	6	3	3	4	4	2
12	2	5	5	3	2	2	1	2
13	2	7	6	4	8	4	1	3
14	3	1	1	2	3	1	1	1
15	3	1	3	2	5	1	2	1

Map Unit	Factor Class							
	Layer 1				Layer 2			
	T_1	V_{P1}	V_{S1}	ρ_1	T_2	V_{P2}	V_{S2}	ρ_2
21	3	5	5	4	5	4	3	2
22	3	5	6	3	8	4	2	2
23	3	5	6	4	5	3	1	3
24	3	7	5	4	1	4	2	3
25	3	7	5	4	3	3	1	2
26	4	3	3	2	5	1	1	1
27	4	4	5	2	5	3	1	1
28	4	6	4	4	3	3	1	2
29	4	6	4	4	5	4	2	2
30	4	6	4	4	8	4	2	2
31	4	6	6	4	6	4	1	2
32	4	6	6	4	8	2	2	3
33	4	6	6	4	8	4	1	3
34	4	7	5	4	2	4	2	3
35	4	7	6	4	8	4	1	3

4

Factor Class	Layer Thickness T, cm	Compression Wave Velocity V_P, m/sec	Shear Wave Velocity V_S, m/sec	Wet Density ρ, g/cm^3
	Factor Value Range, First Refraction Layer			
1	40-65	220-260	75-115	1.00-1.45
2	66-95	261-290	116-135	1.46-1.60
3	96-125	291-320	136-155	1.61-1.80
4	126-165	321-360	156-175	1.81-2.10
5	166-200	361-400	176-190	2.11-2.30
6	201-240	401-240	191-220	
7	241-280	461-525		
8	281-320			
9	321-600			
	Factor Value Range, Second Refraction Layer			

er 2 V_{S2}	ρ_2
3	2
2	2
1	3
2	3
1	2
1	1
1	1
1	2
2	2
2	2
1	2
2	3
1	3

5	1	4	2	2	2	2	1	2	25	5	7	5	4	3	3	1	2
6	1	4	2	4	1	1	1	2	26	4	3	3	2	5	1	1	1
7	1	4	2	4	1	2	1	2	27	4	4	5	2	5	3	1	1
8	2	4	3	3	4	2	3	2	28	4	6	4	4	3	3	1	2
9	2	4	4	4	3	2	2	2	29	4	6	4	4	5	4	2	2
10	2	4	6	2	5	2	2	1	30	4	6	4	4	8	4	2	2
11	2	4	6	3	3	4	4	2	31	4	6	6	4	6	4	1	2
12	2	5	5	3	2	2	1	2	32	4	6	6	4	8	2	2	3
13	2	7	6	4	8	4	1	3	33	4	6	6	4	8	4	1	3
14	3	1	1	2	3	1	1	1	34	4	7	5	4	2	4	2	3
15	3	1	3	2	5	1	2	1	35	4	7	6	4	8	4	1	3
16	3	2	3	2	2	1	2	2	36	6	6	4	4	2	4	2	3
17	3	3	3	3	5	3	2	2	37	9	6	4	4	8	4	2	2
18	3	5	5	3	3	3	1	2	38	9	6	5	4	6	4	2	3
19	3	5	5	3	5	4	2	2	39	9	7	5	4	8	4	2	3
20	3	5	5	4	4	3	3	3	40	9	7	6	4	8	4	1	3

TERRAIN FACTOR COMPLEX MAP F
HAND-EMPLACEMENT

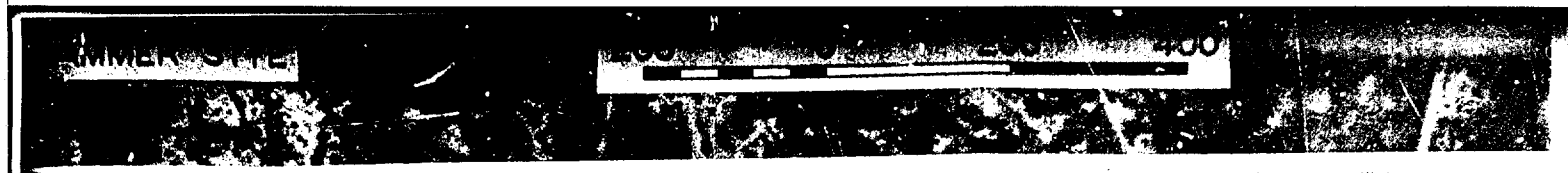

Factor Class						
Layer 1			Layer 2			
T_1	V_{S1}	ρ_1	T_2	V_{P2}	V_{S2}	ρ_2
5	4		5	4	3	2
6	3		8	4	2	2
6	4		5	3	1	3
5	4		1	4	2	3
5	4		3	3	1	2
3	2		5	1	1	1
5	2		5	3	1	1
4	4		3	3	1	2
4	4		5	4	2	2
4	4		8	4	2	2
6	4		6	4	1	2
6	4		8	2	2	3
6	4		8	4	1	3
5	4		2	4	2	3
6	4		8	4	1	3
4	4		2	4	2	3
4	4		8	4	2	2
5	4		6	4	2	3
5	4		8	4	2	3
6	4		8	4	1	3

Factor Class	Layer Thickness T, cm	Compression Wave Velocity V_P, m/sec	Shear Wave Velocity V_S, m/sec	Wet Density ρ, g/cm^3
	Factor Value Range, First Refraction Layer			
1	40-65	220-260	75-115	1.00-1.45
2	66-95	261-290	116-135	1.46-1.60
3	96-125	291-320	136-155	1.61-1.80
4	126-165	321-360	156-175	1.81-2.10
5	166-200	361-400	176-190	2.11-2.30
6	201-240	401-240	191-220	
7	241-280	461-525		
8	281-320			
9	321-600			
	Factor Value Range, Second Refraction Layer			
1	100-150	470-570	235-285	1.61-1.80
2	151-240	571-645	286-335	1.81-2.10
3	241-330	646-750	336-385	2.11-2.30
4	331-480	751-950		
5	481-600	951-1100		
6	601-800	1101-1300		
7	801-1100	1301-1700		
8	1101-2000			

COMPLEX MAP FOR LAYERS 1 AND 2,
D-EMPLACEMENT AREA

MAP 2


8
338
ER
ER
ER
5
5
5
R
341
2
6


3
R
5
337
5
ER
335
ER

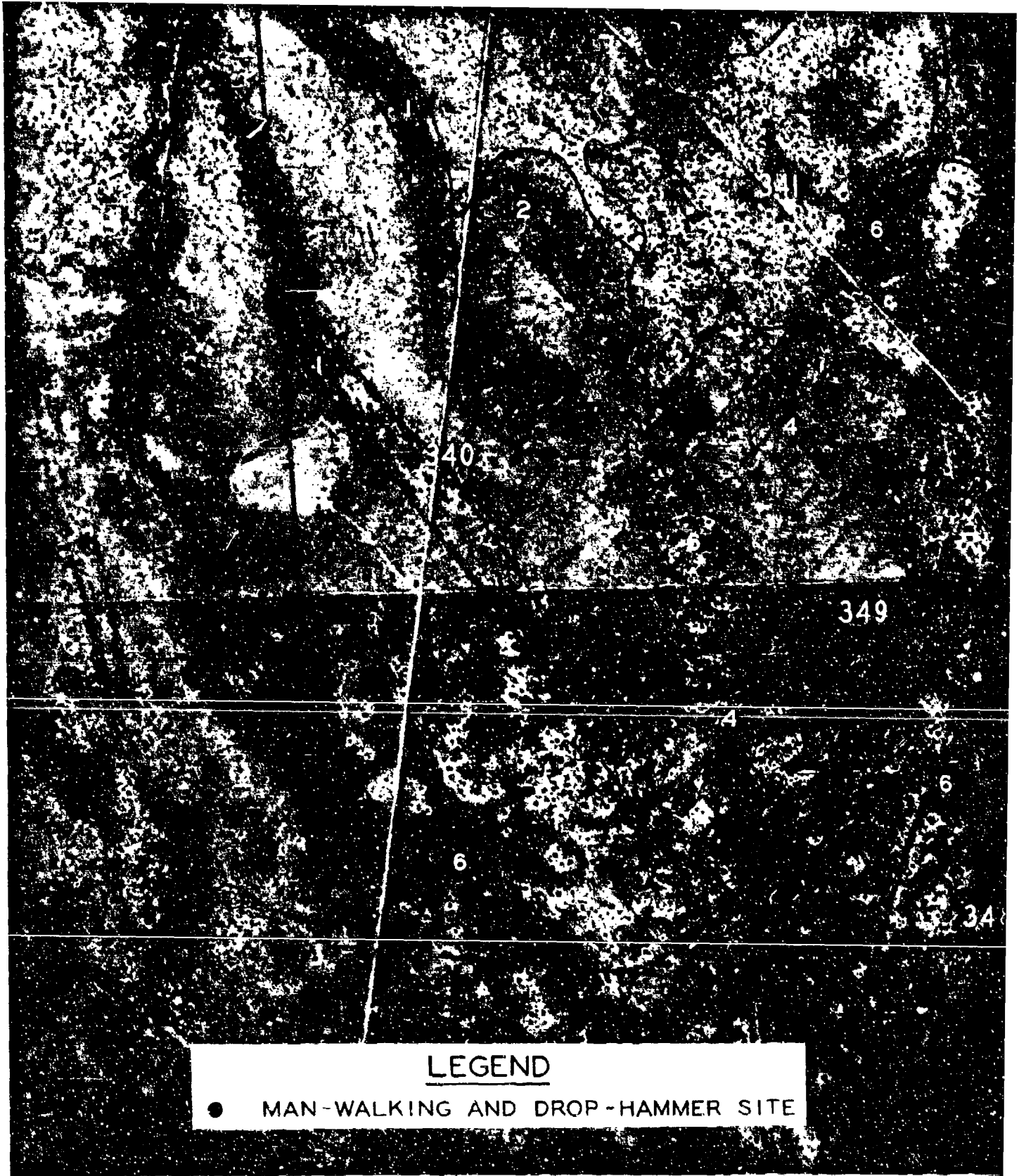

NOTE: ER DENOTES ERRATIC PERFORMANCE. THE ER AREAS ARE ALONG THE ARROYOS (I.E., DRAINAGE CHANNELS) AND CONTAIN SLOPING AND IRREGULAR TERRAIN AND A GRAVELLY SANDY SURFACE MATERIAL. THE SEISMIC RESPONSE IN THIS AREA DEPENDS TO A LARGE EXTENT UPON THE RELATIVE LOCATIONS OF THE DROP HAMMER AND THE SEISMIC DETECTOR.

	Drop Hammer Seismic Response Factor Class																	
	PPV						PSPV						f					
Map	5	10	20	30	40	60	5	10	20	30	40	60	5	10	20	30	40	60
Unit	m	m	m	m	m	m	m	m	m	m	m	m	m	m	m	m	m	m
					1	1	2	2	1	1	1	1	3	3	2	2	2	2

DRAINAGE
Y SURFACE
N THE

40 60
m m

Seismic Response Factor Class	Seismic Response Factor Value Range PPV 10^{-3} cm/sec	PSPV 10^{-3} cm/sec	f Hz
1	0.0 - 0.10	0.0 - 0.10	11 - 16
2	0.11 - 0.30	0.11 - 0.30	17 - 22
3	0.31 - 0.60	0.31 - 0.60	23 - 29
4	0.61 - 1.50	0.61 - 1.00	30 - 36

NOTE: ER DENOTES ERRATIC PERFORMANCE; THE ER AREAS ARE ALONG THE ARROYOS (I.E., DRAINAGE CHANNELS) AND CONTAIN SLOPING AND IRREGULAR TERRAIN AND A GRAVELLY SANDY SURFACE MATERIAL. THE SEISMIC RESPONSE IN THIS AREA DEPENDS TO A LARGE EXTENT UPON THE RELATIVE LOCATIONS OF THE DROP HAMMER AND THE SEISMIC DETECTOR.

	Drop-Hammer Seismic Response Factor Class																	
	PPV						PSPV						f					
Map Unit	5 m	10 m	20 m	30 m	40 m	60 m	5 m	10 m	20 m	30 m	40 m	60 m	5 m	10 m	20 m	30 m	40 m	60 m
1	4	3	2	2	1	1	2	2	1	1	1	1	3	3	2	2	2	2
2	4	3	2	2	1	1	3	2	2	1	1	1	5	5	4	3	3	1
3	4	3	2	2	2	1	2	2	1	1	1	1	4	4	4	3	3	2
4	4	4	2	2	1	1	2	2	1	1	1	1	4	4	4	3	2	1
5	4	4	3	2	1	1	3	2	2	1	1	1	5	5	4	3	3	1
6	4	4	3	2	2	1	3	2	2	1	1	1	4	4	3	3	3	2
7	4	4	3	2	2	1	3	2	2	1	1	1	9	7	5	3	2	2
8	4	4	3	3	2	2	4	3	2	2	2	2	5	5	4	4	3	1

DRY-SEASON DROP-HAMMER SEIS
HAND-EMPLACEMENT

AMMER SITE

SCALE IN METERS

200 0 200 400

THE ARROYOS (I.E., DRAINAGE
A GRAVELLY SANDY SURFACE
LARGE EXTENT UPON THE
ETECTOR.

Class					
f					
5	10	20	30	40	60
m	m	m	m	m	m
3	3	2	2	2	2
5	5	4	3	3	1
4	4	4	3	3	2
4	4	4	3	2	1
5	5	4	3	3	1
4	4	3	3	3	2
9	7	5	3	2	2
5	5	4	4	3	1

Seismic Response Factor Class	Seismic Response Factor Value Range PPV 10^{-3} cm/sec	PSPV 10^{-3} cm/sec	f Hz
1	0.0 - 0.10	0.0 - 0.10	11 - 16
2	0.11 - 0.30	0.11 - 0.30	17 - 22
3	0.31 - 0.60	0.31 - 0.60	23 - 29
4	0.61 - 1.50	0.61 - 1.00	30 - 36
5	1.51 - 3.50	1.01 - 1.50	37 - 43
6	3.51 - 7.00	1.51 - 2.50	44 - 50
7	7.01 - 13.00	2.51 - 3.50	51 - 56
8	13.01 - 28.00	3.51 - 6.00	57 - 62
9	--	6.01 - 13.00	63 - 68
10	--	13.01 - 28.00	69 - 74

6

P-HAMMER SEISMIC RESPONSE MAP,
-EMPLACEMENT AREA

MAP 3


15
14
10
336
ER
ER
12
14
ER
12
14

2

NOTE: MAP BASED ON MAN WEIGHING 66-79 KG;

ER DENOTES ERRATIC PERFORMANCE;
CHANNELS) AND CONTAIN SLOPING AND
MATERIAL. THE DETECTION PERFORM
RELATIVE LOCATIONS OF THE MAN-WAL

NOTE: MAP BASED ON MAN WEIGHING 66-79 KG, WEARING BOOT SIZE 9-11, AVERAGE SPEED, [illegible]

ER DENOTES ERRATIC PERFORMANCE; THE ER AREAS ARE ALONG THE ARROYOS (I.E., DRAINAGE CHANNELS) AND CONTAIN SLOPING AND IRREGULAR TERRAIN AND A GRAVELLY SANDY SURFACE MATERIAL. THE DETECTION PERFORMANCE IN THIS AREA DEPENDS TO A LARGE EXTENT UPON THE RELATIVE LOCATIONS OF THE MAN-WALKING TARGET (FOOTSTEP) AND THE MINISID.

5
2

SID ONE MAN-WALKING DETECTION
HAND-EMPLACEMEN

PER STEP.

DRAINAGE
SURFACE
NT UPON THE

Map Unit	Detection Distance Factor Class: Low Gain	Medium Gain	High Gain
4	1	4	6
5	1	5	8
6	2	3	5
7	2	4	5
8	2	4	6
9	2	4	8
10	2	5	6
11	2	5	8
12	2	5	9
13	3	4	5
14	3	4	6
15	3	5	6
16	3	5	8
17	3	5	9
18	3	7	8

Detection Distance Factor Class	Value Range, m
1	1-4
2	5-10
3	11-20
4	21-30
5	31-40
6	41-50
7	51-60
8	61-80
9	81-110

6

DETECTION PERFORMANCE MAP,
PLACEMENT AREA

MAP 4